

Metabolic Reprogramming of the Cell: Investigating Systemic Signatures and Growth in Cancer

Thesis Submitted to AcSIR
For the Award of the Degree of

DOCTOR OF PHILOSOPHY
In
BIOLOGICAL SCIENCES



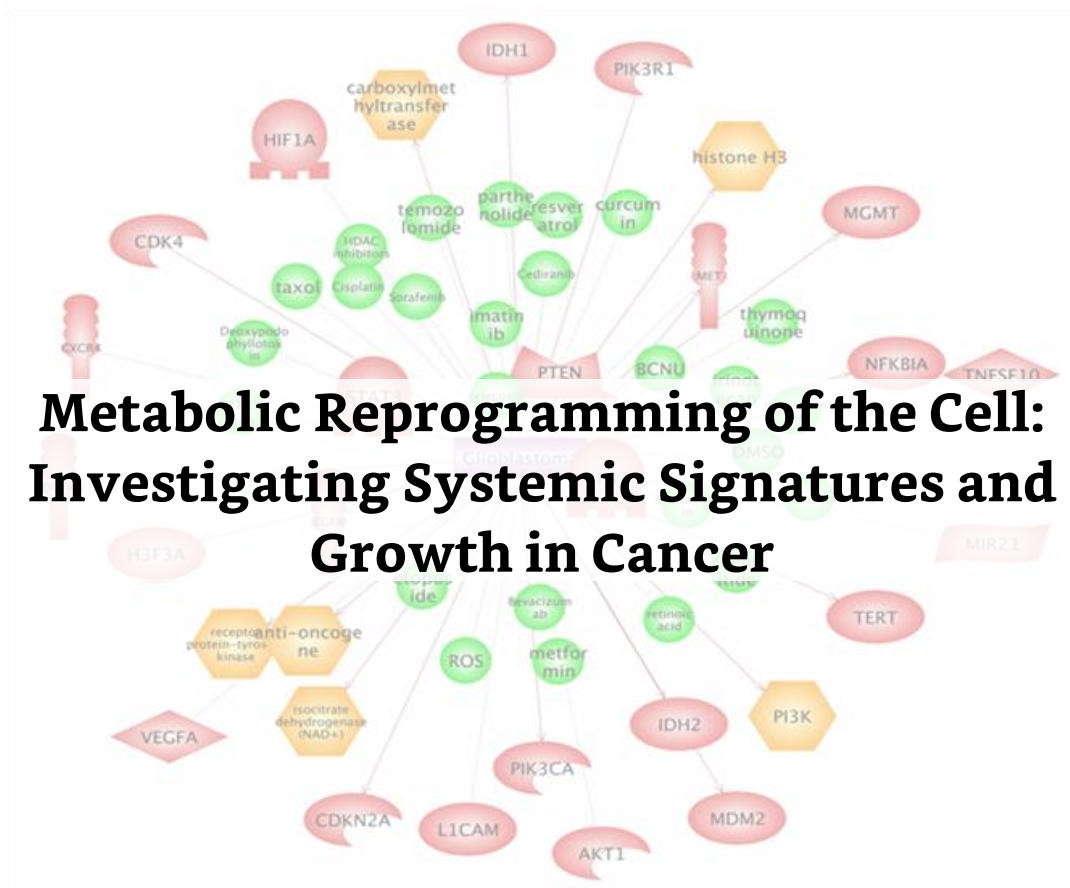
By

SELVA RUPA CHRISTINAL I.
10EB11A26062

Under the guidance of
DR. ANU RAGHUNATHAN
(Research Supervisor)

Chemical Engineering Division
CSIR-National Chemical Laboratory
Pune – 411008, India

September 2018



By
Selva Rupa Christinal I.



सीएसआयआर-राष्ट्रीय रासायनिक प्रयोगशाला

(वैज्ञानिक तथा औद्योगिक अनुसंधान परिषद)

डॉ. होमी भाभा मार्ग, पुणे - 411 008, भारत



CSIR-NATIONAL CHEMICAL LABORATORY


(Council of Scientific & Industrial Research)

Dr. Homi Bhabha Road, Pune - 411008, India

Certificate

This is to certify that the work incorporated in this Ph.D. thesis entitled **Metabolic Reprogramming of the Cell: Investigating Systemic Signatures and Growth in Cancer** submitted by Mrs. **Selva Rupa Christinal I.** to Academy of Scientific and Innovative Research (AcSIR) in fulfillment of the requirements for the award of the Degree of **Doctor of Philosophy**, embodies original research work carried out under my supervision. I further certify that this work has not been submitted to any other University or Institution in part or full for the award of any degree or diploma. Research material obtained from other sources has been duly acknowledged in the thesis. Any text, illustration, table etc., used in the thesis from other sources, have been duly cited and acknowledged.



Selva Rupa Christinal I.
(Student)


Dr. Anu Raghunathan
(PhD Supervisor)
Principal Scientist
Chemical Engineering Division
CSIR-National Chemical Laboratory
Pune-411008

Place: Pune

Date: 17/09/2018

Communication
Channels


NCL Level DID : 2590
NCL Board No. : +91-20-25902000
EPABX : +91-20-25893300
: +91-20-25893400

FAX

Director's Office : +91-20-25902601
COA's Office : +91-20-25902660
COS&P's Office : +91-20-25902664

WEBSITE

www.ncl-india.org

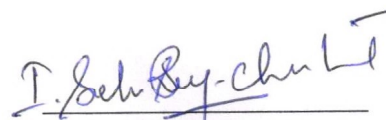
Declaration of Authorship

I hereby declare that this Ph.D. thesis entitled Metabolic Reprogramming of the Cell: Investigating Systemic Signatures and Growth in Cancer was completely carried out by me for the degree of Doctor of Philosophy in Biological Sciences under the guidance and supervision of **Dr. Anu Raghunathan**, Principal Scientist, CSIR-National Chemical Laboratory, Pune, India.

I confirm that this thesis research is my own work while in candidature for a research degree at this institution and the contents of this thesis is original. I also affirm that no part of this thesis has previously been submitted for a degree or any other qualification at this institution or any other institution. Also, the interpretations put forth are based solely on my knowledge and understanding of the original research articles and all resources have been duly cited and acknowledged as and when appropriate.

Place: Pune

Date: 17/09/2018



Selva Rupa Christinal I.

(PhD Student)

Metabolic Inquiry and Cellular Engineering (MICE) Lab

Chemical Engineering Division

CSIR-National Chemical Laboratory

Pune-411008.

The Road Not Taken

*Two roads diverged in a wood, and I—
I took the one less traveled by,
And that has made all the difference.*

- Robert Frost

Preface

My doctoral research discussed in this thesis focuses on understanding **"Metabolic Reprogramming in Cancer": Identification and characterization of drug-resistant cells from final stage Glioblastoma**, the most aggressive brain tumor, **using a systems approach**. I have delineated multi-OMIC datasets starting from Growth → Dose-response → DNA sequence variation (Exome) → mRNA abundances (qPCR) →



metabolite levels (LC-MS/MS) → energy metabolism (Phenotypic microarray). A **comparative analysis across drug-sensitive and drug-resistant cancer cells** eventually led to the development of an integrative combinatorial paradigm for addressing cancer drug resistance. This work holds promising research findings that can become the basis for further development of novel treatment regimens, to control cancer relapse/resistance, also towards personalized medicine in cancer.

Today, as I stand here and look back, the phase of my Ph.D. wasn't that simple and easy. Hence, it's my pleasure to add a few words about this experience. It was on **29th July 2011**, I started my Ph.D. Journey in Chemical Engineering and Process Development (CEPD) Division at CSIR-National Chemical Laboratory, Pune, India with **Dr. Anu Raghunathan**. Having seen my own brother's sufferings due to blood cancer (AML), I have cancer research as my aspiration. Though he, **Selva Raj Jebadurai Immanuel**, is not there with us now, the inspiration he left helped me to face all the challenges. My beloved Father, **Immanuel**, was my biggest support for doing Ph.D. and to reach another region (Maharashtra) from my native (Tamil Nadu), without knowing the regional language (Hindi). I have come across dejection and heartaches in losing my Father in 2012 and also the sudden loss of Dr. APJ Kalam in 2015 who was also my inspiration. Though all this sounded unfavorable and bleak, I began to get many opportunities. I was **an awardee of Newton Bhabha Ph.D. placement from British Council, UK, and DST-India**. I worked for 6 months at the MIB, **University of Manchester, UK** with **Dr. Philip Day and Prof. Douglas Kell** in 2015. This period taught me how to face the world alone, and be much stronger. On my return to India, I was diagnosed with Meningitis. I have survived this illness phase, coming back from my deathbed, yet finished my work and Ph.D. This phase of my life challenged me in every aspect from personal losses, health to financial burden yet I could reach my project goals. **Big achievements and dreams don't just happen; they are gained through hard work, perseverance, and self-confidence**. I hope as a writer that this thesis inspires you both as a reader and a researcher!

I have no special talent, I am only passionately curious
-Albert Einstein

A handwritten signature in black ink that reads "Selva Rupa Christinal Immanuel".

Selva Rupa Christinal Immanuel

Dedicated to.....

My Beloved Father, **Immanuel**

&

My Dearest Brother, **Selva Raj Jebadurai**

Acknowledgements

*All the world's a stage,
And all the men and women merely players;
They have their exits and their entrances
- William Shakespeare*

By God's grace and countless blessings from my beloved father, **Immanuel**, and Brother, **Selva Raj**, I am able to complete my doctoral research and accomplished my Ph.D. with satisfaction and fulfillment.

*The hardest problems of pure and applied science can only be solved
by the open collaboration of the world-wide scientific community.
-Kenneth G. Wilson*

As stated, it is not only to solve the problems of applied sciences but also for the completion of a doctoral thesis, the open collaborations and discussions helped me a lot. My heartfelt and sincere gratitude is to **Dr. Anu Raghunathan** (Anu ma'am as how we address her!). As an advisor, she stood by my side in solving the research problems and gave her hand to strengthen me in all difficulties. I cherish and remember all the thoughtful discussions with her. The freedom that she has given us, starting from ordering the chemicals to designing the experiments (whether it is for the tryptophan project for *E. coli* knockout generation that is now published in BioSystems or for my complete doctoral research), it moulded me step by step to improve my thought-process as a researcher and as a student. As a beginner in systems biology, I had difficulties in integrating large datasets, analyzing and interpreting high-throughput data. Her motivation and many rounds of discussions made me learn how to handle heterogenous data types and do multi-tasking. Though I was thousands of miles away (actually countries apart!), she was right there via phone calls to offer her support. Dear Ma'am, many thanks for all the encouragement and kindly accept my token of appreciation and I hope to receive your continuous support in future.

My profound gratitude is to **Dr. Venkateswarlu Panchagnula** for his research collaboration in acquiring LC-MS/MS data. He has offered his help in many situations. I am also thankful to Drs. **Philip J. Day** and **Douglas Kell**, with whom I worked in the UK for 6 months. They taught me different views in addressing research problems and **Philip** has been a very big support for me till date. It was truly a global experience and excellent international exposure and I got to interact with many scientists during my UK stay. I had a very supportive DAC – Drs. **Venkat, Mugdha Gadgil**, and **Dhiman Sarkar**. I am thankful for their support and inputs during my DAC meetings.

My biggest acknowledgements and love to Ekta Sangtani, Deepak Chand, Prasenjit Bhoumik, Preeti Jain, Deepanwita Banerjee, Mayoreshwar Rajankar, Avinash Ghanate, Madhura Mohole and Priyanka Buddhiwant for their support. Deepa and Mayoer have been with me as lab-mates throughout the journey; our joint efforts for lab establishments and the tea time with them are all worth mentioning. Many thanks to Avinash Ghanate and Dharmesh Parmer, for their help in

acquiring the **LC-MS/MS** data and **FACS facility** at **NCCS, Pune**. I also thank my friends from MBL (where I started my experiments!), Riya Uthup, Shweta Bhat, Arati Deshmukh, Rubina Kazi, Reema Banerjee, Tejal Pant, Tanaya Surve, Vishwanath, Newton Bishoyi, Dipali Kale, Rashmi Godbole and Jyoti Rawat; and my colleagues from NCL - Ashok Kumar, Vasudevan, Lenin, Balaji Anna, Mohan, Edwin, Suman Devi, Aarthy; and "Chithirai Sangamam" (experience as the master of ceremony!).

A special mention for my UK friends and colleagues – Fiona Marriage, Justine Grixti, Caro (Ke Zhang), Andrew Currin, Ilaria Russo, Ming Zu, Alisa, Gabrielle, Samrina, Srijan, Rupesh Bhavsar, Dharamraj, Nathiya and Malkhey Verma for making my UK stay memorable. I cherish the get-together moments with all the Newton Bhabha Fellows 2015 in London, UK. I thank Drs. David Fell and Mark Poolman (Oxford Brookes, UK), C. G. Suresh, Sureshkumar Ramasamy and Chetan Gadgil also for their valuable interactions.

Last, but not the least, I acknowledge **AcSIR** and **CSIR-National Chemical Laboratory**, for allowing me to pursue my doctoral research. I cherish all the memories that CSIR-NCL has given me in the lab premises, hostel residences and the house at B-14, NCL colony. To state, these memories of NCL, starting from chit-chats to RSM dance performances, will stay in the future as unforgettable moments. I offer my sincere thanks to the Directors of my tenure, Drs. **Sourav Pal** and **Ashwini Kumar Nangia**, for providing the pleasant lab atmosphere to work. My special thanks to the people in official desk, Ajinkya Ghorpade (Finance and accounts), Poornima Kolhe and P.V. Iyer (SAO), Vaishali Suryawanshi and Komal A. Patil (AcSIR office) for their support in processing my official documents without much delay. I would like to acknowledge **DST-INSPIRE** for the 5 years Ph.D. fellowship, **Newton fund** under **British council** and **DST-India** for **Newton Bhabha Fellowship** in 2015 for 6 months.

On the personal front, I am grateful to my family who encouraged me throughout. My mom, **Mercy Immanuel**, retired school teacher, is a continuous support for me. As a teacher, she knows a student's mindset and helped in uplifting my thoughts on many occasions. My partner, **Manu M.S.**, is my best friend and a colleague from CSIR-NCL. He has been a good companion in this journey with a constant support in all ups and downs of my life. I still cherish the moment with him when I received the email from BBRC journal when my first paper got accepted. Amidst many differences of opinion, he is a hand that helped, clapped and lifted me in every moment of need. Special thanks to my sister's family (Selvamaray, Vignesh, Thiya, Nitin), in-laws (Manikantan, Saraswathy), Maneesh and entire Shagunthala's family.

For the ones mentioned and for the ones not mentioned but been there in the journey, I wish all of them good luck and my best regards to every person who is connected to this thesis completion.



Selva Rupa Christinal Immanuel

Table of Contents

Certificate	ii
Declaration of Authorship	iii
Preface	v
Acknowledgements	vii
Table of contents	ix
Abbreviations	xv
List of Figures.....	xvii
List of Tables.....	xix

Thesis Abstract	1
------------------------------	----------

Chapter 1: Introduction	3
--------------------------------------	----------

1.1. Cancer - "Uncontrolled growth"	5
1.2. Cancer Metabolism: An Emerging Cancer Hallmark.....	6
1.3. Glioblastoma Multiforme	7
1.4. Temozolomide - "DNA methylating drug"	8
1.5. Oncometabolites - Epigenetics and DNA methylation.....	10
1.6. Intra-tumor Heterogeneity and Drug Resistance	11
1.7. Glioblastoma Multiforme: Systems perspectives	12
1.8. Human Glioblastoma Multiforme - U87MG cell line.....	13
1.9. Cancer Associated Metabolic Changes and its Link to Temozolomide Resistance	14
1.10. Hypothesis and specific aims	15
1.11. Overview of the thesis	16

Chapter 2: Intra-Tumor Heterogeneity And Drug Response: How Differences Make Difference?	19
---	-----------

Abstract.....	20
2.1. Introduction	21
2.2. Methods	24
2.2.1. Cell culture	24
2.2.2. Fluorescence microscopy	25
2.2.3. Flow cytometry.....	25
2.2.4. Sorting of cells by FACS and functional characterization using verapamil	25
2.2.5. Growth/proliferation studies	26
2.2.6. Temozolomide dose-response curves.....	26
2.2.7. In vitro differentiation of NSP.....	26
2.2.8. Sample extraction, dilution and internal standard spiking for LC-MS/MS	27

2.2.9. Metabolomics profiling using liquid chromatography high resolution mass spectrometry (LC-HRMS)	27
2.3. Results	28
2.3.1. Microscopy reveals distinct cell morphology of each population.....	28
2.3.2. FACS profiling identifies differential dye efflux properties in U87MG cells	29
2.3.3. Differential growth kinetics of the side-population	31
2.3.4. Dose-response parameters vary across cells for temozolomide	33
2.3.5. Quantitative exo-metabolite profiling identifies differential dynamics of nutrient uptake in the side-population.....	34
2.3.6. Side-population NSP has the capability of differentiation into glial cell type.....	37
2.4. Discussion.....	39
2.5. Conclusions	42

Chapter 3: Candidate Gene Interaction Networks In Glioblastoma **43**

Abstract.....	44
3.1. Introduction	45
3.1.1. Network analysis using PathwayStudio™	45
3.1.2. Cancer candidate (CAN) genes and their role.....	46
3.1.3. ABC transporters and drug resistance	46
3.2. Methods	47
3.2.1. Selection of CAN genes using Pathway Studio™ (v11.0.5) analysis.....	47
3.2.2. RNA extraction and cDNA synthesis.....	47
3.2.3. GeNorm analysis for stable reference gene identification	49
3.2.4. Real-time PCR using SYBR green-I	50
3.2.5. Real-time PCR using hydrolysis probe assay.....	51
3.2.6. Gene expression of ABC transporters	51
3.3. Results	52
3.3.1. Network of cancer candidate (CAN) genes.....	52
3.3.2. Relative gene expression qPCR analysis of selected CAN genes.....	52
3.3.3. Network analysis of ABC transporter genes	55
3.3.4. mRNA abundances of ABC transporters genes	56
3.4. Discussion.....	60
3.5. Conclusions	61

Chapter 4: Exome Characterization: Towards Genetic Basis For Temozolomide Resistance **63**

Abstract.....	64
4.1. Introduction	65
4.1.1. Next generation sequencing	65

4.1.2. Exome sequencing.....	66
4.1.3. Overall workflow of exome sequencing	67
4.1.4. Application of Exome sequencing in cancer research.....	68
4.2. Methods	68
4.2.1. Genomic DNA extraction.....	68
4.2.2. Exome sequencing.....	68
4.2.3. Functional annotations of Exome data	68
4.3. Results	69
4.3.1. Exome statistics.....	69
4.3.2. Genomic variability across the sensitive and resistant cells.....	70
4.3.3. Distribution of SNPs in chromosomes	70
4.3.4. Functional characterization of the identified exome variants.....	70
4.3.5. Homozygous and heterozygous variants	73
4.3.6. Transversions and transitions	73
4.3.7. Metabolic genes with exome variants	76
4.4. Discussion.....	76
4.4.1. Possible impact of homozygous variants on metabolism of temozolomide-sensitive and temozolomide-resistant cells.....	76
4.5. Conclusions	80

Chapter 5: Phenotypic Plasticity of Growth and Respiration **81**

Abstract.....	82
5.1. Introduction	83
5.1.1. Phenotypic and metabolic plasticity in cancer	83
5.1.2. Nutrient dependencies in cancer.....	84
5.2. Methods	85
5.2.1. Cell culture	85
5.2.2. Phenotype microarray analysis.....	85
5.3. Results	86
5.3.1. Phenotypic plasticity defined by nutrient preferences for growth and respiration.....	86
5.3.2. Euclidean clustering of growth and respiration rates	86
5.3.3. Differential growth and respiration rates across U87MG and Neurospheres	87
5.3.4. Nutrient preferences from 367 C/N sources	90
5.3.5. Differential profile in ions and hormones	91
5.3.6. Chemo-sensitivity of U87MG and NSP to 92 drugs.....	91
5.4. Discussion.....	93
5.5. Conclusions	95

Chapter 6: Metabolic Dynamics And Reprogramming Of The Cell **97**

Abstract.....	98
6.1. Introduction	99
6.1.1. Metabolic phenotypes in cancer and regulation of epigenetics.....	99
6.2. Methods	101
6.2.1. Growth in different concentrations of Temozolomide.....	101
6.2.2. Liquid chromatography-high resolution mass spectrometry (LC- HRMS): Sample extraction, dilution and internal standard spiking	101
6.2.3. Standard preparation.....	102
6.2.4. Metabolites profiling using LC-HRMS.....	102
6.2.5. Selection of metabolites for profiling.....	103
6.2.6. Consumption and Release (CORE) clustering and Principle component analysis (PCA)	104
6.2.7. Variable Importance in Projection (VIP) scores using Partial Least Square Discriminant Analysis (PLSDA)	104
6.3. Results	104
6.3.1. Quantitative metabolite profiling identifies key differences in the metabolic states of the cell in the presence of TMZ.....	104
6.3.2. CORE clustering and PCA.....	105
6.3.3. Concentration profile across time.....	105
6.3.4. Key metabolites and their role in metabolic reprogramming.....	112
6.4. Discussion.....	116
6.5. Conclusions	117

**Chapter 7: An Integrative Paradigm For Temozolomide
Resistance: A Systems Approach** **119**

7.1. How does the expression of drug transporters impacts growth and susceptibility response to temozolomide?.....	120
7.2. How does modulating CAN gene expression impacts the response to alkylating drug TMZ?	121
7.3. How do genomic alterations contribute to temozolomide resistance?	123
7.4. Combinatorial role of CAN genes, ABC transporters, related exome and metabolism on temozolomide resistance.....	124
7.5. Predictive constraints-based metabolic modeling of U87MG and NSP cells	125
7.6. Discussion.....	130
7.7. Conclusion.....	132

Chapter 8: Conclusions and Future Scope **133**

8.1. Recapitulation.....	134
--------------------------	-----

8.2. Unknown frontiers of chemotherapeutic resistance 135
8.3. Future scope and directions 136
8.4. Single cell analysis 136

Appendices 139

A. Appendix A: (All the supplementary data generated in this doctoral research
have been listed in the form of tables and figures) 139
B. Appendix B: (Additional soft data) 155
C. Appendix C: (Contributions to other projects) 156

Bibliography 163

List of Publications 183

Author's curriculum vitae 189

*****~**

Abbreviations

NSP	Neurospheres
Ala	Alanine
Arg	Arginine
Asn	Asparagine
Asp	Aspartic acid
Cys	Cysteine
Gln	Glutamine
Glu	Glutamate
Gly	Glycine
His	Histidine
Leu / Ile	Leucine / Isoleucine
Lys	Lysine
Met	Methionine
Phe	Phenyl alanine
Pro	Proline
Ser	Serine
Thr	Threonine
Trp	Trptophan
Tyr	Tyrosine
Val	Valine
Glc	Glucose
Lac	Lactate
TMZ	Temozolomide
GBM	Glioblastoma Multiforme
ASA	Argininosuccinate
OAA	Oxalo acetic acid
α -KGA	Alpha-Ketoglutaric acid
PEP	Phosphoenolpyruvic acid
3PG	3-Phosphoglyceric acid
G6P	Glucose-6-phosphate
F6P	Fructose-6-phosphate
NAD	Nicotinamide adenine dinucleotide
ACMS	2-amino-3-carboxymuconate semialdehyde

List of Figures

Figure 1.1. Overview of the thesis showing the integrative approach to address drug resistance	3
Figure 1.2. Hallmarks of Cancer	6
Figure 1.3. Types and clinical features of Glioblastoma.....	7
Figure 1.4. Mechanism of temozolomide action and its resistance.....	9
Figure 1.5. Mechanisms that regulate the development, progression and maintenance of tumor heterogeneity	11
Figure 1.6. Systems approach for addressing temozolomide resistance	12
Figure 1.7. Remarkable publications/reports that form the basis of this thesis.....	13
Figure 1.8. Morphology of U87MG cell line grown in DMEM	14
Figure 1.9. Objectives and work plan.....	16
Figure 2.1. Graphical abstract of Chapter 2	19
Figure 2.2. Schematic showing heterogeneity in Glioblastoma Multiforme.....	23
Figure 2.3. Heterogeneous cell population in U87MG as seen using microscopy.....	29
Figure 2.4. FACS profiling of heterogeneity within U87MG cells.....	30
Figure 2.5. Growth profile of heterogeneous population in U87MG.....	32
Figure 2.6. Dose-response curve for temozolomide.....	33
Figure 2.7. Consumption and release profile for selected metabolites.....	35
Figure 2.8. Quantitative exo-metabolite profiling of separated U87MG and neurospheres	36
Figure 2.9. Redifferentiation capability of drug resistant side population cells.....	37
Figure 2.10. NDX cells show distinct growth, dose-response and metabolic dynamics.....	38
Figure 2.11. Predicted cellular metabolism of U87MG and NSP	40
Figure 3.1. Graphical abstract of Chapter 3	43
Figure 3.2. RNA analysis using Agilent 2100 Bioanalyser.....	49
Figure 3.3. GeNorm analysis for stable reference gene identification	50
Figure 3.4. Network analysis of CAN genes	53
Figure 3.5. Relative gene expression analysis of CAN genes	54
Figure 3.6. Localization and distribution of ABC transporters in Human	56
Figure 3.7. Interaction network generated using PathwayStudio™	57
Figure 3.8. Relative gene expression for ABC transporters	58
Figure 3.9. CAN genes and metabolism.....	61
Figure 4.1. Graphical abstract of Chapter 4	63
Figure 4.2. Workflow for Exome sequencing using Ion proton system.....	67
Figure 4.3. Genomic DNA isolated from U87MG and Neurospheres (NSP).	69
Figure 4.4. Exome variants statistics	71
Figure 4.5. Chromosome-wise distribution of exome variants	72
Figure 4.6. Functional characterization of exome variants	74
Figure 4.7. Transversions and transitions.....	75

Figure 4.8. Metabolic gene variants in Exome	76
Figure 4.9. Signaling genes that majorly controls metabolism	77
Figure 4.10. Polyamines and cancer.	78
Figure 5.1. Graphical abstract of Chapter 5	81
Figure 5.2. Metabolic pathways under nutrient-replete and nutrient-deprived conditions	84
Figure 5.3. PMM-1 to 4 analyses using growth (GR) and Respiration (Resp) rates	88
Figure 5.4. PMM-1 analysis of respiration (A) and growth (B) profiles	89
Figure 5.5. Analysis of chemo-sensitivity of U87MG and NSP.	91
Figure 5.6. Chemo-sensitivity profile for U87MG and Neurospheres	92
Figure 5.7. Phenotypic microarray panels (PMM 1 to 14)	94
Figure 5.8. NADH theory of cancer energy metabolism	95
Figure 6.1. Graphical abstract of Chapter 6	97
Figure 6.2. Determinants of the tumor metabolic phenotype	100
Figure 6.3: Metabolites selected for quantification using LC-MS/MS analysis	103
Figure 6.4. Metabolite profiling in the absence and presence of drug (Temozolomide)	106
Figure 6.5. Metabolite concentration profile of U87MG and Neurospheres in the absence of temozolomide	107
Figure 6.6. Metabolite concentration profile of U87MG and Neurospheres in the presence of 10 μ M TMZ	109
Figure 6.7. Metabolite concentration profile of U87MG and Neurospheres in the presence of 100 μ M TMZ	110
Figure 6.8. Metabolite concentration profile of U87MG and Neurospheres in the presence of 10 μ M TMZ	111
Figure 6.9. VIP score for metabolites profiled using LC-MS/MS analysis for U87MG and NSP in the absence of temozolomide	113
Figure 6.10. PLS-DA component analysis scores plot	116
Figure 6.11. Exo-metabolite profile of lactate, pyruvate, succinate and AKG.	115
Figure 6.12. Ornithine profiles from LC-MS/MS analysis.	115
Figure 6.13. Predicted metabolic state of NSP cells.	117
Figure 7.1. The experimental datasets and their key inferences from Chapter 2 to 6 that are used for the integrative analysis in this chapter 7	119
Figure 7.2. ABCG transporter family and its linked transport of molecules	121
Figure 7.3. Figure 7.3: Possible resistance mechanism of NSP cells derived from the inferences on LC-MS/MS and mRNA abundances datasets	122
Figure 7.4. An Integrative paradigm for Temozolomide resistance	124
Figure 7.5. Constraints-based metabolic models and their role in delineating cancer metabolism	125
Figure 7.6. Generation of constraints-based core metabolic model of U87MG and NSP cells	126
Figure 7.7. Core model predictions	126

Figure 7.8. Metabolic reprogramming depicted based on the inferences from all the datasets in this thesis.	131
Figure 8.1. Integrative paradigm developed for cancer drug resistance from this study and its future scope on translational research.	133
Figure 8.2. Encapsulation of samples with cells inside droplets.	136
Figure 8.3. Fluorescence microscope image of droplets created for U87MG cells stained with Hoechst 33342 dye.	137
Figure 8.4. Stability of droplets under varied temperature conditions.	137

*****~**

List of Tables

Table 2.1. Growth parameters determined based on Gompertz growth fit in GraphPad Prism	32
Table 2.2. Summary of dose-response analysis for TMZ.....	34
Table 2.3. Growth parameters for NDx cells.....	38
Table 2.4. Dose-response summary for NDx cells.....	38
Table 3.1. List of cancer candidate genes selected using Pathway Studio 11.0.5	48
Table 3.2. Primers and probes designed for gene expression studies of reference genes (control genes) for GeNORM-based normalization of qPCR data	49
Table 3.3. Primers and probes designed for CAN genes.....	51
Table 3.4. List of ABC transporter genes profiled in this study.....	58
Table 4.1. Genes with homozygous variants in Exome of U87MG and NSP.....	73
Table 4.2. Percentage of heterozygous and homozygous variants	75
Table 5.1. Differential drug response for U87MG and NSP	93
Table 7.1. Exome variants of genes that control metabolism.....	123
Table 7.2. Differential flux distribution across U87MG and NSP in Flux variability analysis.	127
Table 7.3. Details of the exome variants used as constraints.	128

*****~**

Thesis Abstract

The field of cancer research is caught in a data deluge by the advent of inexpensive genome-scale high throughput technologies. The complexity of a living system justifies the need for data acquisition at all molecular levels of cell hierarchy from DNA to metabolites. However, just listing candidate genes (From genomic/ exome data), gene expression signatures (from transcriptomic data), or metabolites (from metabolomics data) are not enough to understand a complex, multi-hit, multifactorial emergent disease like cancer. Although there are many methods that exist to analyze individual data types, no method exists to integrate heterogeneous data-types into a platform or mathematical model and to let alone predict outcomes and cell behaviour. Glioblastoma, the most severe form of brain cancer is even more complex due to its inherent heterogeneity, as the only drug used to treat it is being rendered less useful due to chemoresistance. To understand the difference between cells of glioblastoma that are resistant or susceptible to temozolomide, we have isolated the resistant population of neurospheroidal cells (NSP) from an authenticated model cell line U87MG. These were further characterized extensively using whole exome sequencing, limited gene expression profiling, metabolite profiling, growth-resistance profiling and respiration phenotyping to understand the genotype and the differential phenotypes of its molecular components. Since biological systems are complex and their function is more than the sum of their parts, all the data were integrated to analyze the emergent properties resulting from the interaction. Such integrated analysis unravelled some of the mechanistic aspects of drug resistance to temozolomide, a methylating drug. To complement data-driven analysis, a predictive constraints-based flux balance model of human metabolism was used to develop context-specific models for U87MG and NSP. These models computed accurately the growth phenotypes of each cell and also predicted the metabolic reprogramming through varied flux distribution profiles. Such pipelines are scalable to other cancer types and can be translated to the clinical studies. The multidimensionality of probing such molecular portraits in heterogeneous tumor cells of patients has spurred on personalized medicine approaches and can lead the way to individualized therapy.

Chapter 1

Introduction

"All cancers are alike but they are alike in a unique way."

— Siddhartha Mukherjee, *The Emperor of All Maladies: A Biography of Cancer*

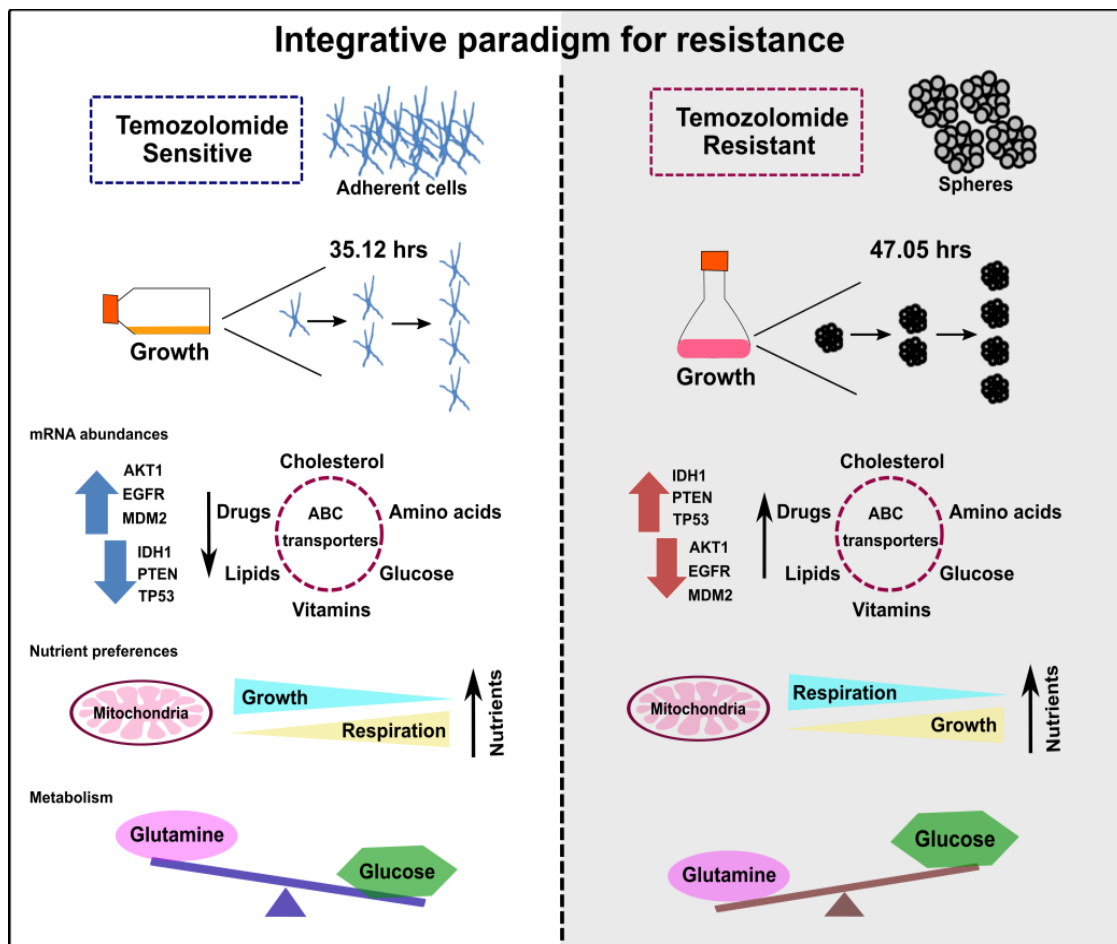


Figure 1.1: Overview of the thesis showing the integrative approach to address drug resistance

The global understanding of metabolic reprogramming and its underpinnings in molecular cell hierarchies is critical to unravel the duality of cell function. Understanding the impact of growth and energy generation for survival of cancer necessitates a systems approach. On the one hand, drug resistance has become one of the most challenging problems to address in cancer relapse. On the other, the presence of stem-like cells that are drug resistant in most cancers, confound the analysis and therapy. These minor subpopulations need to be characterized to overcome resistance developed in the last stages of cancer. **In this thesis, a systems biology approach has been implemented to understand the emergent properties of chemotherapeutic resistance in a Glioblastoma (brain tumor) cell line, U87MG, *in vitro*.** This approach is scalable to other cancer cell-types and can also be used for clinical translation.

1.1. Cancer - "Uncontrolled growth"

Cancer is a multi-factorial disease (Warburg et al. 1923; Warburg 1956; Hanahan & Weinberg 2000; Hsu & Sabatini 2008; Kreeger & Lauffenburger 2009; Xue Xue 2012) that potentially links metabolism to its progression (Feron 2009; Muñoz-Pinedo et al. 2012; Dang 2012; De Berardinis & Chandel 2016; Zielinski et al. 2017). Cancer cells reprogram their energy metabolism in order to satisfy their requirement for biosynthesis and growth (Ward & Thompson 2012; Daye & Wellen 2012; Hainaut & Plymoth 2012). Increased aerobic glycolysis, fatty acid synthesis, and glutamine metabolism have been already known in cancer metabolic reprogramming, yet the real importance have not yet been addressed (Wise et al. 2011; Duckwall et al. 2013; Altman et al. 2016).

Metabolism in cancer is unique in a way that these cells consume more glucose compared to normal cells (Warburg et al. 1923; Hsu & Sabatini 2008; Vander Heiden et al. 2009) but use a small amount of it towards oxidative phosphorylation even in aerobic conditions. Cancer cells proliferate rapidly with a higher growth rate. Therefore, there is a need for more nutrients to drive the faster growth. This is supported by the oncogene-directed metabolic reprogramming (Daye & Wellen 2012; Nieminen et al. 2013; Ríos et al. 2013). Recent findings suggest that metabolites themselves can be oncogenic (Losman & Kaelin 2013; Gaude & Frezza 2014) by altering cell signaling and blocking cellular differentiation. Cancer-associated genomic and metabolomic alterations have a direct impact on the cell growth and survival (Ramão et al. 2012). Thereby, the change in metabolism plays a key role and could be a potential marker in cancer.

1.2. Cancer Metabolism: An Emerging Cancer Hallmark

The metabolic properties of cancer cells diverge significantly from those of normal cells. One of the emerging hallmarks in cancer is that altered metabolism and energy regulation guides the cancer growth and progression (Figure 1.2) (Hanahan & Weinberg 2000; Hanahan & Weinberg 2011).



Figure 1.2: Hallmarks of Cancer. Source: Originally published in Hallmarks of Cancer: The Next Generation, Cell, 646-674, © Elsevier, 2011 (Hanahan & Weinberg 2011).

This metabolic regulation of growth is dependent on the availability of nutrients. Also, many of the oncogenes have an effect on the metabolism of cancer cells. Tumor cells, in contrast to normal cells, display increased metabolic rates, increased uptake rates (taking up nutrients) and metabolizing them in pathways that support growth and proliferation (Warburg et al. 1923; Hsu & Sabatini 2008; Dang 2012).

To state, most of the previous work in tumor cell metabolism focused only on bioenergetics, in particular, increased glycolysis and suppressed oxidative phosphorylation ('Warburg effect'). This altered energy metabolism is widespread in cancer cells of any origin contributing to the traits that have been already accepted as hallmarks in cancer (Hanahan & Weinberg 2000). Hence, the changes in the regulation of metabolism and energy generation (aerobic glycolysis) simply define another

phenotype. The question whether the metabolism is a cause or effect can help with further delineation of cancer mechanisms. This would enable path towards personalized medicine through potential micro-environment tailoring.

1.3. Glioblastoma Multiforme

Glioblastoma multiforme (GBM), is the most common brain tumor (Zhang et al. 2011; Sottoriva et al. 2013; Qazi et al. 2017), and generally shows aggressive characteristics including a very high rapid growth rate (Broadley et al. 2011; Y. P. Ramirez et al. 2013; Yeung et al. 2013; Yuan et al. 2015). It is a Grade IV glioma (Kreth et al. 2010; Y. P. Ramirez et al. 2013; Y. Ramirez et al. 2013), the most malignant and comprises more than a half of all gliomas known so far (Figure 1.3). A lower grade glioma (such as grade I–II tumor) is well differentiated with some cellular anomalies. Grade III tumor is anaplastic, with increased cell density and display differences in cellular morphology (Maher 2001).

Glioblastoma is derived from astrocytes and shows a very poor prognosis than any other tumors in brain. The main reason for this high morbidity is always believed to be its higher growth rate. The survival of GBM patient is approximately 1 year despite under the treatments including chemotherapy, radiotherapy, and surgery (Zhang et al. 2011; Zhao et al. 2013). Normally, the ATP production and neuronal activity in astrocytes are determined and maintained by the metabolic energy flow from lipolysis and glycolysis.

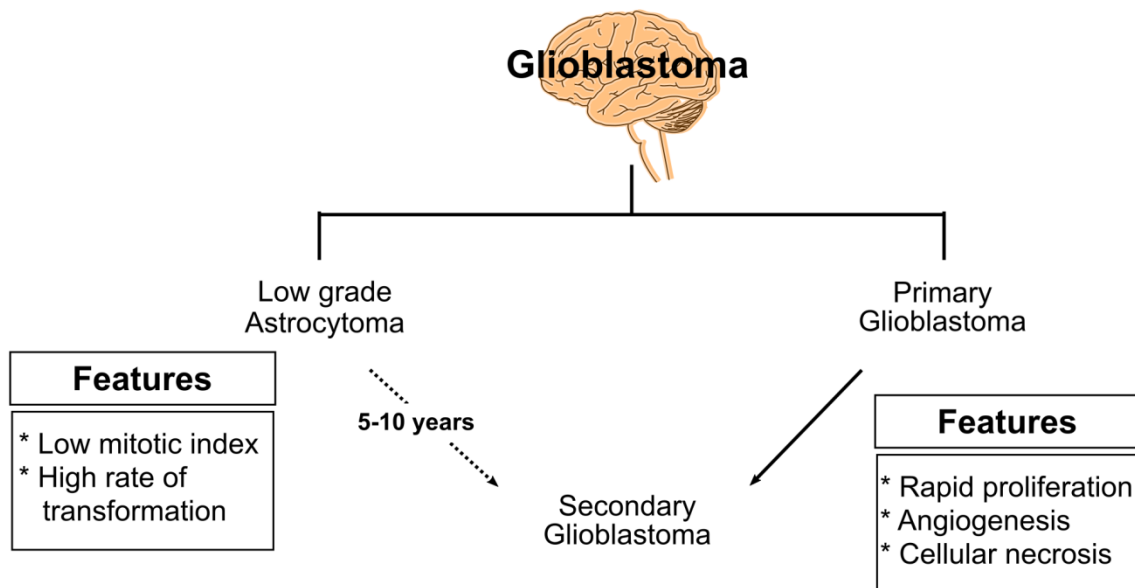


Figure 1.3: Types and clinical features of Glioblastoma.

In contrast to neurons, astrocytes support the lactate production by aerobic glycolysis even in the oxygen replete conditions (Warburg effect), and ATP production by mitochondrial respiration through electron transport chain (Pasteur effect). Lactate was found to be involved in increasing growth by being an energy source (Lactate to Pyruvate shuttle) and also supports the memory formation by getting shuttled between the neurons and astrocytes. Hence, the inherent capability of astrocytes towards lactate secretion could eventually lead to a high rate of tumor formation by supporting glycolytic fluxes (Kim et al. 2015). Recent studies address the presence of a subset of cells with stem-like properties that are found in the final stages of the tumor. This subset of cells was often reported to show chemotherapy resistance and stated to be the key component for tumor relapse (Hirschmann-Jax et al. 2004; Persson & Weiss 2009; Golebiewska et al. 2011; Broadley et al. 2011; Bar 2011). The tumor microenvironment has been shown to be the major determinant for the molecular and phenotypic abnormalities of such cell types and in promoting the growth of resistant populations to sustain the treatment regimens. Understanding the reprogrammed metabolism based on the microenvironmental conditions and the interaction between different cell types within the tumor mass would definitely help to answer the questions on how metabolism modulates the aggressiveness and response to therapy. This would pave way for the innovative treatment regimens to target primary glioblastoma or potentially in cases of relapse.

1.4. Temozolomide - "DNA methylating drug"

Temozolomide (TMZ) is one of the alkylating agents used for chemotherapy in GBM (Friedman et al. 2000; Portnow et al. 2009; Wesolowski et al. 2010; Liu et al. 2012; Qian et al. 2013). Most of the alkylating agents are active in the resting phase of the cell, though they are considered to be cell cycle non-specific. TMZ is an orally administered drug that crosses the Blood Brain Barrier (BBB). It shows good uptake, distribution and tumor localization thus has the clinical approval.

It is a prodrug that undergoes hydrolysis in neutral pH to MTIC (monomethyl triazene 5-(3-methyltriazene-1-yl)-imidazole-4-carboxamide). This MTIC further reacts with water and gives 5-aminoimidazole-4-carboxamide (AIC) and a highly reactive methyl diazonium cation. This active form then methylates DNA (Figure 1.4). Predominantly, DNA is methylated at N7 positions of guanine in guanine-rich regions (70%), but TMZ also methylates N3 adenine (9%) and O6 guanine residues (6%) (Wesolowski et al. 2010; Zhang et al. 2011; Lee 2016).

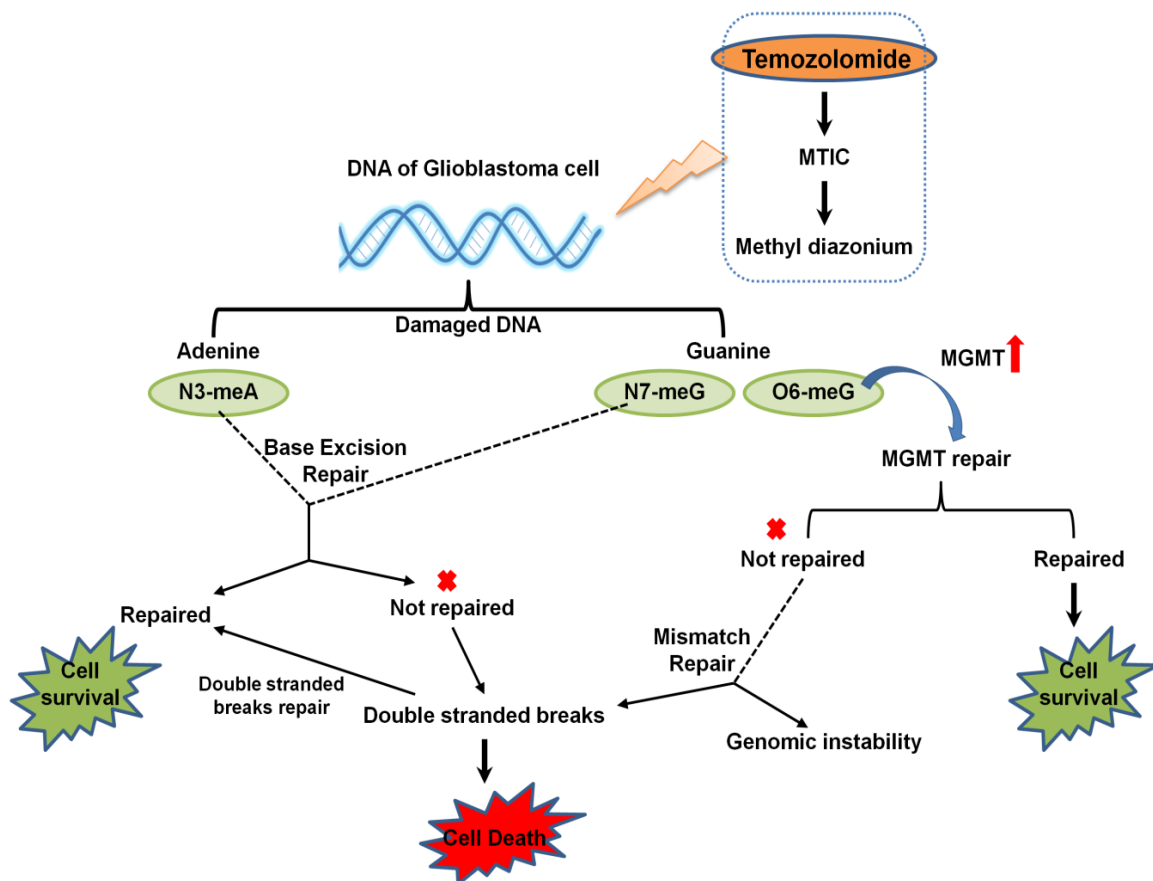


Figure 1.4: Mechanism of temozolomide action and its resistance.

The temozolomide concentration prescribed for patients is $150\text{mg}/\text{m}^2$. $75\text{ mg}/\text{m}^2$ for 42 days followed by the initial maintenance dose of $150\text{mg}/\text{m}^2$ once daily for Days 1-5 of a 28-day cycle of “Temodar” (the commercial name for temozolomide) is prescribed for patients with Glioblastoma for 6 cycles of chemotherapy. The clinical trials for confirming the activity of this drug was performed in the range starting from $300\text{ }\mu\text{M}$ to $1500\text{ }\mu\text{M}$ in model systems of Glioblastoma including U87MG cell line as well (Huang et al. 2012; Johannessen et al. 2013).

The half-life of temozolomide is approximately 1.8 hours. Temozolomide (TMZ) gets converted to MTIC and the active half-life of this metabolite (MTIC) is longer than TMZ. Both the active and inactive forms of TMZ are excreted through kidneys. The plasma levels of TMZ are monitored during the chemotherapy cycles. TMZ is prescribed once daily to maintain the dosage in the plasma and the circulation time gets affected by the food intake and the diet followed by the patients. Side effects include nausea and vomiting which are common among the patients and are usually mild to moderate. A limited number of patients (7%) have shown seizure and thrombocytopenia (Wesolowski

et al. 2010).

1.5. Oncometabolites - Epigenetics and DNA methylation

DNA methylation is a major epigenetic modification that has implications for various biological processes (Ulrey et al. 2005; Weisenberger 2014). This epigenetic modification in DNA is considered stable compared to other epigenetic mechanisms. DNA demethylation also has been studied and known to exist in certain stages of cellular function and destabilizes the programmed gene silencing by DNA methylation (Holohan et al. 2013). Many enzymes are proven to perform active DNA demethylation and multiple mechanisms are being characterized to understand the effect of demethylation.

Most of the DNA modifying enzymes were shown to be dependent on metabolites such as NAD⁺, FAD, ATP, S-adenosylmethionine (SAM), α -ketoglutarate and acetyl-coenzyme A that can influence the epigenetic activities. IDH1 and IDH2 mutants convert glutamine carbon to the oncometabolite 2-hydroxyglutarate to dysregulate epigenetics and cell differentiation (Ward & Thompson 2012). Hence, the nutritional state of the cell might have an important role in maintaining these nuclear activities. The interconnection between epigenetic dynamics and metabolism could contribute to the emergent properties of the resistant cell in the presence of DNA methylating drugs (Ulrey et al. 2005; Hsu & Sabatini 2008; Cantor & Sabatini 2012; Etchegaray & Mostoslavsky 2016).

Profiling the metabolite levels in different conditions (in the presence or absence of the drug) would give us the clues to define whether or not the microenvironment controls the resistance. Detailing how DNA methylation is regulated would eventually broaden our understanding of epigenetic regulation, cell reprogramming and cancer resistance in case of DNA methylating drugs. Taken together, the question whether the epigenetic regulation by metabolism and downstream effects becomes the cause or effect will solve the puzzle in unveiling the resistance development for the drugs that target DNA. One such example for metabolites and their role in epigenetics can be addressed by the study of Ten-eleven translocation (TET) pathway (Carey et al. 2014; Scourzic et al. 2015).

TET proteins are involved in DNA methylation or demethylation and are α -ketoglutarate-dependent dioxygenases in the conversion of 5-methylcytosines (5-mC) to 5-hydroxymethylcytosine (5-hmC), 5-formylcytosine and 5-carboxycytosine. Recently new pathways have been elucidated in the cytosine methylation and demethylation process in human. The α -ketoglutarate-dependent TET activity produces 5-hydroxymethylcytosine.

This can be an intermediate in either passive or active DNA demethylation. The biological relevance of TET inhibition by 2HG (2-hydroxyglutarate) has a strong genetic influence as well. Mutations of IDH1 or IDH2 are found to be responsible for the generation of 2-hydroxyglutarate (Wise et al. 2011; Losman & Kaelin 2013).

1.6. Intra-tumor heterogeneity and drug resistance

Tumor heterogeneity can be used to describe both inter-tumoral and intra-tumoral variability, including differential mutational patterns, intratumoral histological variation and intratumoral polyclonality (Furnari et al. 2015). GBM tumors display striking histological variation within the same mass of the population of cells (Figure 1.5). However, complete characterization has been not done yet. In GBM tumors, the complete genome-scale mutational profiles of the major and minor populations present within, are not yet known but, the overall mutational heterogeneity seems to be similar to those of most other cancer types (Parker et al. 2016; Qazi et al. 2017).

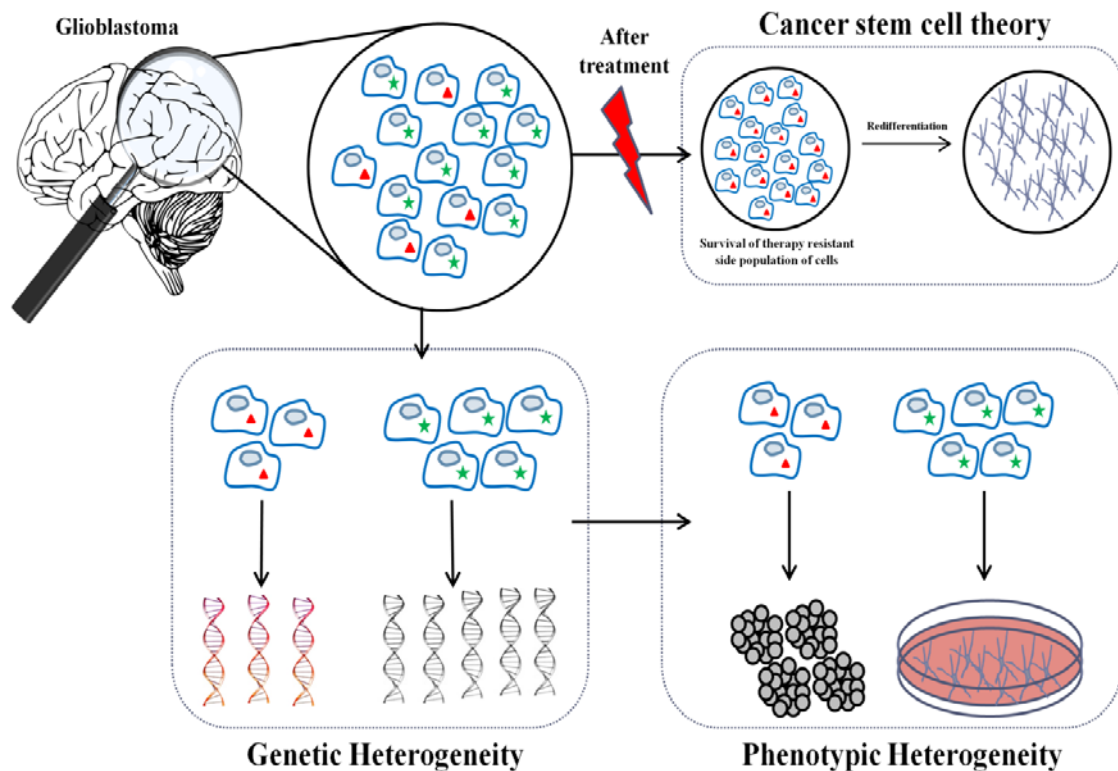


Figure 1.5: Mechanisms that regulate the development, progression, and maintenance of tumor heterogeneity.

Many reports exist about the presence of minority populations in the final stage cancer, responsible for drug resistance and relapse. These sub-populations possess various clinically important phenotypes such as the ability to metastasize and to resist and

survive chemotherapy (Hirschmann-Jax et al. 2004; Persson & Weiss 2009; Golebiewska et al. 2013). This phenotypic diversity can be a combined impact of both genetic and non-genetic influences. Also, recent advances in novel technologies have advanced the molecular understanding of main and sub-populations within and/or across cancers, enabling the identification of targets for better combination therapies and interventions. This is critical to diagnosis and treatment as the most abundant cell type might not necessarily predict the properties of mixed populations (Inda et al. 2014; Mathis et al. 2017).

1.7. Glioblastoma Multiforme: Systems perspectives

Though Glioblastoma is known to be a highly aggressive and deadly brain tumor for more than a decade, there are very few improvements in the treatment regimens due to the complexity of the disease. This necessitates the development of a systems paradigm to address the drug resistance and tumor relapse. A systems approach as developed in this thesis, allow delineation of genotype to phenotype relationships fundamental to the biology of a cancer cell. These include primary phenotypes like growth and drug response that can be influenced by secondary phenotypes like respiration, metabolism, and nutrient preferences (Figure 1.6).

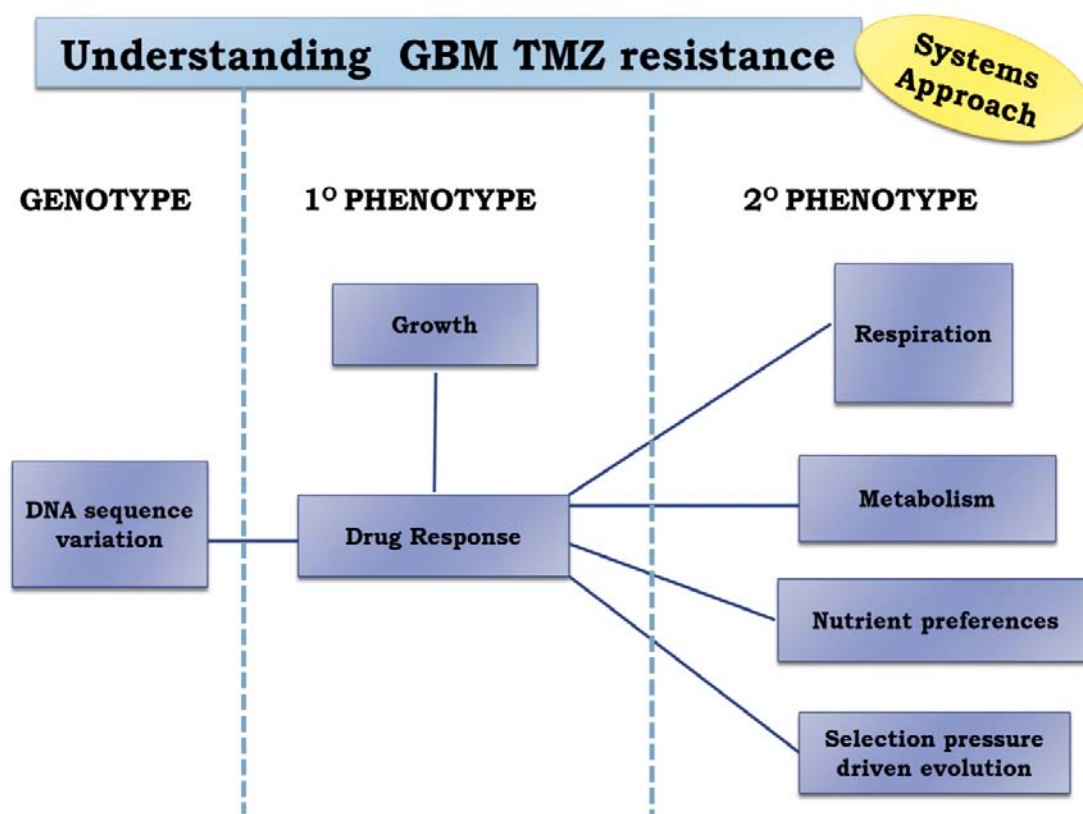


Figure 1.6: Systems approach for addressing temozolomide resistance.

Some of the milestones in researches on Glioblastoma and cancer metabolism that showed the present status of this disease until the work discussed in this thesis commenced have been listed (Figure 1.7).

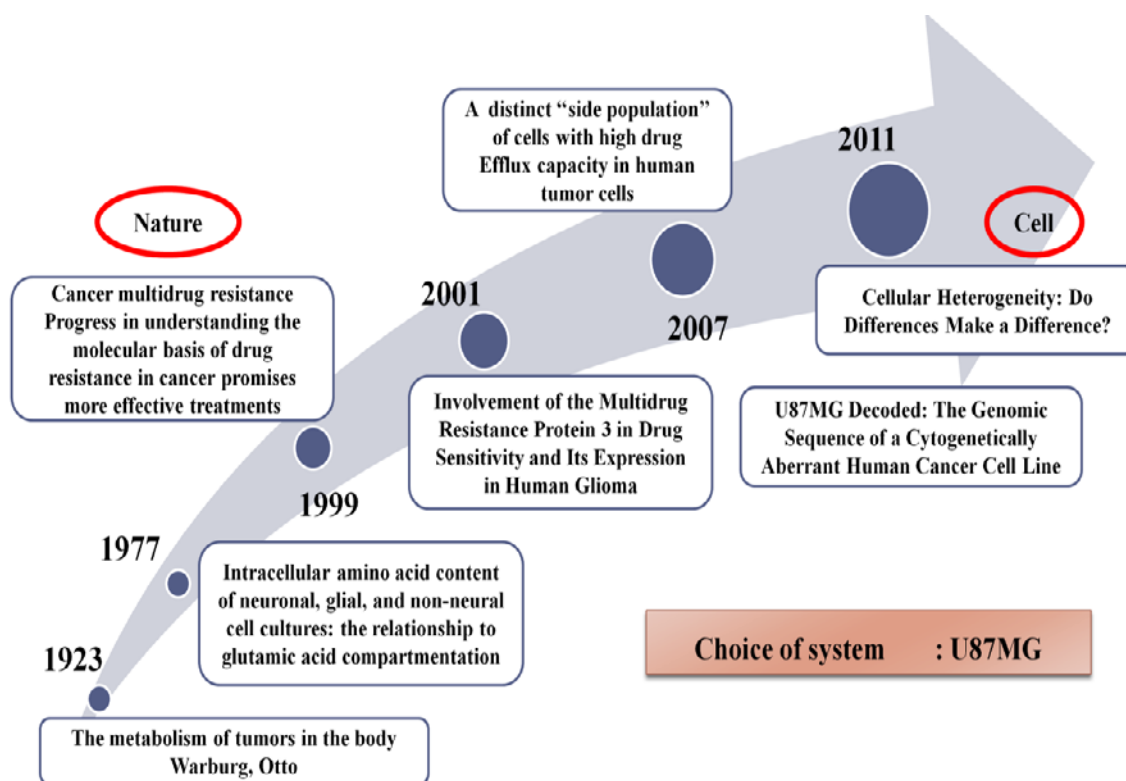


Figure 1.7: Remarkable publications/reports that form the basis of this thesis (Warburg et al. 1923; Drummond & Phillips 1977; Haga et al. 2001; Hirschmann-Jax et al. 2004; Clark, Homer, O’Connor, Chen, Eskin, Lee, Merriman & Stanley F. Nelson 2010; Altschuler & Wu 2010).

Also, how the systems approach benefits the understanding of drug (temozolomide) resistance in Glioblastoma has been highlighted. This complete thesis is based on the experimental and computational analysis of the cell line, U87MG that is well known as a model system of Glioblastoma *in vitro*.

1.8. Human Glioblastoma Multiforme - U87MG cell line

U87MG (HTB-14, Human Glioblastoma Multiforme from ATCC) has epithelial morphology and grows as adherent population of cells *in vitro* (Figure 1.8). This cell line has been authenticated in our study for the confirmation of 9 STR (Short tandem repeats) profile (Appendix A). Also, many reports highlight the use of U87MG as a model cell line for Glioblastoma (Günther et al. 2003; Clark, Homer, O’Connor, Chen, Eskin, Lee, Merriman & Stanley F Nelson 2010; Vacas-Oleas, 2013; Pei et al. 2014; Kim et al. 2015; Zou et al. 2017).

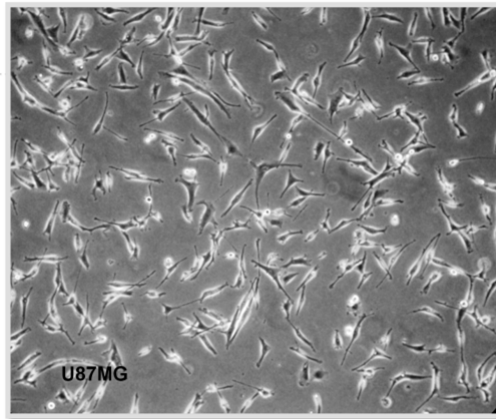


Figure 1.8: Morphology of U87MG cell line grown in DMEM. Microscopic image captured using an EVOS® FLoid® system, ThermoFisher Scientific at a magnification of 20X.

1.9. Cancer-associated metabolic changes and its link to temozolomide resistance

The reasons for the failures of conventional cancer treatments like radiation therapy and chemotherapy remain unanswered. Contributing factors include sub-optimal delivery of drugs to necrotic regions are also potentially less sensitive to ionizing radiation. An ideal response for treatment of cancer depends on the availability of the entire drug dosage at the site of tumor and low-toxicity to nearby healthy tissues. Minimizing side effects while maximizing tumor targeting is the need for current tumor therapeutic protocols. Such improvements may be achieved by looking at reprogrammed metabolism that contributes to drug response only in tumor cells. In the case of Glioblastoma, the chemotherapy is by using Temozolomide (Temodar™). This drug belongs to the class of alkylating drugs that target DNA and hence resistance is mostly related to resistance to DNA methylation. Many intermediate metabolites play a key role in the interplay between the epigenetic response (DNA methylation) and reprogrammed metabolism and may relate to induced resistance (Etchegaray & Mostoslavsky 2016).

Acetyl-CoA, an intermediate in TCA (Tricarboxylic acid cycle/ Citric acid cycle), that is utilized as an acetyl group donor during the histone acetyltransferase-dependent acetylation of nucleosomal histones. NAD (Nicotinamide adenine dinucleotide) is another central metabolite that can be synthesized *de novo* from the amino acid, tryptophan. NAD⁺ functions as a cofactor for SIRT1 and SIRT6 that eventually deacetylate histones. This deacetylation of histone H3 modulates the expression of metabolic genes, thereby causing alterations in the key metabolic pathways such as glycolysis, gluconeogenesis, mitochondrial respiration, fatty acid oxidation, and

lipogenesis (Etchegaray & Mostoslavsky 2016). S-adenosylmethionine (SAM) is the third metabolite that is generated through the methionine biosynthesis pathway. It transfers methyl groups to both histone methyltransferases (HMTs) and DNA methyltransferases (DNMTs). S-adenosyl homocysteine (SAH), on the other hand, functions as a repressor of both DNMTs and histone lysine demethylases (KDMs) (Etchegaray & Mostoslavsky 2016). α -ketoglutarate (a-KG) is a key metabolite that is generated through the TCA cycle. This also functions as an obligatory cofactor for KDMs and ten-eleven translocation (TETs) enzymes. TETs oxidize DNA by catalysis of methylated cytosines into 5-hydroxymethylcytosine (5hmC) (Etchegaray & Mostoslavsky 2016). The involvement of these metabolites in DNA methylation and histone acetylation may play a key role in the temozolomide resistance. This highlights the importance of understanding the reprogrammed metabolism.

1.10. Hypothesis and specific aims

The main hypothesis proposed is that metabolic reprogramming in glioblastoma shapes the response to temozolomide and contributes to drug resistance/sensitivity. While doing so the following unanswered questions may be sorted.

1. How does cancer-cell metabolism differ across drug sensitive and drug-resistant cells?
2. Is metabolism a cause or effect in contributing to drug resistance?
3. Is altered or preferential nutrient uptake a strategy for cell survival and resistance?
4. Is drug resistance an emergent property of the cell or self-driven by microenvironment?

To address these questions and validate the above hypothesis, this thesis explores the use of both reductionist and integrated approaches listed below to unravel differential phenotypes of the glioblastoma cell-line.

- i. Morphology and physiological features (Fluorescence microscopy and FACS profile)
- ii. Growth and drug response,
- iii. Genotyping (Exome sequencing),
- iv. Primary and Secondary phenotype (Phenotypic microarray; gene expression of CAN and ABC transporters genes using real-time qPCR),

v. Metabolite profiling in the presence and absence of drug (LC-MS/MS analysis).

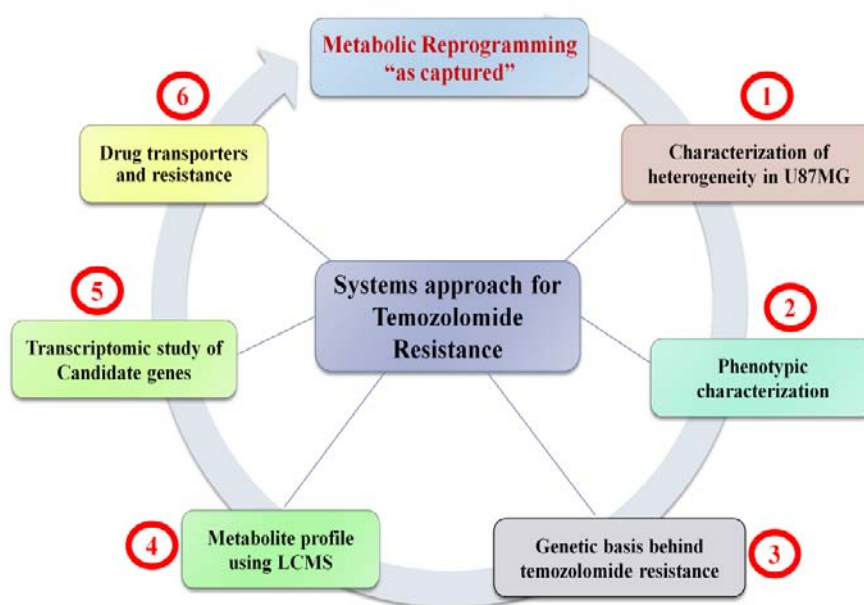


Figure 1.9: Objectives and work plan.

1.11. Overview of the thesis

This work presents an integrated analysis of a glioblastoma cell line, U87MG, to explore the inherent differential genotype-phenotype relationships in **temozolomide sensitive and resistant cells**. The heterogeneity of drug response was investigated using proliferation/growth kinetics, dose-response (Growth inhibition patterns), metabolite analysis (LC-MS/MS profile of key exo-and endo-metabolites in the presence and absence of drug), genotype analysis (Exome sequencing) and connected to observed differential cellular phenotypes (Phenotypic microarray and gene expression). To our knowledge, such poly-OMIC data integration has never before been performed in this way to describe GBM heterogeneity in addressing the reprogrammed metabolism towards resistance.

Chapter 2 discusses the identification and characterization of intra-tumor heterogeneity and drug response. An authenticated U87MG glioblastoma cell line was investigated to identify a sub-population of neurospheroidal (NSP) cells within the main epithelial population (U87MG). The NSP cells sorted using Fluorescence Assisted Cell Sorting (FACS) showed varied morphology, 30% lower growth rates, 40% higher IC₅₀ values for temozolomide drug and could differentiate into the glial cell type (NDx). Metabolite profiling using HR-LCMS identified glucose, glutamine and serine in both populations and tryptophan only in U87MG as growth limiting substrates. Glycine,

alanine, glutamate, and proline were secreted by U87MG; however, proline and glycine were re-utilized in NSP. Exo-metabolite profiling identified differential metabolism of primary carbon sources glucose and derived pyruvate for U87MG; glutamine and derived glutamate metabolism in NSP.

Chapter 3 summarizes the candidate gene interaction networks in Glioblastoma.

The choice of genes for qRT-PCR was based on Pathway Studio™ analysis. A network was generated linking genes with selected functional biological processes to identify cancer candidate (CAN) genes. Network analysis was also carried out to understand the interactions between these CAN genes. Real-time qPCR was used to quantify and detect changes in the mRNA for the selected CAN genes and ABC transporters relative to housekeeping/ reference genes. The differential mRNA abundances (17 higher and 2 lower for NSP) potentially contribute to the efficiency of drug and nutrient metabolite transport and efflux.

Chapter 4 investigates the differential exome characterization of temozolomide sensitive and temozolomide resistant cells to delineate the genetic basis for temozolomide resistance. In addition to the statistical analysis of exome variants, the detailed functional analysis was done using the Oncotator web-tool. These were also analyzed in the context of models of human metabolism to understand the impact of identified mutations in signaling and regulatory regions in controlling metabolism. Altered metabolism and epigenetic profiles that may be potentially genotype driven were identified.

Chapter 5 details the differential nutrient preferences and discussed the phenotypic plasticity of growth and respiration. The cellular energetics and pathways involved in the metabolism of U87MG and NSP cells that eventually define cell-specific metabolic fingerprints were delineated. Differential response to cytotoxic drugs, ions and hormones were also tested against the two cell types (U87MG and NSP) that allowed validation of the reprogrammed metabolism.

Chapter 6 elaborates the metabolic dynamics and reprogramming of the cell in the presence of the drug, Temozolomide. The exo- and endo-metabolite levels in the two cell types (U87MG and NSP) were analyzed and quantified using LC-MS/MS in the presence and absence of the drug at varying concentrations. NSP cells were most likely glutamine-dependent for their survival and growth. CORE (Consumption and Release)

profile analysis and PCA (Principal Component Analysis) was performed to understand the exo- and endo- metabolite state of both the cell types (U87MG and NSP).

Chapter 7 investigates the integrative paradigm developed for understanding temozolomide response, susceptibility vs resistance via a systems approach. In this chapter, all the experimental data (components) obtained using reductionism has been analyzed through integration to understand the drivers of drug resistance. Such analyses across molecular hierarchies in the cell have been delineated that would potentially help design combinatorial treatments by metabolite supplements to overcome drug resistance.

Chapter 8 reflects on the **conclusions of the thesis and highlights the future scope of this study.** Although the existence of small minority populations with differential histology and dye efflux properties within cancer cell lines has been known for decades, the underlying biochemical physiology of how this shapes functional drug response is still incompletely understood.

An integrative paradigm has been developed in this thesis to address temozolomide resistance acquired due to the presence of such minority population of cells. This pipeline thus developed is scalable and can be extended in single cell analysis and also helps in translating the bench side research to bedside for clinical implications.

Taken together, the importance of characterizing drug-resistant sub-populations for growth and gene expression analysis, exome characterization and nutrient consumption/metabolism, is critical in understanding the differential dose-response curves, potency and efficacy parameters that can eventually help in better therapeutic response and drug regimens. The results strongly suggest the need for delineating metabolic preferences of sub-populations in addition to drug efflux and histological examination. Further, these datasets can be analyzed in the context of metabolic models to predict the impact of therapeutic regimens. This would lead the way towards overcoming drug resistance in cancer and drive the path towards personalized medicine and improved combinatorial therapies.

Chapter 2

Intra-Tumor Heterogeneity and Drug Response: How Differences Make Difference?

"Cancer's life is a recapitulation of the body's life, its existence a pathological mirror of our own."

— Siddhartha Mukherjee, *The Emperor of All Maladies: A Biography of Cancer*

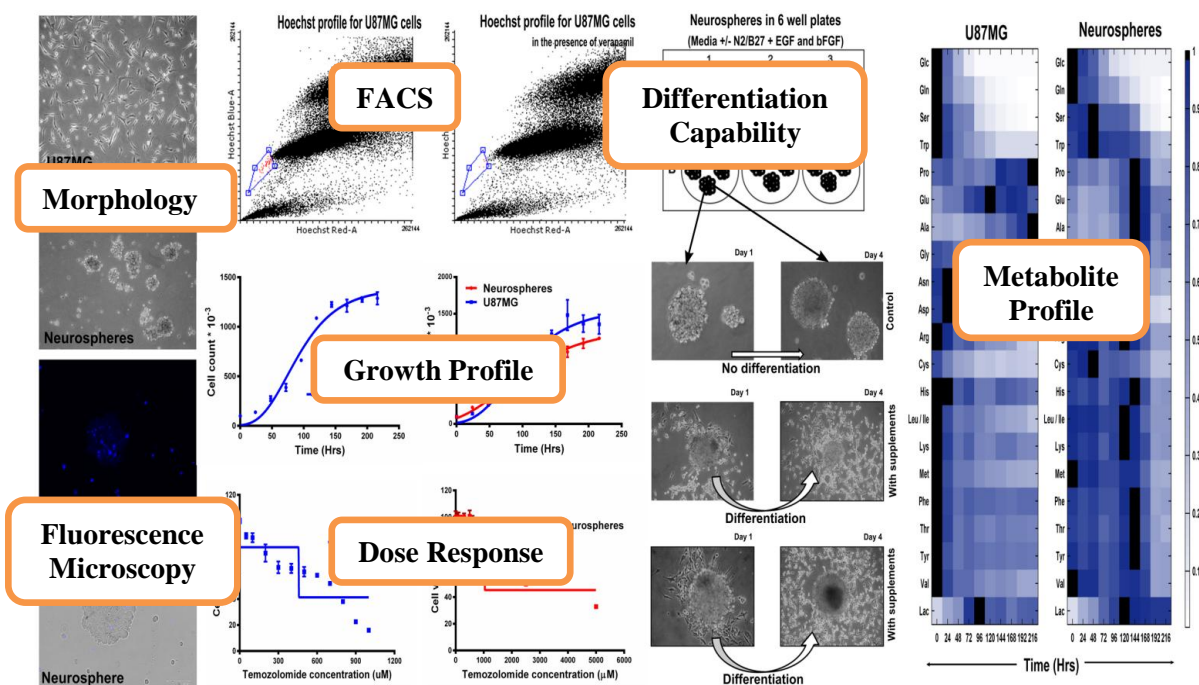


Figure 2.1: Graphical abstract of Chapter 2.

Abstract

The criticality of therapeutic impact arising from tumor heterogeneity is indisputable. Clonal cell lines established as scalable cancer models are known to harbor cellular sub-populations that mirror tumor heterogeneity. Functional characterization of heterogeneity unravels phenotypic plasticity that can be leveraged for desired drug responses. U87MG, a glioblastoma cell line, was investigated to identify side-populations of neurospheroidal (NSP) cells within the main epithelial population (U87MG) with varied morphology and sorted using Fluorescence Assisted Cell Sorting (FACS). The growth of NSP cells in the presence of 1 mM temozolomide indicated 40% higher IC_{50} values. The maximum growth rate was 30% lower for NSP than U87MG cells. Metabolite profiling using HR-LCMS identified growth limiting substrates glucose, glutamine and serine in both populations and tryptophan only in U87MG. Glycine, alanine, glutamate, and proline were secreted by U87MG; however, proline and glycine were re-utilized in the NSP side-population. NSP cells could differentiate into the glial cell type (NDx) that had varied IC_{50} values and metabolic dynamics. Reprogrammed metabolism in the side-population potentially shaped epigenetics leading to temozolomide resistance in NSP cells. The highlights include: (i) Temozolomide (TMZ) resistant Neurospheroids (NSP) identified in U87MG cell line (ii) NSP shows varied dose response, 40% higher IC_{50} and 30% lower growth rate. (iii) Altered Glucose and Glutamine uptake in U87MG and NSP shape metabolic dynamics.

2.1. Introduction

Origins and implications of heterogeneity in tumor manifest *in vivo* as multifactorial responses. Intra-tumor heterogeneity shapes responses for personalized medicine approaches and can limit therapeutic efficacy leading to resistance (Inda et al. 2014; Parker et al. 2015). Resistance to chemotherapy and other targeted therapies are known to dramatically reduce cancer remission rates (Hoey 2010). Evidence supports the presence of a small population of therapy-resistant cells in many cancer types that can eventually result in cancer recurrence (Turner & Reis-Filho 2012; Burrell et al. 2013). Therefore heterogeneity of cancer not only affects the quality of data but may also mask the interpretation of the cancer cell drug response (Sottoriva et al. 2013). More recently, metabolic reprogramming has been recognized as a hallmark with certain neo-metabolites including 2-hydroxyglutarate associated with a gain of function (Wise et al. 2011; Losman & Kaelin 2013). Although, the clinical relevance of human cancer-derived cell lines as model systems is highly debatable they are undoubtedly indispensable as preclinical tumor models to test therapeutic strategies (Qian et al. 2013; Gaspar et al. 2010; Seznec et al. 2010; Angeles & Angeles 2010; Clark et al. 2010). The failure of cell culture models to reflect clinical patterns may also be due to unaccounted tumor micro-environments and dynamics of nutrients available (Persano et al. 2013; Cantor & Sabatini 2012). Researchers have demonstrated that human cancer cell lines harbour minority populations of putative stem-like cells (De Almeida Sassi et al. 2012; Broadley et al. 2011; Khan et al. 2013; Sharma et al. 2011; Persano et al. 2013; Cruz et al. 2012), molecularly defined by dye extrusion phenotypes (Goodell 2005; Med 1996; Bhattacharya et al. 2003). These cancer stem cells (CSC) form integral parts of most tumors and have further advanced the concept of intra-tumoral heterogeneity (De Almeida Sassi et al. 2012; Grasbon-Frodl et al. 2007).

Fundamentally, the CSC concept states that long-term tumor propagation, metastasis, and relapse depend on small populations of phenotypically-distinct cancer cells endowed with unique functional properties (Turner & Reis-Filho 2012; Burrell et al. 2013). These small populations are highly conserved (Golebiewska et al. 2011; Hirschmann-Jax et al. 2004; Golebiewska et al. 2013; Broadley et al. 2011) and have also been identified in human cancer-derived cell lines. Both, the clonal evolution models and the CSC hypothesis support the genesis and maintenance of side populations and their mechanistic role in chemotherapeutic resistance (Safa et al. 2015). Despite their potentially controversial origin, the presence of these cells (Figure 2.2) that form a sub-population is ratified. These

populations have largely been characterized for morphology and drug/dye extrusion properties, although detailed characterization of their dose-response relations does not exist (Marjanovic et al. 2013; Furnari et al. 2015). There is a need to understand the underlying biochemical, molecular and physiological signatures to tackle resistance. While these cell lines continue to be the basis of substantial biological insight, experimental inferences reflective of both the main and the side populations is inevitable.

Glioblastoma multiforme (GBM) the most malignant among astrocytic tumors arising from the glia, is associated with poor prognosis (Brandes et al. 2008; Wrensch et al. 2002) and high levels of both macroscopic and microscopic heterogeneity (Parker et al. 2015). Due to phenotypic plasticity (Marjanovic et al. 2013) and potential switching between cell types via epigenetic regulation (Persano et al. 2013), maintaining a dynamic equilibrium between these differentiated and de-differentiated cell populations is critical. Glioblastoma has four distinct subtypes: proneural, neural, classical and mesenchymal based on gene expression patterns and correlates to clinical characteristics (Verhaak et al. 2010). High prevalence of mutations in isocitrate dehydrogenase isozyme (IDH1/2) (Li et al. 2013), indicates not only a key role in early gliomagenesis but also connections of altered metabolism and clinical outcomes. Due to its highly aggressive and plastic nature and poor therapeutic responses (Kohsaka et al. 2012; Wang et al. 2014), understanding the complex heterogeneity of GBM is of great interest.

Temozolomide (TMZ) is an imidazotetrazine derivative of the alkylating agent dacarbazine and an anti-cancer prodrug of Temodar™, the primary oral alkylating agent used to treat GBM. The therapeutic index is dependent on molecular markers like O⁶-methylguanine methyltransferase (MGMT) and/or lack of a DNA repair pathway in GBM cells, isocitrate dehydrogenase type 1 and type 2 (IDH1/2) mutation (Megova et al. 2014) and glioma cytosine-phosphate-guanine (CpG) island methylator phenotype (G-CIMP) (Noushmehr et al. 2010; Ostrom et al. n.d.). U87MG, a commonly studied (Angeles & Angeles 2010; Vacas-Oleas, 2013) grade IV glioma cell line, known to show sensitivity to temozolomide, has been analyzed and subjected to molecular/functional characterization over the last four decades (Pei et al. 2014; Bernhart et al. 2013). The whole genome sequence of U87MG has been delineated (Clark et al. 2010) and the sequence analysis of U87MG provides an unparalleled level of mutational resolution compared to any cell line to date (Angeles & Angeles 2010). U87MG is wildtype for IDH1/IDH2 (Wise et al. 2011) in contrast to many gliomas whose hallmark is the production of a neo-metabolite 2 hydroxyglutarate (Losman

& Kaelin 2013; Wise et al. 2011). However, side-populations have not been identified and characterized phenotypically or functionally.

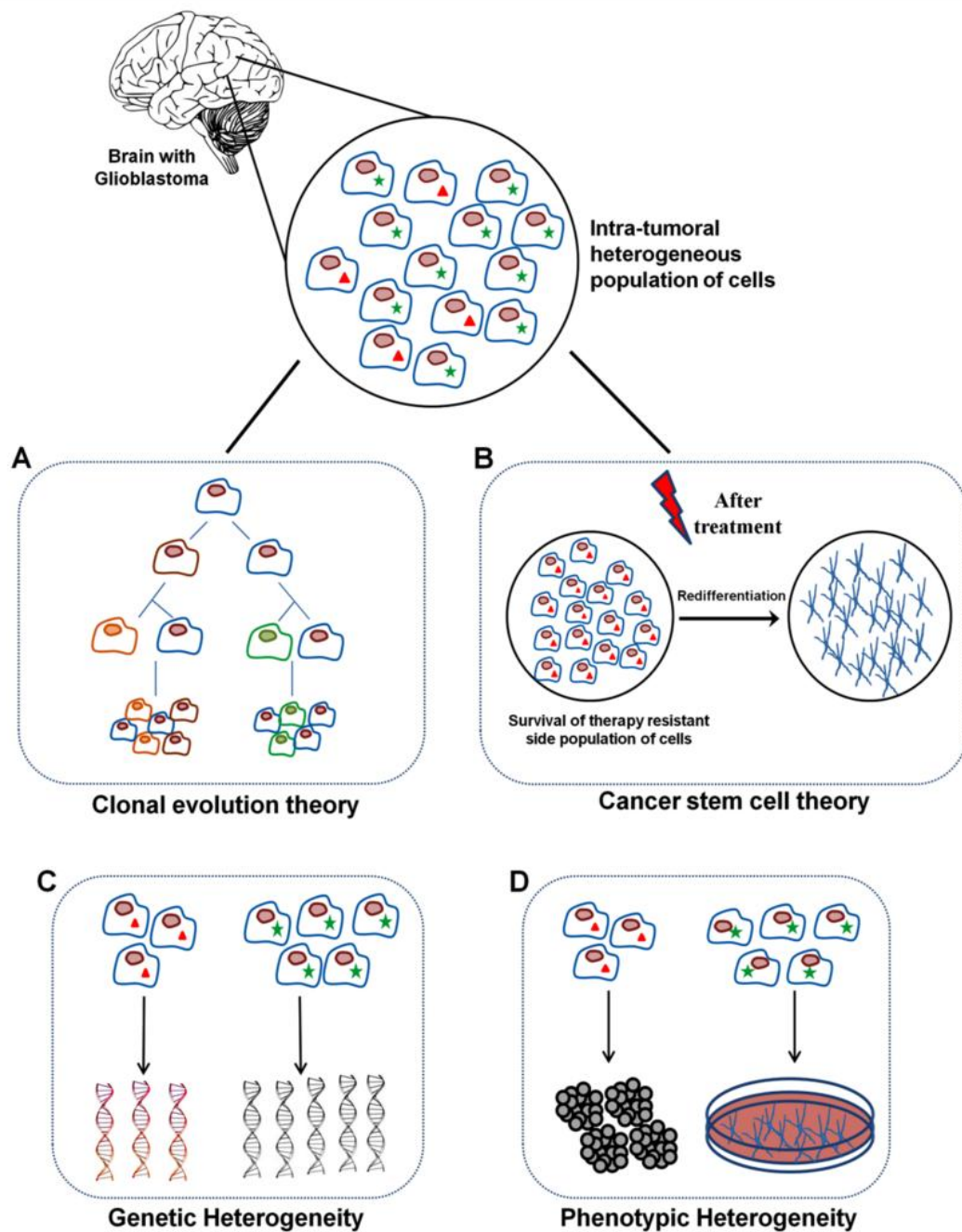


Figure 2.2: Schematic showing heterogeneity in Glioblastoma Multiforme. (A) Clonal evolution theory: Epigenetic elements are conserved during evolution which results in somatic clonal evolution. (B) Cancer stem cell theory: A sub-population of cells in the intra-tumor region (which gains resistance to the drug) undergoes re-differentiation after treatment to give rise to cancer, thus having stemness characteristics. (C) Genetic heterogeneity: Any changes in the genetic makeup of the cells that give rise to two different cell types within tumors. (D) Phenotypic heterogeneity: Accounting for the complete effect of oncogenic mutations and tumor microenvironment on the morphology of the cells.

The Cancer Genome Atlas (TCGA) and Parsons et al. analyzed 20,661 protein-coding genes in 22 human GBM samples by using Sanger sequencing (Parsons et al. 2010). These Candidate Cancer Genes (CAN-Genes) included TP53, PTEN, CDKN2A, RB1, EGFR, NF1, PIK3CA, and PIK3R, have been previously implicated in gliomas (Frattini et al. 2013; Marjanovic et al. 2013). The methylation status of the MGMT may be causal in intra-tumoral chemotherapeutic heterogeneity observed in GBM and other cancers (Snuderl et al. 2011; Little et al. 2012).

Receptor tyrosine kinases (RTKs) including EGFR, MET and PDGFRA have been identified with varying levels of amplification (Snuderl et al. 2011; Little et al. 2012; Szerlip et al. 2012). Intra-tumoral variation was observed in single-cell RNA sequencing and gene expression from five primary GBMs (Patel et al. 2014). There are many gene expression studies for selected signaling pathways like PPARG, JAK-STAT, EGFR, MGMT, and DNA repair enzymes and some metabolic genes like IDH1/IDH2, LDH, SDH that have been reported in the literature (Yeung et al. 2013; Szerlip et al. 2012; Kohsaka et al. 2012). However, none of these functional or molecular or physiological studies focuses on the side-population that could potentially exist.

A side-population/ sub-population of neurospheroidal cells (NSP) that are morphologically distinct from epithelial cells were identified in U87MG (Grade-IV GBM cell line) and sorted using Fluorescence Assisted Cell Sorting (FACS). A detailed phenotypic and functional characterization of the side-population's heterogeneous phenotype vis-a-vis the main tumor cell line population (U87MG) was performed.

To our knowledge, this is the first study addressing the functional characterization in relation to growth/proliferation and metabolite profiling to understand nutrient uptake of side-population cells within a cell line. The differential growth kinetics of the two populations has also been delineated in addition to their differential response to the chemotherapeutic drug, Temozolomide. The glucose/ amino acid utilization profiles and differential metabolism is characterized using LC/MS.

2.2. Methods

2.2.1. Cell culture: U87MG cell line (HTB-14; Human Glioblastoma Multiforme) was cultured in DMEM (Dulbecco's Modified Eagle's Medium). Glucose (1 mg/mL) and L-glutamine (0.584 mg/ml) with added 10% fetal bovine serum (FBS, Gibco™,

ThermoFisher Scientific) and 1% non-essential amino acids (Sigma-Aldrich) was used. Cells lines were maintained at 37°C in a humidified atmosphere of 5% CO₂/95% air. This cell line has been authenticated by STR profiling (Appendix A) to ensure the ATCC STR profiles (10 marker loci). Among 16 marker loci, 9 marker loci were used for the confirmation of authentication (Appendix A). After separation using FACS, NSP was initially maintained in neurobasal medium (Gibco™, ThermoFisher Scientific) supplemented with B27 supplement (Gibco™, ThermoFisher Scientific), 0.2 µg/mL of epidermal growth factor, EGF (ThermoFisher Scientific) and 0.2 µg/mL of basic fibroblast growth factor, bFGF (ThermoFisher Scientific). Further sub-culturing and passaging of NSP was carried out using the similar medium as U87MG to avoid any contribution from different micro-environments and delineating heterogeneity of molecular signatures. NSP were cultured as free-floating spheres in the appropriate low attachment T-75 flasks or 6 well/24 well plates (Nunc™, ThermoScientific™).

2.2.2. Fluorescence microscopy: Hoechst 33342 stain (ThermoFisher Scientific) at a concentration of 1 mg/mL was used for all fluorescence studies on EVOS® FLoid® cell imaging system (ThermoFisher Scientific). The side-population assay exploits the excitation of Hoechst 33342 in the blue fluorescence range (351 to 364 nm with a 450/20 band-pass filter) and emission in the red fluorescence (675-nm long-pass edge filter). The differential fluorescence intensity (390/40 nm excitation and 446/33 nm emission) reflected the varied Hoechst dye uptake by cells.

2.2.3. Flow cytometry: The side-population assay as previously described (Goodell 2005) was performed with cells at 70% to 80% confluency. Cells were trypsinized, washed and resuspended in phosphate buffer saline (PBS) supplemented with 2% FBS to a final concentration of 10⁶ cells per milliliter. Cells were incubated at 37°C, with 5 µg/ml Hoechst 33342, in dark, for 120 minutes, with regular mixing at 30-minute intervals followed by incubation at 4°C. Propidium iodide (4 µM) was added for viability assessment. Efflux of Hoechst 33342 was determined using flow cytometry with BD FACS Aria III machine (BD Biosciences Ltd). Intensity data using the appropriate channels were collected in linear mode.

2.2.4. Sorting of cells by FACS and functional characterization using verapamil: Cells with the ability to efflux Hoechst dye were characterized and sorted by their fluorescent profile into Hoechst high (Hoechst positive) and Hoechst low (Hoechst negative) using BD FACS Aria III. Cells were suspended to 2-4 x 10⁶ cells per milliliters and sorted using

FACS. A two-way sort yielded both the main population (Hoechst high/U87MG) and side-population (Hoechst low/NSP). Hoechst low FACS profile of cells was confirmed using Verapamil (a calcium channel blocker). All data were collected in linear mode and analyzed using BD FACSDiva™ software v6.1.3. Cells were displayed on dot plots gated on live cells, PI negative, and viewed in a Hoechst Blue versus Hoechst Red dot plot to capture the effect of Verapamil and to confirm the dye efflux.

2.2.5. Growth/proliferation studies: Growth of the cells separated by FACS (U87MG and NSP) and the heterogeneous population (Het U87MG) were studied by monitoring their proliferation via cell count over a period of 216 hours (9 days). The initial seeding set the starting population (*No*) at ~10000 cells per well. The growth profile was studied in a 24 well plate (Nunc tissue culture-treated) for ease of harvesting. Both U87MG and NSP cells were harvested every 24 hours and counted using hemocytometer based on trypan blue dye exclusion assay. Before counting, the NSP population was disaggregated by trypsinization. The growth curve was graphed with the number of cells on the Y-axis and time on the X-axis. The data were fitted using Gompertz function using GraphPad Prism software and the growth parameters calculated. The same protocol was followed for the growth studies of NDx cells.

2.2.6. Temozolomide dose-response curves: For dose-response experiments, we plated cells in four replicates at 20,000 cells per well in 96-well plates (Nunc™ tissue culture treated, ThermoScientific™) in full growth medium for 24 h and then treated them with different doses of TMZ in serial dilutions (0.05M to 5M) and tested them for cell viability using the MTT assay. Cell control (without TMZ treatment) in every individual replicate was considered as 100% viable, and the IC₅₀ value was calculated as the dosage at which 50% viable cells are present with respect to control cells in each representative replicate. Three biological replicates were performed with three technical replicates in each biological replicate on a 96-well plate (Nunc™ tissue culture treated, ThermoScientific™).

2.2.7. *In vitro* differentiation of NSP: NSP were grown initially in DMEM followed by addition of N-2 supplement (Thermofischer Scientific Ltd). Growth factors, bFGF and EGF were reconstituted with 0.1% BSA solution at a concentration of 100 µg/mL. 20 µL from this working stock was added to 100 mL of complete medium. Unused portions were frozen and kept in aliquots until further use. All other conditions were maintained the same as used in the proliferation/growth study. The NDx cells were cultured separately by following the same method of culture of U87MG cells and frozen in cryo-vials for further

studies.

2.2.8. Sample extraction, dilution and internal standard spiking for LC-MS/MS: The 9 samples harvested during growth every 24 hours over a period of nine days were used for the metabolic profiling to understand nutrient uptake and kinetics. Culture samples were thawed in an ice bath to aliquot 100µL of the sample for extraction. The aliquot was transferred into a fresh 1.5 mL centrifuge tube. 400 µL of chilled methanol (previously stored at -80°C) was added. The solution was thoroughly mixed for 2 min followed by centrifugation for 15 min at 5000 rpm (4°C). The tubes were carefully removed, 300 µL of supernatant was withdrawn and transferred into a fresh tube (Dilution level: 5X). A two-step serial dilution of the supernatant was performed using 50% acetonitrile in water. In the first step, 50 µL of supernatant was thoroughly mixed with 450 µL of diluent (Dilution level: 50X). This solution was further diluted by mixing 100 µL of the sample solution with 400 µL of diluent (Dilution level: 250X). Before injection, 100 µL of the sample solution was mixed with an equal volume internal standard solution containing 4.4 µM verapamil in 50% acetonitrile in water with 0.2 % formic acid. **Standard preparation:** Standards of metabolites were prepared using chemically defined minimal essential media (MEM), non-essential amino acid media (NEAA). Stock solutions were serially diluted to generate the various calibration levels for quantitative estimations (Appendix B).

2.2.9. Metabolomics profiling using liquid chromatography high-resolution mass spectrometry (LC-HRMS): Metabolic profiling of samples was carried out by Accela 1250 ultra-performance liquid chromatography (UPLC) in tandem with Thermo Q-exactive high-resolution mass spectrometer (HRMS) using heated electrospray ionization (HESI) interface. The UPLC and MS were operated using Xcalibur (Thermo, Version 2.0) software platform, whereas HESI source parameters were set using Tune module (Thermo, version 2.1). Samples were stored in a temperature controlled Accela autosampler maintained at 4°C during LC-HRMS analysis. A reverse-phase C18 hypersil gold column (10cm x 2.1mm x 3.0µm) was used for chromatography. The mobile phase consisted of 0.1% formic acid in deionized water (Mobile phase 'A') and 0.1% formic acid in acetonitrile (Mobile phase 'B'). The elution gradient was set as 70% of mobile phase A (0.0-2.5 min), 10% A (3.5-5.5 min), 70% A (5.5-8.0 min) with a constant flow rate at 1000 µL/min.

The HESI source spray voltage was set at 3.7kV with capillary temperature 300°C, sheath

gas 45 units, auxiliary gas 10 units, heater temperature 390°C and S-lens RF at 50 units. The mass spectrometer was set to m/z range of 60-900, resolution of 70,000 FWHM with automated gain control target 1e6 and maximum injection time of 50 ms. 5µL of samples was injected for analysis using the auto-sampler unit. The data was acquired in both positive and negative ion mode in two separate batches. Metabolomics data analysis was carried out by the Qual and Quan browser modules of Xcalibur (Thermo). [M+H]⁺ and [M-H]⁻ ions were used for all sets of data analysis in positive and negative ion mode respectively.

A Qual/Quan approach of data processing was employed. First, accurate mass-extracted ion chromatogram (AM-XIC) of various metabolites using 20 ppm mass extraction window (MEW) were generated and peaks were confirmed using MS/MS spectral peak matching. As the latter part of the Qual/Quan approach, the metabolites confirmed through the qualitative analysis were quantified in various intra- and extra-cellular samples using internal standard normalized linear regression models generated from standards. The detail of MS/MS confirmations, concentration ranges and regression fits of various metabolites is provided in Appendix B.

2.3. Results

The glioblastoma cell line U87MG contained a side-population (0.1%) of Hoechst-effluxing cells. The side-population cells were confirmed with Verapamil, an ABC transporter L-type calcium channel blocker and inhibitor of Hoechst 33342 dye efflux. The separated populations were tested for morphological and phenotypic heterogeneity. Morphology was studied by microscopy for both cell types and also the ability of the spheroid cells to differentiate back into the glial cell type. Phenotypic heterogeneity was tested by comparing growth kinetics and the nutrient uptake from complex media in addition to the response to Temozolomide (Temodar™) used to treat glioblastoma.

2.3.1. Microscopy reveals distinct cell morphology of each population. Under bright field microscopy, cultures of the separated U87MG showed characteristics of glial cells with epithelial cell morphology (Figure 2.3A). Neurospheres (NSP) were seen as small rounded cells that form floating aggregates in culture (Figure 2.3B). Fluorescent microscopy further suggested a difference in fluorescence intensity between the NSP and U87MG cells in the heterogeneous population (Figures 2.3C and 2.3D). This is indicative of potential efflux of the Hoechst dye by a small population of cells, the side-population

within the major population.

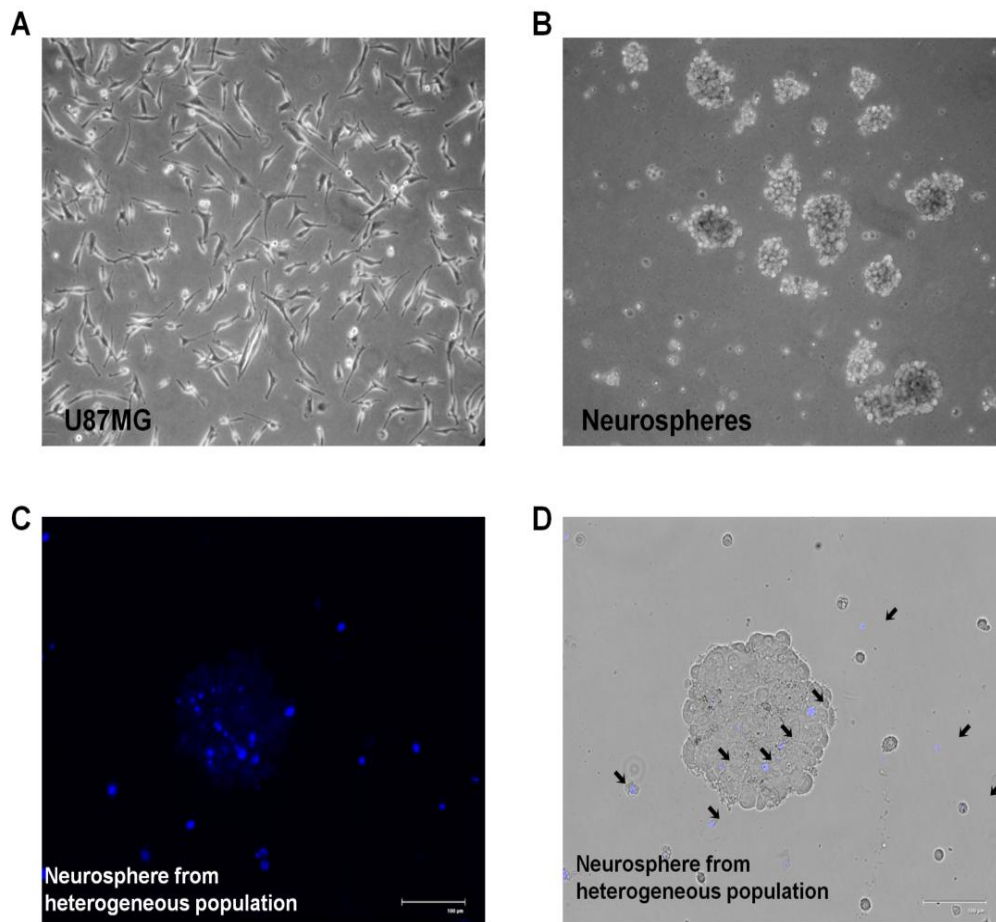


Figure 2.3: Heterogeneous cell population in U87MG as seen using microscopy. (A) U87MG cells grown in DMEM medium, forming epithelial morphology with adherent profile (B) Separated NSP cells grown in low attachment surfaces as spheres (C) Fluorescence microscopy of a neurosphere from heterogeneous population before sorting using FACS; The difference in fluorescence intensity of dye uptake (Hoechst 33342 staining) is shown in the blue fluorescence image. (D) Bright-field light microscopy merged image of C. All microscopic images were captured in an EVOS® FLoid® system, ThermoFisher Scientific. Scale bar: (A) and (B) at 20X magnification; (C) and (D) was captured with a scale of 100 μ M.

2.3.2. FACS profiling identifies differential dye efflux properties in U87MG cells. To confirm differential dye uptake, flow cytometric analysis was performed and side-population were identified, characterized as NSP. The side-population cells were detected in parental GBM cells, at a frequency of 0.1%. The NSPs were confirmed by use of Verapamil. The fluorescence profile (Figure 2.4A) of viable cell population allowed identification of the side-population that can be sorted further.

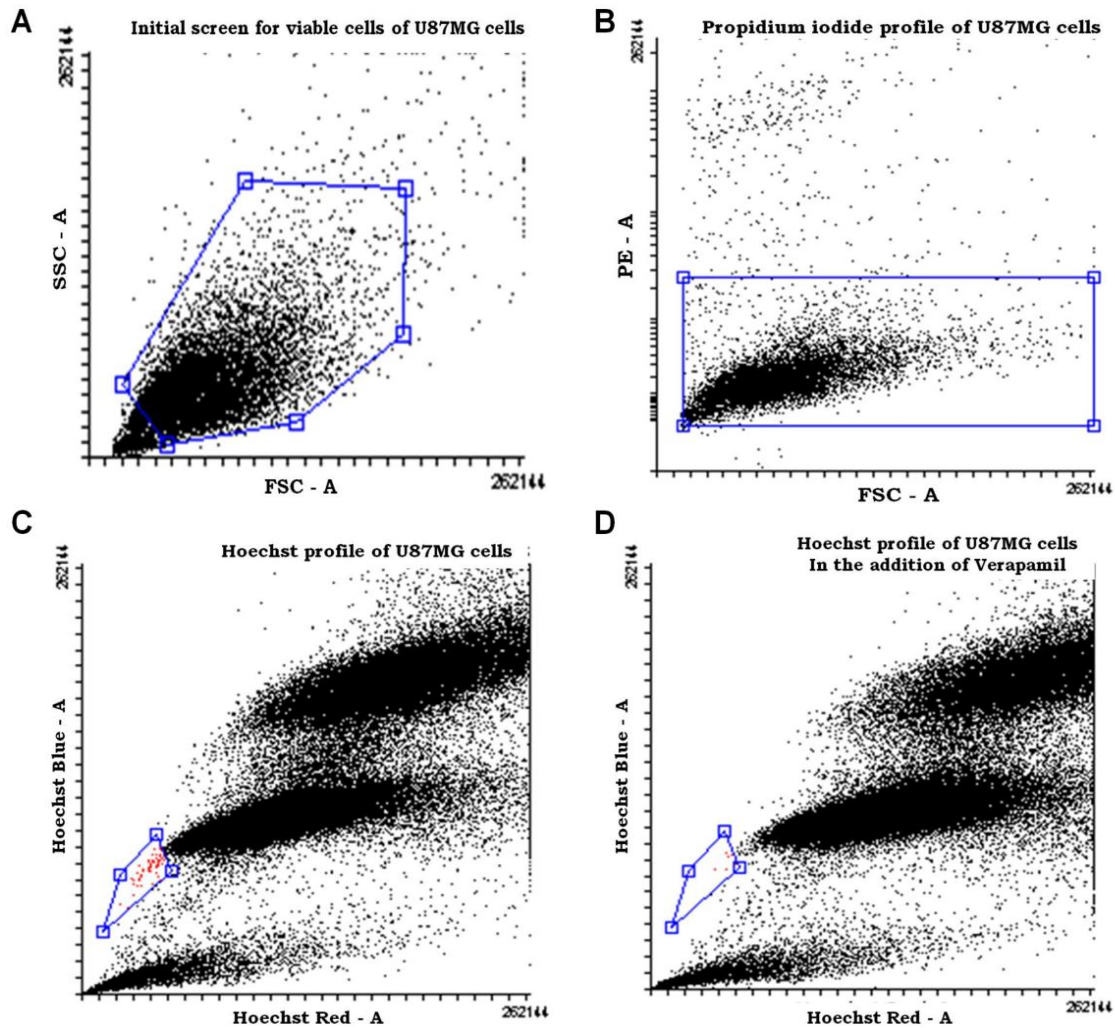


Figure 2.4: FACS profiling of heterogeneity within U87MG cells. (A) Initial screening for viable cells of U87MG cells: Cells were distinguished from debris using FSC (Forward scatter, related to cell size). (B) Propidium Iodide (PI) profile of U87MG cells: PI is mainly taken up by the dead cells. Gated cells were representative of viable cells. (C) Hoechst profile of U87MG cells: Hoechst Red versus Hoechst Blue was compared for the dot plot where the side-population of cells was gated. NSP cells were recognized as a small tail extending first on the left side of the G₀/G₁ phase cells towards the lower “Hoechst Blue” signal. (D) Hoechst profile of U87MG in the presence of Verapamil: the cells were treated with Verapamil and analyzed for the blocking of dye efflux as a confirmation of side-population profile. In the presence of Verapamil, the gated side-population decreases to a few cells confirming the blocking of dye efflux and this confirmation helped the sorting of NSP cells.

The multi-step gating strategy was critical for characterizing the side-population and discriminating the main population. The flow-cytometric profile based on the forward scatter (FSC, indicative of cell size) and side scatter (SSC, indicative of cell granularity) allowed distinguishing viable cells from cell debris. To assure that a detected signal arose from single cells, cell doublets and aggregates were gated-out based on their properties displayed on the SSC area (SSC-A) versus FSC area (FSC-A) dot plot (Figure 2.4A). Dead

cells were recognized for their strong positivity for the dead cell discrimination marker, propidium iodide (Figure 2.4B). This gating strategy primarily allowed the definition of Hoechst profile of viable populations. Sub-population cells were recognized as a dim tail extending first on the left side towards the lower ‘‘Hoechst Blue’’ signal (Figure 2.4C). The mechanism of Hoechst dye uptake depended on the activation of the ABCG2 transporter system and this can be inhibited by the use of the calcium channel blocker, Verapamil hydrochloride. The side-population was confirmed based on Hoechst 33342 efflux through the Verapamil-sensitive ATP-binding cassette (ABC) transporter, ABCG2 (Figure 2.4D).

2.3.3. Differential growth kinetics of the side-population

The growth of cells with differential dye efflux capability was studied based on a ten-day experiment monitoring their proliferation (Figure 2.5). Viable counts of the specific cell type were graphed as a function of time and then fitted to the Gompertz model using GraphPad PRISM V4.0 (GraphPad Software, San Diego, CA, USA) to determine maximum specific growth rate (μ_{max}), and maximum population density (N_{max}).

The Gompertz function used to model the growth kinetics of both the cell types was as follows:

$$N(t) = N_0 \exp (\ln(N(t)/N_0) [1 - \exp(-kt)]$$

where N_0 defines the initial seeding density of the cells, Nt is the number of cells at time t , and k is the maximum specific growth constant (Table 2.1).

The doubling times calculated from the growth rates (Table 2.1) were 35.12 and 47.05 hours for the U87MG and the NSP populations respectively. This function unlike the traditional exponential model gives a better fit (Figures 2.5B and 2.5C) by the three parameters used and predicts decelerated growth towards the end by accounting for lack of resources or space. Thus the fitted Gompertz function reaches its horizontal asymptote for U87MG and NSP after 6.17 and 4.8 doublings respectively. The maximum specific growth rates calculated were 0.014 and 0.02 hr^{-1} for NSP and U87MG respectively. The NSP population growth rate is 30% lower than the main population and thus the maximum population density reached at the end of 216 hours was higher for U87MG as compared to NSP. The heterogeneous population had a growth rate of 0.02 hr^{-1} and a doubling time of 36 hours.

Table 2.1: Growth parameters determined based on Gompertz growth fit in GraphPad Prism software

Gompertz growth parameters	Nmax (cell numbers)	μ Max (hr ⁻¹)		R Squared
		Gompertz	Monod's	
Neurospheres	1.304*10 ⁶	0.01473	0.0145	0.9733
U87MG	1.556*10 ⁶	0.01973	0.0219	0.9421
Heterogeneous U87MG	1.383*10 ⁶	0.02316	0.0186	0.9690

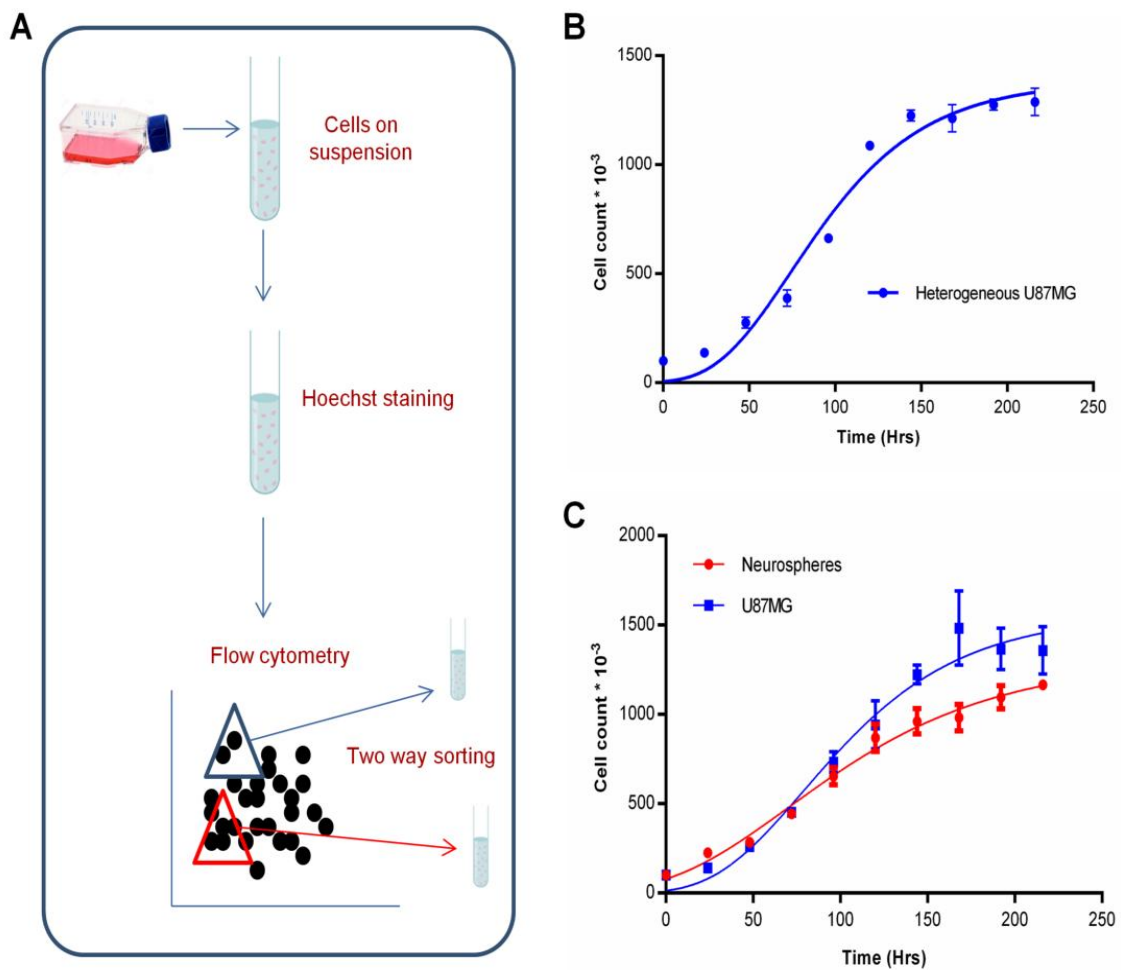


Figure 2.5: Growth profile of the heterogeneous population in U87MG. (A) Workflow used to obtain a homogeneous population of cells by FACS that were growth profiled. (B) The growth of the heterogeneous population of cells U87MG and (C) The growth profile (mean of 3 biological replicates) over 9 days for the separated NSPs & U87MG seeded at the same density and graphed using the cell count every 24 hours. The Gompertz growth kinetic model was fitted using GraphPad Prism. A comparison of (A), (B) and (C) shows differential lag times and U87MG was observed to have a higher growth rate as compared to NSP as indicated in the summary of growth kinetic parameters (Table 2.1).

2.3.4. Dose-response parameters vary across cells for temozolomide

The objective of determining the dose-response curves for TMZ (Temodar), was to detect and analyze any potentially different growth inhibition patterns exhibited by the side-population NSP. The dose-response of U87MG and NSP are varied as seen in the steepness of the dose-response curve (Figure 2.6), differences in maximum effect and the more classical drug potency measurements (IC_{50} and E_{max}).

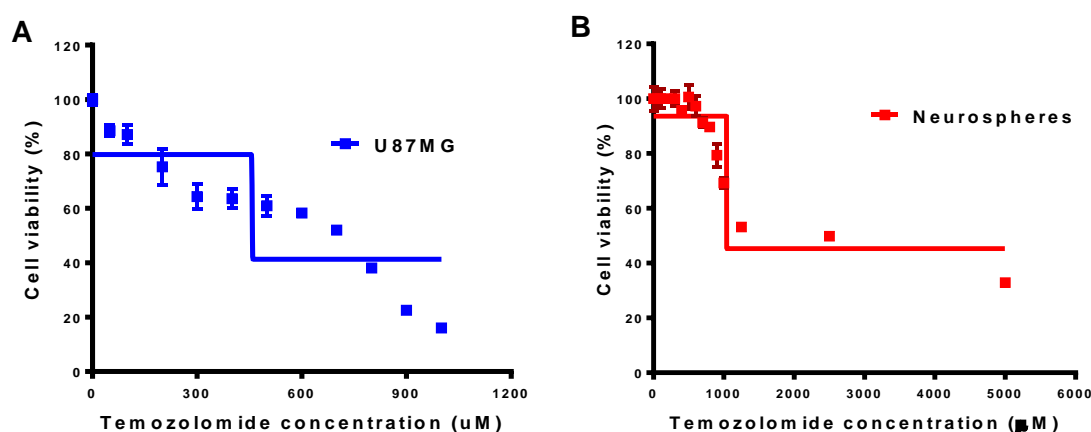


Figure 2.6: Dose-response curve for temozolomide. The dose-response summary was graphed as cell viability (reported as % compared to control) against the concentrations for TMZ. (A) U87MG showed the IC_{50} value of 745.6 μ M while (B) and NSP IC_{50} was calculated to be higher at 1,039 μ M using a non-linear regression curve fit using GraphPad Prism. A detailed summary of all dose-response parameters is given in Table 2.

The summary (Table 2.2) indicates IC_{50} values indicative of the potency of the drug, E_{max} values a measure of efficacy, Hill Slopes (HS) indicating effect per unit of drug and area under the curves (AUC) that reflect the overall response of the cell lines to the drug. All measurements were based on the estimation of % cell viability (run in quadruplicates) obtained from MTT assay after 24 hours incubation with TMZ. The incubation time was determined as 24 hrs after testing the time dependent effect of TMZ on NSP (Appendix A). A lower IC_{50} value for U87MG cells (745.6 μ M) indicates the higher potency of TMZ against these cells (Figure 2.6A). A higher IC_{50} for NSP (1039 μ M) indicates a potential lower efficacy of the drug on these cells (Figure 2.6B). The fold resistance was calculated to be 40%. The E_{max} values for NSP are almost three-fold higher than that of U87MG indicating higher efficacy of TMZ on the main cell line as compared to the side-population (Table 2.2). However, an HS value of near 1 for NSP indicates a potentially higher efficacy, at least in culture. AUC combines potency and efficacy of a drug into a single parameter. AUC values were compared across U87MG and NSP exposed to the same range of TMZ concentrations indicate a higher impact of the drug on U87MG.

Temozolomide is potentially also shown to be efficacious in controlling the side-population growth but only at concentrations that are 40% higher (indicated by fold resistance ratio 1.41).

Table 2.2: Summary of dose-response analysis for TMZ.

Dose response summary	U87MG	Neurospheres
IC ₅₀ (μM)	745.6	1039
E _{max}	25.53	45.28
Log ₂ (Hill Slope)	-1.95904	0
AUC	53039	276836

2.3.5. Quantitative exo-metabolite profiling identifies differential dynamics of nutrient uptake in the side-population

LC-MS/MS was used to monitor the differential nutrient uptake of glucose and amino acids required for growth (Figures 2.7A, B, and C). Consumption of major nutrient glucose correlated with the release of by-product lactate consistent with the well-documented Warburg effect in transformed cells (Vander Heiden et al. 2009; Feron 2009; Warburg et al. 1923). The extent of the Warburg effect was also measured through estimation of the lactate secreted in relation to the glucose consumed. Glucose was taken-up linearly during growth of U87MG. The side-population NSP had a slight lag before glucose uptake and was consumed exponentially. Glucose influx is also seen to be differential between NSP and U87MG (Figure 2.7C). Among the amino acids, glutamine consumption (Figure 2.7D) was quantitatively the highest and closely mirrored glutamate secretion in the media. The nutrients that were completely depleted during the time frame growth as monitored in both U87MG and NSP were glucose, glutamine and serine although with varied dynamics (Figures 2.7D, E and F). Tryptophan was utilized completely by U87MG only indicating potentially different functional roles in NSP (Figure 2.7G). The maximum uptake rates of these amino acids in U87MG being highest in the first 24 hours decreasing several folds by the end of 96 hours (Figures 2.7D-H). NSP, however, seems to show maximum uptake of these amino acids in the 24-48hr time frame indicating a potential lag in the first 24 hours. Interestingly, the patterns of utilization seem to indicate a linear decrease of these nutrients for U87MG while NSP growth is supported through the exponential decrease of the same nutrients with a time delay of about 48 hours in their uptake corresponding to the end of the first observed doubling (Figures 2.8A, B). Ala, Glu, Gly, and Pro were secreted by the U87MG population as shown in a clade different from the rest of the metabolites that are

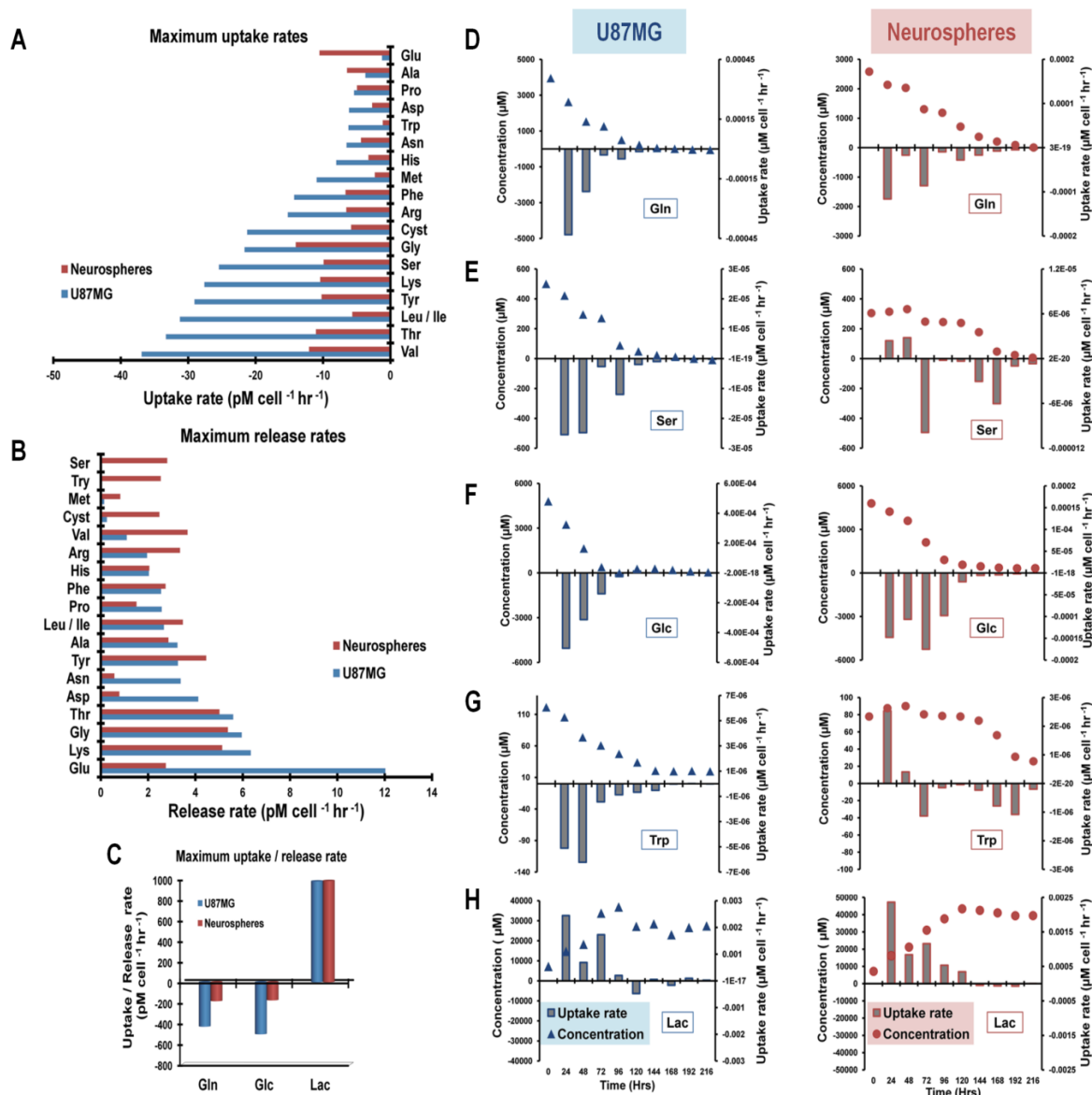


Figure 2.7: Consumption and release profile for selected metabolites. Consumption and excretion rates of glucose, lactate, and amino acids by U87MG and NSP cells. Amino acids are ranked in descending order by absolute magnitude of their maximum uptake and release fluxes in U87MG (A, B). Each bar represents the slope from a linear fit of $n = 3$ replicates \pm SE. Standard three-letter abbreviations are used for amino acids. (C) Maximum uptake/release rate of Gln, Glc and Lac. Glc-glucose; Lac-lactate. Rapidly proliferating cells of U87MG/NSP in a culture consumed Gln (D) and (E) serine and (F) glucose in excess of other nutrients while only U87MG consumed (G) tryptophan in excess. U87MG utilized Gln at a faster rate compared to NSP cells. NSP cells were found not to utilize tryptophan until 144 hrs (6 days) of growth. Uptake of glucose was faster in U87MG and slower in NSPs. (H) Lactate release was found to be proportional to the utilized glucose concentration and was stable from 120 hrs in NSP cells.

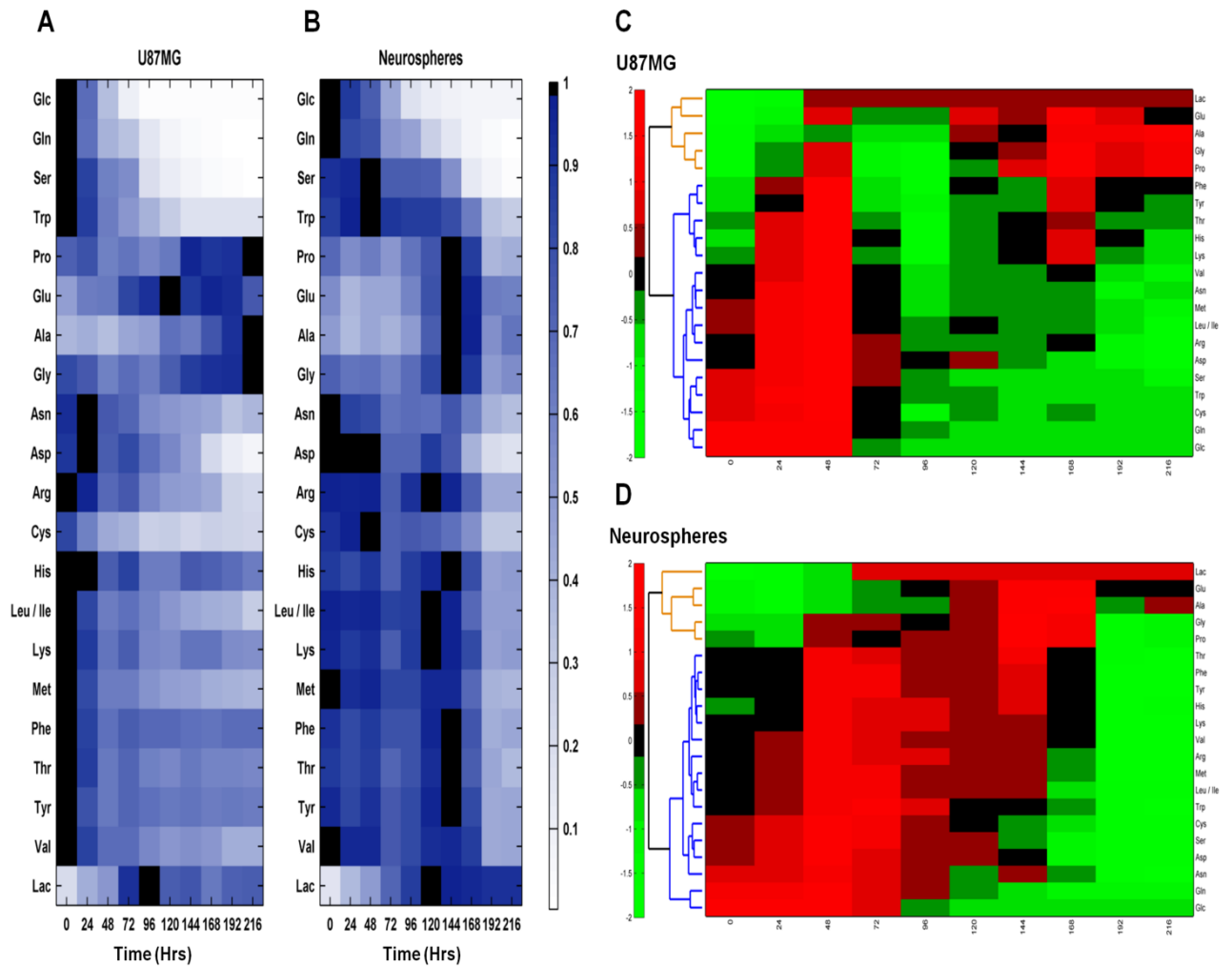


Figure 2.8: Quantitative exo-metabolite profiling of separated U87MG and neurospheres. Normalized dynamics of LCMS-based concentration profiles of amino acids over time was plotted as a heat map for U87MG (A) and NSP (B). The heat map indicates the consumption/release of the amino acids in the extracellular medium over time. The profile varies across a scale of 0 to 1 wherein 1 corresponds to release/accumulation and 0 corresponds to the least value/uptake. The clustergram of U87MG (C) and NSP (D) shows the relative concentration of all amino acids in the external environment over time.

all consumed (Figures 2.8C and D).

This phenomenon has been seen in previously studied glioblastoma cells. The NSP population however only secreted alanine and glutamate. Glycine and glutamate were secreted initially in fast dividing cells and then taken-up later suggesting a metabolic functional role for them in the NSP (Figures 2.8A and B). Several amino acids including Cys, Leu/Ile, Lys, Gly, Met, Phy, Ser, Thr, Tyr, and Val were utilized linearly in the first 48 hours of growth only by U87MG (Figure 2.8A). NSP was observed to utilize these only after the first doubling (Figure 2.8B). Another feature distinct from U87MG was the

utilization of the amino acids Tyr, Trp, Val, Thr, Ser, Pro, Met, Phe, Lys, Leu/Ile, His in NSP cells somewhere between 120- 168 hours and continued until growth was monitored at 216 hours (Figures 2.8A and B). This indicated that the demand for these nutrients at that time may exceed the endogenous synthetic capacity in NSP and thus necessitate uptake.

2.3.6. Side-population NSP has the capability of differentiation into a glial cell type

The ability of the side-population to undergo differentiation and form specialized cell types was confirmed in an assay that provided growth factors for such differentiation (Figure 2.9). The differentiated neurospheroidal cells (NDx) exhibited glial morphology and were adherent in contrast to the NSP (spheroidal) side-population. NDx cells showed a TMZ dose response in between NSP and U87MG, exhibiting an IC_{50} value of $817.5 \mu M$ and growth rate of 0.01634 hr^{-1} (Figures 2.10A, B and Tables 2.3 and 2.4).

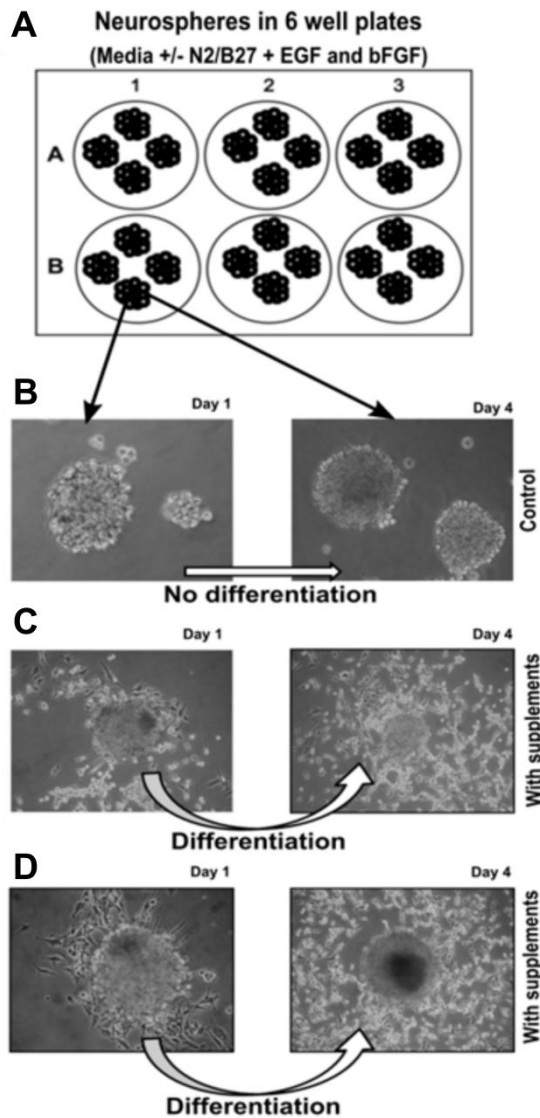


Figure 2.9: Redifferentiation capability of drug resistant side population cells.

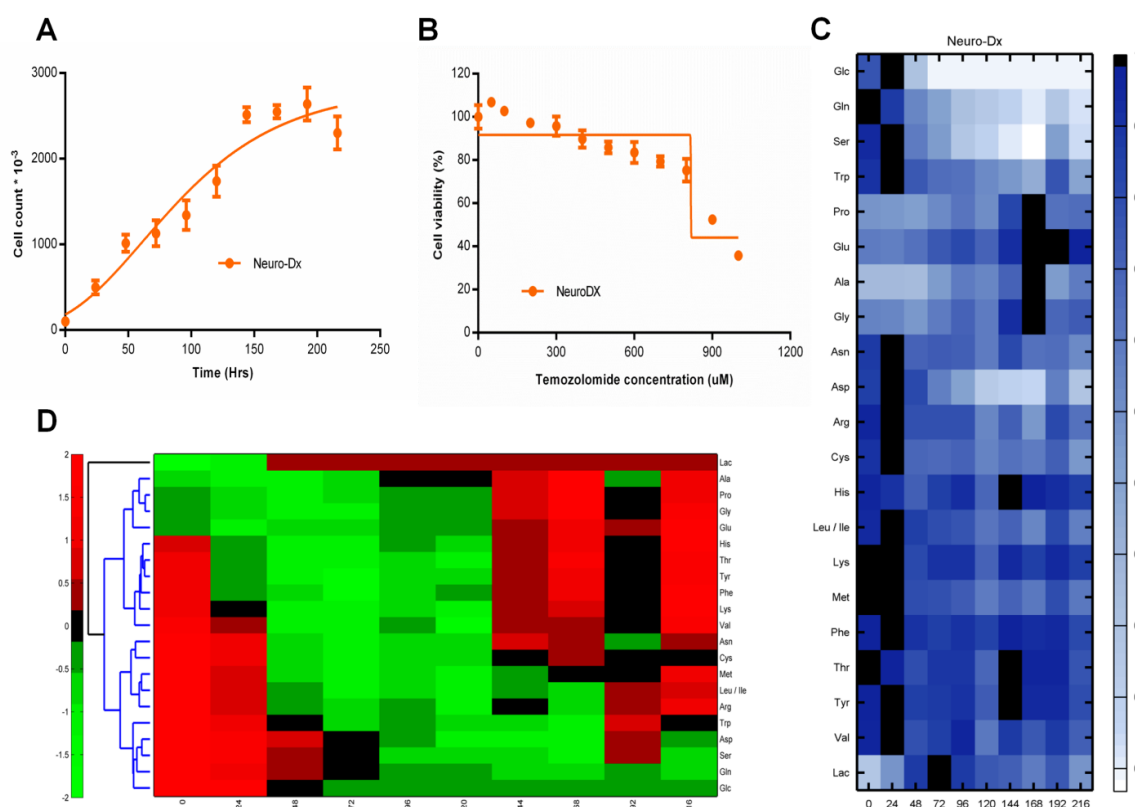
(A) Experimental setup for study: 6 well plate containing the NSP in media supplemented with or without growth factors, bFGF and EGF. Column 1 in the plate contains media without growth factors as control for the experiment (B) Microscopic image of one NSP on day 1 (24 hours after seeding) and day 4 supplemented with media without EGF/bFGF; (C) Microscopic image of NSP on day 1, differentiating into adherent cells on day 4. (D) Microscopic image of another neurosphere (NSP cell) undergoing differentiation from day 1 to day 4.

Table 2.3: Growth parameters for NDx cells.

Growth parameters	NDx cells
Growth rate (hr^{-1})	0.01634
Nmax (cell numbers)	2.826×10^6
R square	0.9325

Table 2.4: Dose-response summary for NDx cells.

Dose-response summary	NDx cells
IC ₅₀ (μM)	817.5
E _{max}	44.10
Log ₂ (Hill Slope)	~ -1.000
AUC	83256

**Figure 2.10: NDx cells show distinct growth, dose-response, and metabolic dynamics.**

(A) The growth of NDx cells: Gompertz growth fit is used for calculating the growth parameters. Growth rate = 0.01634 hr^{-1} . (B) Dose-response of NDx cells to TMZ: IC₅₀ is found to be $817.5 \mu\text{M}$ which is higher than U87MG and lesser than NSP. The complete dose-response summary is given in Table S2. (C) Heatmap of max normalized values of exo-metabolite concentration measured by LCMS analysis at every 24 hours of growth. The consumption and release of different metabolite profile differ from that of U87MG and NSP. (D) Clustergram of exo-metabolite concentration max normalized to time points to highlight the presence of highly concentrated metabolite in each time point.

The exo-metabolome analysis of growth samples also showed similarities to U87MG especially with respect to glucose and glutamine consumption. Serine, tryptophan and glutamate profiles mimicked NSP cells (Figure 2.10C, and D).

2.4. Discussion

Although the existence of small minority populations with differential histology and dye efflux properties within cancer cell lines has been known for decades (Golebiewska et al. 2011; Hirschmann-Jax et al. 2004; Golebiewska et al. 2013; Broadley et al. 2011), the underlying biochemical physiology of how this shapes functional heterogeneity is still incompletely understood. Here we report the functional characterization of differential growth & proliferation of a cellular side-population isolated from the U87MG glioblastoma cell line. The identification of differential dose response and resistance of the side-population to TMZ, a clinically approved DNA methylating drug to treat glioblastoma, highlights the need to unravel functional heterogeneity. The incredible genetic and histological heterogeneity of tumors seems to involve the common induction of a finite set of pathways to support core functions including anabolism, catabolism, and redox balance (Ros et al. 2012). This study revealed novel heterogeneity in the context of varied growth-limiting nutrients and uptake rates in addition to micro-environmental changes. To our knowledge, such functional physiological responses have not been correlated to drug response till date for the side-population (NSP) of GBM cells.

U87MG showed a high rate of glucose consumption indicated the flux via aerobic glycolysis to satisfy the bioenergetics of ATP demand (Figure 2.11) depicted by using LCMS metabolite profiles, resembled many cancer cell lines. The dynamic exo-metabolite profiles show higher utilization rates for glucose in U87MG cells and changes in metabolic fluxes occur in primary response to growth-factor signaling (AKT), independent of changes in ATP. Proliferating cells are in much greater need of reduced carbon and reduced nitrogen, as well as cytosolic NADPH for reductive biosynthetic reactions.

The reprogramming of cellular metabolism toward macromolecular synthesis is critical to supplying enough nucleotides, proteins, and lipids for a cell to increase its total biomass and then divide to produce two daughter cells. Glucose and glutamine are rapidly consumed simultaneously by U87MG cells during proliferation suggesting the induction of the MYC transcriptional program. Glutamine conversion to AKG by glutamate

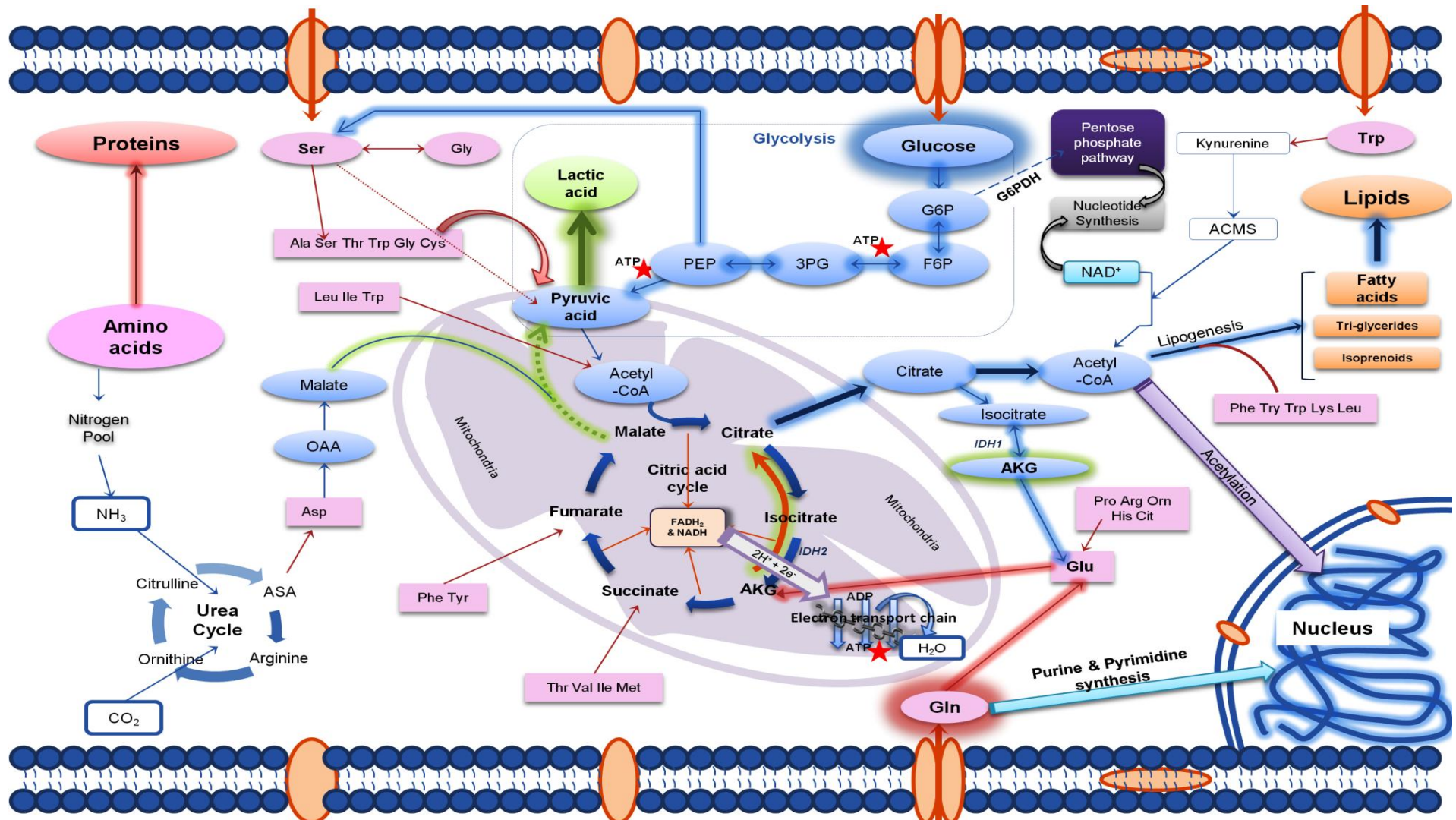


Figure 2.11: Predicted cellular metabolism of U87MG and NSP. The reprogramming of cellular metabolism towards macromolecular biosynthesis is shown. U87MG predominantly uses glucose (highlighted in blue) and glutamine (highlighted in red) simultaneously thus triggering aerobic glycolysis for bioenergetics demand and glutaminolysis for anaplerosis of TCA cycle. NSP cell population preferentially utilizes glutamine and concomitantly increases AKG even in the presence of glucose. This reprograms the TCA cycle.

dehydrogenase (GDH) or by transamination reactions, remove the α -amino group from glutamate transferring it to non-essential amino acids secreted from the cell, like; alanine, glycine, and proline via transaminases (as seen in Figure 2.8A for U87MG). The majority of acetyl-CoA in U87MG cells is derived from glucose, while OAA is derived from glutamine.

Consistent with this hypothesis (Figure 2.11), activation of the tumor suppressor p53 transcriptional program has been shown to be critical for cell survival following glucose depletion (Jones et al. 2005) that could potentially turn on adenylate kinases to meet ATP demand. This activity is required to maintain the TCA cycle under conditions when cells use citrate as a biosynthetic precursor of lipids, cholesterol and fatty acids via the AKT controlled ATP citrate lyase. Glutamine was utilized in excess of its nitrogen requirements and potentially used as intermediates in NSP cells in the presence of minimal amounts of glucose (Figure 2.11).

Differential tryptophan metabolism suggests the role of this carbon source for fatty acid synthesis suggesting a source of NADPH (the electron donor for fatty acid synthesis) and anapleurosis to replenish TCA cycle of picolinate carboxylase activity in maintaining a balance between nicotinamide nucleotide synthesis and acetyl-CoA production that may further affect acetylation (Figure 2.11). The differentiated population NDx from NSP was closer to U87MG in its metabolite consumption patterns and growth profiles. Since TMZ is a DNA methylating drug, the potential effects of metabolism on epigenetics are critical in drug action and cell susceptibility. A reduction in flux through aerobic glycolysis reflective of higher NAD levels could possibly control the SIRTUIN family transcriptional repressors and silence chromatin via decreasing histone acetylation marks.

The non-dependency on glutamine also suggests normal levels of methylation marks in U87MG. The high levels of AKG may potentially turn on high levels of the histone demethylases that prevent the methylation and thus increase the amount of drug (IC_{50}) needed for cidal activity of the side- population. Further experiments are needed to be done to explore the implication of AKG in the demethylation of DNA and its effect on drug sensitivity. In line with this hypothesis, the side-population exhibited properties of 30-40% fold resistance (indicated by higher IC_{50} values) during the studied chemotherapeutic response to the drug.

2.5. Conclusions

The importance of characterizing sub-populations (NSP) within the main population (U87MG) is critical to understanding the contribution of each cell type to overall growth and metabolism of tumor cells. The influence of the presence of sub-populations as those discussed in this chapter on drug dose-response, potency and efficacy may eventually help in better drug regimens and treatment strategies. Drug resistance of these side populations of cells characterized as neurospheres (NSP) in this **Chapter 2** is further studied for its genotypic variations and also characterized for secondary phenotypes. The differential genotype-phenotype relations compared to the main population (U87MG) are delineated and discussed in subsequent chapters of this thesis. Moreover, the results strongly indicate the role of altered metabolism in NSP in addition to drug efflux as a driver for temozolomide resistance.

Chapter 3

Candidate Gene Interaction Networks in Glioblastoma

"Epigenetics doesn't change the genetic code, it changes how that's read".

- Bruce Lipton

"DNA, like a tape recording, carries a message in which there are specific instructions for a job to be done".

-Arthur Kornberg

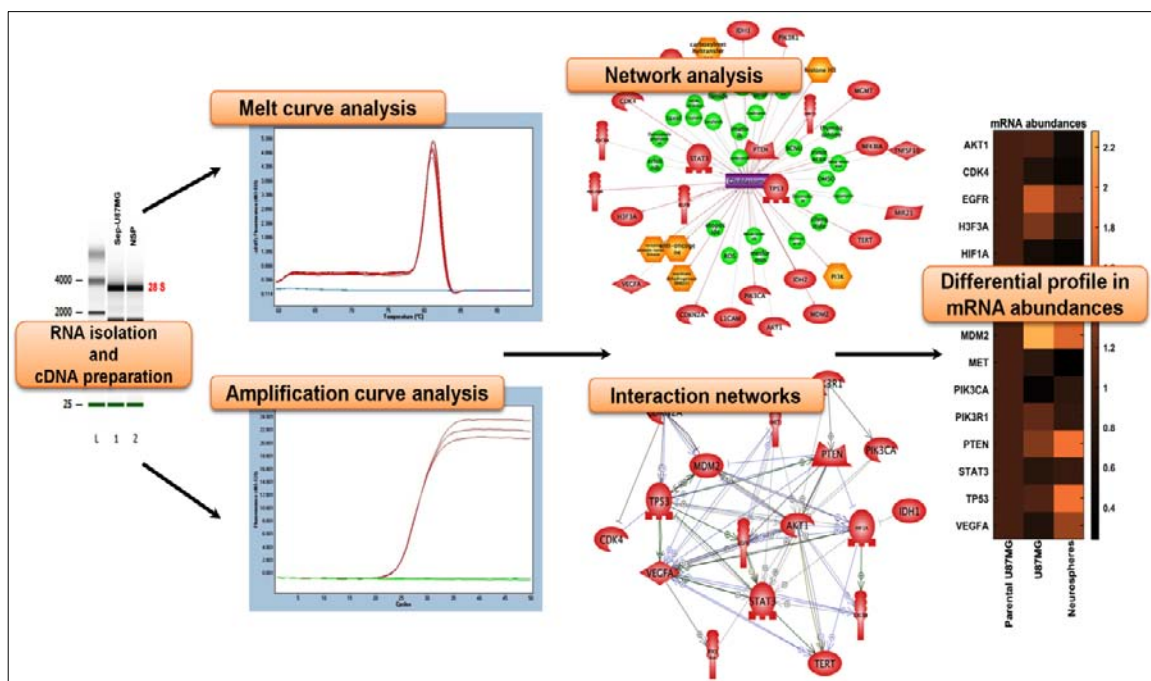


Figure 3.1: Graphical abstract of chapter 3.

Abstract

There is a need to profile ABC transporters along with candidate cancer (CAN) genes for a system-level understanding of drug resistance. This **chapter 3** illustrates the use and application of network analysis guided real-time quantitative PCR (qPCR) to discern differential gene expression comparing drug-sensitive cells (U87MG) having the adherent state of growth to cells that are drug resistant (NSP) and forms spheroids. Patterns of gene expression by cells could yield the mRNA abundances of the key gene markers (CAN-genes and ABC transporters) and help in characterizing drug resistance towards understanding the metabolic rewiring in the resistant cells.

This chapter discusses our findings highlighting the variation in mRNA transcript abundances and differential expression of genes AKT1, TP53, PTEN, EGFR and MET across the populations identified from U87MG. Relative quantitation of gene expression measurements of ABC transporters in NSP showed two to three-fold variations as compared to U87MG. Differential mRNA abundance of AKT1, PTEN, PIK3CA controlling substrate uptake, and metabolism, drug efflux through ABC transporters, nutrient transport, and epigenetic control MDM2 are potentially critical in shaping DNA methylation effects of temozolomide mechanism, causing resistance.

3.1. Introduction

Glioblastoma has four distinct subtypes: proneural, neural, classical and mesenchymal based on gene expression patterns and correlates to clinical characteristics (Verhaak et al. 2010). However, little is known about the distinct phenotype and possible activation of genetic and cellular programs in the biology of minor populations, that distinguish them from major cell types in the tumor environment (Hirschmann-Jax et al. 2004; Bleau et al. 2009). Microarray technology has proven to be very useful in the complete molecular characterization of tumor grades, thus generating evidence of a transition that is unique in every stage of cancer (Khodursky et al. 2000; Hoelzinger et al. 2005). Gene expression analysis not only helps in histopathological diagnosis known so far but also in identifying new signatures especially of non-characterized sub-population that causes drug resistance (Immanuel et al. 2018; Hoelzinger et al. 2005).

It is also expected that molecular characterization of drug-resistant cells would eventually lead to the application of customized therapy to a particular tumor microenvironment. Increasingly gene expression signatures and detailed molecular characterization are routinely used in the clinic as prognostic markers to classify tumors and stratify patient risk/treatment groups. Adaptive signature design through gene expression profiling is being used to characterize the sensitivity of the patient to therapy. This association of gene expression is highly dependent on the purity of the tissue sampled and identification of genes with so-called static signatures.

3.1.1. Network analysis using PathwayStudio™

Information about gene to protein function and cellular pathways is central to the system-level understanding of human disease. The knowledge about the key cancer candidate (CAN) genes specific to each cancer type is routinely characterized and reported in numerous scientific publications. There is a huge need to bring the relevant information together using automated software systems to validate, organize and study pathway implications from legacy data.

PathwayStudio™ is a web-based software and tool developed for analysis of molecular networks by text-mining from databases that contain the cancer candidate gene information (Nikitin et al. 2003). The choices of cancer candidate genes can be delineated by using this web-based software to rank the genes that are linked to glioblastoma with the highest

relevance to the published dataset. The unique feature of PathwayStudio is the inbuilt natural language processing module MedScan (Nikitin et al. 2003) that can convert the keywords of PubMed into pathway diagrams. Gene interaction networks also can be built by using the known legacy data that can benefit from addressing the effect of these genes on a network/pathway.

3.1.2. Cancer candidate (CAN) genes and their role

The Cancer Genome Atlas (TCGA) and Parsons et al. analyzed 20,661 protein-coding genes, in 22 human GBM samples, by using Sanger sequencing. These candidate cancer genes included TP53, PTEN, CDKN2A, RB1, EGFR, NF1, PIK3CA, and PIK3R, that have been previously implicated in gliomas (Frattini et al. 2013). The methylation status of the MGMT may be causal in intra-tumoral chemotherapeutic heterogeneity observed in GBM and other cancers (Little et al. 2012; Szerlip et al. 2012). Receptor tyrosine kinases (RTKs) including EGFR, MET, and PDGFRA has been identified with varying levels of amplification (Snuderl et al. 2011; Szerlip et al. 2012; Little et al. 2012). Intra-tumoral variation was observed in single-cell RNA sequencing and gene expression from five primary GBMs (Patel et al. 2014).

There are many gene expression studies for selected signaling pathways like PPARG, JAK-STAT, EGFR, MGMT, and DNA repair enzymes and some metabolic genes like IDH1/IDH2, LDH, SDH that have been reported in the literature (Yeung et al. 2013; Szerlip et al. 2012; Kohsaka et al. 2012). With the increased discovery of gene and protein expression signatures [4] and detailed molecular characterization to characterize the drug sensitivity, rigorous phenotyping of the subpopulations (NSP), in addition to morphology and drug efflux is critical to understand the resistance.

3.1.3. ABC transporters and drug resistance

One of the largest protein families is ABC (ATP-binding cassette) proteins and these transporter families are present in all living organisms ranging from microbes to humans (Higgins 2001; Štefková et al. 2004). This kind of widespread presence of these proteins suggests a fundamental role. Members of the ABC superfamily are involved in a broad spectrum of functions, including detoxification (ABCB1/MDR1, ABCC1/MRP1, ABCG2) (Chang 2003), defense mechanism against foreign substances and oxidative stress (ABCCs/MRPs), uptake and secretion processes (MDRs, MRPs), lipid metabolism (ABCA1, MDR3, ABCGs) and antigen presentation (ABCB2/TAP1 and ABCB3/TAP2)

(Szakács et al. 2008; Higgins 2001; Štefková et al. 2004; Vasiliou et al. 2009). ABC transporters with multidrug transporter function (ABCB1/MDR1, ABCC1/MRP1, ABCG2) are present in almost all tissue types by showing a good expression profile, proving their importance in cellular defense mechanism (Szakács et al. 2008). 44 ABC transporters are selected and profiled for mRNA abundances in this study that accounts for most of the drug transportation related to cancer.

3.2. Methods

3.2.1. Selection of CAN genes using Pathway Studio™ (v11.0.5) analysis: Pathway Studio 11.0.5 software from Elsevier (<https://product.pathwaystudio.com/mammalcedfx/>) was used to select specifically for CAN genes in silico. Initial pathways/networks (legacy data) implicated in GBM were reconstructed by specifying related key terms including oncoproteins. This resulted in deciphering sub-networks and pathways that included inter-relationships with a confidence score of 3. To further validate networks and infer causal pathways filters were applied to include >25 references. This analysis resulted in a pathway containing 23 genes (Table 3.1) and 1 miRNA. These 23 genes were then expression profiled to quantitate relative mRNA abundance using qPCR.

3.2.2. RNA extraction and cDNA synthesis: Cultured cells were counted using a c-chip hemocytometer (Labtech International Ltd, East Sussex, UK). Cells (10×10^6 cells) were centrifuged at 8000xg for 10 minutes, the supernatant was discarded and the remaining cell pellet was used for RNA extraction using the RNeasy mini-extraction kit (Qiagen, Manchester, UK). In the final step of the protocol, the column was placed on to a nuclease-free 1.5 mL tube and 50 μ L of RNase-free water (Thermofisher Scientific Ltd) was added to the membrane for RNA-elution. After 1 minute incubation at room temperature, followed by centrifugation for 1 minute at 8000xg, the eluted RNA samples were stored at -20°C for short-term storage and at -80°C for long-term storage. Quality of RNA was checked using RIN value (Figure 3.2) determined using Bioanalyzer (Agilent Pvt. Ltd). To remove any DNA contamination, a TURBO DNA-Free treatment (Ambion, Thermofisher Scientific Ltd.) was performed before cDNA synthesis. RNA was reverse transcribed using Superscript III (Thermofisher Scientific Ltd) using the manufacturer's protocol. The synthesized cDNA was stored at -20°C for further use.

Table 3.1: List of cancer candidate genes selected using Pathway Studio 11.0.5

Gene Symbol	Gene Name	Human chromosome position	Cell Localization
AKT1	V-akt murine thymoma viral oncogene homolog 1	14q32.32	Nucleus; Cytoplasm; Cell membrane
CDK4	Cyclin-dependent kinase 4	12q14	Membrane; Nucleus; Cytoplasm
CDKN2A	Cyclin-dependent kinase inhibitor 2A	9p21	Mitochondrion; Nucleoplasm; Nucleus; Cytoplasm; Nucleolus
CXCR4	Chemokine (C-X-C motif) receptor 4	2q21	Plasma membrane; Cell junction; Lysosome; Early endosome; Late endosome; Cell membrane
EGFR	Epidermal growth factor receptor	7p12	Endosome membrane; Plasma membrane; Endosome; Golgi apparatus membrane; Nucleus; Endoplasmic reticulum membrane; Nucleus membrane; Secreted; Cell membrane
H3F3A	H3 histone, family 3A	1q42.12	Chromosome; Nucleus
HIF1A	Hypoxia inducible factor 1, alpha subunit (basic helix-loop-helix transcription factor)	14q23.2	Nucleus; Cytoplasm
IDH1	Isocitrate dehydrogenase 1 (NADP+), soluble	2q33.3	Cytoplasm; Peroxisome; Mitochondria
IDH2	Isocitrate dehydrogenase 2 (NADP+), mitochondrial	15q26.1	Mitochondrion; Mitochondria
L1CAM	L1 cell adhesion molecule	Xq28	Cell membrane
MDM2	MDM2 oncogene, E3 ubiquitin protein ligase	12q14.3-q15	Nucleoplasm; Nucleus; Cytoplasm; Nucleolus
MET	Met proto-oncogene	7q31	Plasma membrane; Membrane; Secreted
MGMT	O-6-methylguanine-DNA methyltransferase	10q26	Nucleus
MIR21	MicroRNA 21	17q23.1	Cytoplasm
NFKBIA	Nuclear factor of kappa light polypeptide gene enhancer in B-cells inhibitor, alpha	14q13	Nucleus; Cytoplasm
PDGFRA	Platelet-derived growth factor receptor, alpha polypeptide	4q12	Plasma membrane; Cell membrane
PIK3CA	Phosphatidylinositol-4,5-bisphosphate 3-kinase, catalytic subunit alpha	3q26.3	Cytoplasm
PIK3R1	Phosphoinositide-3-kinase, regulatory subunit 1 (alpha)	5q13.1	Cytoplasm
PTEN	Phosphatase and tensin homolog	10q23.3	Nucleus; PML body; Cytoplasm
STAT3	Signal transducer and activator of transcription 3 (acute-phase response factor)	17q21.31	Nucleus; Cytoplasm
TERT	Telomerase reverse transcriptase	5p15.33	Chromosome; Telomere; Nucleoplasm; Nucleus; PML body; Cytoplasm; Nucleolus
TNFSF10	Tumor necrosis factor (ligand) superfamily, member 10	3q26	Membrane; Extracellular
TP53	Tumor protein p53	17p13.1	Mitochondrion matrix; Nucleus; PML body; Cytoplasm; Endoplasmic reticulum
VEGFA	Vascular endothelial growth factor A	6p12	Secreted; Extracellular; Cell membrane

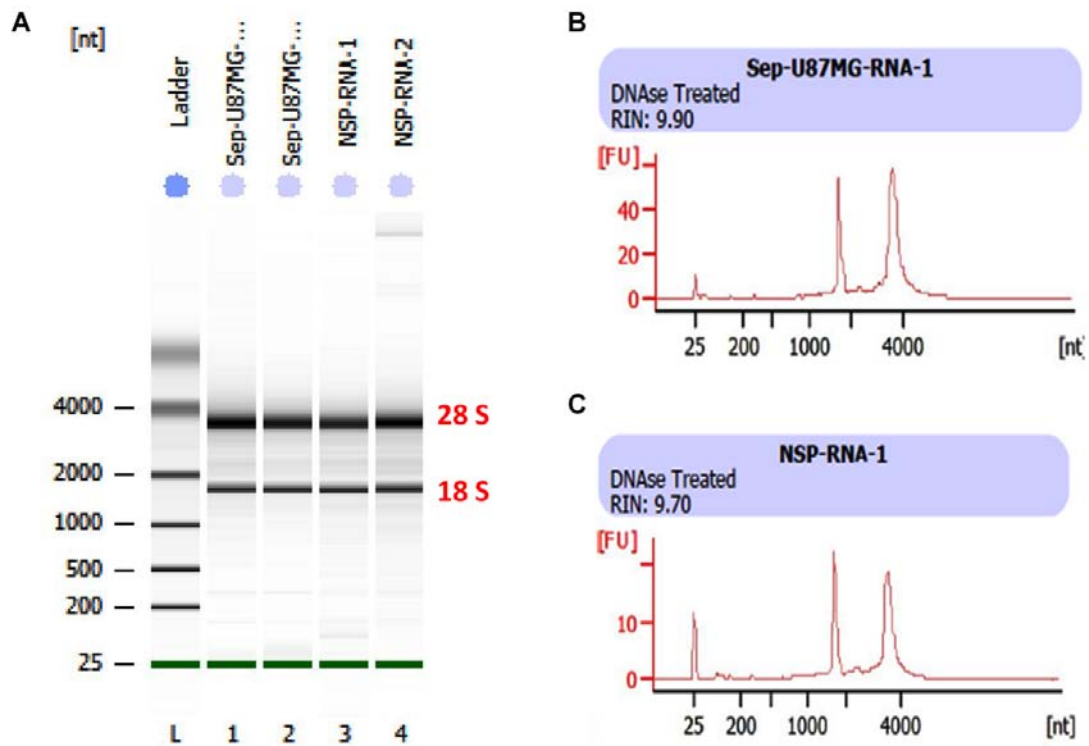


Figure 3.2: RNA analysis using Agilent 2100 Bioanalyser. (A) Gel picture for RNA samples run using RNA Nano-chip from Agilent. Electropherograms of RNA from Separated U87MG cells (B) and (C) NSP showing the predicted RIN values > 9.70.

Table 3.2: Primers and probes designed for gene expression studies of reference genes (control genes) for GeNORM-based normalization of qPCR data

Gene Symbol	Gene Name	Transcript	Forward Primer	Reverse Primer	Probe Number
GAPDH	Glyceraldehyde 3-Phosphate Dehydrogenase	NM_00204 6	AGCCACATCGCT CAGACAC	GCCCAATACGACC AAATCC	60
ACTB	Beta-Actin	NM_00110 1	ATTGGCAATGAG CGGTTC	GGATGCCACAGGA CTCCAT	11
B2M	Beta-2 Microglobulin	NM_00404 8	TTCTGGCCTGGA GGCTATC	TCAGGAAATTTGA CTTCCATC	42
HPRT1	Hypoxanthine Phosphoribosyltransferase 1	NM_00019 4	TGACCTTGATTT ATTTTGCATACC	CGAGCAAGACGTT CAGTCCT	73
RPL32	RPL32 ribosomal protein L32	NM_00099 4	GAAGTTCCTGGT CCACAACG	GCGATCTCGGCAC AGTAAG	17
SDHA	Succinate dehydrogenase complex, subunit A	NM_00416 8	AGAAGCCCTTTG AGGAGCA	CGATTACGGGTCT ATATTCCAGA	69
HMBS	Hydroxymethylbilane Synthase	NM_00019 0	AGCTATGAAGGA TGGGCAAC	TGTTATGCTATCTG AGCCGTCTA	25
RPL13A	RPL13 ribosomal protein L13	NM_01242 3	GAGGCCCTACC ACTTC	TGTGGGGCAGCAT ACCTC	28

3.2.3. GeNorm analysis for stable reference gene identification: Real-time qPCR was initially carried out on all three cell types (Parental U87MG, U87MG, and NSP) for 8

reference genes (Table 3.2) selected based on a previous study (Vandesompele et al. 2002). The primers designed for all these reference genes were based on the Primer3web solutions (<http://primer3.ut.ee/>) and further validated for the primer-dimer formation and any non-specificity using NCBI BLAST (Basic Local Alignment Search Tool) (<http://www.ncbi.nlm.nih.gov/BLAST>), in order to reduce the chance of primers binding non-specifically. The Cq values obtained from the qPCR were analyzed using the GeNorm software (Vandesompele et al. 2002), to calculate the stability of transcripts. Based on this data, GAPDH and RPL13A were selected as control genes (Figure 3.3) based on an average expression stability (M) value of less than 0.4 (Vandesompele et al. 2002).

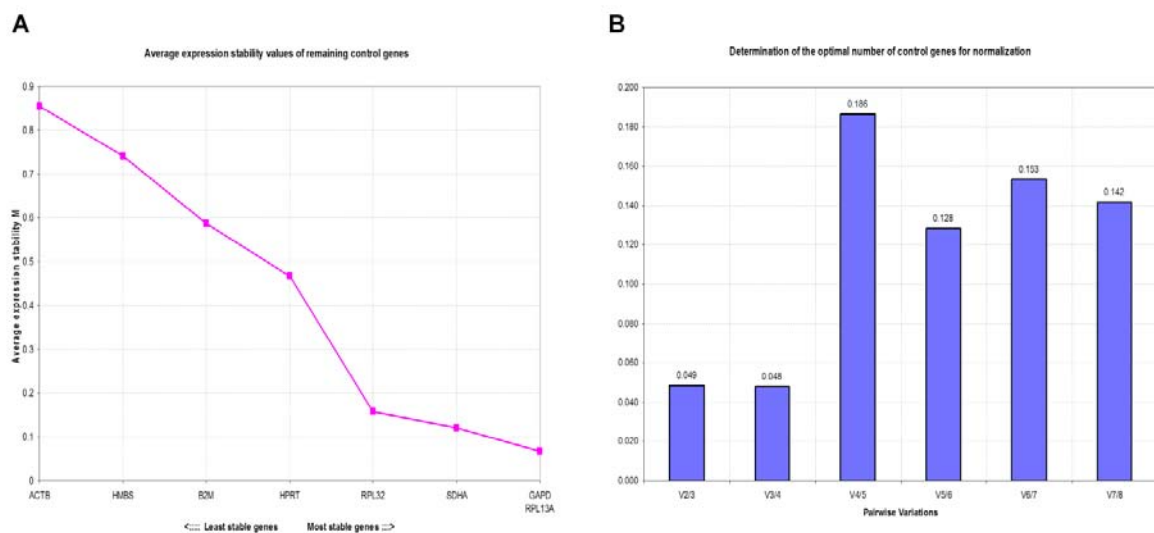


Figure 3.3: GeNorm analysis for stable reference gene identification. (a) Graph showing the average expression stability value (M) for all the 8 reference genes selected (Table 3.2). GAPDH and RPL13A were predicted to be highly stable among the selected genes. (b) Determination of the optimal number of control genes for normalization was carried out using GeNorm. These predictions showed that 2 reference genes, GAPDH and RPL13A were sufficient for the optimal normalization as control genes.

3.2.4. Real-time PCR using SYBR green-I: Real-Time quantitative PCR (RT-qPCR) was used to quantify gene expression of selected CAN genes. All primers designed for this study were based on the Primer3web (<http://primer3.ut.ee/>) solutions and validated using NCBI BLAST (<http://www.ncbi.nlm.nih.gov/BLAST>), to reduce the chance of primers binding non-specifically. SYBR Green I was used as a reporter in the SYBR green assay to increase the sensitivity of detection. qPCR was run on a Light Cycler 480 instrument from Roche Applied Sciences. MIQE (Minimum Information for Publication of Quantitative

Real-Time PCR Experiments) (Bustin et al. 2009) guidelines were complied-with for all the protocols.

Table 3.3. Primers and probes designed for CAN genes

Gene Symbol	Transcript	Forward Primer	Reverse Primer	Probe No.	Amplicon Size (bp)
AKT1	ENST00000349310.3 ENSG00000142208.11	GGCTATTGTGAAGGAGGGTTG	TCCTTGTAGCCAATGAAGGTG	69	108
CDK4	ENST00000257904.5 ENSG00000135446.11	GTGCAGTCGGTGGTACCTG	TTCGCTTGTGTGGGTTAAAA	25	82
CDKN2A	ENST00000304494.5 ENSG00000147889.10	GTGGACCTGGCTGAGGAG	TCTTTCAATCGGGGATGTCT	34	133
CXCR4	ENST00000241393.3 ENSG00000121966.5	GGTGGTCTATGTTGGCGTCT	ACTGACGTTGGCAAAGATGA	18	73
EGFR	ENST00000275493.2 ENSG00000146648.10	GCCTTGACTGAGGACAGCA	TTTGGGAACGGACTGGTTTA	69	72
H3F3A	ENST00000366815.3 ENSG00000163041.5	GCCATCTTTCAATTGTGTTCCG	GGTACAGAGACCTCCTTACTTACCC	19	124
HIF1A	ENST00000337138.4 ENSG00000100644.10	TTTTTCAAGCAGTAGGAATTGGA	GTGATGTAGTAGCTGCATGATCG	66	66
IDH1	ENST00000345146.2 ENSG00000138413.9	GGTGACATACCTGGTACATAACTTTG	GTGTGCAAAAATCTTCAATTGACTT	77	91
IDH2	ENST00000330062.3 ENSG00000182054.4	TGGCAGTTCATCAAGGAGAA	CAGTCTGGTCACGGTTTGG	42	91
L1CAM	ENST00000370060.1 ENSG00000198910.7	CGATGAAAGATGAGACCTTCG	AAGGCCTTCTCCTCGTTGTC	80	64
MDM2	ENST00000462284.1 ENSG00000135679.15	GACTCCAAGCGCGAAAAC	GGTGGTTACAGCACCATCAGT	68	89
MET	ENST00000318493.6 ENSG00000105976.9	CAGAGACTTGGCTGCAAGAA	GGCAAGACAAAATCAGCA	42	73
MGMT	ENST00000306010.7 ENSG00000170430.9	GTGATTCTTACCAGCAATTAGCA	CTGCTGCAGACCACTCTGTG	52	125
NFKBIA	ENST00000216797.5 ENSG00000100906.6	GTCAAGGAGCTGCAGGAGAT	ATGGCCAAGTGCAGGAAC	38	110
PDGFRA	ENST00000257290.5 ENSG00000134853.7	AGGTGGTTGACCTTCAATGG	TTTGATTCTTCCAGCATTGTG	80	74
PIK3CA	ENST00000263967.3 ENSG00000121879.3	CGAGATCCTCTCTGAAATCAC	GAATTTCCGGGATAGTTACACAA	2	85
PIK3R1	ENST00000521381.1 ENSG00000145675.10	AATGAACGACAGCCTGCAC	CCGTTGTTGGCTACAGTAGTAGG	16	68
PTEN	ENST00000371953.3 ENSG00000171862.5	TCCACAAAACAGAAAGATGCTA	CGATTCTTGATCACATAGACTTCC	6	129
STAT3	ENST00000264657.4 ENSG00000168610.9	GAGCAGAGATGTGGGAATGG	CGGTCTCAAAGGTGATCAGG	17	88
TERT	ENST00000310581.5 ENSG00000164362.14	GCCTTCAAGAGCCACGTC	CCACGAACTGTCGCATGT	19	61
TNFSF10	ENST00000241261.2 ENSG00000121858.6	CCTCAGAGAGTAGCAGCTCACA	GGCCCAGAGCCTTTTCAT	6	91
TP53	ENST00000269305.4 ENSG00000141510.8	AGGCCTTGGAACTCAAGGAT	CCCTTTTGGACTTCAGGTG	12	85
VEGFA	ENST00000372067.3 ENSG00000112715.16	TTAAACGAACGTACTTGCAGATG	GAGAGATCTGGTTCCCGAAA	12	93

3.2.5. Real-time PCR using hydrolysis probe assay: LNA hydrolysis probes were used in the qPCR assay to increase specificity and reduce primer dimer formation and detection. Probes were designed (Table 3.3) using the universal probe library assay design center from Roche Applied Science, Ltd. (<http://www.universalprobelibrary.com>). qPCR was run on a Light Cycler 480 and all the protocols followed MIQE guidelines similar to the SYBR Green assays.

3.2.6. Gene expression of ABC transporters: Real-Time quantitative PCR (RT-qPCR) was used to quantify gene expression of ABC transporter gene array (ThermoFisher Scientific, TaqMan Array Human ABC Transporter Panel). This 96 well plate array consisted of duplicate wells with primers and hydrolysis probes for 44 ABC transporter

genes having 4 housekeeping genes as control (primers and probes were optimized for its high specificity feature by the manufacturer). TaqMan probes were used as a reporter in the assay to increase the specificity in comparison to SYBR green dyes. 10 µl of reaction mix containing the synthesized cDNA from U87MG and NSP cells with TaqMan master mix was used in each well of the plate for the study. Gene expression profiling was run on a Light Cycler 480 instrument from Roche Applied Sciences. All the analyses were performed in the LCS480 1.5.1.62 software.

3.3. Results

3.3.1. Network of cancer candidate (CAN) genes: PathwayStudio™ web-based software was used that runs the in-built text-mining MedScan module to link the published data from PubMed to correlate it with the key terms specified by the user. The choice of genes for qRT-PCR was based on this Pathway Studio™ analysis. A network was generated linking genes with selected functional biological processes, regulatory networks and glioblastoma to identify CAN genes. References related to each selection were validated by enrichment analysis by ranking the genes based on the maximum number of references. The final prediction included 23 genes and 1 miRNA that are highly relevant to gliomagenesis (Figure 3.4A). Network analysis was also carried out to understand the interactions between these CAN genes (Figure 3.4A, B). 23 genes were selected (Table 3.1) based on high confidence scores. The interaction network highlighted maximum interactions between AKT1, PTEN, TP53, VEGFA and STAT3 genes indicating the link to cell metabolism and uptake of nutrients as discussed in Chapter 2.

3.3.2. Relative gene expression qPCR analysis of selected CAN genes: Real-time qPCR was used to quantify and detect changes in the gene expression for the selected 23 CAN genes relative to housekeeping/reference genes (Table 3.2). Of the workflows used, as expected, higher sensitivity was observed for the SYBR Green I workflow while the hydrolysis probe-based workflow demonstrated higher specificity. To compare across the cell types, relative quantification was computed using the delta-delta Cq method ($\Delta\Delta Cq$) and expression fold change represented as $2^{-(\Delta\Delta Cq)}$. The qPCR assay results (Figures 3.5A, C) were reported for two biological replicates with three technical replicates within each experiment. Statistically significant variation in gene expression was observed for genes between the parental U87MG and NSP side-population (Figure 3.5A). Thus, heterogeneity of mRNA expression was established through the significant distinct gene expression

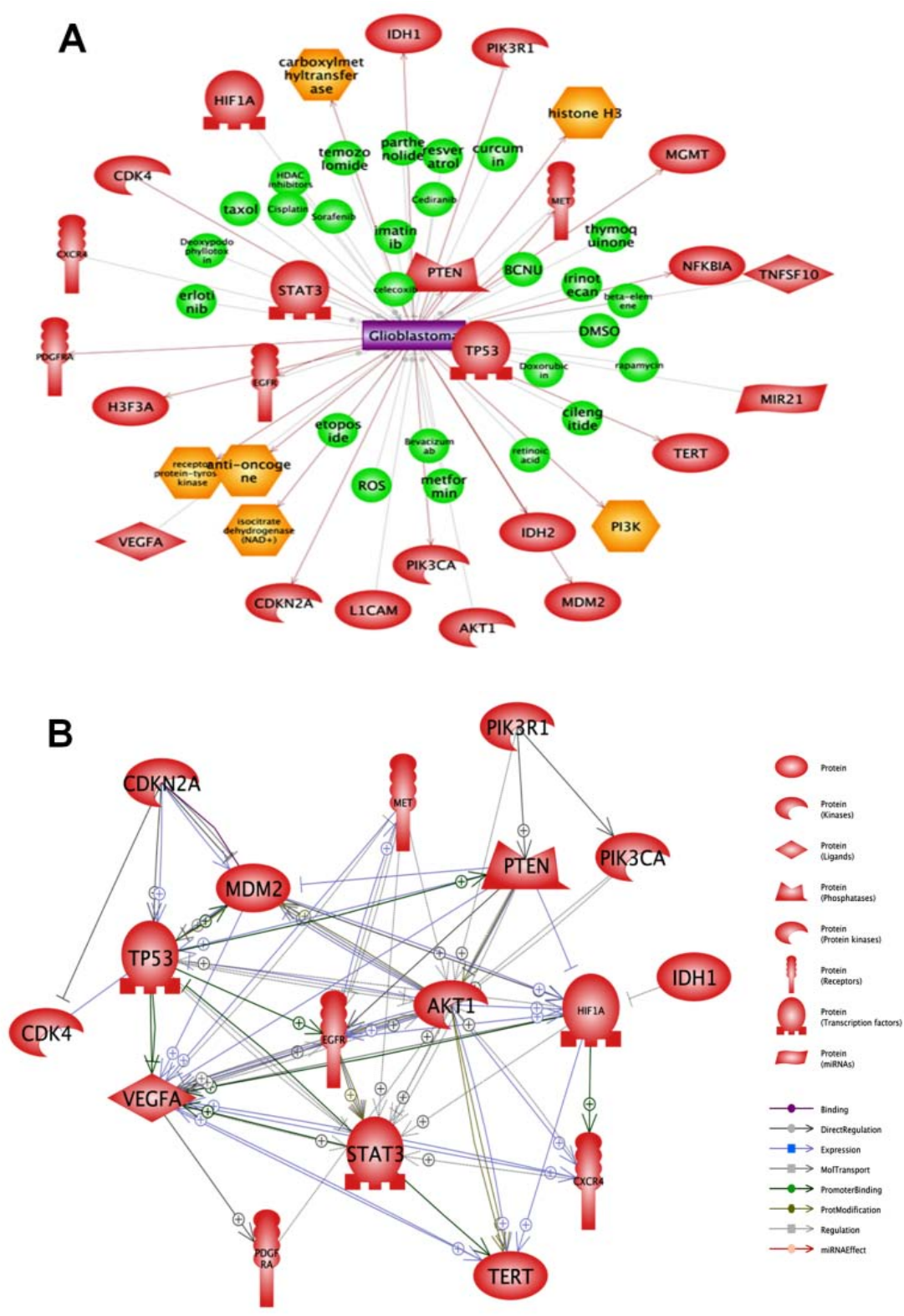


Figure 3.4: Network analysis of CAN genes. A) Prediction using Pathway Studio™ to select the most relevant candidate genes on (confidence score of 3) for gene expression analysis. 23 genes were selected as most critical to glioblastoma pathogenesis for validation. B) Interaction network generated to understand the possible interaction between the selected CAN genes.

signatures observed between the heterogeneous population and separated populations (Figure 3.5A). The differential mRNA abundances of signaling pathway controllers, histone deacetylases and methyl transferases potentially contribute to the varying dynamics of nutrient uptake during proliferation and could dictate indirectly changes observed in TMZ dose-response relation (increasing IC_{50} values and decreasing sensitivity).

It is well known that p53 and PTEN play a pivotal role in tumor suppression and are both down-regulated (less mRNA level) in the U87MG cells with respect to NSP (Figure 3.5C).

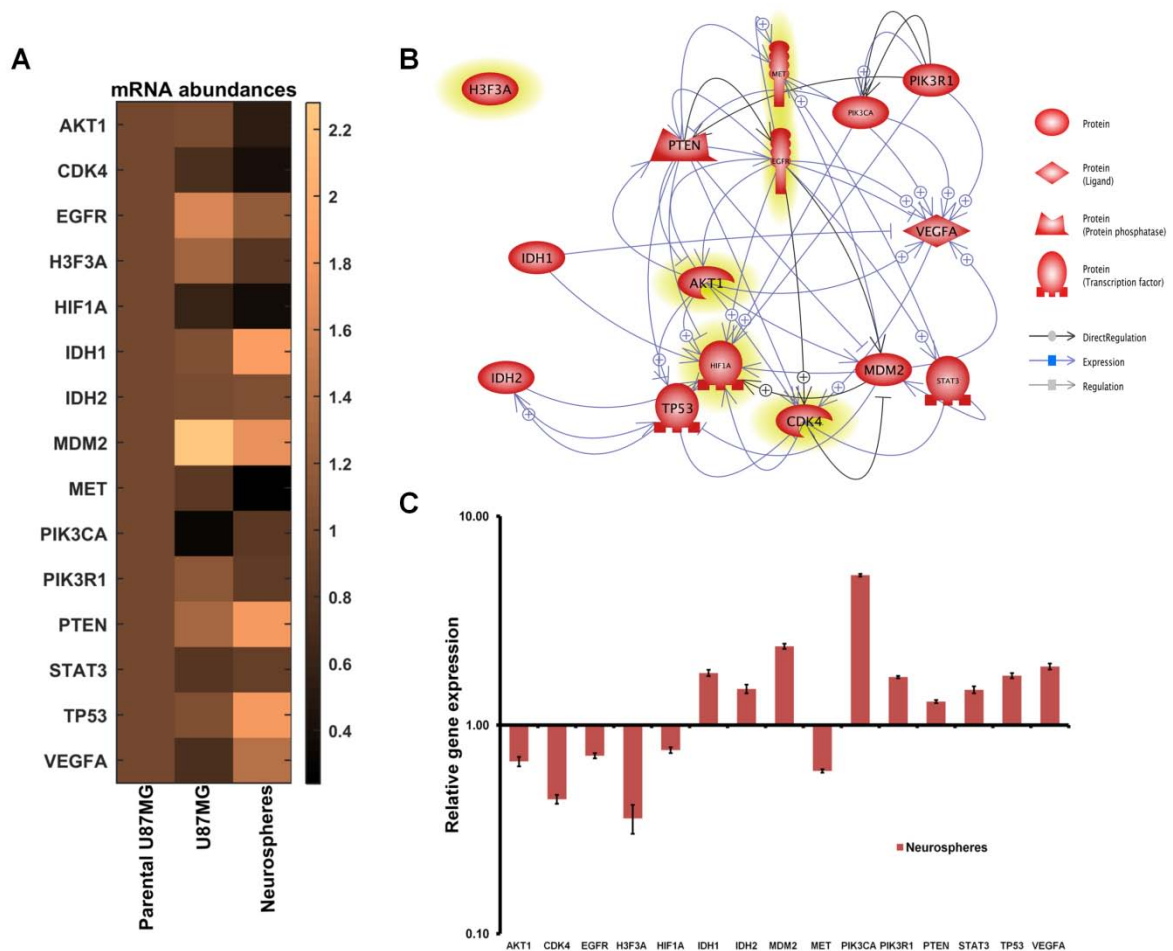


Figure 3.5: Relative gene expression analysis of CAN genes. A) Heatmap of relative gene expression of CAN genes with respect to heterogeneous population (parental U87MG) that shows the potential ramifications of expression signatures in side-populations. (B) Network of interactions between the differentially expressed CAN genes: To study the interactions between the differentially expressed genes, *in silico* enrichment analysis were carried out and the pathway given. Highlighted entries are the genes showing lesser expression in NSP cells with respect to U87MG cells. (C) Relative gene expression of differentially expressed CAN genes between the separated population of U87MG and side-population NSP is shown.

Up-regulation (higher mRNA level) of AKT1 in U87MG with respect to NSP is evident in the differential glucose and amino acid uptake patterns as shown in Chapter 2. IDH1/IDH2 over-expression (higher mRNA level) in the NSP population in comparison with U87MG indicates potential reprogramming of the pathways around AKG that could eventually cause downstream effects on the acetylation profiles. Increased PIK3CA (5 fold change) in NSP could potentially dictate changes involving phosphorylation governing differential nutrient uptake. VEGFA and MDM2 are also highly expressed (higher mRNA levels) in the resistant population NSP compared to U87MG. The cyclin-dependent kinase CDK4 is down-regulated as compared to U87MG indicating a potential cell cycle arrest that needs to be overcome for NSP to proliferate.

Lowered H3F3A expression (lesser mRNA levels) in NSP indicates potential changes in histone acetylation patterns. The interaction network (Figure 3.5B) with highlighted entries shows the genes having more variations in their mRNA levels in NSP. These highlighted genes (Figure 3.5B) included H3F3A, AKT1, HIF1A, CDK4, EGFR and MET indicating a highly possible involvement of cell metabolism in defining the temozolomide resistance. Although the dysregulation of the NSP population is reported here with reference to the cancer cell line U87MG, it is plausible that such correlations may still hold when analyzed in the context of a normal cell as well. The primary goal of this part of the study was to highlight the potential of error due to the presence of sub-population of cells, in the interpretation of the gene expression signatures based on varied sampling strategies and also suggest contributing factors to the integrative analysis of the resistant phenotype.

3.3.3. Network analysis of ABC transporter genes:

To understand drug resistance, it is important to delineate the efficiency of drug transporters that are known for drug transport across the cell membrane. For further elucidation of the efficiency of drug transporters, primarily, the network interaction across the transporters and the drug/molecules is studied using PathwayStudio™ web tool. Initial network was generated to study the localization and distribution of the ABC transporters inside the cell. This network (Figure 3.6) shows the distribution of ABC transporters in the cell membrane, endoplasmic reticulum (ER), mitochondria and cytoplasm. This helps in understanding the localization of these transporters and how they will eventually affect the cell metabolism. Further, the interaction between these transporters and other molecules (Drug/metabolites/small molecules) were studied through pathway analysis.

Interaction networks were generated for 5 out of 7 families of ABC transporters. ABCE and ABCF have been identified recently and hence their entries are either less or not present in the analysis. ABCA, ABCB, ABCC, ABCD, and ABCG contribute majorly to the transport of drugs in human. Amongst all the 7 sub-families of ABC transporters (Table 3.4), ABCB has the highest connectivity to the drugs and small molecules.

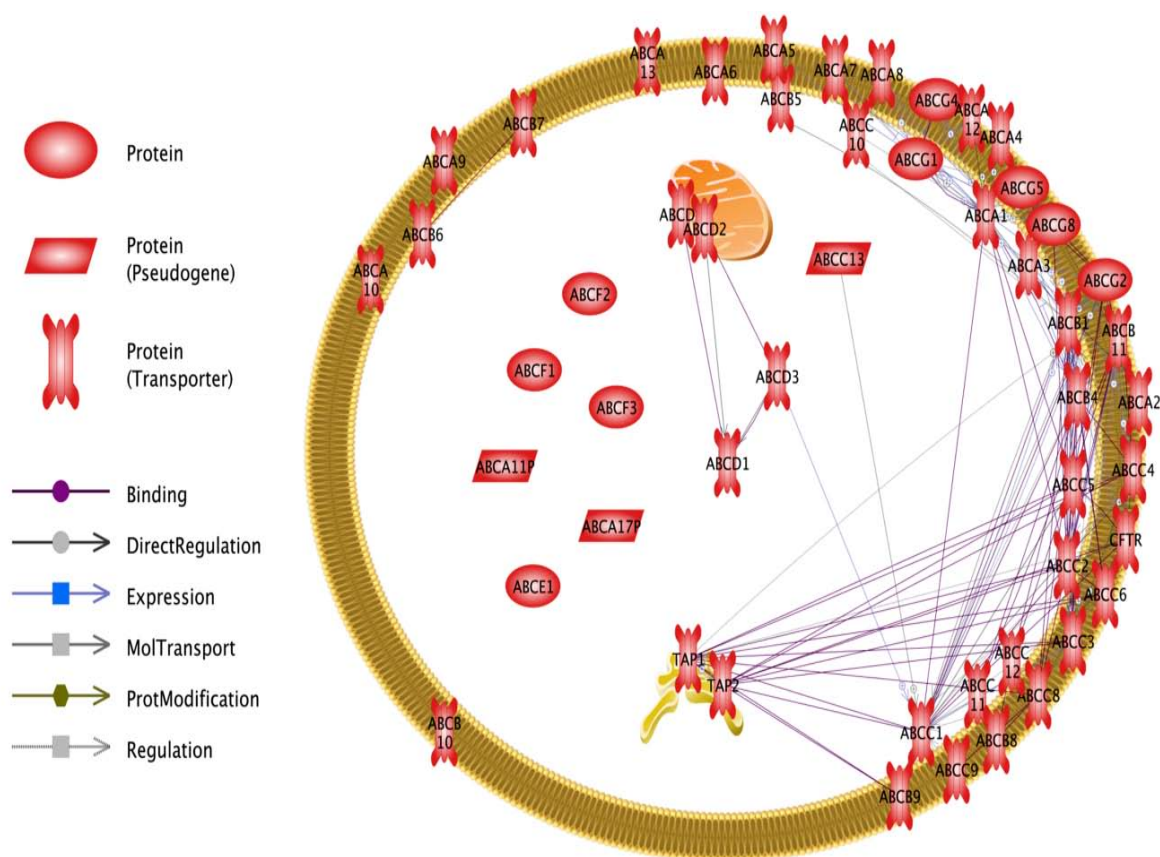


Figure 3.6: Localization and distribution of ABC transporters in Human. ABC transporters are found in the cell membrane, endoplasmic reticulum, mitochondria and cytoplasm as shown in the network generated using PathwayStudio™.

ABCA1 and ABCB1 are the most connected transporters in the pathway analysis of interaction networks (Figure 3.7). The molecules that are majorly connected to these transporters are provided in Appendix B. This interaction network highlights that these ABC transporters play an important role in the cell by mediating the transport of most of the key metabolites and drugs. ABCG2, the transporter of Hoechst dye and Temozolomide drug, also found to be interacting with many compounds in the network.

3.3.4. mRNA abundances of ABC transporters genes: The gene expression of 19 out of the 44 ATP-binding cassette (ABC) transporters profiled was varied between NSP and

U87MG (Figure 3.8). The differential mRNA abundances (17 higher and 2 lower for NSP) potentially contribute to the efficiency of drug and nutrient metabolite transport and efflux.

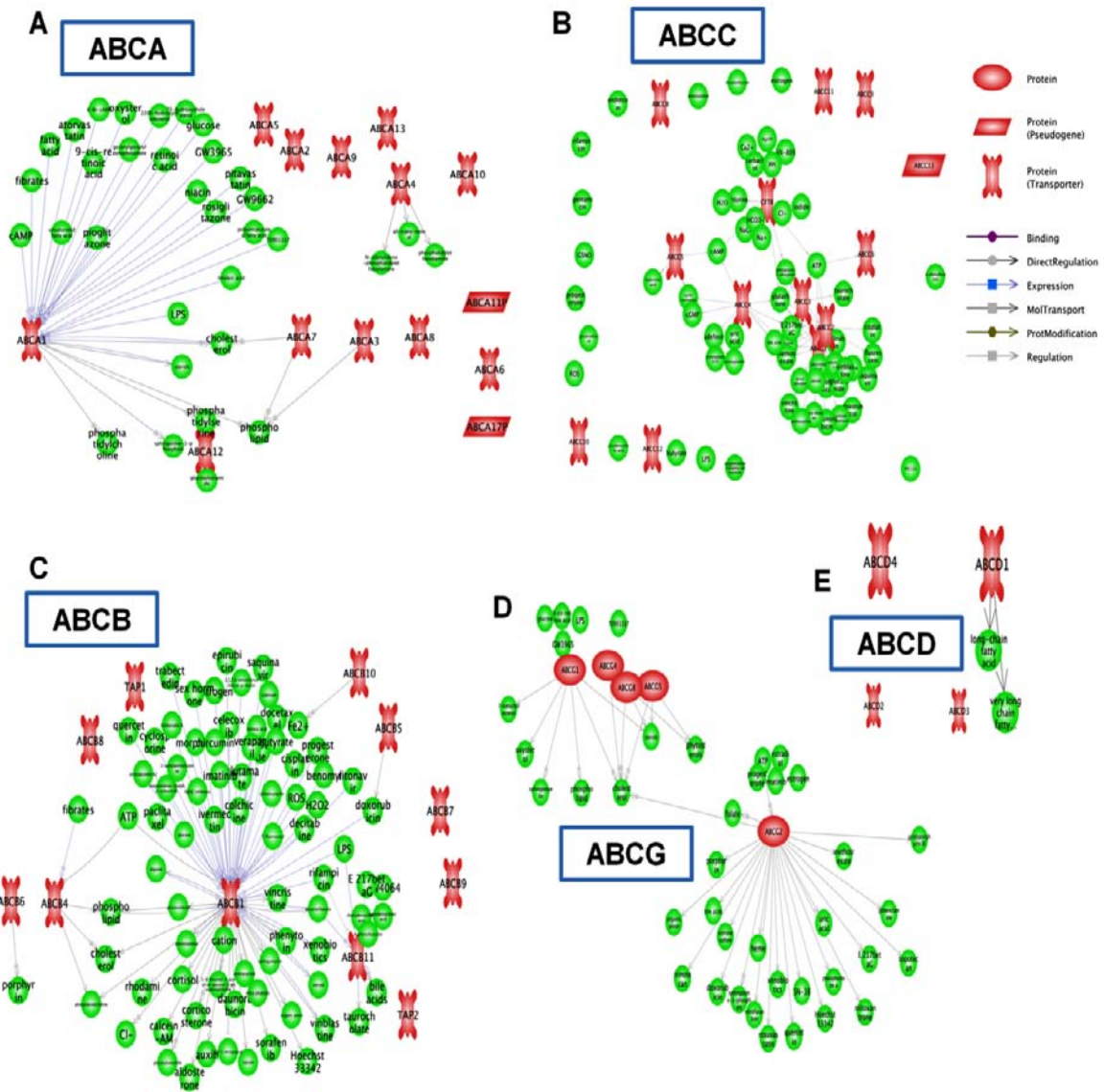


Figure 3.7: Interaction network generated using PathwayStudio™ highlighting the potential transport of metabolites in addition to drugs. ABC transporters are involved in the influx/efflux of drugs/metabolites.

Relative expression highlighted ABCB7 and ABCE1 to be lower for NSP with respect to U87MG. ABCC5 had the highest variation and showed a 10-fold increase in mRNA abundances. Maximum variation was seen in the ABCC subfamily. ABCG2, linked to TMZ transport and Verapamil, showed a 20% increase in mRNA in NSP cells. The varied abundance of transporters was also linked to metabolite transport in the network analysis and is provided in the table in Appendix B.

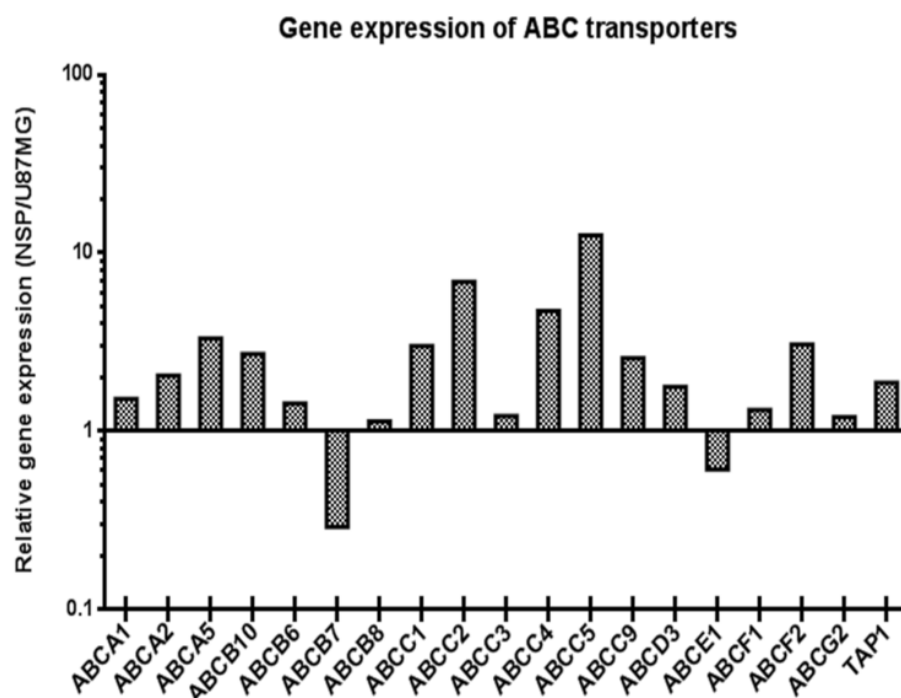


Figure 3.8: Relative gene expression for ABC transporters. The fold change (NSP/U87MG) has been plotted to show their differential mRNA abundances.

Table 3.4: List of ABC transporter genes profiled in this study

Gene Symbol	Approved Name	Synonyms	Chromosome
ATP-binding cassette transporters, subfamily A :			
ABCA1	ATP binding cassette subfamily A member 1	TGD	9q31
ABCA2	ATP binding cassette subfamily A member 2		9q34
ABCA3	ATP binding cassette subfamily A member 3	ABC-C, EST111653, LBM180	16p13.3
ABCA4	ATP binding cassette subfamily A member 4	FFM, ARMD2, CORD3	1p22
ABCA5	ATP binding cassette subfamily A member 5	EST90625	17q24.3
ABCA6	ATP binding cassette subfamily A member 6	EST155051	17q21
ABCA7	ATP binding cassette subfamily A member 7	ABCX	19p13.3
ABCA8	ATP binding cassette subfamily A member 8	KIAA0822	17q24
ABCA9	ATP binding cassette subfamily A member 9	EST640918	17q24
ABCA10	ATP binding cassette subfamily A member 10	EST698739	17q24
ABCA11P	ATP binding cassette subfamily A member 11, pseudogene	EST1133530, FLJ14297	4p16.3
ABCA12	ATP binding cassette subfamily A member 12	DKFZP434G232, LI2	2q34
ABCA13	ATP binding cassette subfamily A member 13	FLJ33876, FLJ33951	7p12.3
ABCA17P	ATP binding cassette subfamily A member 17, pseudogene		16p13.3
ATP-binding cassette transporters, subfamily B :			
ABCB1	ATP binding cassette subfamily B member 1	P-gp, CD243, GP170, ABC20	7q21.12
TAP1	transporter 1, ATP-binding cassette, subfamily B (MDR/TAP)	PSF1, RING4, D6S114E	6p21.3

Gene Symbol	Approved Name	Synonyms	Chromosome
TAP2	transporter 2, ATP-binding cassette, sub-family B (MDR/TAP)	PSF2, RING11, D6S217E	6p21.3
ABCB4	ATP binding cassette subfamily B member 4	MDR2, PFIC-3, GBD1	7q21
ABCB5	ATP binding cassette subfamily B member 5	EST422562, ABCB5beta, ABCB5alpha	7p14
ABCB6	ATP binding cassette subfamily B member 6	EST45597, umat, MTABC3	2q36
ABCB7	ATP binding cassette subfamily B member 7	EST140535, Atm1p, ASAT	Xq13.3
ABCB8	ATP binding cassette subfamily B member 8	EST328128, M-ABC1, MABC1	7q36.1
ABCB9	ATP binding cassette subfamily B member 9	EST122234	12q24
ABCB10	ATP binding cassette subfamily B member 10	EST20237, M-ABC2, MTABC2	1q32
ABCB11	ATP binding cassette subfamily B member 11	ABC16, SPGP, PFIC-2, PGY4	2q24
ATP-binding cassette transporters, subfamily C :			
ABCC1	ATP binding cassette subfamily C member 1	GS-X	16p13.1
ABCC2	ATP binding cassette subfamily C member 2	DJS, MRP2, cMRP	10q24
ABCC3	ATP binding cassette subfamily C member 3	MRP3, cMOAT2, EST90757, MLP2, MOAT-D	17q21
ABCC4	ATP binding cassette subfamily C member 4	MRP4, EST170205, MOAT-B, MOATB	13q31
ABCC5	ATP binding cassette subfamily C member 5	MRP5, SMRP, EST277145, MOAT-C	3q27
ABCC6	ATP binding cassette subfamily C member 6	MRP6, EST349056, MLP1, URG7	16p13.11
CFTR	cystic fibrosis transmembrane conductance regulator	MRP7, ABC35, TNR-CFTR, dJ760C5.1, CFTR/MRP	7q31.2
ABCC8	ATP binding cassette subfamily C member 8	HI, PHHI, SUR1, MRP8, ABC36, HHF1, TNDM2	11p15.1
ABCC9	ATP binding cassette subfamily C member 9	SUR2, CMD10	12p12.1
ABCC10	ATP binding cassette subfamily C member 10	EST182763, MRP7, SIMRP7	6p12.3
ABCC11	ATP binding cassette subfamily C member 11	MRP8	16q12
ABCC12	ATP binding cassette subfamily C member 12	MRP9	16q12.1
ABCC13	ATP binding cassette subfamily C member 13	PRED6, C21orf73, ABCC13P	21q11.2
ATP-binding cassette transporters, subfamily D :			
ABCD1	ATP binding cassette subfamily D member 1	AMN, ALDP, adrenoleukodystrophy	Xq28
ABCD2	ATP binding cassette subfamily D member 2	ALDR, ALDRP	12q12
ABCD3	ATP binding cassette subfamily D member 3	PMP70, ZWS2	1p21.3
ABCD4	ATP binding cassette subfamily D member 4	PMP69, P70R, EST352188	14q24
ATP-binding cassette transporters, subfamily E :			
ABCE1	ATP binding cassette subfamily E member 1	RLI, OABP	4q31
ATP-binding cassette transporters, subfamily F :			
ABCF1	ATP binding cassette subfamily F member 1	EST123147	6p21.33
ABCF2	ATP binding cassette subfamily F member 2	EST133090, ABC28, M-ABC1, HUSSY-18	7q36.1
ABCF3	ATP binding cassette subfamily F member 3	EST201864	3q27.1

Gene Symbol	Approved Name	Synonyms	Chromosome
ATP-binding cassette transporters, subfamily G :			
ABCG1	ATP binding cassette subfamily G member 1	ABC8	21q22.3
ABCG2	ATP binding cassette subfamily G member 2 (Junior blood group)	EST157481, MXR, BCRP, ABCP, CD338	4q22.1
ABCG4	ATP binding cassette subfamily G member 4	WHITE2	11q23
ABCG5	ATP binding cassette subfamily G member 5	STSL	2p21
ABCG8	ATP binding cassette subfamily G member 8	GBD4	2p21

3.4. Discussion

Chapter 3 provides key evidence for differences in measured gene expression within the GBM heterogeneous cell line U87MG. Our study underscores the significance and challenge of identifying heterogeneous populations as important to gene expression analysis. The mRNA abundances in the NSP cells possibly reflect metabolism in a microenvironment of low glucose and high glutamine (also supported by the data from **Chapter 2**). The differential growth factor signaling mediated by AKT1 that showed differential mRNA abundances is seen as a consequence of relatively low glucose levels in the microenvironment of NSP. The glutamine is converted to glutamate and AKG and the TCA may operate in the opposite direction and provides anaplerotic AKG to make glycolysis slower and reprogram it into ribose synthesis through PKM2 (Figure 3.9). AKG was shuttled through reductive carboxylation to shuttle NADPH equivalents needed for pyrimidine or fatty acid biosynthesis (Mazurek et al. 2005) events.

The increased expression (high mRNA abundances) of IDH1 and IDH2 are a means to shuttle and derive more cytosolic NADPH needed to support pyrimidine/fatty acid synthesis. The simultaneous negative regulation of ACL by AKT1 lowers the acetyl CoA pool and hence the acetate potentially available for histone acetylation (reflected in the lower levels of histone acetylase H3F3A). The higher mRNA levels of cytokines STAT3 turn on the transcriptional program of MYC and induce consumption of glutamine in NSP that is reflected in the metabolite profiles of the environment in **Chapter 2**. The MGMT levels are similar in the absence of TMZ. HIF1A also has differential mRNA abundances across the heterogeneous populations in comparison to the parental population. This highlights a differential regulation in the glycolysis of these two cell types that may contribute to the differential glucose uptake in the metabolite profile in the LC-MS/MS analysis of extracellular profiles. 19 out of the 44 ATP-binding cassette (ABC) transporters profiled, were varied between NSP and U87MG. Relative gene expression highlighted

ABCB7 and ABCE1 to be lesser in the expression for NSP with respect to U87MG. ABCC5 had the highest variation and showed a 10-fold increase in the gene expression.

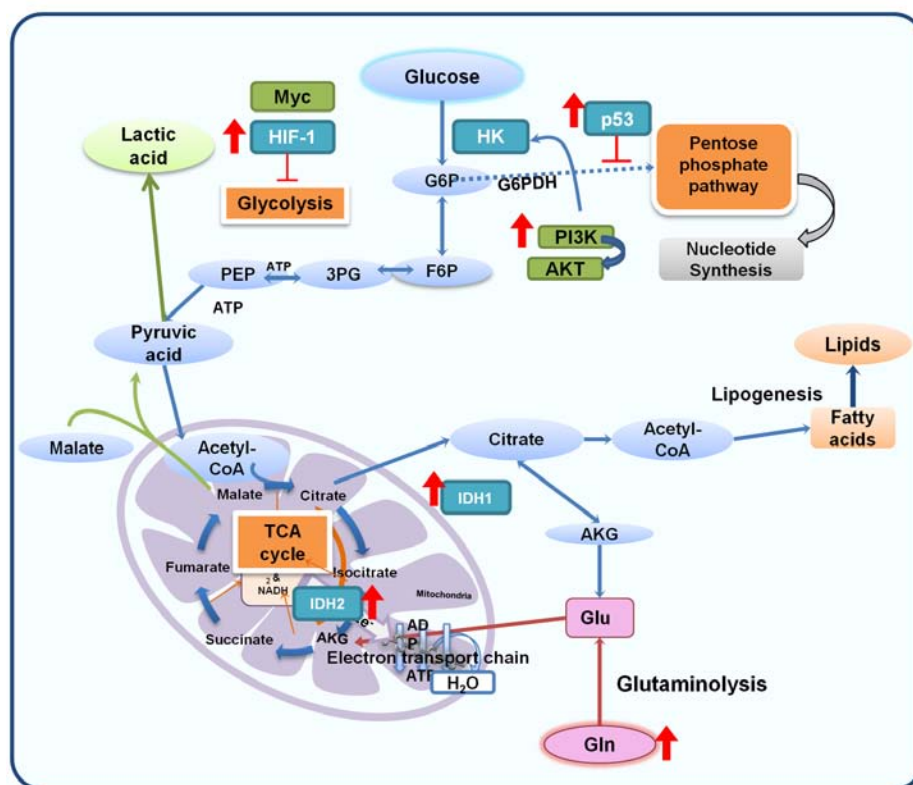


Figure 3.9: CAN genes and metabolism. Red arrows indicate the inferences from mRNA abundances profiled using qPCR and its influence on metabolism.

In an overall comparison of mRNA abundances, the ABCC subfamily of ABC transporters had the maximum variations. ABCG2 that is linked to the transport of temozolomide and verapamil, showed 20% increased gene expression in NSP. Literature evidence for ABC transporters to be responsible for the transport for other metabolites are also existing (Sahoo et al. 2014). By complimenting to the transport of the key metabolites, ABC transports not only help in the drug efflux but also in the cell metabolism for the cell to survive in the selection pressure, thereby eventually increase the chances of cancer relapse.

3.5. Conclusions

The work described herein provokes a new insight into the drug resistance problem and highlights the potential role of cell metabolism along with drug efflux mechanism of the cells by profiling the CAN genes and ABC transporters. These results suggest that the

mRNA abundances of CAN genes potentially regulate the cell metabolism in addition to the differential mRNA abundances of ABC transporters. Also, these transporters that show a differential expression profiles in NSP may potentially not only transport drugs but also other metabolites like cholesterol critical for growth and proliferation. Hence, indicating that the drug resistance in NSP might be a combined effect of CAN genes, drug transporters, and metabolism.

Chapter 4

Exome Characterization: Towards Genetic Basis for Temozolomide Resistance

"It is not the strongest of the species that survives, nor the most intelligent that survives. It is the one that is most adaptable to change".

- Charles Darwin

"Only time and money stands between us and knowing the composition of every gene in the human genome".

-Francis Crick

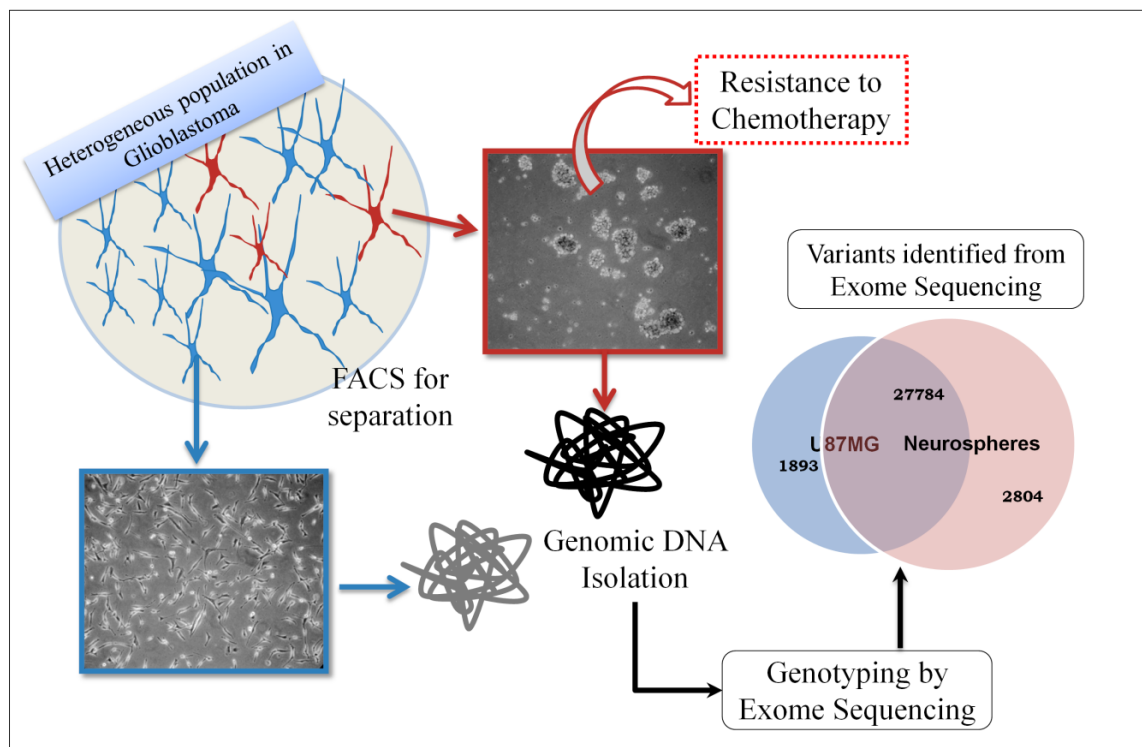


Figure 4.1: Graphical abstract of Chapter 4.

Abstract

Genomic alterations play a vital role in oncogenesis, tumor progression and tumor response to therapy. Single nucleotide polymorphisms specific to certain cancer types become biomarkers that can drive precision medicine. The main focus of cancer systems biology is on unraveling genome sequence variation in the context of SNP databases to identify the heretofore unknown genetic basis of the multifactorial response. Targeted Exome (coding regions of the genome) Capture, a recent advancement in Next-Generation Sequencing (NGS), is cost effective and can be used to unveil these genomic alterations effectively without any further validation. In this chapter, U87MG and Neurospheres are exome characterized and the genetic alterations identified including the known SNPs in key signaling genes such as PTEN, TP53, KRAS, and MTOR and other INDELs by aligning the sequence to the human genome (hg19, build 37). The total number of variants identified from U87MG exome was 30,704 (SNPs - 97%; INDELs - 3%) and from NSP was 31,776 (SNPs - 96%; INDELs - 4%). Functional effect of these mutations has been analyzed using Oncotator (Oncotator v0.4.1.8) web-based tool which annotates point mutations and INDELs. This genomic and protein annotations include the identification of gene names, functional consequence (e.g. Missense, silent, Intron), PolyPhen-2 predictions, common SNP annotation from dbSNP, and cancer-specific annotations from resources such as COSMIC, Tumorscape, and published MutSig results. Further, the metabolic and non-metabolic genes were analyzed using the gene set from Recon 1 (Human metabolic reconstruction model). Thereby, this part of the thesis drives the way towards systems-level characterization using Exome sequencing for the better understanding of the genomic basis behind the temozolomide resistance.

4.1. Introduction

Cancer is a complex disease, that involves genetic, epigenetic, transcriptomic and proteomic differences in comparison with the normal/healthy state of the cell and eventually leads to metabolic rewiring (Hsu & Sabatini 2008; Gaude & Frezza 2014; Cantor & Sabatini 2012). As this complex disease has always been thought of as a genetic disease, characterization of the genotype of the cancer cell in terms of somatic or germline mutations is very important especially to understand drug resistance (Auger et al. 2006; Turner & Reis-Filho 2012). **This chapter** comprises of the genetic characterization of the identified temozolomide resistant versus the sensitive population of cells from U87MG. In recent years, the impact of new DNA sequencing technologies on the detection, diagnosis, and treatment of cancer is becoming significant in many ways (Mardis 2008). U87MG is one of the commonly used cell lines to study Glioblastoma. This cell line is derived from grade IV glioblastoma patient and it has been addressed in more than 1800 publications till date (Pei et al. 2014; Bernhart et al. 2013; Vacas-Oleas, 2013; Immanuel et al. 2018). The genomic landscape of this cell line has already been of interest due to the criticality of genome-based transition in the disease prognosis (Frattini et al. 2013). In addition, the whole genome of this cell line has been completely sequenced (Clark et al. 2010) with higher sequence coverage. To characterize the complete genome, greater than 30x genomic sequence coverage has been used with a novel 50-base mate-paired strategy containing ~1.4kb insert library (Clark et al. 2010).

4.1.1. Next-generation sequencing

Recent advances in sequencing technologies enable many researchers to delineate the genotype of the systems under study. Whole genome sequencing has become available in a very easy and affordable way because of the next generation sequencing (NGS) technologies (Metzker 2010). These technologies allow many worldwide collaborative efforts including the International Genome Consortium (ICGC) and The Cancer Genome Atlas (TCGA) project to easily catalog thousands of cancer genomes and also for many other diseases thereby supporting the detailed study on disease prognosis and diagnosis. These technologies will eventually contribute to the better understanding of the diseases to bridge the new era of molecular biology advances to personalized medicine (Meldrum et al. 2011). By the use of NGS, it is no longer the narrow-down approach to sequence genes one by one but to a higher extent of sequencing all genes in a single experiment and

correlate it to disease-causing variants. Instead of sequencing the targeted genes and comparing, the whole genome can be compared with the healthy human genome and the variants can be identified with high coverage score precisely. However, finding the causal variants from thousands of identified variant can be challenging.

4.1.2. Exome sequencing

Sanger et al in 1977 first described the dideoxy-nucleotide sequencing of DNA that has now improved and many such findings added the essence of sequencing then. This improved the technology to a fast, economic and large-scale sequencing of the human genome. The complete genome of human was published on 15th February 2001 in Nature journal. This covered only 90% of the euchromatic genome with 250,000 gaps and contained some errors in the nucleotide sequence. From then, the sequencing technologies have undergone a steady improvement and growth with the computer databases having specialized instrumentations.

It is well known and established that the changes in the genome play a very important role in oncogenesis, disease progression and drug response of tumors to chemotherapy. The improvements and advances in next-generation sequencing technologies (NGS) would definitely provide capabilities to sequence the complete genomes for changes including single nucleotide polymorphisms (SNPs), point mutations, deletions, insertions and changes in chromosomal copy number. However, the amount of data generated in genome sequencing and the cost for whole genome sequencing still prevents the routine application of NGS in many types of research. On the other hand, the capturing and sequencing of only the coding regions of genes - exons constituting the “exome” can be a cost-effective and less-data generation approach for identifying changes in genes that result in alteration of protein sequences.

Genomic alterations of coding regions in cancer cells change the normal functions and pathways of the cell including proliferation and apoptosis. These pathways are essential for tumor genesis, growth, and metastasis in the cancer cell. Also, the unique combination of mutations in its genome makes the cancer cell-specific and it can lead to heterogeneity in cancer prognosis and responses to therapy. Exome sequencing methods can be used for such analyses and can deliver sequencing information (SNPs and INDELs) for functionally relevant genome at increased coverage and reduced cost. Human cancer cell line models play a critical role in the understanding of cancer prognosis, identification, and validation

of causal genes and to screen for potential drug targets. Though these cell lines acquire some mutations during the cell line development and passage stages, these cell lines definitely carry the genetic and somatic mutations from their source. Hence, comparisons between cell lines that are sensitive to drugs to that of resistant cells, reveal any heterogeneity in genomic mutations and could help in identifying the causal pathways.

4.1.3. Overall workflow of exome sequencing

The term "Exome" is used to describe the complete set of exons (coding regions) in the genome. These regions are transcribed into mRNA (messenger RNA) thereby expressed as proteins. Exome sequencing technology captures the variants in the coding region of the genome that could possibly affect the protein function. The workflow (Figure 4.2) required to sequence and to analyze an exome using Ion Proton™ systems (Life technologies Pvt. Ltd., India) is as follows:

1. Genomic DNA isolation from the sample (cells).
2. Fragmentation of the genomic DNA for capture and short read using NGS.
3. Construction of a library.
4. Targeted capture of exons using biotinylated probes (Template).
5. Amplify captured targets.
6. Sequence using an instrument with a 2x100 or 2x150 read length.
7. Analyze captured information, call variants using TorrentSuite and Ion Reporter software.



Figure 4.2: Workflow for Exome sequencing using the Ion proton system. Source: Life technologies pvt.ltd. manual and website.

While there are ~180,000 exons in the human genome, that constitutes less than 2% of the total genome, the exome possibly contains ~80-90% of known disease-causing variants making it a cost-effective alternative to whole genome sequencing (WGS).

4.1.4. Application of Exome sequencing in cancer research

One of the major challenges facing the field of cancer genome sequencing is to identify and validate the mutations in cancer-associated genes that drive the cancer phenotype. The most effective way of identifying these causative mutations is through the NGS. Exome sequencing is a high-throughput technique that can be used to analyze a large number of samples simultaneously. Recent studies highlight the use of exome sequencing to profile the mutational impacts on NCI60 cell lines for systems pharmacology applications (Cheng et al. 2014; Abaan et al. 2013). Many types of research use exome sequencing as a tool to identify and characterize the disease state (Ng 2008; Ng et al. 2010; Wei et al. 2011; Ng et al. 2009; Chang et al. 2011; Liu et al. 2012; King et al. 2011). These technologies are revolutionizing medical diagnostics and help in improving our understanding of the basis behind every stage of cancer.

4.2. Methods

4.2.1. Genomic DNA extraction: The complete/genomic DNA extraction from cultured U87MG and NSP cells were performed using DNeasy Blood & Tissue Kits Spin-column protocol (Qiagen, India). A total of 4×10^6 each U87MG and NSP cells were centrifuged for 5 min at 300 x g and resuspended in 200 μ l PBS each. 20 μ l proteinase K was used in the initial step to lyse the cells. The manufacturer's protocol was closely followed. 4 μ l RNase A (100 mg/ml) was used to remove any RNA contamination from the extracted DNA by incubating for 5 min at room temperature. ~15 μ g of genomic DNA was extracted from each sample. This extracted DNA (Figure 4.3) was used for the Exome sequencing.

4.2.2. Exome sequencing: Exome workflow of Ion Proton™ systems (Life technologies Pvt. Ltd., India) was used to obtain the Exome sequences of U87MG and NSP cells. Ion TargetSeq™ Exome Kit and Ion Proton™ sequencer was used for acquiring the Exome data that was further processed through TorrentSuite and Ion Reporter software to identify the variants and for the coverage analysis.

4.2.3. Functional annotations of Exome data: The variants of U87MG and NSP cells thus identified by Exome sequencing had been analyzed for its functional effect using

Oncotator web tool (<https://portals.broadinstitute.org/oncotator/>). Oncotator is a web-based application that is used for annotating human genomic point mutations including Single Nucleotide Polymorphisms (SNPs) and Insertions & Deletions (INDELS).

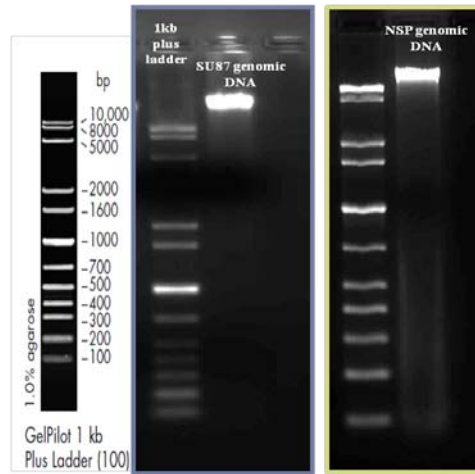


Figure 4.3: Genomic DNA isolated from U87MG and Neurospheres (NSP). Quality of the DNA was checked by running on an agarose gel.

This includes genomic annotations (Gene, transcript, and functional consequence annotations for the hg19 database), protein annotations (Site-specific protein annotations from UniProt, functional impact predictions from dbNSFP and cancer variant annotations), and common SNP annotations from the dbSNP database. The input file contained the details of the position in chromosomes, reference and its corresponding variants identified that was uploaded in the web tool for analysis. The output file had the results with details of the gene name, gene IDs, HUGO symbol, variant classifications (Silent, 5'-UTR, 3'-UTR, Intron, Missense, Frameshift deletions), gene description, protein/amino acid change and its biological functions. These details were further used in the analysis and interpretations.

4.3. Results

4.3.1. Exome statistics

Exome, the coding part of the genome consisting of the complete set of exons, was sequenced using next-generation sequencing platform to assess the genomic variability across the two cell types (U87MG and NSP). With exome sequencing, in addition to faster turnaround time and cost-effectiveness, data analysis and interpretation is less complex. In order to identify the DNA variants most possibly contributing to the heterogeneity and

temozolomide resistance, within exome - 1% of the genome (protein coding sequence), the genomic DNA of both these cell types was pipelined in the exome sequencing workflow. The identified variants were considered from the targets with base coverage at 20x with 92.22% recovery in U87MG exome and 95.00% recovery in NSP exome (Figure 4.4). Further, to account for the somatic variants (from dbSNP and COSMIC databases), the identified variants were first cross-checked with the known reference variants of the human genome (hg19 – NCBI build 37). The total number of variants identified from U87MG exome was 30,704 (SNPs - 97%; INDELs - 3%) and from NSP was 31,776 (SNPs - 96%; INDELs – 4%). Concordance between dbSNP and COSMIC databases entry identified 1,804 variants as novel (uniquely from our study) in U87MG exome and 795 in NSP (Figure 4.4).

4.3.2. Genomic variability across the sensitive and resistant cells

A total of 11,733 genes from NSP and 11,571 genes from U87MG has the variants identified (SNPs and INDELs). 11,174 genes were found to be common between U87MG and NSP identifying 559 and 397 unique genes for NSP and U87MG respectively (Figure 4.4). The same analysis was extended to genes with only SNPs (Common – 11,002; Unique in U87MG – 292; Unique in NSP – 453), SNPs by position (Common – 27,784; Unique in U87MG – 1893; Unique in NSP – 2804), insertion by position (Common – 143; Unique in U87MG – 62; Unique in NSP – 395) and deletion by position (Common – 408; Unique in U87MG – 412; Unique in NSP – 230). Such analyses highlighted the differential exomic variants identified across the drug-sensitive (U87MG) and resistant (NSP) cells, characterizing these populations as different.

4.3.3. Distribution of SNPs in chromosomes

Overall distribution of variants was assessed by chromosome-wide analysis (Figure 4.5). The number of unique SNPs in NSP and U87MG was different indicating that these two cell types possibly share genomic variability. Variant span with variant frequency (data from variant calling) had been plotted to have an overall view of the effect of this genomic variability on the chromosome and to identify the highly altered chromosome (Figure 4.5). Chromosome 2 and 19 showed maximum variants profiled in both U87MG and NSP.

4.3.4. Functional characterization of the identified exome variants

Functional characterization of the variants was delineated using Oncotator web tool that further classified the SNPs as 3'UTR, 5'UTR, 5'Flank, IGR, intron, missense mutation,

nonsense mutation, nonstop mutation, RNA, silent, splice site, and translation start site.

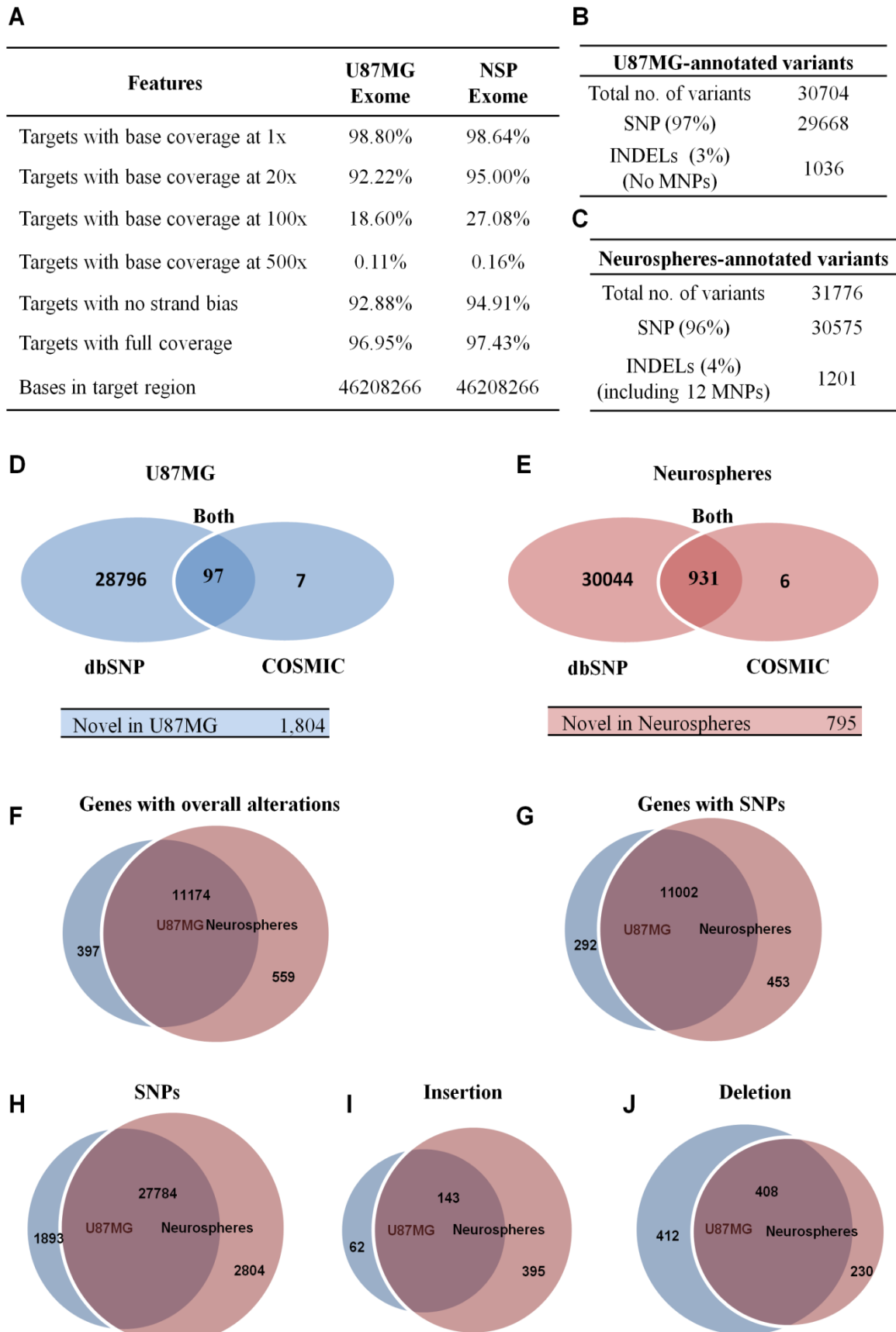


Figure 4.4: Exome variants statistics.

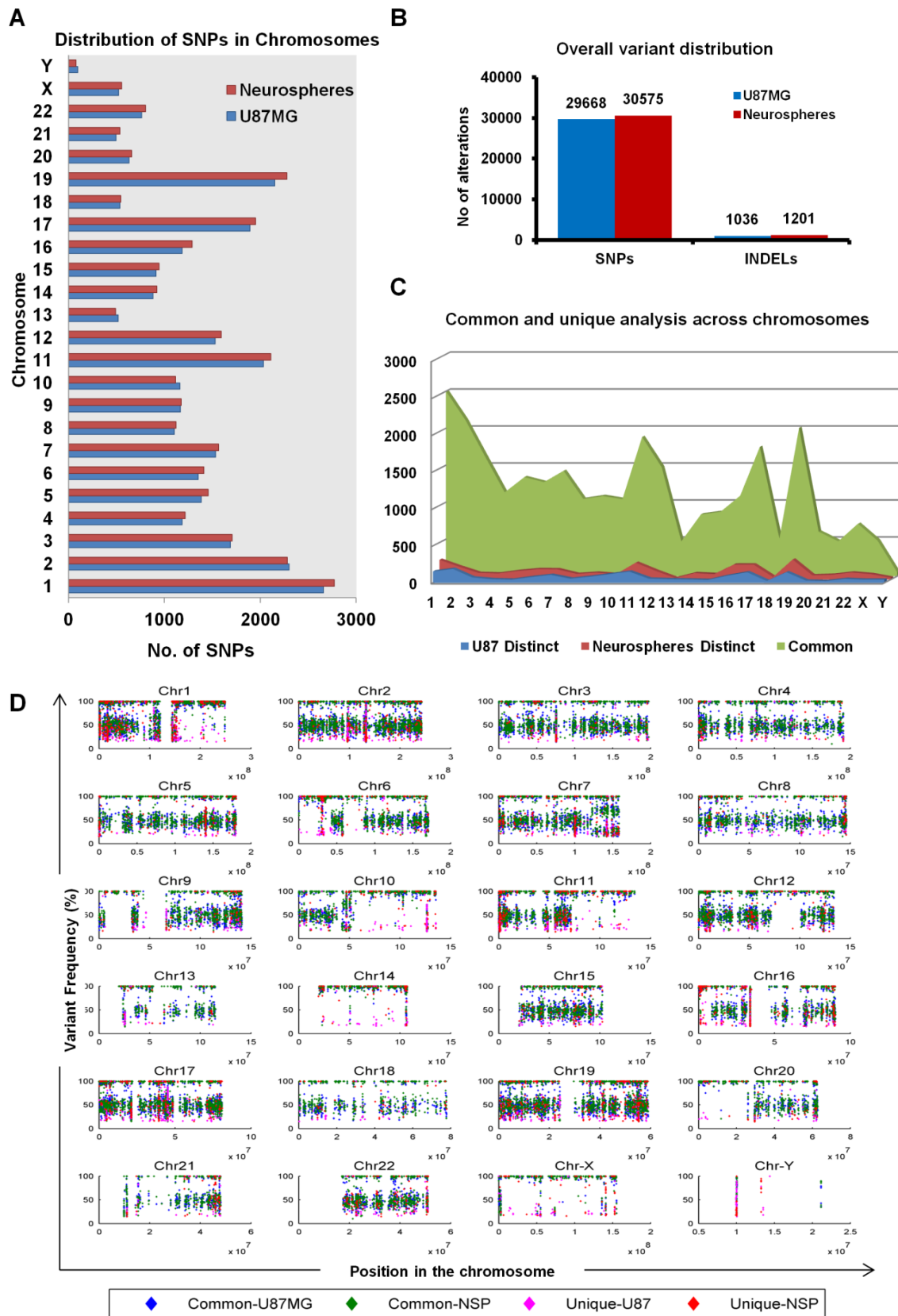


Figure 4.5: Chromosome-wise distribution of exome variants.

These annotations also output the gene name associated with the variants based on their

position in the chromosomes and protein descriptions (Figure 4.6A). These genomic annotations are further classified for the effect on protein function using site-specific protein annotations from UniProt, druggable target data from DrugBank and functional impact predictions from PolyPhen-2 for all the identified variants. Cancer annotations also have been performed using Oncotator web tool to identify the known gene alterations that are present in the databases including COSMIC, Cancer Gene Census, Tumorscape, TCGA Copy Number Portal, Overlapping Oncomap mutations from the Cancer Cell Line Encyclopedia and MutSig analyses. Of the variants classified, silent mutations (9819 - U87MG; 10344 - NSP) and missense mutations (9161 - U87MG; 9382 - NSP) form the majority of identified variants in U87MG and NSP (Figure 4.6 B and C).

4.3.5. Homozygous and heterozygous variants

A total of 11,733 genes from NSP and 11,571 genes from U87MG had the variants in the study, of which, 7055 genes from NSP and 6722 genes from U87MG has homozygous entries (>90% variant frequency calling). 6603 genes are common across these two populations wherein 452 and 119 genes are unique in NSP and U87MG respectively. Similarly, the same analyses have been performed for common and unique genes in heterozygous variants from Exome (Table 4.1 and 4.2).

Table 4.1. Genes with homozygous variants in Exome of U87MG and NSP.

U87MG		
	Total	Homozygous
Total Genes	11571	6722
Common	11174	6603
Unique	397	119
Neurospheres		
	Total	Homozygous
Total Genes	11733	7055
Common	11174	6603
Unique	559	452

4.3.6. Transversions and transitions

Transversions are point mutations (SNPs) that changes a purine to pyrimidine (A to C; A to T; C to A; C to G; G to C; G to T; T to A and T to G) and transitions are SNPs that changes a purine to another purine (A to G; G to A; T to C; and C to T). The ratio between transition/transversion for U87MG= 24.99/12.49 = 2; and for NSP= 24.99/12.495 = 2. (Figure 4.7)

A

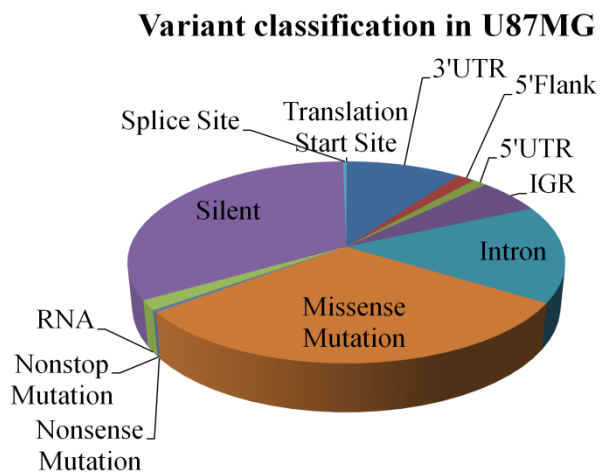
Genomic Annotations
 UCSC KnownGenes hg19 and mirBase reference sets.
 Common SNP annotations from dbSNP

Protein Annotations
 Site-specific protein annotations from UniProt.
 Druggable target data from DrugBank.
 Functional impact predictions from PolyPhen-2.

Cancer Annotations
 COSMIC.
 Cancer Gene Census.
 Tumorscape and theTCGA Copy Number Portal.
 Overlapping Oncomap mutations from the Cancer Cell Line Encyclopedia.
 MutSig analyses.

B

Variant Type	U87MG
3'UTR	2951
5'Flank	445
5'UTR	369
IGR	1651
Intron	4622
Missense Mutation	9161
Nonsense Mutation	98
Nonstop Mutation	8
RNA	472
Silent	9819
Splice Site	72
Translation Start Site	10



C

Variant Type	Neurospheres
3'UTR	3012
5'Flank	439
5'UTR	402
IGR	1628
Intron	4723
Missense Mutation	9382
Nonsense Mutation	97
Nonstop Mutation	7
RNA	481
Silent	10344
Splice Site	63
Translation Start Site	10

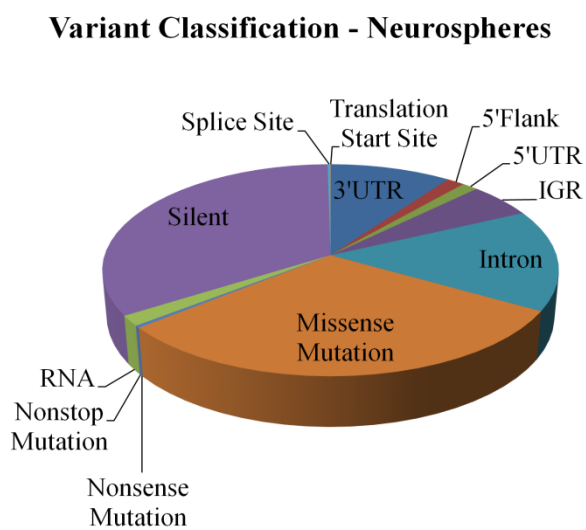


Figure 4.6: Functional characterization of exome variants.

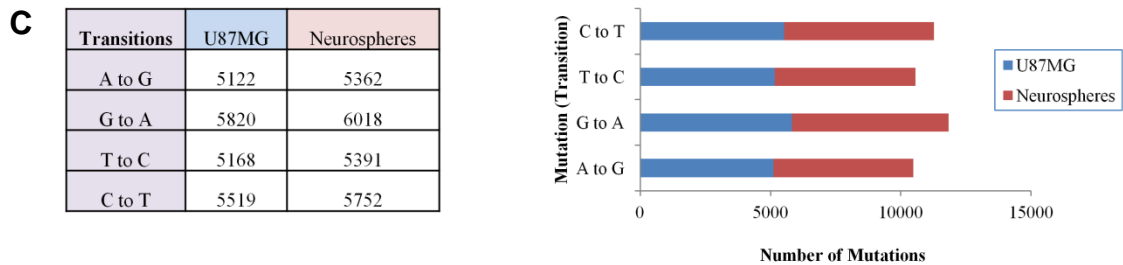
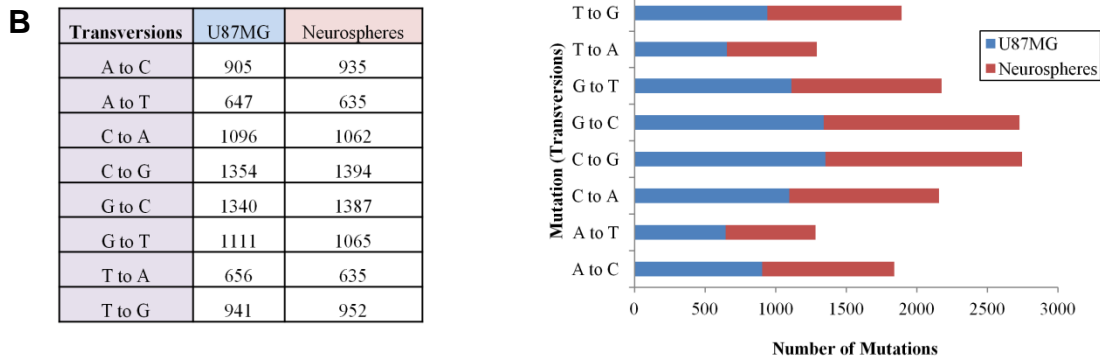
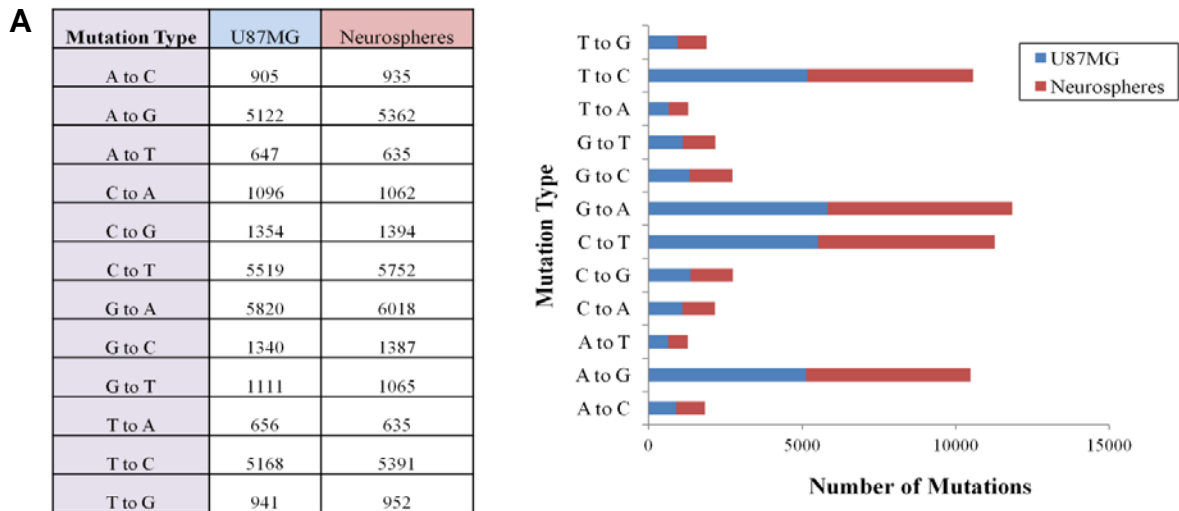


Figure 4.7: Transversions and transitions.

Table 4.2. Percentage of heterozygous and homozygous variants.

Details	U87MG	Neurospheres
Heterozygous (SNP)	16813	16730
Homozygous (SNP)	12866	13858
Total (SNP)	29679	30588
% Heterozygous	56.64%	54.69%
% Homozygous	43.35%	45.30%

4.3.7. Metabolic genes with exome variants

Metabolic genes were selected based on the Recon1 (Human metabolic reconstruction model) (Rolfsson et al. 2011) to understand the variant distribution across these two cell types. A total of 540 (NSP) and 511 (U87MG) genes were identified (with VarFreq >70)

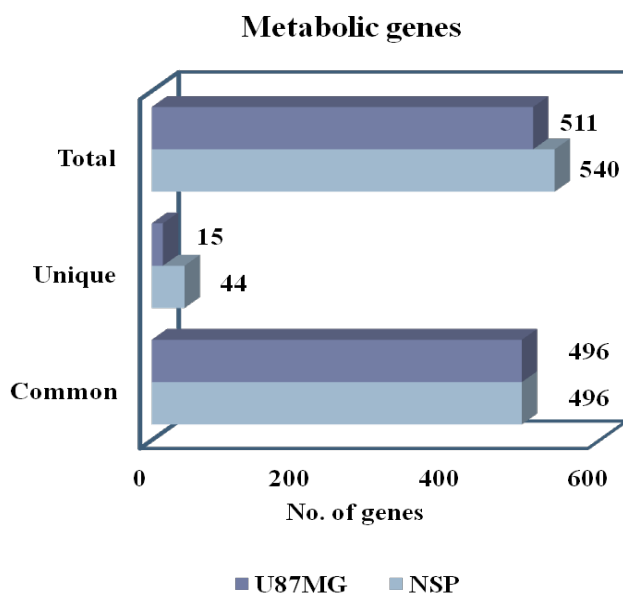


Figure 4.8: Metabolic gene variants in Exome.

with variants, of which, 44 (NSP) and 15 (U87MG) were found to be unique (Figure 4.8). These unique genes in NSP included GPX1, ME1, GCLM, GCLC, PGK2, GSS, ADK, CYC1, NDUFS7 and SLC14A1 (Urea transporter). U87MG cells have GK, SORD, NDUFA11, ABCC5, and SLC2A11 (Glucose transporter isoform C) among the 15 unique genes. These unique genes potentially contribute to the rewiring of metabolism in NSP that

supports resistance and growth. These predictions of functional analyses could thereby highlight the differences in the genetic makeup of resistant and sensitive cells in U87MG, suggesting further needs to access the functional impact of these alterations *in vitro*.

4.4. Discussion

4.4.1. Possible impact of homozygous variants on the metabolism of temozolomide-sensitive and temozolomide-resistant cells

The exome variants were further characterized and classified into homozygous synonymous and non-synonymous mutations. A synonymous substitution (also known as "silent substitution") is the substitution of one nucleotide base for another nucleotide base in the protein-coding part of the gene (exon), in such a way that the protein or the amino acid sequence is not modified due to the redundancy of the genetic code. Synonymous substitution usually occurs in the third position of the codon, changing the codon alone but not the amino acid. On the other hand, a nonsynonymous substitution is a nucleotide change that alters the amino acid sequence of a protein. Nonsynonymous substitutions differ from synonymous substitutions, in such a way that the substitutions occur in the first

and second position in the codon thereby leading to an amino acid change in the protein, eventually modifying the protein sequence. The homozygous (>90% of variant frequency in the variant calling) and nonsynonymous mutations are expected to have a protein change with an expectancy of more than 85%. Though these modifications need experimental confirmations, they can lead to a firm hypothesis as such, owing to its nature of decreased or blocked protein activity. By considering this fact, the possible impact of these homozygous nonsynonymous mutations is delineated in our study.

The genes that are involved in the signaling pathways often contribute to metabolism (Yecies & Manning 2011; Ríos et al. 2013; Hardie 2013; Nieminen et al. 2013). By addressing the effect of these dysregulated pathways may have an insight into the altered metabolism. TSC1, one of the controllers of mTORC1 (Figure 4.9), has a unique deletion in U87MG in homozygous entries. The stimulation of the TSC1-TSC2 complex by oncogenic regulation by tumor suppressors and oncogenes may inhibit the activation of mTORC1. This hypothesis highlights the impact of mTORC1 on glucose uptake and glycolysis (Figure 4.9). U87MG is proposed to prefer glucose uptake over glutamine and prefers more glycolysis than TCA cycle as discussed in **Chapter 2**. These mutations from exome data also support this hypothesis that was based on the metabolite levels from LC-MS/MS data in these cells, wherein the inhibition of mTORC1 is possibly prevented by the TSC1 mutation in U87MG.

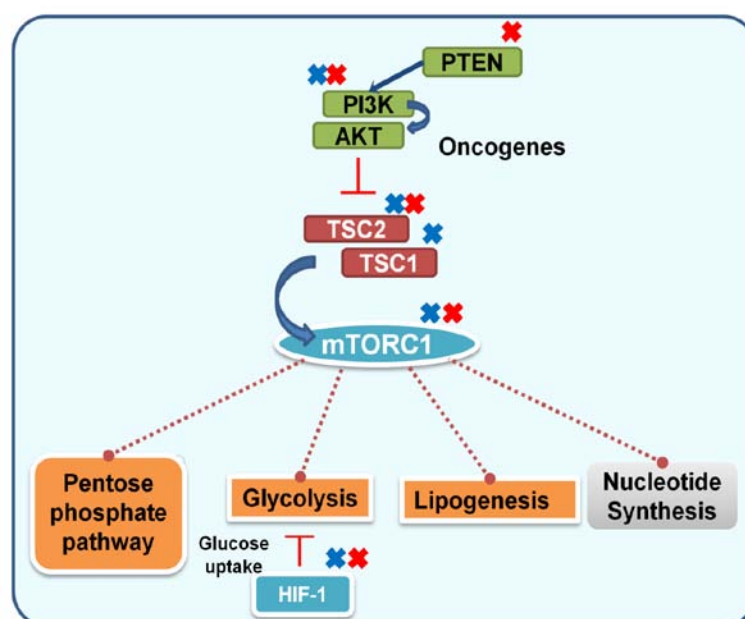


Figure 4.9: Signaling genes that majorly controls metabolism. Red cross indicates mutation in NSP and a blue cross indicates mutation in U87MG from the exome data.

Another potential impact is on the cellular levels of polyamines that would possibly help for the survival of cells, by “MYC” guided activation of ODC (Ornithine Decarboxylase) Enzyme. ODC Enzyme is well characterized in human. It is involved in polyamine biosynthesis. It is the key enzyme that controls the initial step of conversion of ornithine to putrescine. The polyamines such as putrescine, spermine and spermidine play an important role in cell cycle and proliferation (Gerner & Meyskens 2004).

In the exome data, APC gene has seven mutations in both the cells. APC suppresses transcription of MYC. MYC is an activator of ornithine decarboxylase (ODC). ODC antizyme (OAZ) is a protein that regulates ODC activity by targeting it for degradation (Figure 4.10).

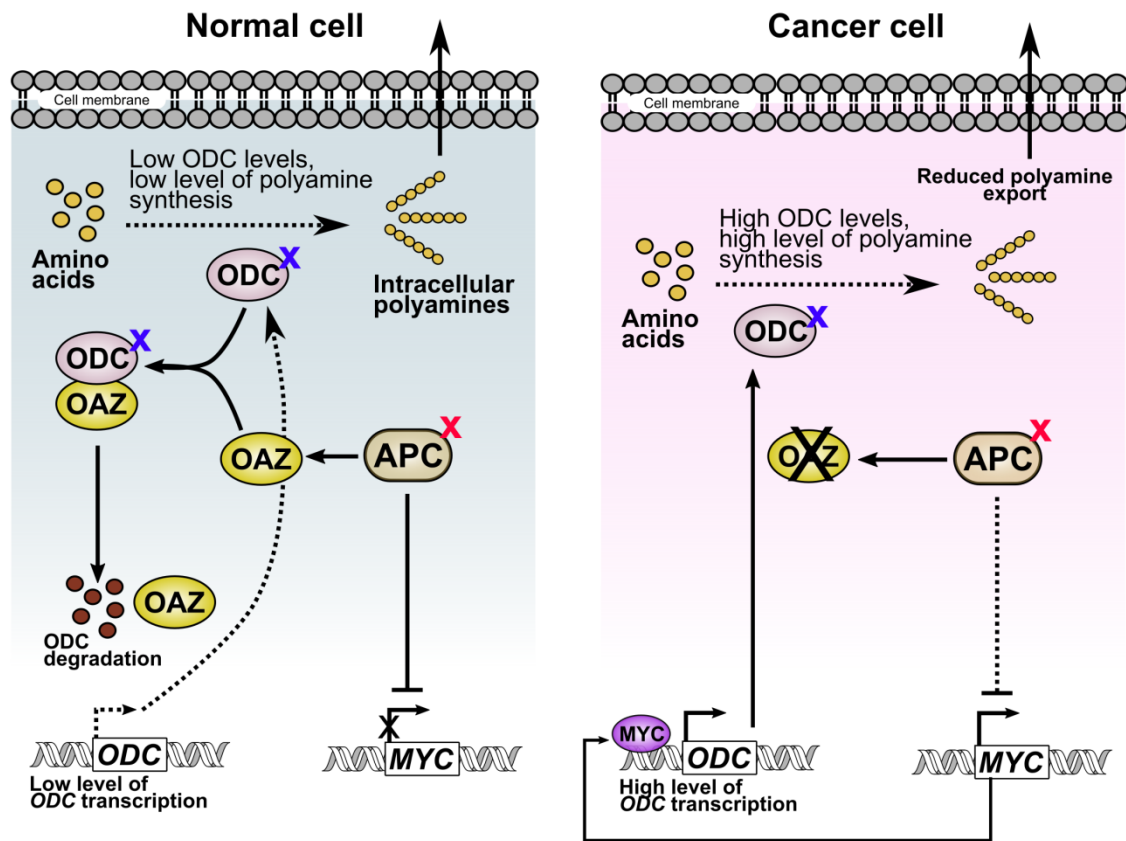


Figure 4.10: Polyamines and cancer. The differences in the normal cell metabolism and cancer cell metabolism are shown based on Gerner & Meyskens 2004. Red cross indicates mutation in NSP and a blue cross indicates mutation in U87MG from the exome data.

OAZ1 has mutations in U87MG alone. KRAS has 4 mutations in U87 and 5 mutations in NSP. KRAS leads to reduced proliferation, increased apoptosis, and reduced neoplasia. One of the tumor suppressors, peroxisome proliferator-activated receptor (PPAR), activates spermidine /spermine N1-acetyltransferase (SSAT) transcription and is repressed by active

KRAS in normal cells. This PPAR gene has mutations in both. Hence, there is a firm possibility that the regulation of MYC guided ODC activation can lead to the survival of neurospheres and that is different in the case of U87MG.

Some of the other unique mutation profiles that could potentially shape metabolic response in U87MG include mutations in AMY2A that could modulate glucose availability through starch hydrolysis. The genetic variations in fucose pathways with a unique change in FUT8 also indicate a disruption in the GDP-GTP pool. The redox balance through NADH/NADP synthesis could be potentially affected by unique mutations in AMT and HSD17B3 respectively. This could be coupled to differential folate accumulation and steroid estradiol synthesis. So, U87MG could potentially have reducing equivalents in excess of that produced by NSP due to its varied mutational profile and thus possibly need to recycle more NAD than NSP.

The unique mutation profile that shapes metabolic response in NSP included transporters SLC38A3, SLC38A4, SLC1A5 all involved in amino acid transport. These could potentially be responsible for the differential exo-metabolite profiles for amino acids and uptake rates as discussed in Chapter 2 and the following chapters. Also, Glutathione metabolism via unique mutational profiles of GCLM, GGT2, and GPX1 coupled with a compromised oxidative phosphorylation complex III and ATPase (ATP4A, CYC1 mutations) is also identified. A dysfunctional ATPase may allow accumulation of ATP. CYC1 inhibition is known to prevent neuronal differentiation and could be why NSP cells remain spheroidal. The origins, however, cannot be commented on.

Nucleotide metabolism and signaling (ADK mutations) could alter the ATP: AMP balance leading to increased ATP while guanylyl cyclase dysfunction may affect GTP accumulation. The only known receptor for Nitric Oxide (NO) is soluble guanylyl cyclase (sGC) leading to dysregulation of iNOS (Inducible nitric oxide synthase) and excess NO. NO-mediated cellular regulation may be responsible for some of the arginine related metabolic differences between the two cell types. NO could also bind to the binuclear center of complex IV, COX (cytochrome c oxidase) and potentially inhibit mitochondrial respiration. There may be a greater need for NADPH leading to NADPH oxidase inhibition. ROS generation triggers PI3K-Akt-mTORC1- dependent autophagy signaling pathway and significantly increases autophagic flux. These could be compromised through Phosphoinositol metabolism and the negative regulatory effect of PI3K, PTEN via mutations in PLCD3 and SYNJ1. Also, pyruvate metabolism could be

varied through mutations in ME1 leading to differential secretion profiles in presence of high concentrations of the drug. Heme Biosynthesis may also be affected by mutations in HMBS. All these identified mutations can thus form the base for more hypotheses. Further characterization by site-specific sequencing and site-directed mutagenesis would benefit in understanding the causal effects on metabolism.

4.5. Conclusions

The genetic landscape of tumors is continually evolving and can be an impediment to the clinical management of cancer patients with recurrent disease. Continuous genotypic characterization throughout the progression of the disease drives the identification of candidate mutations that are induced through microenvironment changes and the presence of the drug. Such mutations can be used as diagnostic tools for identification of the severity of the disease. Our study identified varied mutational profiles in temozolomide resistant (NSP) and sensitive (U87MG) population of cells. This leads to validations of established physiological phenotypes in resistance and also the development of hypothesis and biological discovery. Further validation of impact by specific gene silencing would help in developing novel strategies to control the drug resistance.

Chapter 5

Phenotypic Plasticity of Growth and Respiration

"When you cannot measure, your knowledge is meager and unsatisfactory"

-Lord Kelvin

"No Disease, including cancer can live in an alkaline environment"

- Otto Warburg

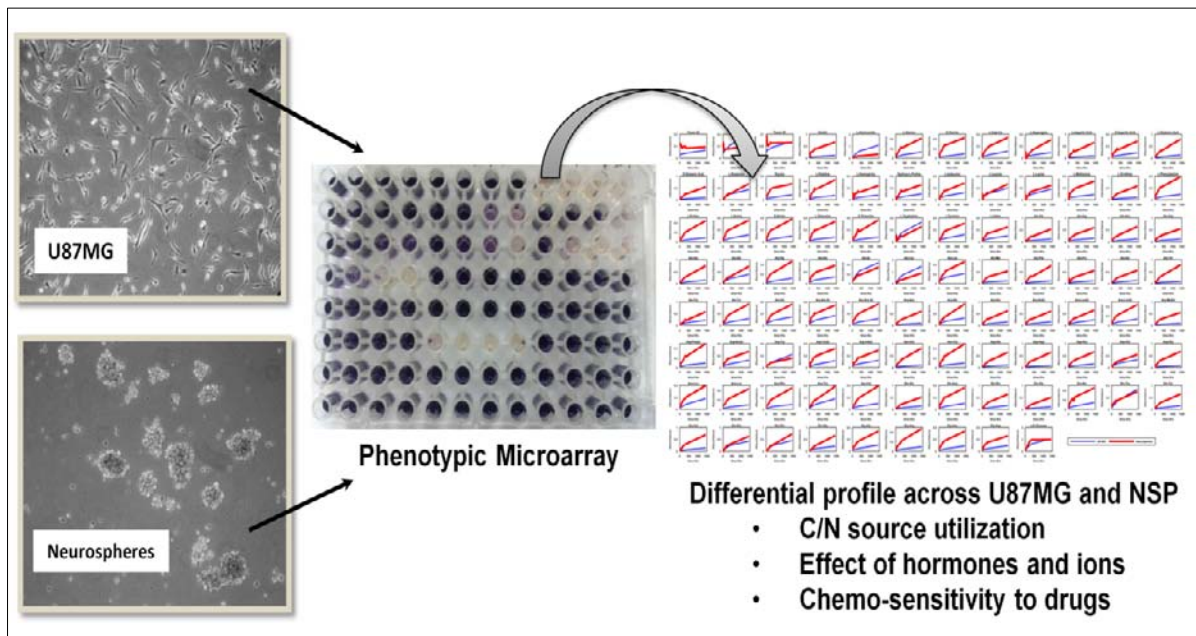


Figure 5.1: Graphical abstract of Chapter 5.

Abstract

Two principal dimensions of life that define cell function are growth and energy generation. Metabolic networks potentially orchestrate this duality of cell function critical for survival and proliferation. The ability to utilize a nutrient by the cell is determined by their genetic and phenotypic background that potentially rewires the metabolism to support the growth and survival. Altered metabolism is known to support the anabolic growth of cancer cells during nutrient replete conditions and catabolic pathways to support the survival of cells during nutrient limitation or nutrient deplete conditions. These metabolic preferences may be driven by oncogene activation and gene mutational profiles. In this **Chapter 5**, the capability of temozolomide resistant (Neurospheres) cells and temozolomide sensitive (U87MG) cells to respire and grow on different substrates has been delineated using phenotypic microarrays. Nutrient preferences thus profiled, showed that U87MG could utilize mannose and pyruvate for maximal growth in comparison to glutamine and glutamate for NSP. Ions and hormones also showed differential responses. Of the 92 drugs tested, Neurospheres were sensitive to Rotenone (80% inhibition), Rifaximin, Berberine chloride, and Deguelin. Our study provides a new insight into the differential growth and respiration profiles and highlights the coupled respiration and growth in Neurospheres and decoupled respiration and growth in U87MG. These results thus suggest the existence of cell adaptive mechanisms towards nutrient preferences and would possibly contribute to drug resistance.

5.1. Introduction

The heterogeneous composition of the cancer microenvironment plays a major role in defining the phenotype of cancer cells. Physical, biological and chemical regulators in the microenvironment potentially control and guide cell survival (Mathis et al. 2017; Persano et al. 2013; Calibasi Kocal et al. 2016; Cantor & Sabatini 2012). Microenvironment-driven dynamic heterogeneity causes phenotypic plasticity that drives the evolution of varied response and may cause resistance to therapy. In response to changing microenvironmental conditions, like hypoxia and nutrient starvation, proliferative cancer cells can switch to a more aggressive/invasive and metastatic state. Recent evidence also suggests the presence of sub-population of cells that undergo a phenotypic switch to a more stem-like state (Golebiewska et al. 2011; Persson & Weiss 2009; Broadley et al. 2011; Golebiewska et al. 2013).

In this chapter, a comprehensive analysis of the differential nutrient utilization that supports respiration and growth of both drug-resistant population (Neurospheres) and drug sensitive population (U87MG) is performed and discussed in the context. Also, this chapter summarizes the potential novel therapeutic strategies from the chemosensitivity analysis that can help to target these drug-resistant, Neurospheres.

5.1.1. Phenotypic and metabolic plasticity in cancer

Aerobic glycolysis is the dominant metabolic phenotype in cancer cells (Hsu & Sabatini 2008). Mitochondrial energy pathways are reprogrammed although mitochondria in most tumors are capable of oxidative phosphorylation (OXPHOS) and are not defective. This increases the ability to compensate for high-energy demand, macromolecular synthesis and rapid cell division (Gaude & Frezza 2014). Retrograde signaling and post-translational modification of oncoproteins occur via energy reprogramming. Neoplastic mitochondria also engage in crosstalk with the micro-environment (Kim et al. 2015).

A hybrid glycolysis/OXPHOS phenotype for energy and biomass synthesis can occur in cancer cells and facilitates metabolic plasticity associated with therapy-resistance. Further, tumor cells are capable of switching their metabolic phenotypes in response to external stimuli for survival (De Berardinis & Chandel 2016; Gaude & Frezza 2014; Kim et al. 2015). Therapies targeting cancer metabolic dependency can be made more effective by taking into account this metabolic heterogeneity and plasticity.

5.1.2. Nutrient dependencies in cancer

Cancer cells reprogram their pathways of nutrient acquisition and cell metabolism to meet the demands of bioenergetic, biosynthetic, and redox balance under nutrient replete and deprived conditions (Figure 5.2). Altered metabolism supports the cancer cells for its survival in nutrient replete and nutrient-deprived conditions (De Berardinis & Chandel 2016). Metabolic dependencies can also be used as targets for therapies. Such dependencies other than glucose for survival in the presence of drug can also overcome resistance.

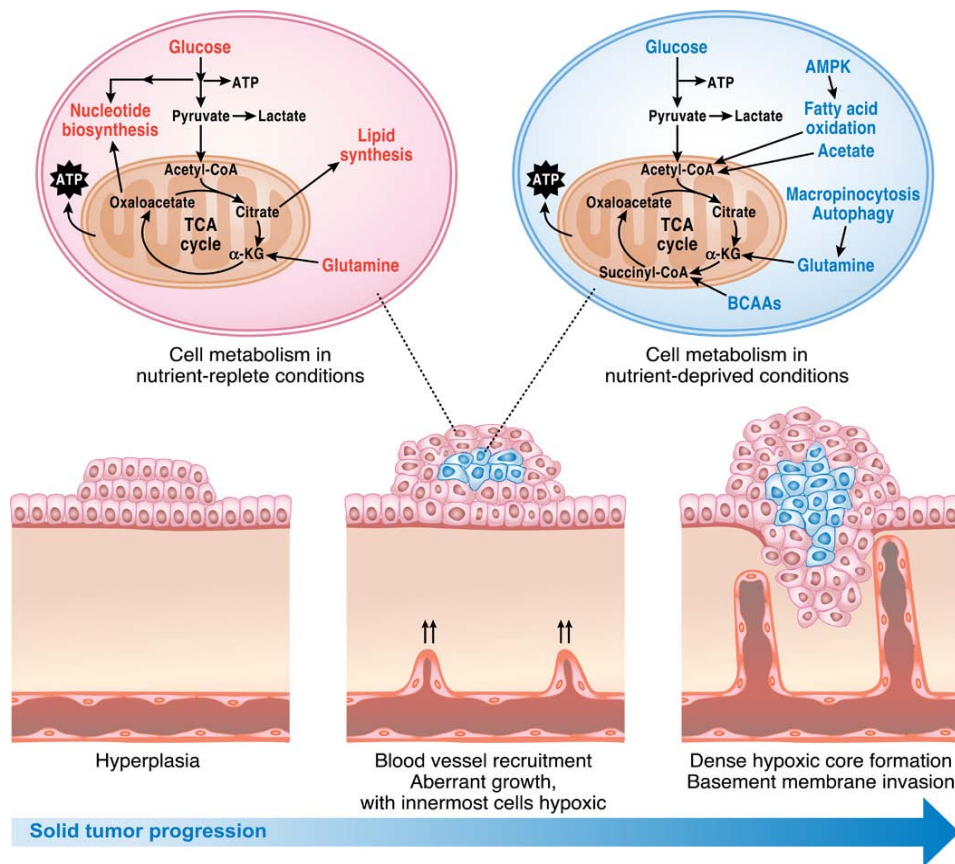


Figure 5.2: Metabolic pathways under nutrient-replete and nutrient-deprived conditions. Figure adapted from R.J. DeBerardinis, N.S. Chandel, *Fundamentals of cancer metabolism*, *Sci. Adv.* 2 (2016) e1600200–e1600200. doi:10.1126/sciadv.1600200 (DeBerardinis & Chandel 2016).

In this **chapter 5**, the nutritional preferences of temozolomide sensitive (U87MG) versus temozolomide resistant (Neurospheres) cells that are profiled so far, are characterized based on their ability to respire and grow on 367 carbon and nitrogen (C/N) sources using BIOLOG phenotypic microarray plates (PMM1 to 4). Also, the selected ions and hormones (PMM5 to 8) are tested for these two populations. Chemo-sensitivity of drug sensitive and drug resistant cells has been assessed for 92 chemotherapy drugs in the PMM11 to 14

panels.

5.2. Methods

5.2.1. Cell culture: U87MG cell line (HTB-14; Human Glioblastoma Multiforme from ATCC) was cultured in DMEM (Dulbecco's Modified Eagle's Medium, Gibco) with Glucose (1 mg/mL) and L-glutamine (0.584 mg/ml). 10% fetal bovine serum (FBS, Gibco™, ThermoFisher Scientific) and 1% non-essential amino acids (Sigma-Aldrich) was used additionally for growth. Cell lines were maintained at 37°C in a humidified atmosphere of 5% CO₂/95% air. Neurospheres (NSP) were initially maintained in neurobasal medium (Gibco™, ThermoFisher Scientific) supplemented with B27 supplement (Gibco™, ThermoFisher Scientific), 0.2 µg/mL of epidermal growth factor, EGF (ThermoFisher Scientific) and 0.2 µg/mL of basic fibroblast growth factor, bFGF (ThermoFisher Scientific). Further sub-culturing and passaging of NSP was carried out using the similar medium as U87MG to avoid any contribution from different micro-environments and delineating heterogeneity of molecular signatures. NSP were cultured as free-floating spheres in the appropriate low attachment T-75 flasks or 6 well/24 well plates (Nunc™, ThermoScientific™) for the study.

5.2.2. Phenotype microarray analysis: Biolog Phenotype MicroArrays™ (PM-M1 to PM-M14) from Biolog, Inc. USA (www.biolog.com) consist of panels of PMM screening assays - (i) Energy metabolism pathways; (ii) Ion and hormone effects on cells and (iii) Sensitivity to anti-cancer agents. These are based on an easy-to-use technology for measuring the energy metabolism pathways present in mammalian cell types from *in vitro* cultured cells to primary cells.

In PM-M1 to PM-M4, the metabolic pathway activities were assayed by using the cell suspension (~20,000 cells/well) prepared in an inoculating fluid (IF-M1 or IF-M2) that lacks carbon and energy sources (provided with the BIOLOG plates). These cells adapt to their new environment of different carbon and energy sources in the various wells. Biolog Redox Dye Mix MA or Biolog Redox Dye Mix MB was added to all wells. This measurement employs a tetrazolium dye that can be reduced to a purple formazan that can be measured at 590nm with a microplate reader. The redox energy produced when a cell metabolizes a substrate is used to convert the color from yellow to purple formazan. The rate of formazan production is linear with time and corresponds to the number of viable cells. iMark™ Microplate Absorbance Reader (Bio-Rad), with a wavelength range of 400–

750 nm, had been used in our study to measure the absorbance.

PM-M5 to PM-M8 plates are coated with different ions, hormones, and other metabolic effectors; and PM-M11 to PM-M14 are coated with different anticancer agents. Cell suspension (~20,000 cells/well in a culture medium that is serum-free and containing D-glucose and L-glutamine) was used for PM-M 5 to 8 and PM-M 11 to 14. All plates were incubated at 37°C in CO₂ incubator. The absorbance readings were measured after an initial incubation (48 hours) of cell growth, followed by adding the dye and reading for 24 hours of study (with initial intervals at 15, 30, 45 and 60 min; 1hr intervals from 2 to 6 hrs; and final reading at 24 hours of incubation).

5.3. Results

5.3.1. Phenotypic plasticity defined by nutrient preferences for growth and respiration

The cellular energetics and pathways involved in the metabolism of U87MG and NSP cells during the nutrient restriction state (only one source/nutrient preferences) were addressed by using Biolog Phenotype MicroArrays™ (PM-M1 to PM-M4) plates. PM-M1 to PM-M4 uses different carbon and nitrogen sources to test for 367 potential metabolic sources and pathways simultaneously that contribute to the conversion of these substrates to energy. These could eventually form distinct profiles of metabolic activity that gives the cell-specific metabolic fingerprints/phenotypic profiles. The data generated were analyzed for respiration and growth separately to understand whether the specific source/nutrient contribute by coupling or decoupling towards respiration (NADH generation) and growth (ATP synthesis).

The respiration profiles were categorized, based on a threshold value into true respiration (includes respiration from initial time points and respiration after certain time gaps/lagged respiration) and no respiration. Of these categories, the source/nutrient that enhances respiration in a specific cell type may or may not result in measurable growth in that cell type. Hence, the same way of categorization was applied in case of growth profiles as well with a different threshold value identified from the cell counts.

5.3.2. Euclidean clustering of growth and respiration rates

73 carbon and nitrogen sources were primarily selected from the panel of PM-M1 to PM-M4, based on their role in the core metabolic pathways and analyzed using Euclidean

clustering. These included glucose, glutamine, and all proteinogenic amino acids. Clustering according to the ability to grow on all 73 C/N sources was able to distinguish U87MG from NSP. Primary column cluster was between the respiration profiles (U87MG and NSP) and the further clusters were connected to this primary cluster in a series (NSP growth followed by U87MG growth) illustrating the correlation.

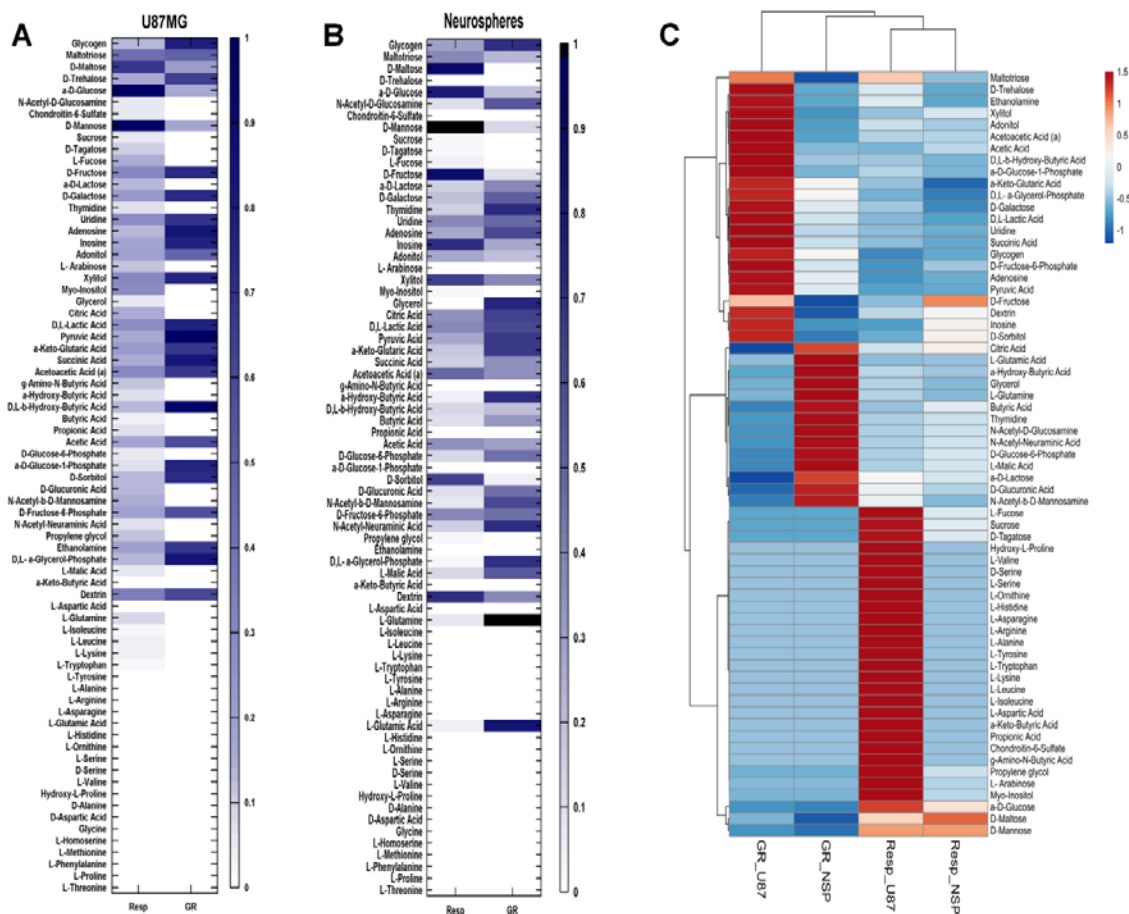
Row-wise clustering with the tightest cluster first in tree ordering highlighted a primary cluster with all amino acids, all carboxylic acids, and all polysaccharides separately followed by interconnection. Dextrin, inosine, and sorbitol formed a separate cluster that was further connected to the primary clusters.

Glutamate and Glutamine supported growth in NSP predominantly compared to D- glucose and D- mannose in U87MG. Pyruvate, AKG, and Succinate supported growth in U87MG but lower than in NSP suggestive of the divergent microenvironments as seen in the exo-metabolite profile of these 3 metabolites (Figure 5.3).

5.3.3. Differential growth and respiration rates across U87MG and Neurospheres

The rate of respiration and growth was further analyzed for all panels of PM-M plates. PM-M1 contains an array of carbon sources including simple sugars, polysaccharides, and carboxylic acids. Both the cell populations utilized glucose for respiration as well as growth along with 31 other metabolites. U87MG cells additionally metabolize 13 metabolites (L-Glucose, D-Salicin, Chondroitin-6-sulfate, D-Melezitose, Palatinose, L-Sorbose, L-Rhamnose, D-Fucose, D-Arabinose, D-Malic acid, γ -Amino-N-butyric acid, α -Keto-butyric acid, and Propionic acid) with no measurable growth. α -D-Glucose-1-Phosphate, Ethanolamine, and D-Trehalose show unique profiles for U87MG for respiration as well as growth. NSP cells can utilize β -Gentiobiose as its source for respiration and growth.

D-cellobiose was not utilized by both cell populations. Out of the 10 methylated substrates (PM-M1), U87MG showed respiration capability in all of them with no measurable growth except mono-methyl succinate. In addition to mono-methyl succinate, two more methylated substrates (α -Methyl-D-mannoside and β -Methyl-D-galactoside) were shown to support respiration as well as growth by NSP (Figure 5.4 and Appendix A).



D Decoupling NAD(P)H oxidase activity and Cell Growth

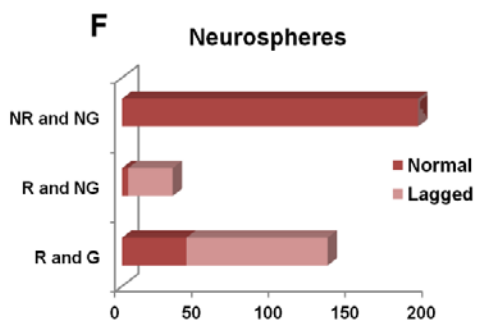
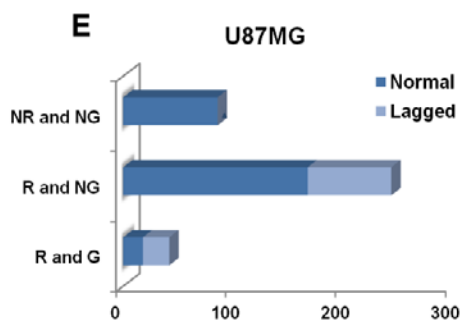
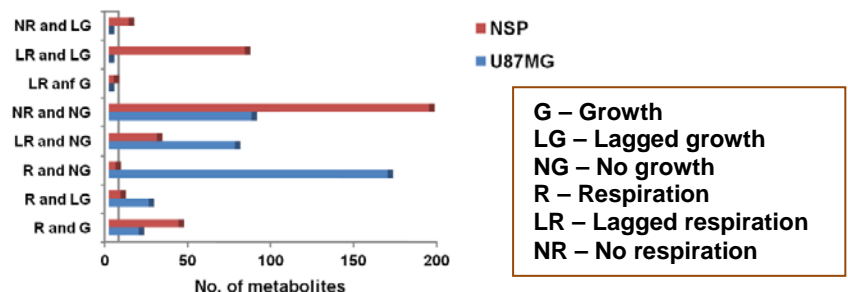


Figure 5.3: PM-M1 to 4 analyses using growth (GR) and Respiration (Resp) rates, clustering using clustergram and identifying coupling and decoupling of growth and respiration. Lagged growth represents the delay in growth due to the carbon source getting converted to another secondary metabolite that can be used by the cells.

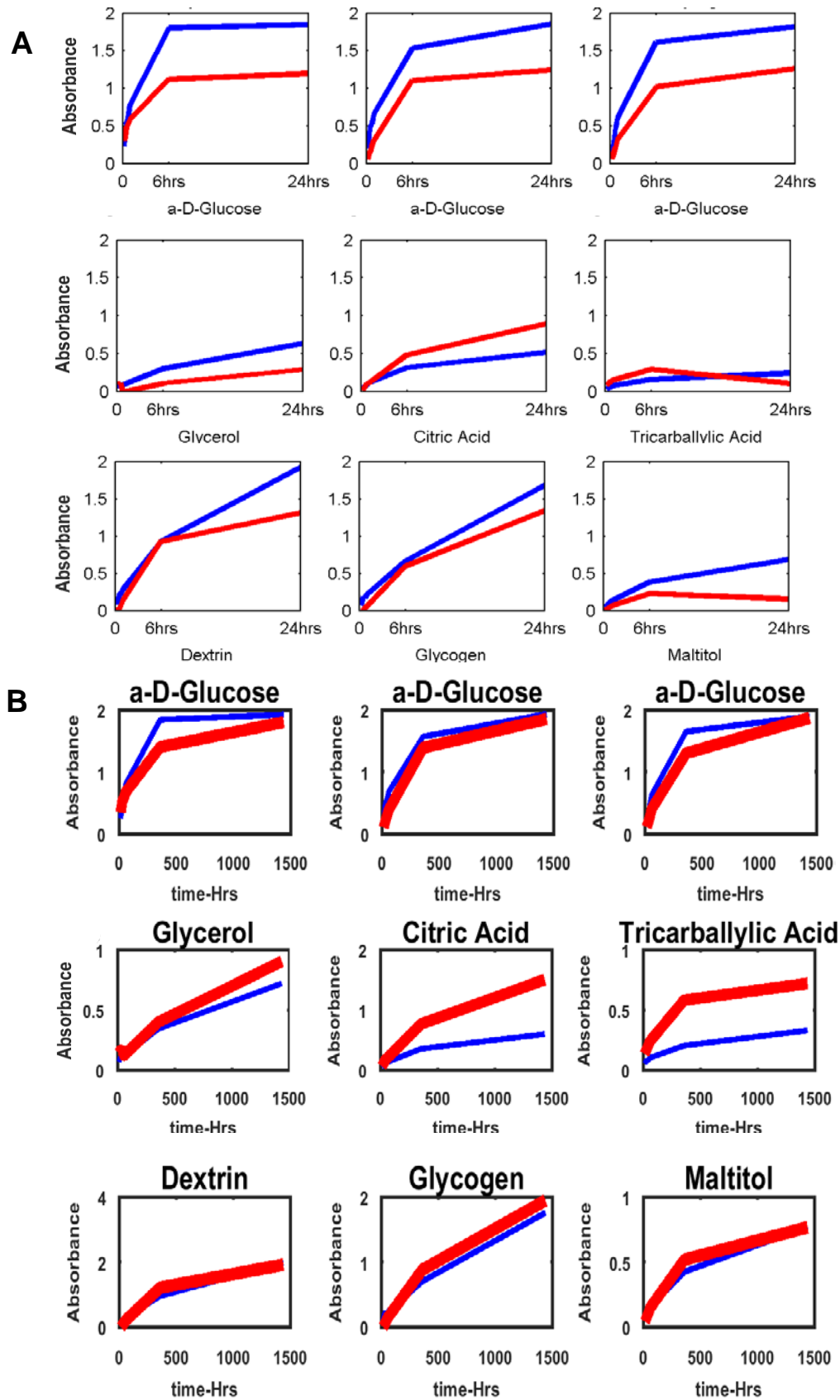


Figure 5.4: PMM-1 analysis of respiration (A) and growth (B) profiles. Selected differential profiles of respiration and growth are shown for the sole carbon sources that are mentioned as title in the subplots. See Appendix A for the complete panel of plates.

PM-M2 to PM-M4 plates have lipids and protein-derived nutrients, primarily individual L-amino acids and dipeptide combinations. In the case of dipeptides, 57 substrates were utilized by both cell populations. Ala-Leu was metabolized for growth and respiration by both cell types but in a slower rate in case of NSP.

Ala-Pro, Thr-Gln, Val-Glu, and Val-Gln were utilized for true respiration by both with no measurable growth in case of U87MG. Ala-Asp and His-Ser were also used for respiration with no measurable growth in U87 and very less growth in NSP. 38 dipeptides were not utilized by both. 114 dipeptides were used by U87MG (respiration but no growth). Leu-Ala is the only substrate (from 114 dipeptides) that resulted in respiration with some growth in U87MG. 35 dipeptides were utilized by NSP and not by U87MG. Thr-Ala was the only one utilized for true respiration and growth by NSP. 11 substrates other than dipeptides (like L-Homoserine) showed no response in both the cases. Other amino acids that not utilized by both cell populations include Glycine, L-Phenyl alanine, D-Alanine, D-Aspartic Acid, and D-Threonine (Appendix A).

5.3.4. Nutrient preferences from 367 C/N sources

Among 367 substrates, 123 substrates (other than dipeptides) which include various carbon and nitrogen sources, 43% i.e. 53 substrates have a common respiration profile in both the cell lines. One-third of all the substrates have a true respiration in both cell lines. This category consists of carbohydrates such as glucose, fructose, galactose; carboxylic acids such as pyruvate, lactate, citrate; sugar alcohols such as 2,3-butanediol sorbitol, maltitol; polysaccharides such as dextrin, glycogen and three methylated substrates - a-methyl mannoside, b-methyl galactoside, and mono methyl succinate. 12 substrates were not utilized for respiration.

For the remaining 70 substrates, the two cell lines have different respiration profiles. With respect to U87MG respiration, more than 84% i.e. 59 substrates are utilized for respiration and more than 14% i.e. 10 substrates were utilized with a lag for respiration (NR in NSP). In contrast, NSP respired on only one substrate but not in U87MG and 60% i.e. 42 substrates were not utilized for respiration by NSP and only 39% i.e. 27 substrates are utilized slowly for respiration by NSP.

5.3.5. Differential profile in ions and hormones

PM-M5 to PM-M8 is designed to profile for effects of ions, hormones, and other metabolic effectors on the metabolism, via respiration and growth rate. In total, 67 different metabolites were screened, of which, 4 ions (Manganese chloride, Zinc chloride, Copper (II) chloride, and Sodium orthovanadate) were not utilized by both the cell populations. 14 metabolites (Ammonium chloride, Sodium selenite, Potassium chloride, Cobalt chloride, Sodium sulfate, Potassium chromate, Sodium Nitrate, Sodium Nitrite, 3-Isobutyl-1-methylxanthine, Thyroxine, IL-2, Prolactin, Calcitriol, 1 α ,25-Dihydroxyvitamin, TNF- α) were shown to be differential profiles in a way that NSP could utilize them for growth but not U87MG. 2 of the metabolites (Magnesium chloride, (Arg8) –Vasopressin) cannot be utilized by NSP but can be utilized by U87MG. 48 substrates were utilized by both the cell populations with maximum growth for U87MG in IL-6 and Adrenocorticotrophic hormone human (ACTH) in NSP (Appendix A).

5.3.6. Chemo-sensitivity of U87MG and NSP to 92 drugs

PM-M11 to PM-M14 is designed to profile for the sensitivity of cells to a diverse set of anti-cancer agents that can affect the cell growth by different modes of action. The anti-cancer agents can target and alter cell metabolism, growth rate, or productivity. 92 cytotoxic drugs in this panel were tested against the two cell types (U87MG and NSP) that showed the difference in their nutrient preferences. 78 drugs were non-cytotoxic to both the cell types (Figure 5.5, Appendix A and Figure 5.6).

Chemosensitivity of U87MG and NSP

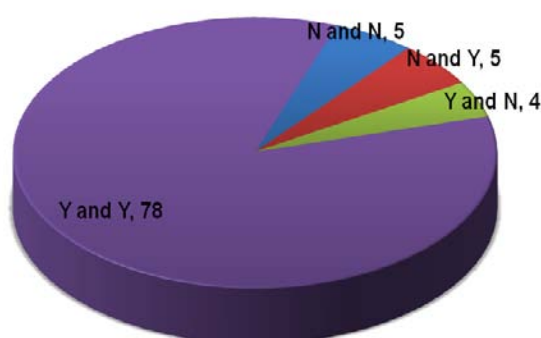


Figure 5.5: Analysis of chemo-sensitivity of U87MG and NSP. U87MG and NSP showed a differential profile in only 9 drugs. Growth in the presence of drugs is considered as “Y” and No growth as “N”.

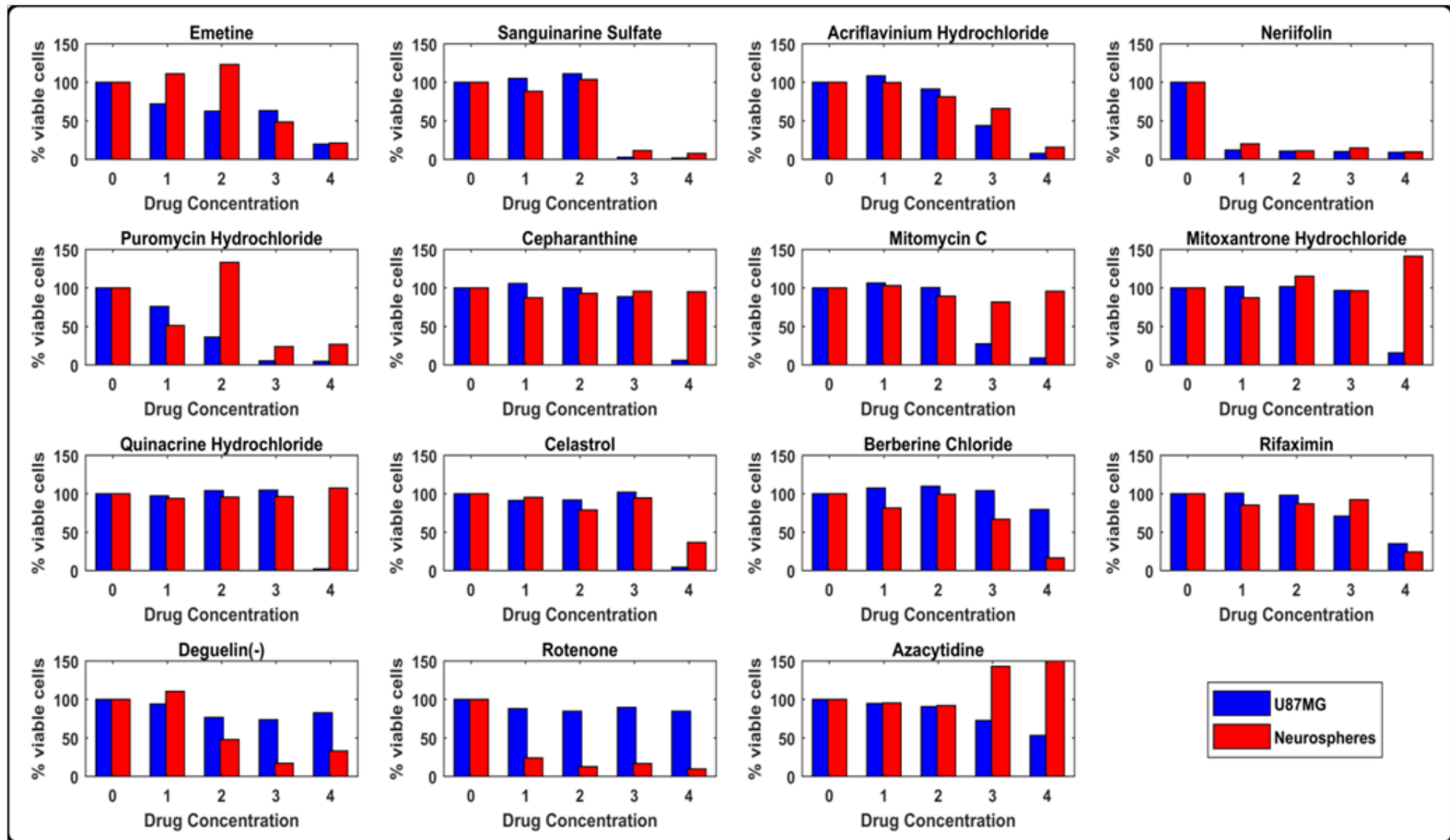


Figure 5.6: Chemo-sensitivity profile for U87MG and Neurospheres. Out of 92 drugs, the differential inhibition profiles are shown. ETC inhibitors like Rotenone and Deguelin affect the NSP population specifically than the U87MG cells.

5 drugs were cytotoxic to both the cell types (Emetine, Sanguinarine, Acriflavinium, Neriifolin, and Puromycin. Differential profile was observed in the drugs listed in Table 5.1. NSP was susceptible to Berberine, Rapamycin, Deguelin, and Rotenone. All these drugs target the complex I in the ETC. Hence, it is possible that the rewired survival strategy of NSP lies in the dependency of ETC, and it is been targeted by these drugs. In a combined therapy, by administering these 4 drugs along with temozolomide can be a most promising therapeutic regimen to target and kill the resistant population, Neurospheres.

Table 5.1: Differential drug response for U87MG and NSP.

No.	Drug Name	U87MG	NSP	Known mechanism / Target
1	Cepharanthine	-	+	It is an anti-inflammatory and antineoplastic compound isolated from <i>Stephania</i>
2	Mitomycin C	-	+	Mitomycin C is a potent DNA cross-linker.
3	Mitoxantrone Hydrochloride	-	+	antibiotic with antineoplastic activity
4	Quinacrine Hydrochloride	-	+	It is an antimalarial drug and also used as an antibiotic.
5	Celastrol	-	+	Celastrol, a plant-derived triterpene, has antioxidant and anti-inflammatory activity that may prevent neuronal degeneration in Alzheimer's disease (AD)
1	Berberine Chloride	+	-	A compound extracted from herbs for its anti-diabetic effects; targets complex I in ETC.
2	Rapamycin	+	-	Rapamycin is a macrolide compound obtained from <i>Streptomyces hygroscopicus</i> that acts by selectively blocking the transcriptional activation of cytokines.
3	Deguelin(-)	+	-	Deguelin is a derivative of rotenone. Both are compounds classified as rotenoids of the flavonoid family and are naturally occurring insecticides
4	Rotenone	+	-	Rotenone works by interfering with the ETC in mitochondria. It inhibits the transfer of electrons from iron-sulfur centers in complex I to ubiquinone.

5.4. Discussion

The phenotypic microarray results are based on the conversion of BIOLOG dye by the cellular oxidoreductases. These assays (Figure 5.10) reflect the production of NADH by the cells from various substrates. The fraction of NADH produced in mitochondria differs for different energy substrates when given as a sole carbon or nitrogen source. The ability

of a cell to use a particular nutrient as a source of energy is evitable; yet this does not support or sufficient to use the same source as a growth substrate.

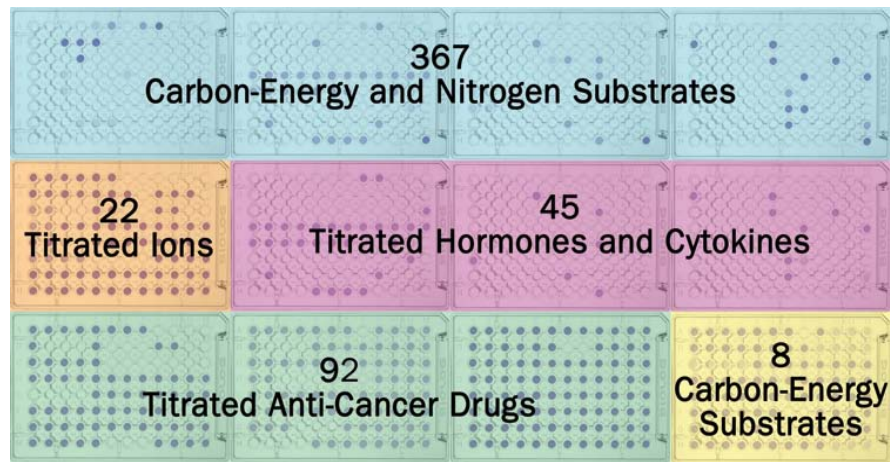


Figure 5.7: Phenotypic microarray panels (PMM 1 to 14). Source: Biolog website. http://www.biolog.com/products-static/phenotype_mammalian_cells_overview.php

To be used as a growth substrate, the sole carbon or nitrogen source should be sufficient to drive metabolism and proliferation. The fraction of cytosolic and mitochondrial NADH produced by the conversion of substrates is measured as cell viability in these assays and hence it supports the cytosolic NADH theory (Figure 5.11). The function of mitochondrial energy metabolism is also dependent on the NADH/NAD⁺ ratios that are present in the mitochondria to support the electron transport chain. In a recent study (Titov et al. 2016), the role of electron transport has been dissected into two separate processes: 1) Proton motive force and 2) ATP synthesis. The process of electron transfer can be considered as cellular respiration and the ATP synthesis further drives the cell growth.

In this chapter 5, the analysis of PMM data has been performed to characterize whether or not these two processes of cellular respiration and growth are coupled or decoupled in the given substrate by the cell. By such analyses, it is observed that U87MG respire in many substrates whereas NSP utilizes the substrates for both respiration and growth. This supports the hypothesis that NSP cells potentially couple their respiration to growth but U87MG cells although utilize many substrates for respiration, grows in fewer substrates (Figure 5.3D, E and F). Also, the metabolite profiling in Chapter 2, highlighted the glutamine preference for Neurospheres in the LC-MS/MS data.

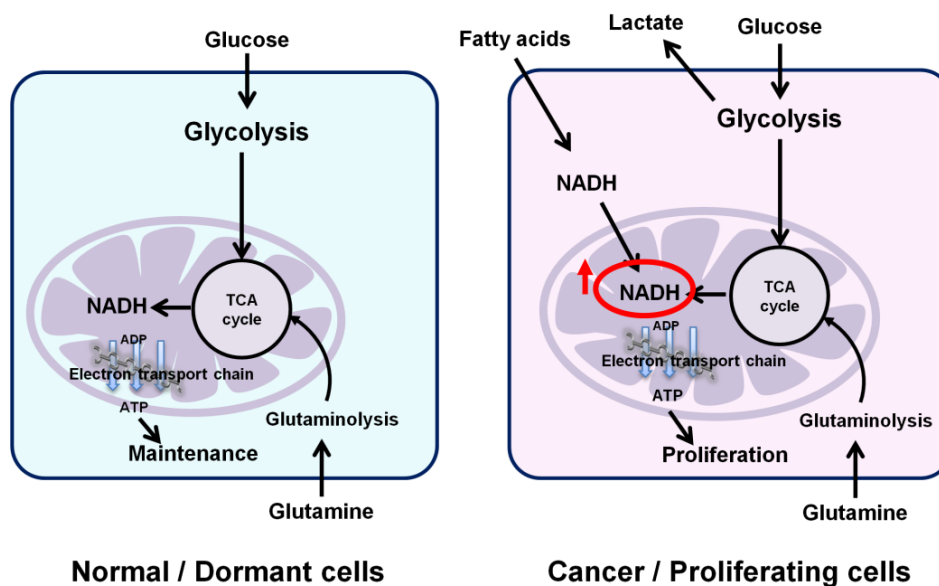


Figure 5.8: NADH theory of cancer energy metabolism. A major source of the electron is considered as cytosolic NADH in cancer cells compared to normal cells.

Herein, the profile for glutamine in the BIOLOG profile shows that NSP can utilize glutamine and glutamate for growth and respiration whereas U87MG can only respire with these with low growth. These datasets support the preferential utilization of glutamine by Neurospheres for their survival.

In the chemo-sensitivity profile, it is observed that NSp cannot grow in the presence of 4 drugs (Berberine, Rapamycin, Deguelin, and Rotenone). All these 4 drugs are known to target complex I in the electron transport chain (ETC). Since growth and respiration are coupled in NSP, the electron transport chain function is crucial for NSP survival. While, Rotenone being the most inhibiting (80% inhibition), other 3 drugs also show inhibition in the concentrations provided in the BIOLOG panel. Although further experiments are needed to study the combined effect of temozolomide and these drugs, it is evident that these drugs can be cytotoxic to NSP.

5.5. Conclusions

In this **Chapter 5**, the PMM analysis has highlighted the differences in growth requirements, nutrient utilization profiles and drug responses of U87MG (temozolomide-sensitive) and NSP (temozolomide-resistant) cells. The use of phenotypic microarray technology delineated the metabolic phenotype profile of U87MG and NSP cells using their capability to utilize nutrients for growth and respiration (Glucose and Pyruvate for

U87MG; Glutamine and Glutamate for NSP). High-throughput screening of these cells on sole carbon and nitrogen sources helped in delineating the cell-specific preferential utilization of substrates. Also, the chemosensitivity panel helped in the identification of 4 candidate drugs - Berberine, Rapamycin, Deguelin and Rotenone that can be cytotoxic to the resistant cells (NSP) with the highest inhibition for Rotenone.

Chapter 6

Metabolic Dynamics and Reprogramming of the Cell

"Genes load the gun, but environment pulls the trigger".

- Bruce Lipton

"The way you understand and investigate time is by moving inward, into metabolism. The human body is a knot in time".

-Terence Mckenna

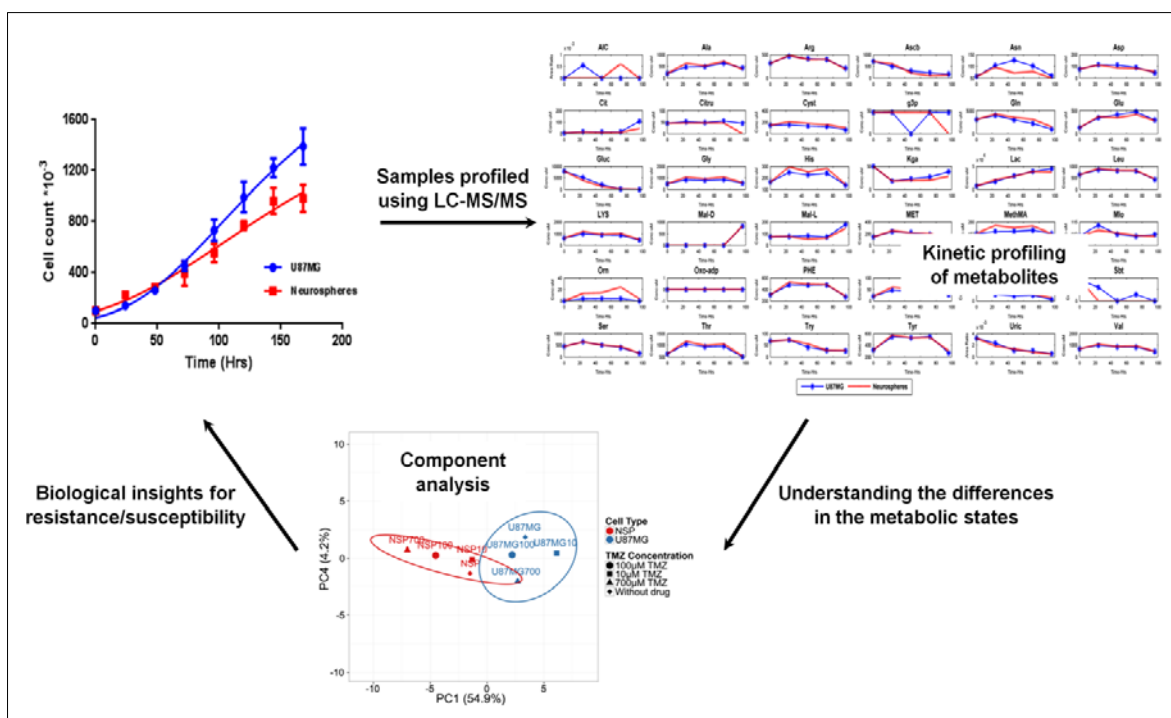


Figure 6.1: Graphical abstract of Chapter 6.

Abstract

The metabolic state of the cell determines how the cell responds to the environment or other stimuli. It is important to know the metabolic features of the cell in order to understand its impact on growth and survival. In this Chapter 6, the metabolite levels in the two cell types (U87MG and NSP) were analyzed and quantified using LC-MS/MS for 5 samples (0 to 96 hours) from varied conditions (Without drug and three different concentrations of temozolomide as 10, 100 and 700 μM TMZ). 34 metabolites were selected based on their important role in central carbon and nitrogen metabolism. This data again indicated that the growth limiting substrates (Glucose, glutamine, serine, and tryptophan) were completely depleted by 96 hours by both the cell types except glucose and serine in U87MG at 700 μM TMZ. Glucose and Glutamine were utilized by both the cell types in the absence of the drug in a linear way but NSP has a slower glucose uptake. CORE (Consumption and Release) profile analysis and PCA (Principal Component Analysis) was performed. Euclidean clustering predicted relevant clusters for succinate-ornithine; glycine-proline, alanine-lactate; arginine-citrulline; and aspartate-tryptophan throughout the varied TMZ concentrations. Most variation was predicted in the 10 μM TMZ and 700 μM TMZ. PCA1 versus PCA2 outlined the two-component spheres to converge, in contrast to PCA1 versus PCA5 which differentiated the 700 μM TMZ profile from others. CORE clustering of endo-metabolite profiling (concentration normalized to cell number) projected NSP-700 profile as a distinct column cluster among others. In conclusion, the differential metabolite profile identified the most variance in the metabolite profiles in the presence of TMZ than the samples in the absence of TMZ, indicating its impact on resistance.

6.1. Introduction

Otto Warburg observed that proliferating mammalian tumor cells converted the majority of the glucose carbon to lactate even in oxygen-rich conditions. Warburg hypothesized that this altered metabolism was specific to cancer cells and attributed it to mitochondrial defects (Warburg et al. 1923; Warburg 1956). Thus mitochondrial dysfunction or its poor ability to oxidize glucose to CO₂ was proposed to cause cancer (Koppenol et al., 2011). Warburg's seminal finding has been exploited extensively in clinical studies as 18F-deoxyglucose positron emission tomography (FDG-PET) (Vlashi et al. 2011). However, it has now been identified that tumor mitochondria are not defective in oxidative phosphorylation, but metabolism in them is reprogrammed for macromolecular synthesis.

Proliferating cells do not attempt to maximize ATP yield, but rather maximize the flux of carbon into macromolecular anabolic pathways. Metabolic rewiring has been regarded as a consequence of malignant transformation driven by aberrant signal transduction mediated by oncogenes and tumor suppressors. The identification of “oncometabolite” (R)-2-hydroxyglutarate [(R)-2HG] in gliomas as a result of mutations in isocitrate dehydrogenase (IDH) has provided direct evidence linking altered metabolism and cancer (Losman & Kaelin 2013).

A less studied but recently emerged concept is that information about a cell's metabolic state is also integrated into the regulation of epigenetics and transcription. The complexity and dynamics of epigenetic modifications in the presence of DNA methylating drugs like TMZ could provide a link between the extracellular environments. Substrate channeling, a common event in cellular metabolism suggests local concentration gradients of metabolites. Compartmentalized metabolic enzymes could provide a local supply of substrates/cofactors to the complexes like methionine adenosyltransferase II α (MATII α), which generates SAM. System biology approaches are needed to fully grasp the complexity of the connections between metabolism, signaling, transcription, and epigenetics. A deeper understanding of these connections may help to shed light on our understanding of the etiology and treatment of a multifactorial disease like glioblastoma.

6.1.1. Metabolic phenotypes in cancer and regulation of epigenetics

Cancer cells adapt, survive and proliferate on dynamically changing harsh microenvironments. They are less dependent on exogenous growth factors and cell-to-cell

interactions. Vigilant monitoring of intracellular metabolites through pathway regulation may allow them to work through this apparent paradox. Metabolism in cancer cells is influenced by internal stimuli such as oncogenic signal transduction and external cues such as nutrient and oxygen availability. Monitoring intracellular levels of metabolites are thus crucial for cells to appropriately gauge their nutritional resources. Evolutionarily conserved ‘nutrient-sensing’ mechanisms like AMP-activated protein kinase (AMPK), related to varying AMP: ATP ratios, illustrate the ability of mammalian cells to switch to a more catabolic state when they perceive a nutrient stress. In contrast, mTOR signaling promotes growth and is active when cells sense a favorable, nutrient-replete environment.

Enzymes responsible for adding or removing epigenetic modifications include but are not limited to histone acetyltransferases (HATs), histone deacetylases (HDACs), histone methyltransferases (HMTs), histone demethylases (HDMs), DNA methyltransferases (DNMTs) and DNA hydroxylases (DNHDs). Metabolic substrates or cofactor levels regulate activities of such chromatin-modifying enzymes by diffusion to deliver metabolic information to nuclear transcription. The interplay between the tumor microenvironment and cellular metabolism is thus not a simple cause-and-effect theory, because most of the secretory metabolites from biochemical reactions and conditions in the tumor constantly influence tumor microenvironment and hence the cellular metabolism (Figure 6.2).

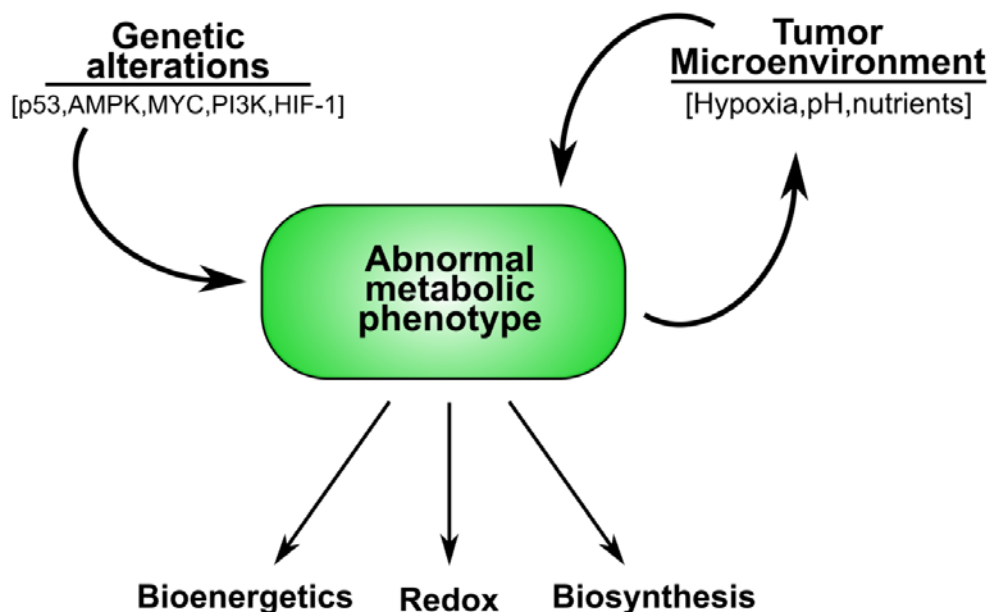


Figure 6.2: Determinants of the tumor metabolic phenotype. The metabolic phenotype of tumor cells is controlled by intrinsic genetic mutations and external responses to the tumor microenvironment.

Due to this dynamic nature of the tumor microenvironment, it is possible that the metabolic phenotype of tumor cells can vary across cell types to adapt to prevailing local conditions/microenvironment (Persano et al. 2013; Calibasi Kocal et al. 2016; Kucharzewska et al. 2015). By addressing these differences in the metabolic changes, the drug-resistant cells can be targeted and it can lead to the development of new therapeutic regimens.

6.2. Methods

6.2.1. Growth in different concentrations of Temozolomide: Growth of the cells (U87MG and NSP) were studied by monitoring their proliferation via cell count over a period of 5 days at different concentrations of TMZ. The initial seeding set has the starting population (N_0) at ~10000 cells per well. The growth profile was studied in a 24 well plate (Nunc tissue culture-treated) for ease of harvesting. Both U87MG and NSP cells were harvested every 24 hours and counted using hemocytometer based on trypan blue dye exclusion assay. Before counting, the NSP population was also disaggregated by trypsinization. For different concentration of drug experiments, cells were plated in replicate wells at ~20,000 cells per well in 24-well plates (Nunc™ tissue culture treated, ThermoScientific™) in full growth medium for 24 h and then treated them with different doses of TMZ (10μM, 100μM, and 700μM). Three biological replicates were performed with two technical replicates in each biological replicate on a 24-well plate (Nunc™ tissue culture treated, ThermoScientific™). Growth and temozolomide response curves were graphed with the number of cells on the Y-axis and time on the X-axis. The data were fitted using Gompertz function using GraphPad Prism software and the growth parameters calculated.

6.2.2. Liquid chromatography-high resolution mass spectrometry (LC-HRMS):
Sample extraction, dilution and internal standard spiking: The 8 samples from each experiment setup (Without drug, 10 μM TMZ, 100 μM TMZ and 700 μM TMZ) were harvested every 24 hours over a period of seven days and used for the metabolic profiling to understand nutrient uptake and release kinetics. Sampling pooling strategy (Cheung et al. 2005; Kline & Richmond 1981) was applied to reduce the number of samples and to make the analysis as a high-throughput quantification. Each replicate-pooled sample was prepared and stored at -80°C; thawed on an ice bath to aliquot 100μL of the sample for extraction. The aliquot was transferred into a fresh 1.5 mL centrifuge tube. 400 μL of

chilled methanol (previously stored at -80°C) was added. The solution was thoroughly mixed for 2 min followed by centrifugation for 15 min at 5000 rpm (4°C). The tubes were carefully removed, 300 μL of supernatant was withdrawn and transferred into a fresh tube (Dilution level: 5X). A two-step serial dilution of the supernatant was performed using 50% acetonitrile in water. In the first step, 50 μL of supernatant was thoroughly mixed with 450 μL of diluent (Dilution level: 50X). This solution was further diluted by mixing 100 μL of the sample solution with 400 μL of diluent (Dilution level: 250X). Before injection, 100 μL of the sample solution was mixed with an equal volume internal standard solution containing 4.4 μM verapamil in 50% acetonitrile in water with 0.2 % formic acid.

6.2.3. Standard preparation: Standards of metabolites were prepared using chemically defined minimal essential media (MEM), and non-essential amino acid media (NEAA) from Sigma. Stock solutions were serially diluted to generate the various calibration levels for quantitative estimations.

6.2.4. Metabolites profiling using LC-HRMS: Metabolic profiling of samples was carried out using Accela 1250 ultra-performance liquid chromatography (UPLC) in tandem with Thermo Q-exactive high-resolution mass spectrometer (HRMS) using heated electrospray ionization (HESI) interface. The UPLC and MS were operated using Xcalibur (Thermo, Version 2.0) software platform, whereas HESI source parameters were set using Tune module (Thermo, version 2.1). Samples were stored in a temperature controlled Accela autosampler maintained at 4°C during LC-HRMS analysis. A reverse-phase C18 hypersil GOLD column (10cm x 2.1mm x 3.0 μm) was used for chromatography. The mobile phase consisted of 0.1% formic acid in deionized water (Mobile phase 'A') and 0.1% formic acid in acetonitrile (Mobile phase 'B'). The elution gradient was set as 70% of mobile phase A (0.0-2.5 min), 10% A (3.5-5.5 min), 70% A (5.5-8.0 min) with a constant flow rate at 1000 $\mu\text{L}/\text{min}$. The HESI source spray voltage was set at 3.7kV with capillary temperature - 300°C ; sheath gas - 45 units; auxiliary gas - 10 units, heater temperature - 390°C and S-lens RF at 50 units. The mass spectrometer was set to m/z range of 60-900, resolution of 70,000 FWHM (Full width at half maximum) with automated gain control target $1e^6$ and maximum injection time of 50 ms. 5 μL of the sample was injected for analysis using the auto-sampler unit. The data was acquired in both positive and negative ion mode in two separate batches. Metabolomics data analysis was carried out by the Qual and Quan browser modules of Xcalibur (Thermo Scientific). $[\text{M}^+\text{H}]^+$ and $[\text{M}\text{H}]^-$ ions were used for all sets of data analysis in positive and negative ion mode respectively. A

Qual/Quan approach of data processing was employed. The initial step of analysis was the generation of accurate mass-extracted ion chromatogram (AM-XIC) of various metabolites using 20 ppm mass extraction window (MEW) and peaks were confirmed using MS/MS spectral peak matching. In the next step, the metabolites (confirmed in the qualitative analysis) were quantified in various intra and extracellular samples using the internal standard normalized linear regression models generated from standards.

6.2.5. Selection of metabolites for profiling: The metabolomic characterization of temozolomide sensitive and temozolomide resistant cells was performed on a targeted way of estimation of concentrations. The central carbon and nitrogen metabolism was targeted in this study. 34 metabolites were selected based on their impact on the metabolism (Figure 6.3). These metabolites include all amino acids, glucose, lactate, alpha-ketoglutarate, citrate, oxaloacetate, succinate, malate, and pyruvate.

34 metabolites are selected

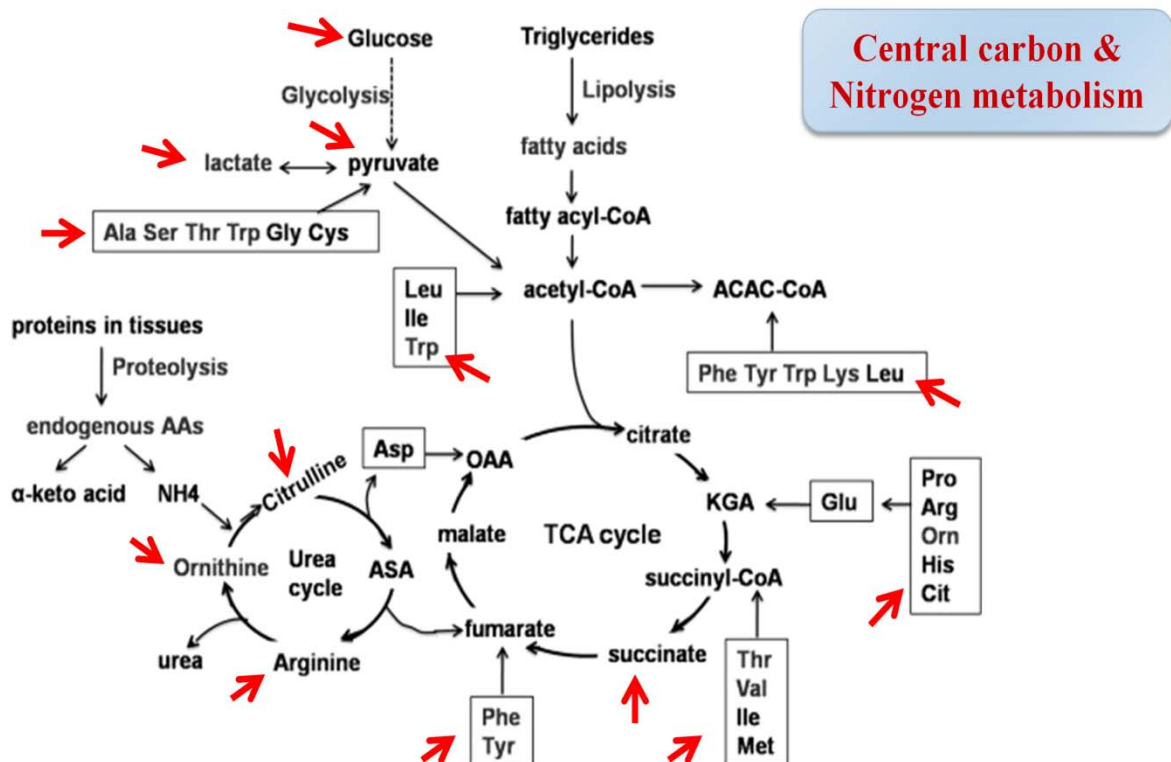


Figure 6.3: Metabolites selected for quantification using LC-MS/MS analysis. Pathway figure is adapted from Y. Zhao et al., BMC Med. 10, 153 (2012) (Zhao et al. 2012).

The targeted analysis was performed in LC-MS/MS for absolute quantification using standards for all these metabolites. Both extracellular and intracellular samples from drug-treated and drug-untreated groups were used for profiling for both U87MG and NSP.

Samples were extracted using the method mentioned in 6.2.2 section and were stored at -80°C until use.

6.2.6. Consumption and Release (CORE) clustering and Principle component analysis (PCA): The concentrations for all 35 metabolites identified from LC-MS/MS analysis were further clustered using ClustVis web tool (<http://biit.cs.ut.ee/clustvis/>). Consumption and release concentrations were calculated by subtracting the concentration at 0 and 96 hrs. These values were used as inputs for generating heat maps and for PCA. Heat maps and clustering was performed with the criteria of unit variance scaling (applied to rows) where all 35 metabolites were the rows in the heat maps. Both rows and columns were clustered using correlation distance and average linkage with the tightest cluster first in tree order. PCA was carried out by using SVD with imputation algorithm specified in the ClustVis tool. In some specific cases, the Euclidean algorithm was used for clustering to interpret the data.

6.2.7. Variable Importance in Projection (VIP) scores using Partial Least Square Discriminant Analysis (PLS-DA): MetaboAnalyst, a web-based statistical tool (MetaboAnalyst - statistical, functional and integrative analysis of metabolomics data) (Xia et al. 2009; Chong et al. 2018; Xia et al. 2015; Xia & David S Wishart 2011; Xia et al. 2012; Xia & David S. Wishart 2011; Xia & Wishart 2016) was used for calculating the VIP scores and the PLS-DA components were plotted to interpret the variance across the cell types. Pareto scaling (mean-centered and divided by the square root of the standard deviation of each variable) was used initially in order to normalize the LC-MS/MS data for the analysis. The 2D and 3D score plots from PLS-DA were generated in the online tool and the interpretations were made accordingly.

6.3. Results

6.3.1. Quantitative metabolite profiling identifies key differences in the metabolic states of the cell in the presence of TMZ

The metabolite levels in the two cell types (U87MG and NSP) over a period of 96 hours of growth/inhibition were analyzed and quantified using LC-MS/MS in the presence of varying concentrations of temozolomide. This was compared to growth in the absence of TMZ. In the absence of TMZ, exo-metabolite profiling showed glucose uptake correlated with lactate secretion, consistent with the well-documented Warburg effect of cancer cells

(Warburg 1956; Hsu & Sabatini 2008; Vander Heiden et al. 2009; Ward & Thompson 2012; Warburg et al. 1923; Dang 2012). The growth limiting substrates (Glucose, glutamine, serine, and tryptophan) were completely depleted by 96 hours by both the cell types except glucose and serine in U87MG at 700 μ M TMZ. Glucose and Glutamine were taken-up linearly by both the cell types in the absence of the drug but NSP showed some lagged uptake in case of glucose. NSP cells were observed to be glutamine-dependent for their survival and growth. Serine and tryptophan had dynamic changes in NSP in the presence of drug exo-metabolite profile compared to U87MG. This was significant at 72 hrs in all concentrations of drug-treated samples (Figure 6.4A).

6.3.2. CORE clustering and PCA

CORE profile analysis and PCA was performed to understand the exo- and endo-metabolite state of both the cell types (U87MG and NSP). Unit variance scaling was applied to CORE (both exo and endo) clustering for the combined 4 experimental setups and 2 cell type analysis with all 35 metabolites in rows. Both rows and columns were clustered using correlation distance and average linkage with the tightest cluster first in tree order. Relevant clustering has been predicted in the combination of succinate-ornithine; glycine-proline, alanine-lactate; arginine-citrulline; and aspartate-tryptophan throughout the varied TMZ concentrations. Most variation was predicted in the 10 μ M TMZ and 700 μ M TMZ (as seen by the color intensity across U87MG and NSP) (Figure 6.4 B and C).

Exo-metabolite PCA output has 5 components where-in PC1, PC2 and PC5 were considered for correlation visualizations. PC1 to PC2 comparison outlined the two-component spheres to converge. In contrast, comparing PC1 to PC5 differentiated the 700 μ M TMZ profile from others. CORE clustering of endo-metabolite profiling projected NSP-700 profile as a distinct column cluster among others. Most variance was observed in the profiles of cells in the presence of drug (highest in NSP-700, NSP-100, and U87MG-10). Among the 5 PCA outputs of the endo-metabolite profile, PC1, PC2 and PC4 were selected for analysis. PC1 to PC2 component spheres clustered NSP and U87MG as separate identifying them as metabolically different intracellularly, yet PC1 to PC4 had some intersection with U87MG (Figure 6.4 D and E).

6.3.3. Concentration profile across time

Concentration was profiled over time to delineate the dynamics. Out of the 35 key metabolites selected for the study, 6 metabolites (Asparagine, citrulline, G3P, histidine,

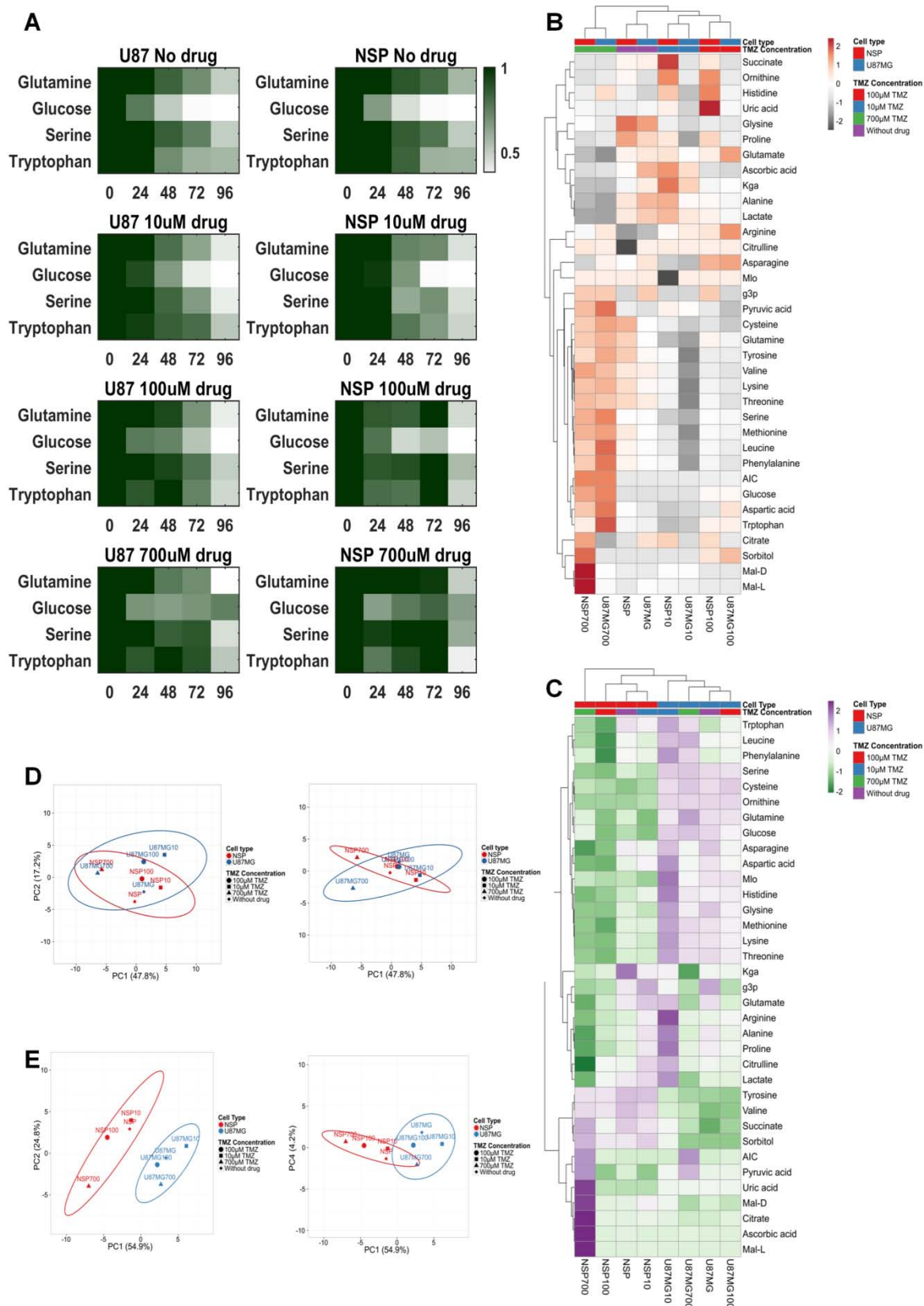


Figure 6.4: Metabolite profiling in the absence and presence of drug (Temozolomide). A) Heat map of growth limiting substrates. Clustergram of Extracellular (B) and Intracellular (C) profiles. PCA analysis of Extracellular (D) and Intracellular (E).

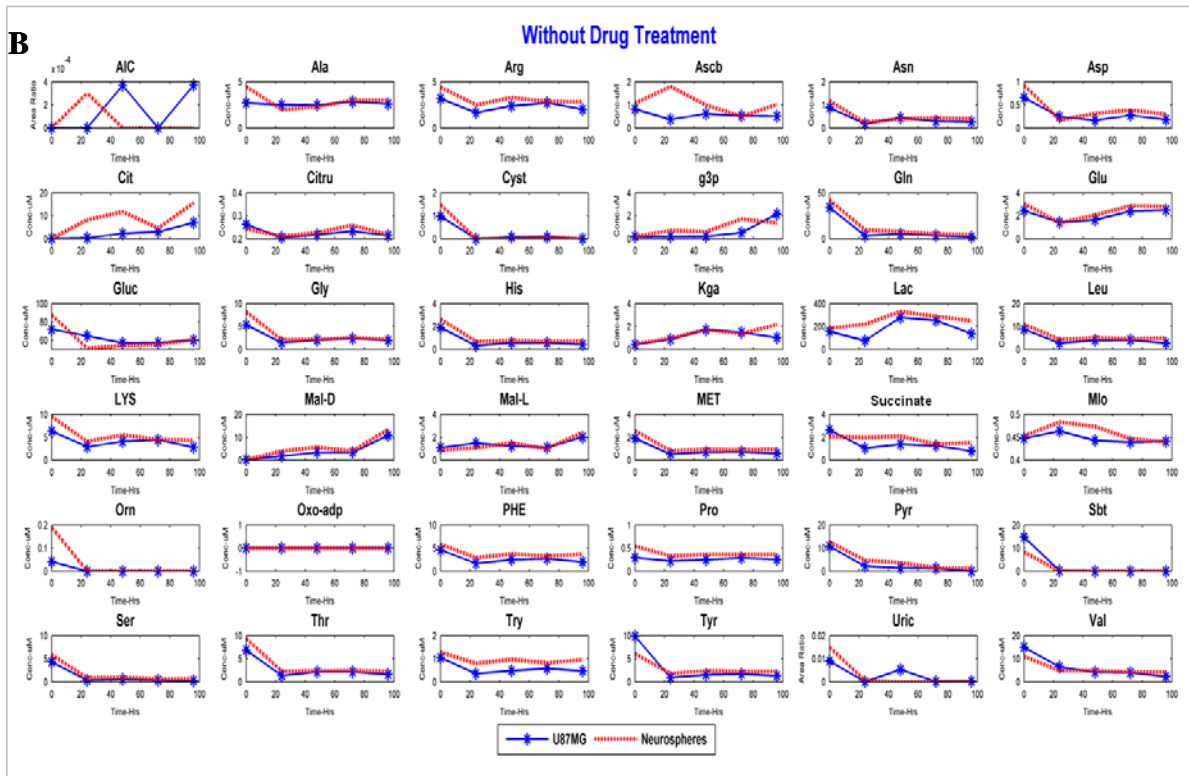
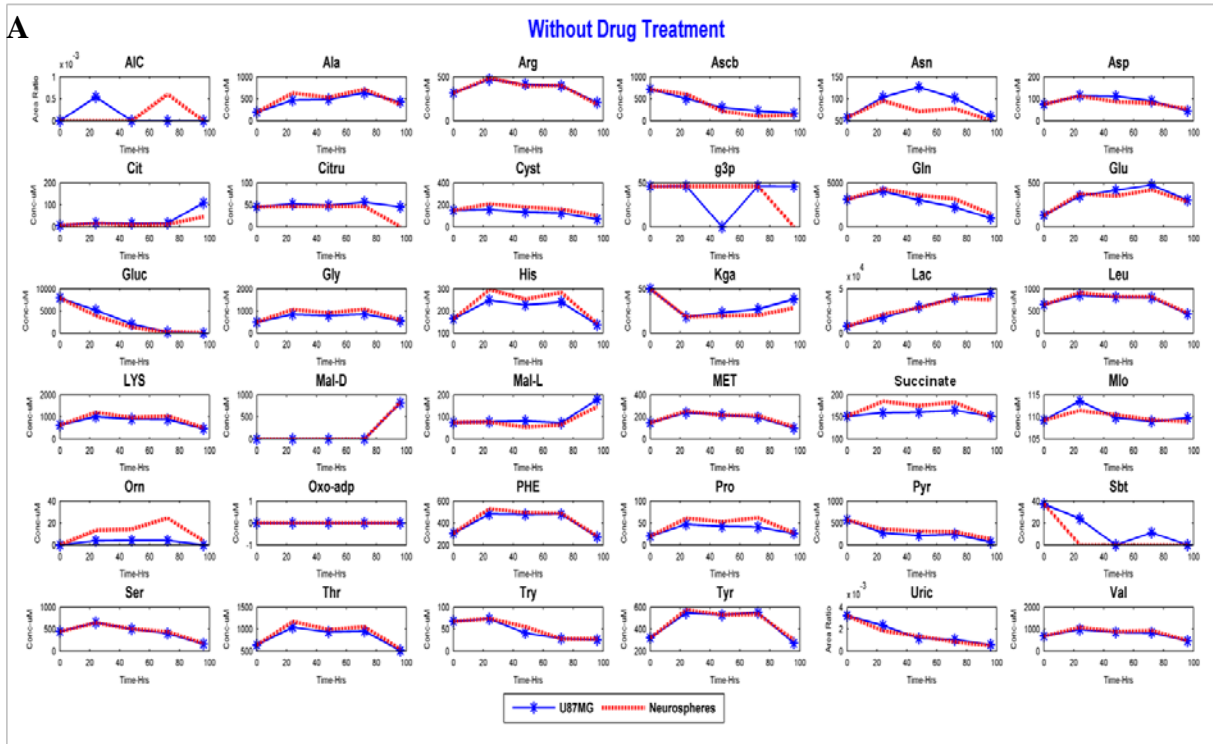


Figure 6.5: Metabolite concentration profile of U87MG and Neurospheres in the absence of temozolomide. A) Extracellular B) Intracellular. The absolute concentrations are plotted with 'Concentration' in Y-axis vs 'Time' in X-axis.

ornithine and proline) showed a differential exo-metabolite profile in the absence of drug (Figure 6.5).

This suggests a possible change in nitrogen flux distribution across the two cell types to maintain their inherent metabolic capability. Alanine, lactate, and glutamate were released by these cells, thus confirming previously discovered glioblastoma signature profiles. Ornithine was found to be a distinct profile in NSP compared to U87MG in all the conditions (No drug, 10 μ M TMZ, 100 μ M TMZ and 700 μ M TMZ). Pyruvate showed differences only in the presence of high concentrations of the drug (700 μ M TMZ). 20 metabolites (Alanine, ascorbic acid, citrate/isocitrate, citrulline, cysteine, glycine, histidine, lactate, leucine/isoleucine, methionine, ornithine, phenylalanine, proline, pyruvate, sorbitol, succinate, threonine, tyrosine and valine) showed difference in their extracellular profile at low concentration of TMZ (10 μ M). The 10 μ M TMZ growth profile was similar to without drug (no significant growth inhibition by TMZ), yet these 20 metabolites showed a concentration change with highest difference in ornithine (~20 fold increase in NSP for no drug profile - 72 hrs; no/least ornithine detection in U87MG in the presence of the drug) followed by pyruvate and alanine (Figure 6.6).

Exo-metabolite profile in the presence of 100 μ M TMZ highlighted 16 metabolites (Alanine, asparagine, citrulline, cysteine, glutamine, glycine, lysine, methionine, succinate, ornithine, phenylalanine, proline, pyruvate, sorbitol, threonine and tyrosine) as different in their concentrations (Figure 6.7). In the presence of 700 μ M TMZ, where U87MG had a negative rate of growth (Appendix A, Table A2) and NSP survived up to 24 hrs in contrast to U87MG. 11 metabolites (Arginine, citrulline, glycine, histidine, lactate, lysine, ornithine, serine, threonine, tyrosine and valine) were different in their exo-metabolite profile in this state (Figure 6.8).

Endo-metabolite concentration profiles and dynamics of 35 metabolites was assessed by normalizing the concentration by cell number to account for increasing cell number/mass at the specific time intervals. Glycine, threonine, and arginine varied similarly in their endo-metabolite profile in the absence and presence of all concentrations of the drug. Six metabolites (Alanine, leucine/isoleucine, lysine, pyruvate, tyrosine, and valine) were differential in the absence of the drug. Pyruvate and alanine were among the 8 metabolites that differed in both 10 μ M TMZ and 100 μ M TMZ. Tyrosine and methionine were unique in the presence of 10 μ M TMZ while Citrulline and D- malic acid unique in the presence of

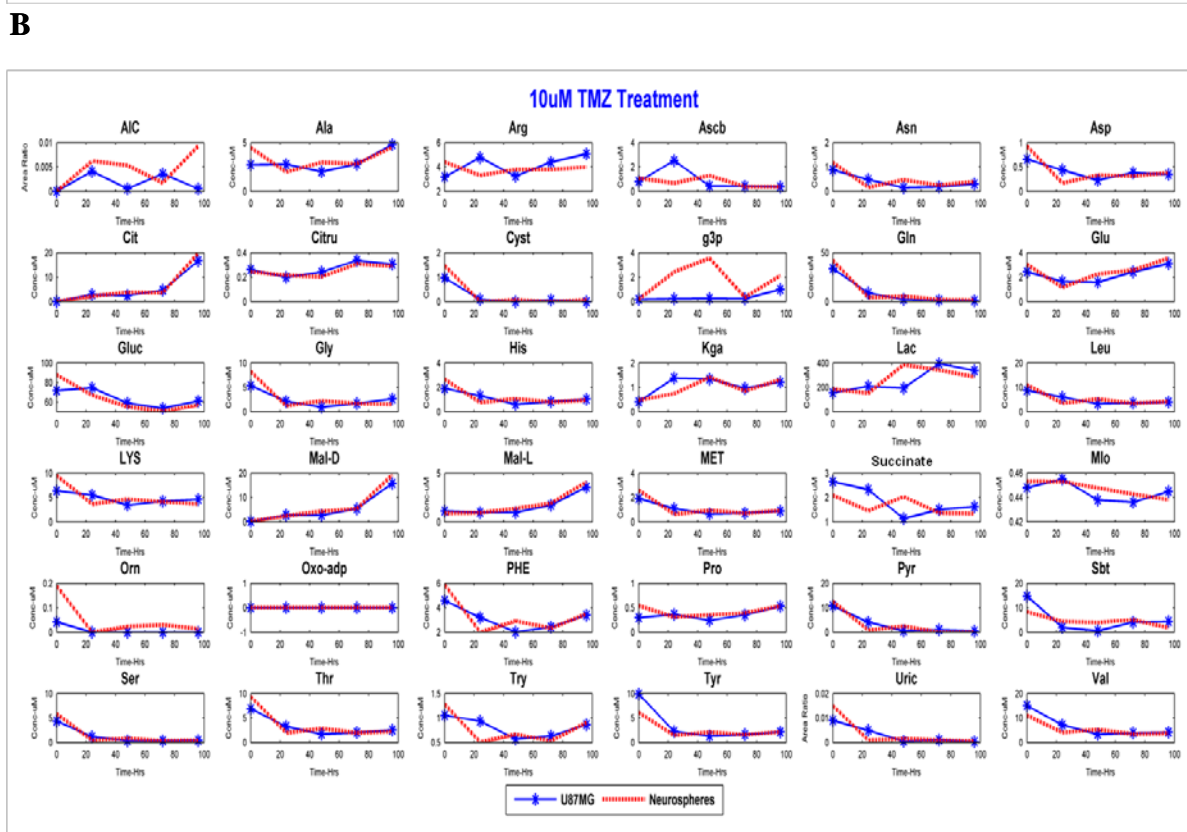
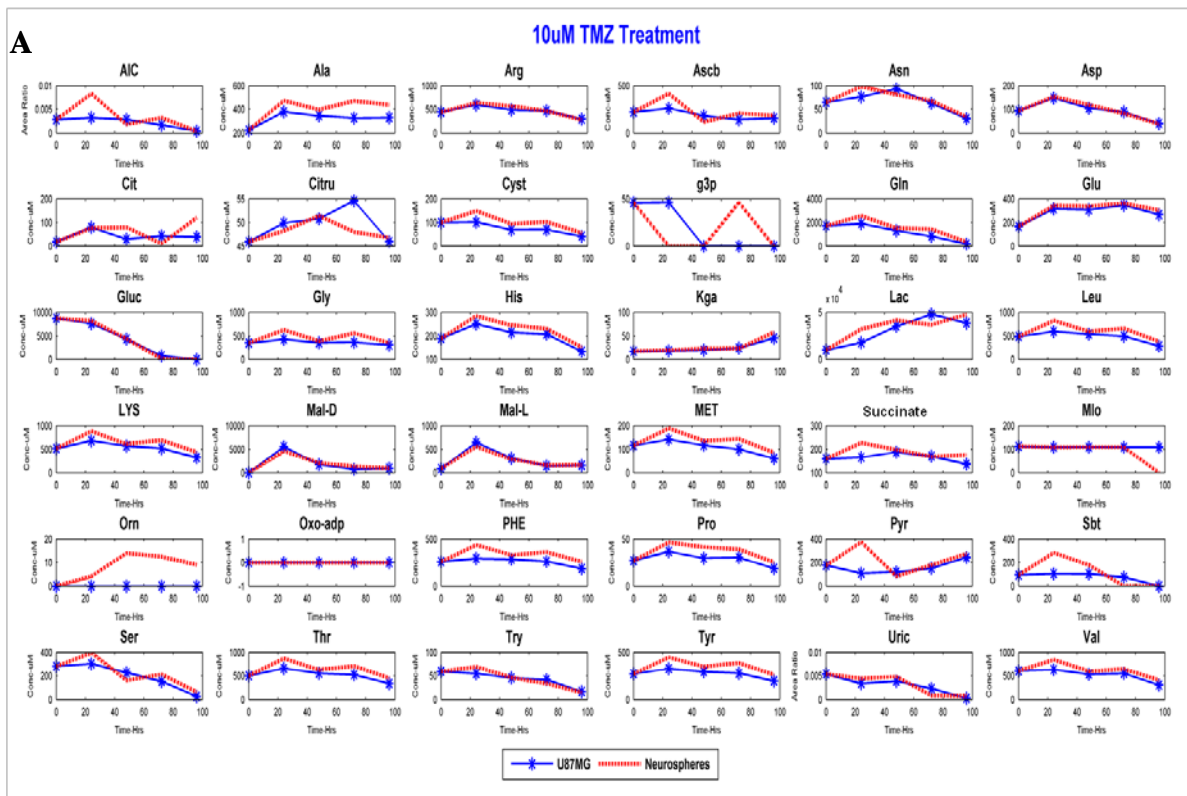


Figure 6.6: Metabolite concentration profile of U87MG (blue) and Neurospheres (red) in the presence of 10 μ M TMZ. A) Extracellular B) Intracellular. The absolute concentrations are plotted with ‘Concentration’ in Y-axis vs ‘Time’ in X-axis.

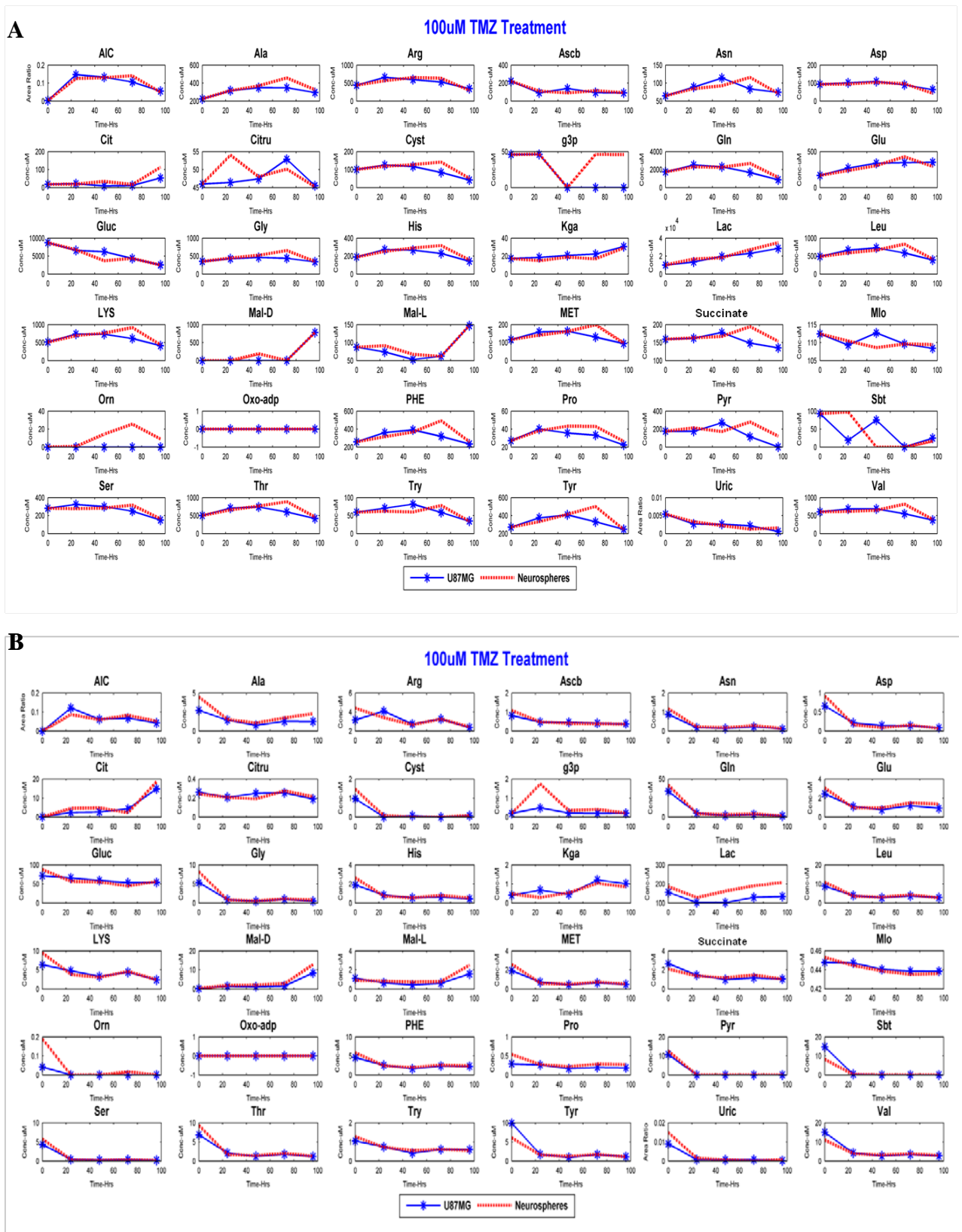


Figure 6.7: Metabolite concentration profile of U87MG (blue) and Neurospheres (red) in the presence of 100 μ M TMZ. A) Extracellular B) Intracellular. The absolute concentrations are plotted with ‘Concentration’ in Y-axis vs ‘Time’ in X-axis.

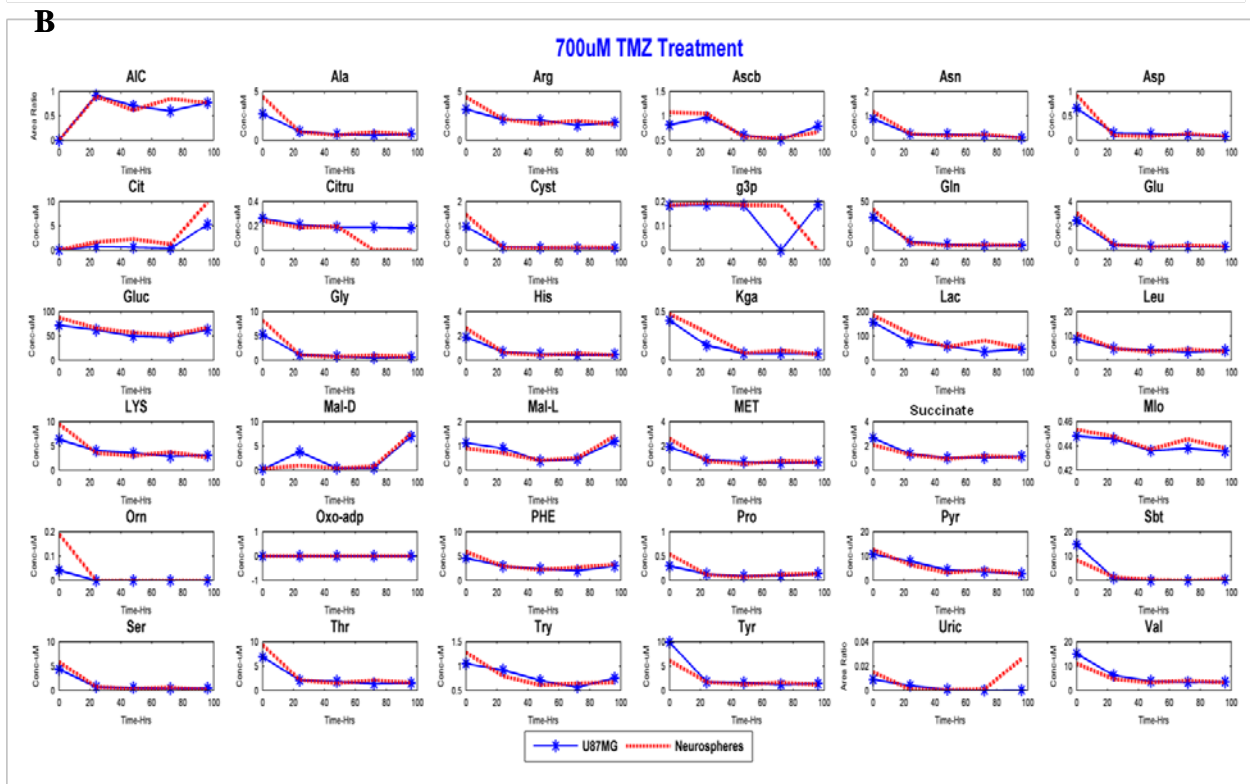
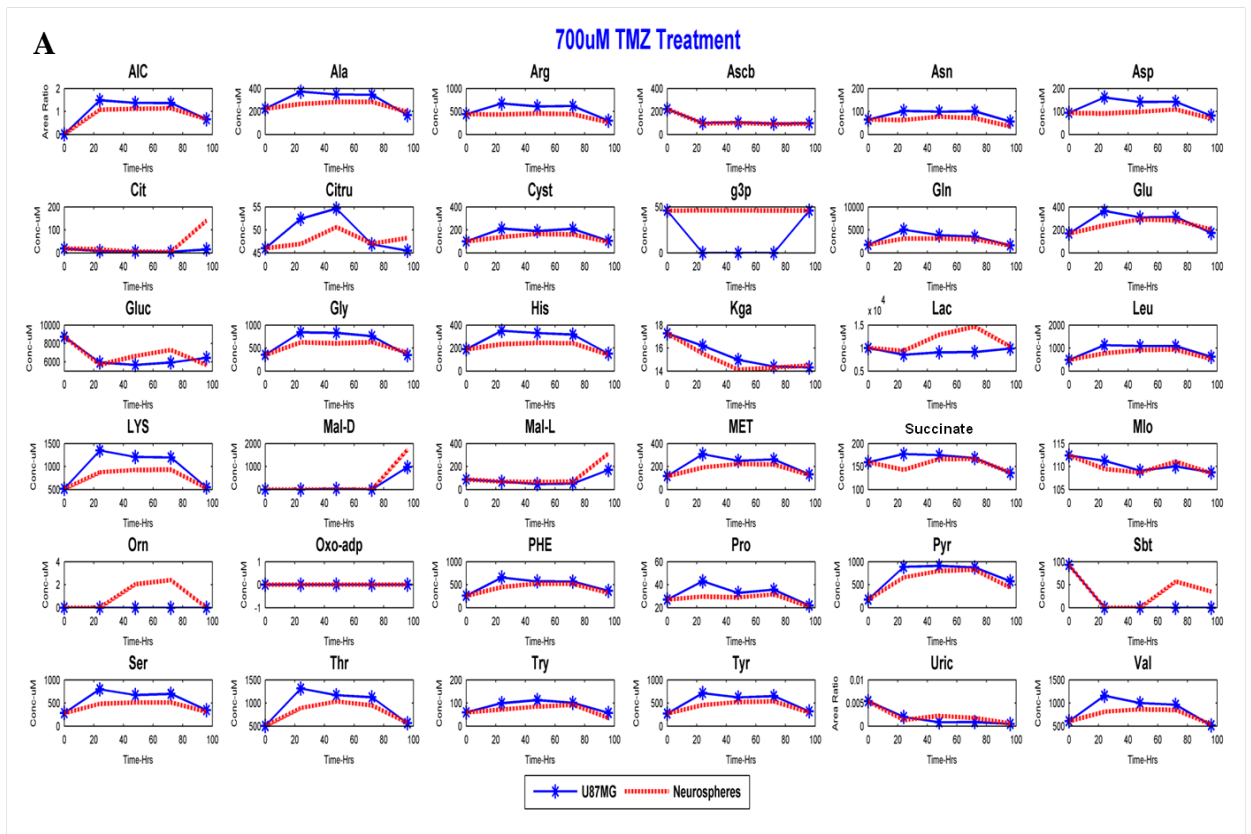


Figure 6.8: Metabolite concentration profile of U87MG (blue) and Neurospheres (red) in the presence of 700 μ M TMZ. A) Extracellular B) Intracellular. The absolute concentrations are plotted with ‘Concentration’ in Y-axis vs ‘Time’ in X-axis.

100 μM TMZ. A 60% change in overall concentration span change was observed in the presence of 700 μM TMZ for all metabolites (Figure 6.4 to 6.8 B sections). Succinate levels diverged significantly in the endo-metabolite profile in the presence of 700 μM TMZ. These analyses showed the demand for these metabolites may differ based on microenvironments. Local conditions may contribute towards choices related to quiescence, proliferation, differentiation or migration in NSP and U87MG.

6.3.4. Key metabolites and their role in metabolic reprogramming

To identify the importance of individual metabolite on the systems under study (U87MG and NSP), it is necessary to use the statistical analysis tools for analyzing the LC-MS/MS data acquired. Identification of the hierarchical importance of metabolites for the cell growth and proliferation of U87MG and NSP was performed in the analysis by calculating their Variable Importance in Projection (VIP) scores using Partial Least Square Discriminant Analysis (PLS-DA). This VIP score is often used to calculate the importance of individual metabolite features in spectra (Farrés et al. 2015).

The extracellular samples from U87MG and NSP cells were analyzed using PLS-DA and their VIP scores were calculated using **MetaboAnalyst**, a web-based statistical tool (MetaboAnalyst - statistical, functional and integrative analysis of metabolomics data) (Xia et al. 2009; Chong et al. 2018; Xia et al. 2015; Xia & David S Wishart 2011; Xia et al. 2012; Xia & David S. Wishart 2011; Xia & Wishart 2016). These results support the initial hypothesis of **Chapter 2**, that NSP prefers glutamine metabolism over glycolysis. Glutamine ranks highest during growth and proliferation of NSP cells while U87MG shows lactate (Figure 6.9). This signifies the importance of glutamine in the temozolomide resistant cells.

In contrast, U87MG cells identified lactate as an important variable potentially due to the potential coupling of Warburg effect and Cori cycle that allows maximizing ATP yields in the absence of Oxidative phosphorylation.

PLS-DA analysis also identified differences in the profiles of U87MG, NSP, and NDx (differentiated from NSP) cells. Pareto scaling (mean-centered and divided by the square root of the standard deviation of each variable) was used to normalize the data points before the PLS-DA analysis. This analysis clearly separated U87MG and NSP as separate clusters and NDx forming the intermediate profile. From this analysis, the metabolic state of NDx cells that are differentiated from NSP has been delineated to be partially between

U87MG and NSP cells (Figure 6.10). The same profile was reflected in the metabolite profile analysis in **Chapter 2**.

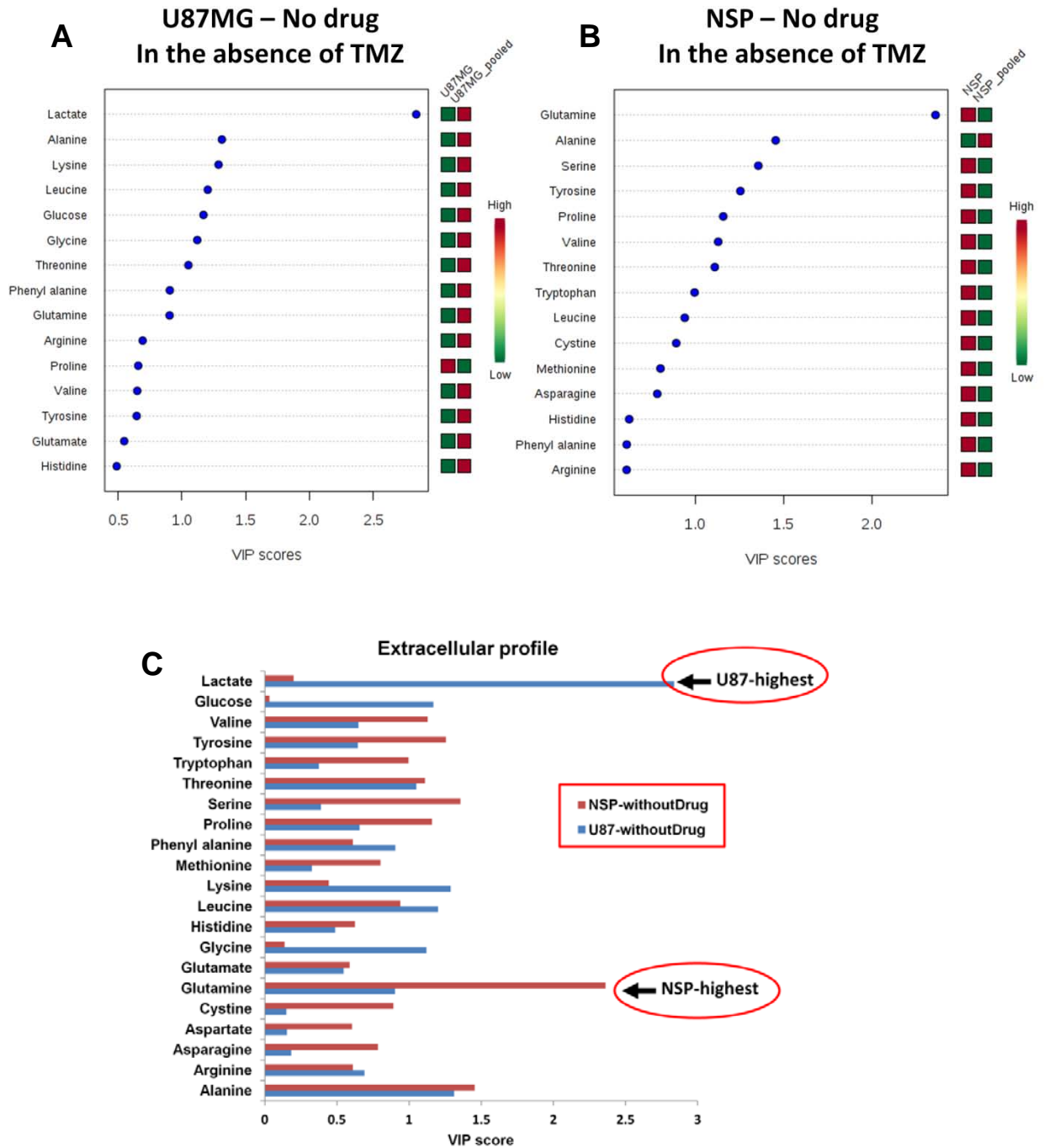


Figure 6.9: VIP score for metabolites profiled using LC-MS/MS analysis for U87MG and NSP in the absence of temozolomide

Differential glycolysis rate is reflected in the ratio between lactate and pyruvate (Figure 6.11A) calculated from the exo-metabolite profile using LC-MS/MS. The ratio of succinate and alpha-ketoglutarate (AKG) in the quantification profiles in extracellular samples

(Figure 6.11B) highlights a major role in regulating the DNA methylation. This ratio regulates the TETs and KDMs in DNA demethylation. NSP cells show a higher ratio and hence the DNA demethylation could potentially be higher in NSP than U87MG cells. This could be a possible reason why the activity of temozolomide i.e. the methylation of DNA does not affect NSP at the IC₅₀ value of U87MG and it requires more dosage to reach the IC₅₀. Our analysis from this thesis identified for the first time, the dependency of temozolomide resistant cells on glutamine and glutamate for its survival and resistance via increased DNA demethylation and repair.

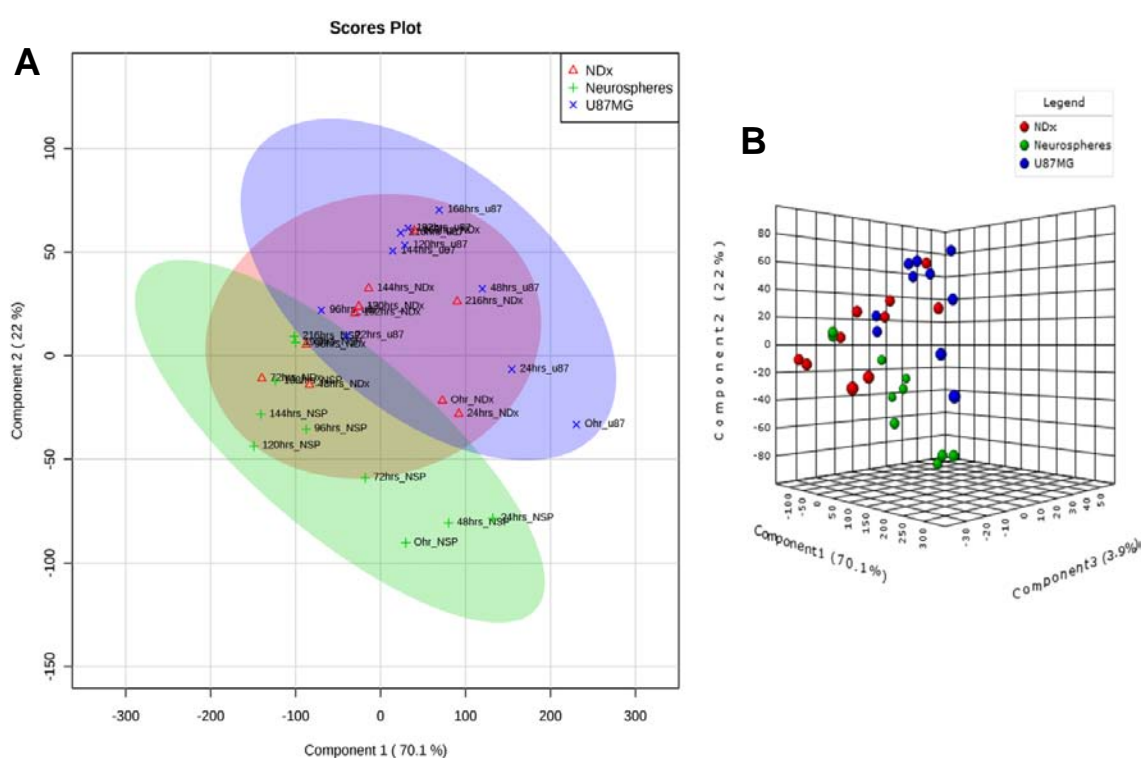


Figure 6.10: PLS-DA component analysis scores plot. A) 2D plot B) 3D plot

Also, ornithine concentrations across U87MG and NSP were found to be differential both in the presence and absence of the drug (Figure 6.12A). This profile was distinct from other amino acids in a way that the difference is consistent in the presence and absence of temozolomide. The presence of a unique deletion in the ODC gene in the exome data from **Chapter 4**, in U87MG cells alone may drive this metabolic change. Also, change in the glutamine concentrations (from low - 0.2mM to high – 2mM) in the media allowed the U87MG cells to accumulate ornithine (Figure 6.12B). This experiment thus explains the reason for the increase in ornithine profile in NSP because of the preferential utilization of glutamine as discussed in **Chapter 2**.

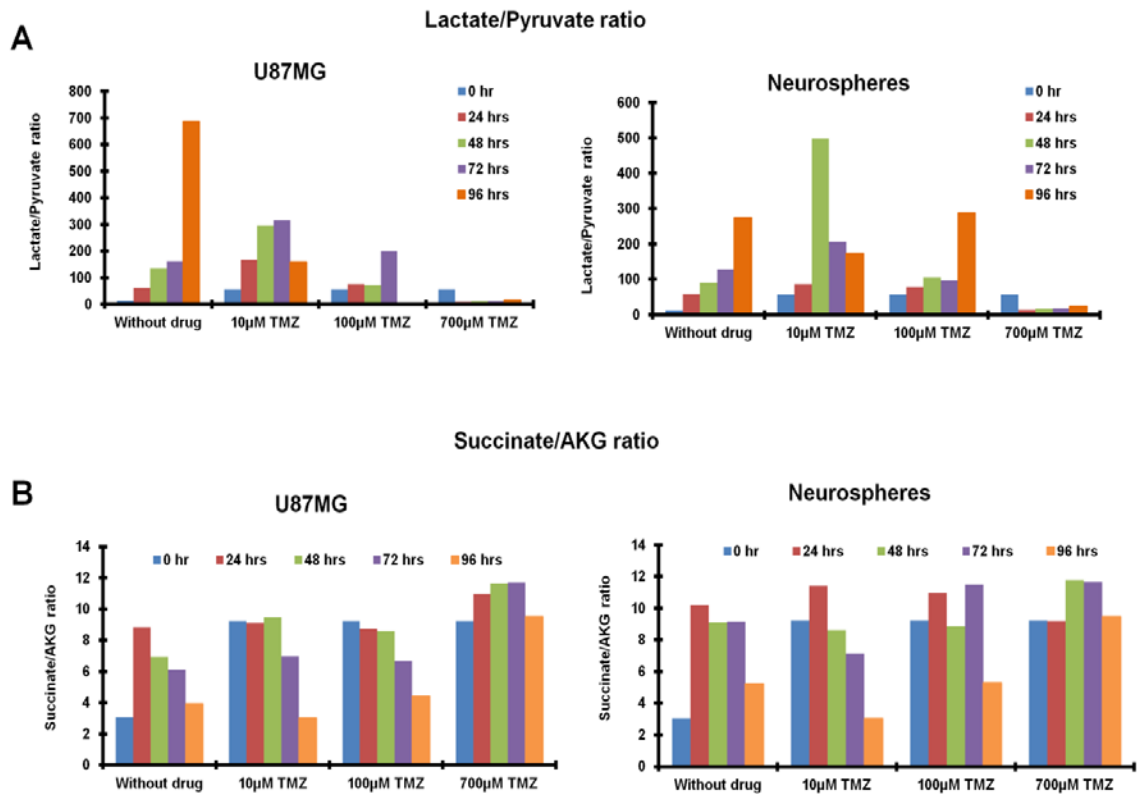


Figure 6.11: Exo-metabolite profile of lactate, pyruvate, succinate, and AKG. A) Ratio of lactate/ pyruvate B) Ratio of succinate/AKG.

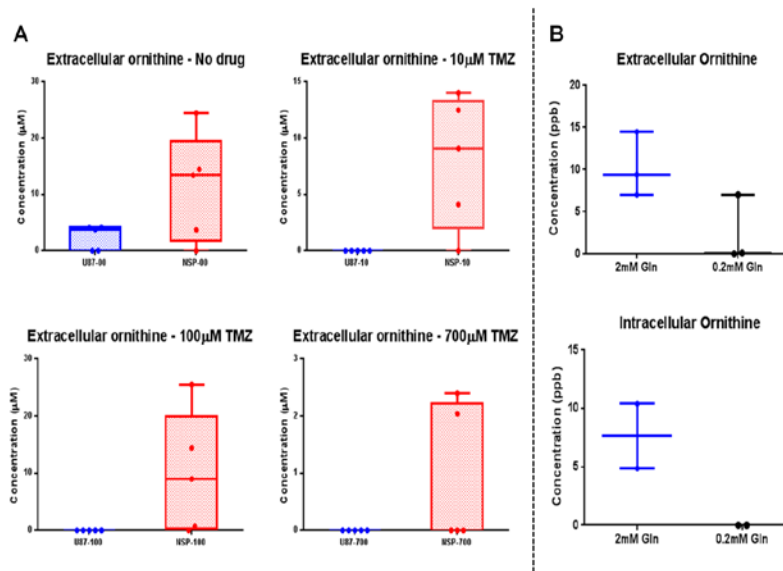


Figure 6.12. Ornithine profiles from LC-MS/MS analysis. A) Exo-metabolite profiles from 4 different experimental conditions (No drug, 10 μ M TMZ, 100 μ M TMZ and 700 μ M TMZ) at different time points (0, 24, 48, 72 and 96 hrs). B) Ornithine profile in low glutamine (0.2mM) and high glutamine (2mM) in U87MG cells.

The major metabolic reprogramming is potentially due to glutaminolysis and its contribution to ornithine via carbamoyl phosphate (Figure 6.13). Hence, the rewired

metabolism is due to the preferential utilization of glutamine as reported from our analysis (Immanuel et al. 2018) along with the potential contributions from genotypic changes in the signal and regulatory networks.

6.4. Discussion

Resistance developed by the cells can be linked to its metabolic state in the presence of the drug as the cell rewires its metabolism to survive in those conditions. Also, delineating the inherent capability of the cell in the absence of the drug would eventually lead to the understanding of rewired metabolism under the influence of the drug. In this **Chapter 6**, the metabolite levels of both temozolomide sensitive and resistant cells were profiled in the conditions where temozolomide is either present or absent in the microenvironment to understand the metabolic reprogramming. Sublethal concentrations (10 μM and 100 μM TMZ) of the drugs and one lethal concentration (700 μM TMZ) was chosen for the analysis. Differential levels of metabolites were identified during survival and death in the presence of temozolomide. This indicates the possible selection through adaptation of metabolites preferred by the cell in the presence of TMZ. By combining all the inferences from the analysis of extracellular and intracellular metabolite levels, the possible metabolic state of NSP that support its growth can be delineated (Figure 6.13).

Glutamine uptake is preferred by NSP more than glucose uptake, highlighting a major contribution of glutamine in the rewired metabolism as also reported in our analysis (Immanuel et al. 2018) and stated in Chapter 2. Glutamine gets converted glutamate via glutaminolysis and can accumulate alpha-ketoglutarate into the TCA cycle. Other important findings are the levels of ornithine from extracellular profile both in the presence and absence of temozolomide that differ highly across U87MG and NSP.

Ornithine levels are very high in NSP compared to U87MG that can possibly rewire the urea cycle to aid in increasing the levels of aspartate and fumarate towards TCA cycle (Figures 6.4 to 6.8 extracellular panels). These results strongly suggest a path towards TCA cycle and ETC for the generation of ATP in contrast to U87MG that depends on Warburg effect to generate ATP. Such analyses have never been performed before to understand the metabolism in the presence of drug to characterize resistance. Hence our study allows identification of a metabolic basis for drug response, susceptibility, and resistance. It provides key evidence for the role of metabolic pathways in the survival of resistant cells.

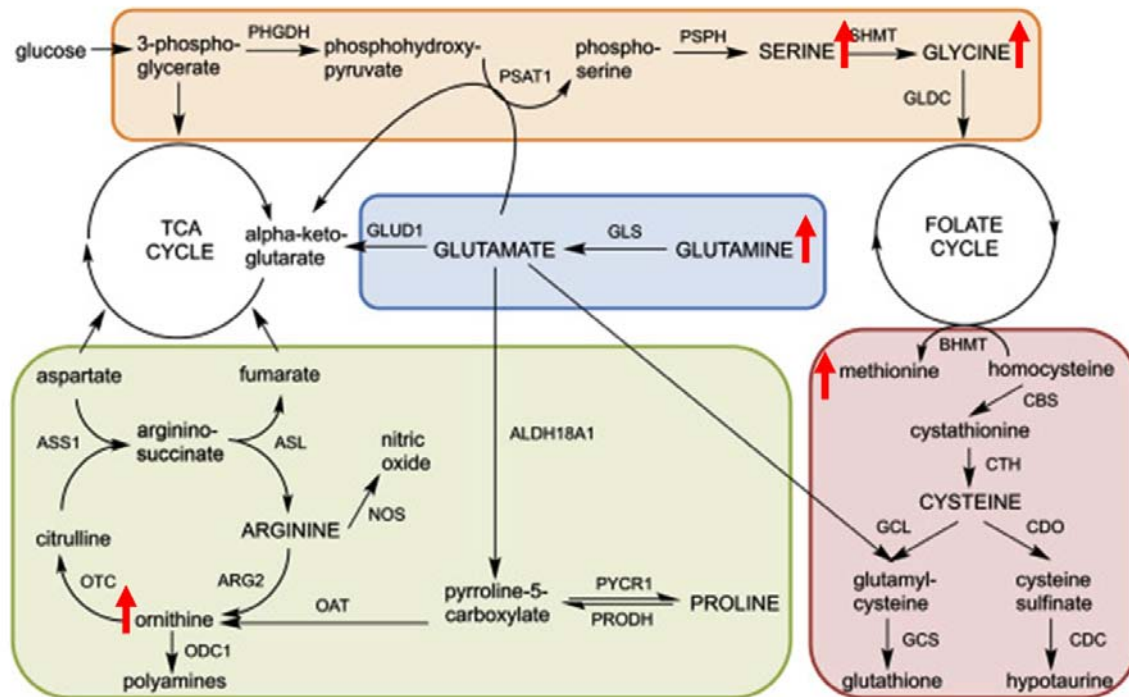


Figure 6.13: Predicted metabolic state of NSP cells. Pathway figure adapted from Geck, R. C., and Toker, A. Nonessential amino acid metabolism in breast cancer, *Advances in Biological Regulation*, 62, 11–17 (2016) (Geck & Toker 2016). **Red arrows indicate the inferences from this study.**

6.5. Conclusions

Absolute quantification of metabolites using LC-MS/MS analysis has always been a promising technique to identify the key metabolites that are responsible for cancer progression and drug resistance. In our study, we have used this technique to identify the potential rewired metabolism that is linked to drug resistance. Glutamine and ornithine were identified to be the most important differential profiles in comparison across U87MG and NSP in both the presence and absence of temozolomide.

Overall profiles of all 34 metabolites were different in the 700 μM TMZ condition for NSP compared to all other profiles. Clustering and PCA analyses also indicated the metabolic phenotype differences across these two populations. From these, it is evident that the metabolite profiles dictate the cell state and can be used to identify causal metabolites. Further, a metabolite supplementation/depletion strategy could be developed to address and inhibit the uncontrolled growth of temozolomide resistant cells.

Chapter 7

An Integrative Paradigm for Temozolomide Resistance: A Systems Approach

"The significant problems we have cannot be solved at the same level of thinking with which we created them".

- Albert Einstein

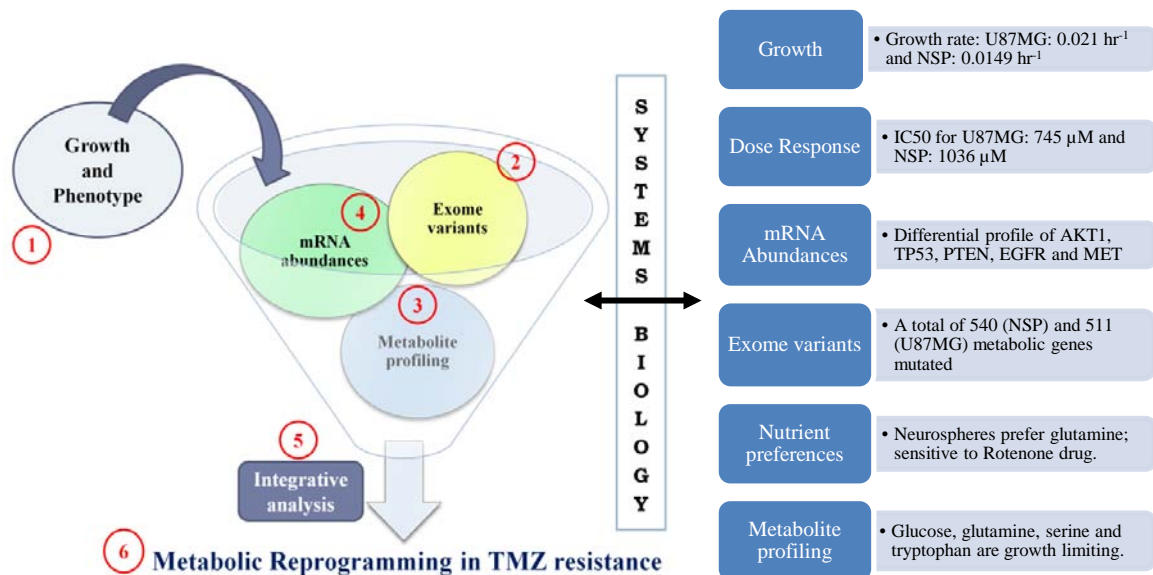


Figure 7.1: The experimental datasets and their key inferences from Chapters 2 to 6 that are used for the integrative analysis in this chapter 7.

The so-called “War on Cancer” approaches the half-century mark and a new paradigm to guide cancer treatment may be needed for the 21st century. Current treatments for cancer include surgery, radiotherapy, cytotoxic chemotherapy, hormonal therapy, immunotherapy, and targeted therapies, however; the cure for cancer is still at bay due to acquired resistance and metastasis. For new paradigms based on reductionist and systems biology approaches established in the previous century, *in vitro*, *in vivo*, clinical models need to be established. The prior chapters of the thesis discussed multiple molecular approaches to probe drug resistant and susceptible glioblastoma cells. Data integration to understand the combinatorial effect and crosstalk among molecular hierarchies (as discussed in this chapter) would help develop strategies against resistant cells in the future. The results from the reductionist approaches applied and discussed in **chapters 2 to 6** were unified to develop context-specific inferences. The outcome of this analysis is the development of an integrative paradigm that helps in understanding drug resistance to aid in systems-level characterization. In the next few sections, inferences from piece-wise molecular data integration will be discussed to answer some open questions.

7.1. How does the expression of drug transporters impacts growth and susceptibility response to temozolomide?

The gene expression of ATP-binding cassette (ABC) transporters delineated using real-time PCR in Chapter 3. These transporters constitute an important superfamily of integral membrane proteins that involves the transport of drugs (Higgins 2001; Rees et al. 2009; Glavinas et al. 2008; Vasiliou et al. 2009; Chang 2003). The mRNA abundances could eventually contribute to drug efflux thereby contributing to drug resistance. Differential transcript levels were observed for all the 7 sub-family ABC transporters. ABCC5 showed a maximum of 10 fold variation in transcript levels. Network analysis predicted that ABCC5 is linked to four drugs (6-mercaptopurine, methotrexate, 6-thioguanine, and 5-fluorouracil).

These drugs tested on the BIOLOG panel (Chapter 5) showed differential efficacy on U87MG and NSP cell viability. Also, through exome analysis (Chapter 4) two novel missense mutations in ABCC5 were identified only in U87MG that could potentially be causal for lowered gene expression. Most transporters belonging to the ABCC sub-family were highly differential in expression. ABCG2 also linked to the transport of 12 drugs (represented on the BIOLOG panel) had increased gene expression in NSP cells though there was no genomic variability (Figure 7.2). 17 ABC transporter genes had increased

gene expression in NSP cells that could account for the drug response in NSP cells. The same transporters were also linked to metabolite and small molecule transport as elucidated in the network analysis (Figure 7.2) from PathwayStudio™ tool.

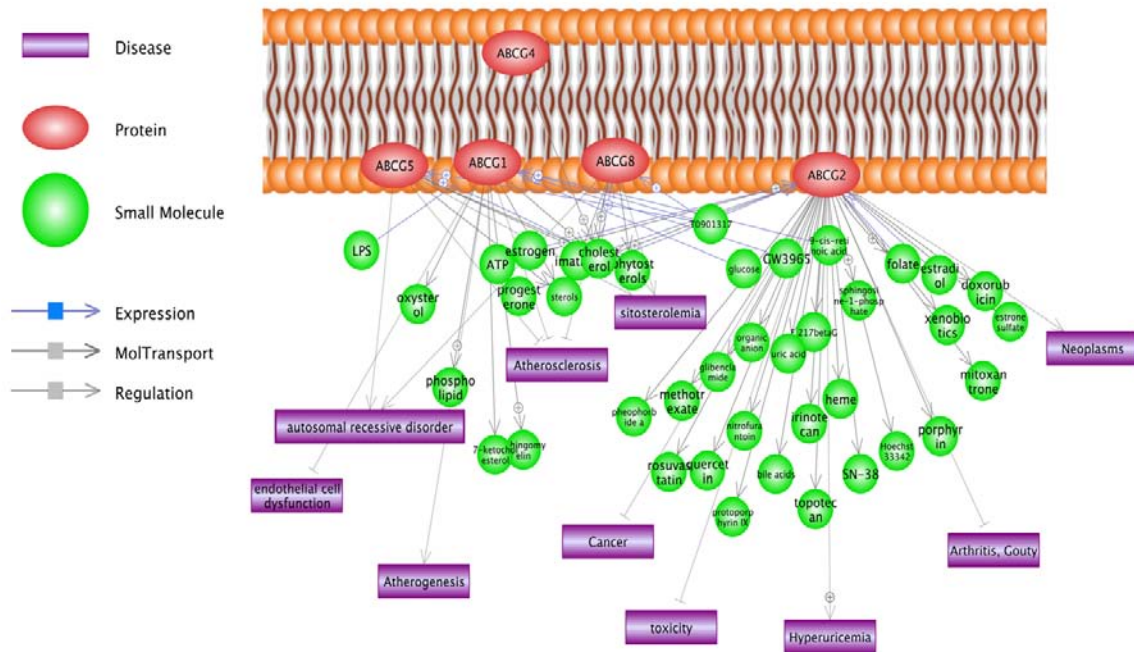


Figure 7.2: ABCG transporter family and its linked transport of molecules. Pathway Studio™ driven elucidation of activity of ABCG transporters.

By complimenting drug efflux with the transport of specific metabolites, these ABC transporters could potentially modulate the microenvironment that would shape growth and proliferation of the cells.

7.2. How does modulating CAN gene expression impacts the response to alkylating drug TMZ?

CAN genes that include AKT, IDH1, IDH2, STAT3, MGMT, and PTEN showed differential mRNA abundances in the qPCR analyses (Chapter 3). These genes contribute to the control of nutrient uptake, metabolic rewiring and epigenetic control of other genes. Higher mRNA abundances of cytokine STAT3 in NSP potentially turn on the MYC transcriptional program and induces preferential consumption of glutamine as shown in the LC-MS/MS data (Chapter 2/Chapter 6). The simultaneous negative regulation of ACL by AKT1 as shown in Chapter 3, potentially lowers the acetyl CoA pool and hence the acetate available for histone acetylation. A reduced aerobic glycolytic flux reflective of higher NAD levels potentially control SIRTUIN family transcriptional repressors and silence

chromatin via decreasing histone acetylation. This partially explains differential tryptophan metabolism (growth limiting for U87MG in Chapter 2) and suggests a role for picolinate carboxylase in the balance between NAD derived nucleotide synthesis and acetyl-CoA driven acetylation. Higher levels of AKG (TCA pool) also indicate epigenetic connections to the Jumonji family of histone de-methylases that could prevent methylation of histones (Figure 7.3).

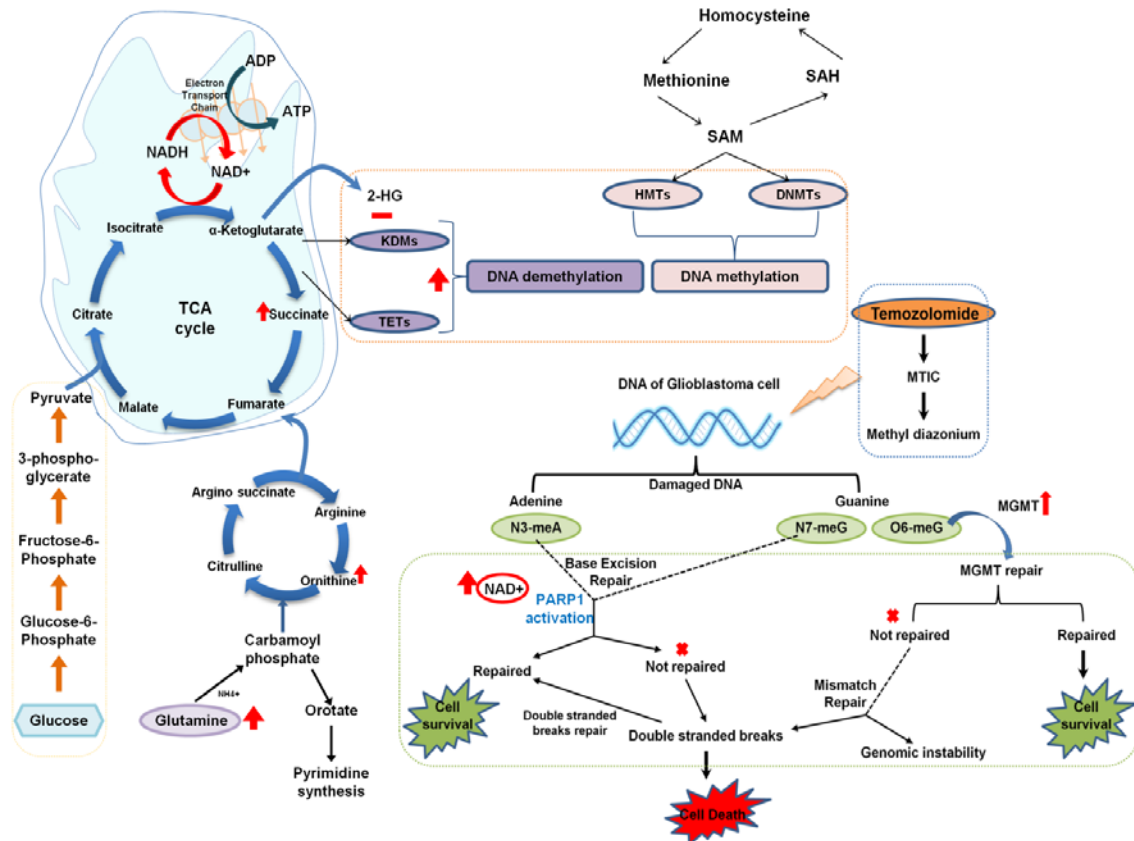


Figure 7.3: Possible resistance mechanism of NSP cells derived from the inferences on LC-MS/MS and mRNA abundances datasets.

This may also explain the varied dose-response relations and increased IC_{50} for TMZ. The dependency on glucose and pyruvate; and not glutamine for growth/respiration also suggests normal levels of methylation in U87MG. Similar MGMT mRNA abundances suggest functional DNA repair in the absence of TMZ. Adaptive TMZ resistant GBM cells have been reported to show activation of JNK, up-regulation of metabolism related to citrate, and an increase in histone demethylase KDM5A gene expression (Banelli et al. 2015). In line with this hypothesis (Figure 7.3), validated through metabolite profiling, NSP exhibited up to 2-fold resistance (indicated by higher IC_{50} , E_{max} and AUC values)

during the studied chemotherapeutic response to TMZ in Chapter 2.

7.3. How do genomic alterations contribute to temozolomide resistance?

All genes that have alterations only in one cell type or have unique mutations from exome data have been classified as metabolic, signaling genes, regulatory genes and epigenetics related genes. The genes with homozygous and nonsynonymous mutations are known to affect protein function (85% confidence). Such unique changes (Chapter 4) in the genome potentially shape the reprogramming of metabolism (Chapter 2/6) in temozolomide resistant NSP cells. The number of variants identified in exome characterization for these key genes is listed in Table 7.1. These genes have an important role in shaping the metabolism as highlighted in Figure 7.8.

Table 7.1. Exome variants of genes that control metabolism

Gene Symbol	Gene Description	No. of variants	
		U87MG	NSP
HIF1A	Hypoxia-inducible factor 1, alpha subunit	1	1
PTENP1	Phosphatase and tensin homolog 2	2	2
TP53	Tumor protein p53 isoform a	1	1
MTOR	FK506 binding protein 12-rapamycin associated	3	3
PIK3R1	Phosphoinositide-3-kinase, regulatory subunit 1	2	1
TSC1	Tuberous sclerosis 1 protein isoform 1	1	0
TSC2	Tuberous sclerosis 2 isoform 1	2	2
GPX1	Glutathione peroxidase 1 isoform 1	0	1
APC	Adenomatous polyposis coli	7	7
OAZ1	Ornithine decarboxylase antizyme 1	1	0
ODC1	Ornithine decarboxylase 1	1	0
AMY2A	Pancreatic amylase alpha 2A precursor	1	0
SLC38A3	Solute carrier family 38, member 3	0	1
SLC38A4	Solute carrier family 38, member 4	2	2
SLC1A5	Solute carrier family 1 member 5 isoform 1	0	1
GCLM	Glutamate-cysteine ligase regulatory protein	0	1
GGT2	Gamma-glutamyltransferase 2	1	2
ATP4A	Hydrogen/potassium-exchanging atpase 4A	1	1
CYC1	Cytochrome c-1	1	2
PLCD3	Phospholipase C delta 3	1	2
SYNJ1	Synaptojanin 1 isoform a	5	7
ME1	Cytosolic malic enzyme 1	0	1
HMBS	Hydroxymethylbilane synthase isoform 1	0	1

7.4. Combinatorial role of CAN genes, ABC transporters, related exome and metabolism on temozolomide resistance

Since TMZ is a DNA methylating drug, the potential effects of regulating metabolism on epigenetics are critical in drug action and cell susceptibility. From the integrated analyses discussed in the previous sections, it is obvious that the emergent properties of these resistant cells are not only from their differential gene expression of drug transporters but a combined effect from CAN genes that drove metabolic reprogramming (Figure 7.4).

Together, by interlinking these connections, one can identify the specific metabolic state of the resistant cells that can be targeted by the novel data-driven development of therapeutic regimens.

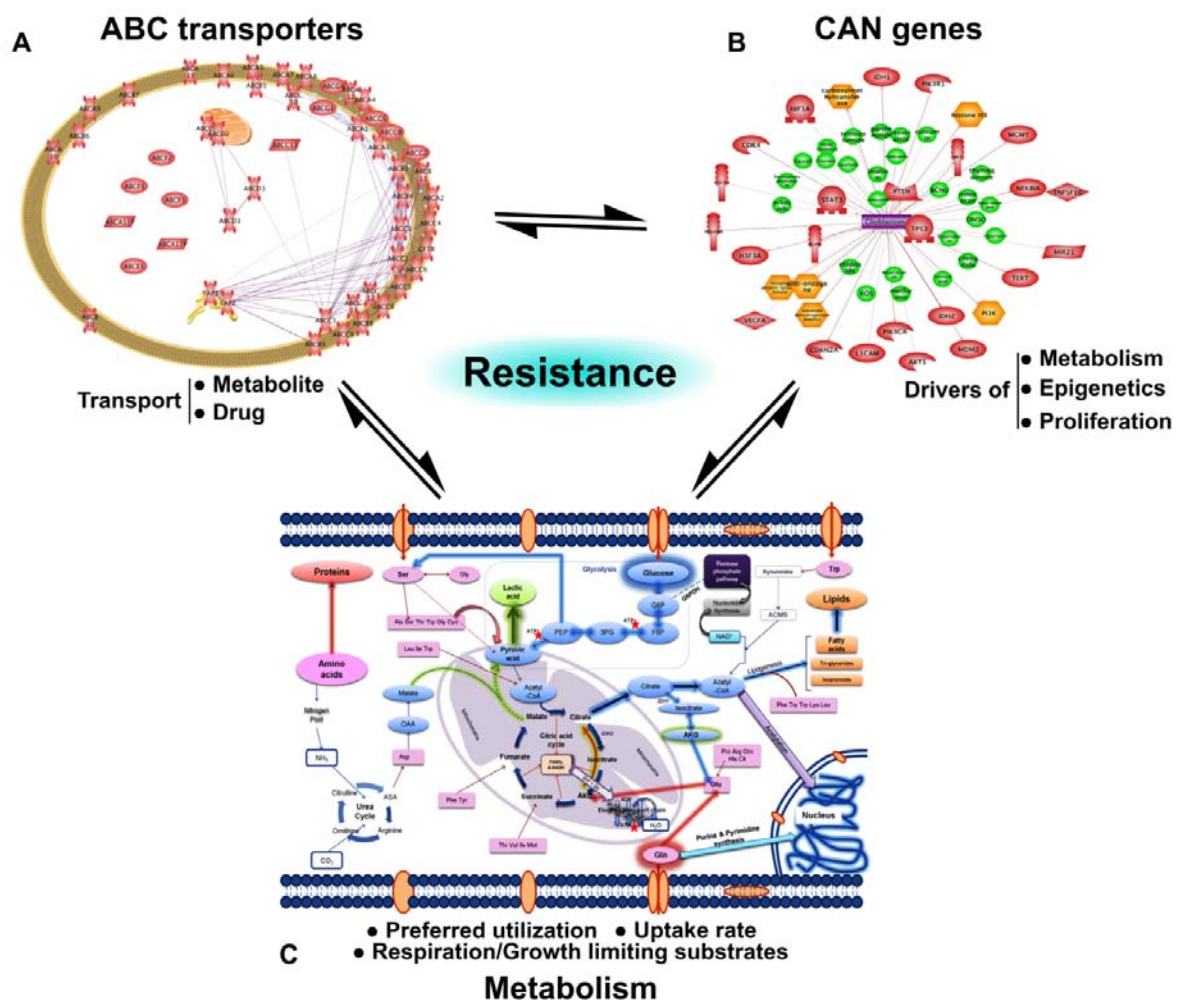


Figure 7.4: An Integrative paradigm for Temozolomide resistance. Contributions in part by metabolism, mRNA abundances of ABC transporters and CAN genes to TMZ resistance in NSP are depicted. Representation of (A) the localization of ABC transporters in the cell (B) network analysis of 23 CAN genes using Pathway StudioTM and (C) potential metabolic rewiring indicated by red (NSP) and blue (U87MG) arrows.

Our study thus highlights the need for a new paradigm for research on drug resistance focusing on the global picture of the cell at the systems level.

7.5. Predictive constraints-based metabolic modeling of U87MG and NSP cells

Constraints-based approaches enable one to integrate multiple data-types (Figure 7.5A) in the context of a model to help predict emergent properties. These models have been reported to help understand cancer metabolism and predict phenotypes that are specific to the constraints. These models are also able to elucidate differential pathway wiring based on constraints. Metabolism is not just a hallmark of cancer but can cross-talk with most of the other hallmarks (Figure 7.5B).

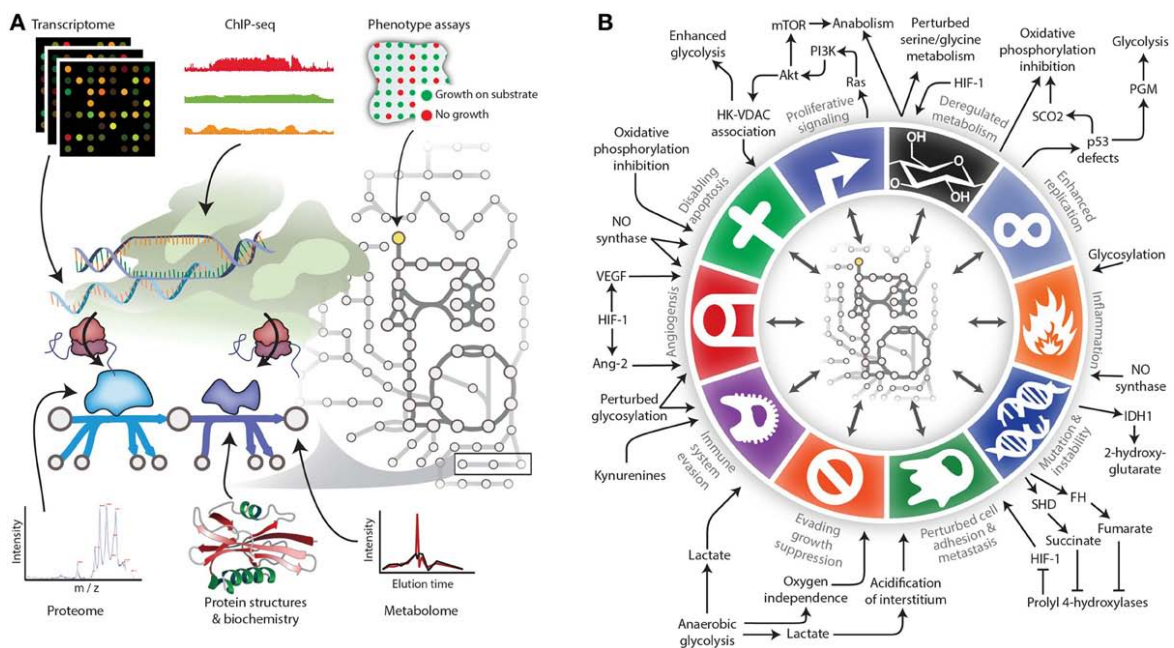


Figure 7.5: Constraints-based metabolic models (A) and their role in delineating cancer metabolism (B). Adapted from N. E. Lewis, A. M. Abdel-Haleem, The evolution of genome-scale models of cancer metabolism. *Front. Physiol.* 4, 237 (2013) (Lewis & Abdel-Haleem 2013).

In this approach, we have integrated all the experimental data discussed so far into a core metabolic model to develop *in silico* representations of U87MG and NSP. A previously published core model of human metabolism (Figure 7.6) consisting of 380 reactions (Zielinski et al. 2017) was contextualized using CORE data obtained in Chapter 2. This core model includes reactions from all the central metabolic pathways including glycolysis, gluconeogenesis, pentose phosphate pathway, TCA cycle etc. The cell-specific models (Figure 7.6) were defined using experimental constraints from growth, uptake rates of different metabolites (LC-MS/MS data) and genomic variants from Exome data mentioned

in the **Chapters 2 to 6** in this thesis. The prediction accuracy for growth rates of the *in silico* cells of u87MG and NSP was 94% for U87MG and 92% for NSP (Figure 7.7A). The oxygen uptake rate was fixed using legacy data for a grade III glioblastoma cell line, U251 (Zielinski et al. 2017).

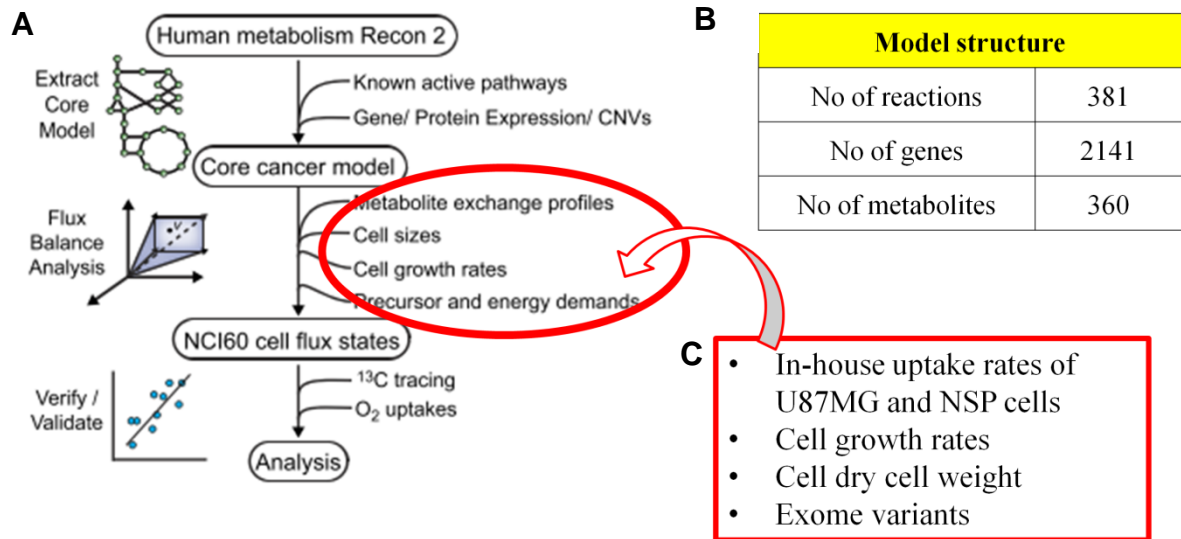


Figure 7.6: Generation of constraints-based core metabolic model of U87MG and NSP cells. A) Base model reported. Figure adapted from Zielinski, D. C. et al. Systems biology analysis of drivers underlying hallmarks of cancer cell metabolism, Scientific Reports 7, 41241 (2017). B) Model structure C) Constraints used from in-house experimental datasets.

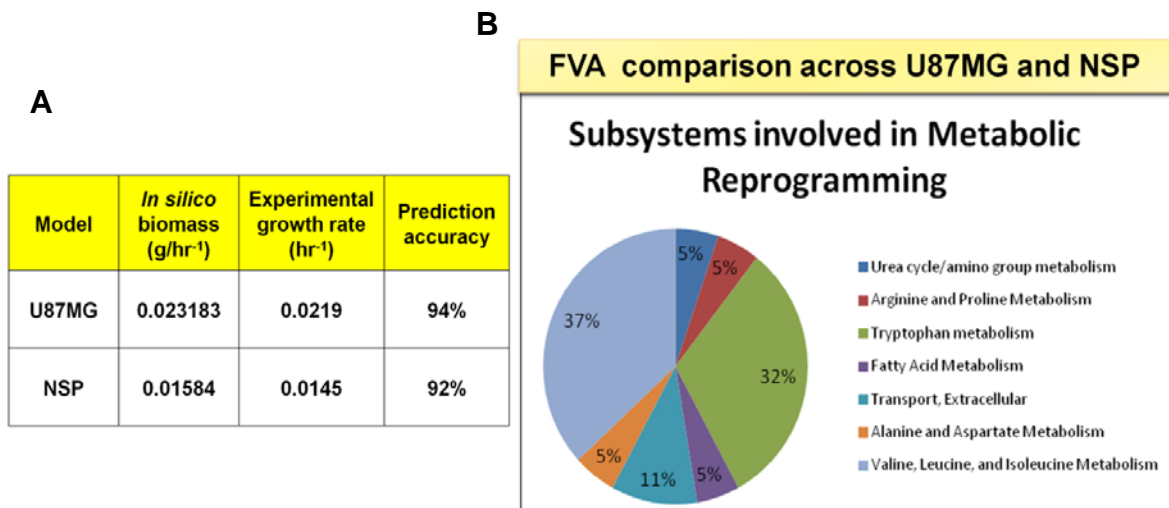


Figure 7.7: Core model predictions. A) Biomass B) Flux variability analysis.

Table 7.2. Differential flux distribution across U87MG and NSP in Flux variability analysis.

Reaction Name	Reaction	U87MG		NSP	
		Minimum	Maximum	Minimum	Maximum
ornithine carbamoyltransferase, irreversible	OCBTm	-4.4E-16	1.398211	4.42E-17	0.74598
pyrroline-5-carboxylate reductase (m)	P5CRm	-5.9E-05	0.001356	0.00261	0.003223
L-Tryptophan exchange	EX_trp_L(e)	-0.03063	-0.02659	-0.00121	-0.00121
3-hydroxyanthranilate 3,4-dioxygenase	3HAO	0.024801	0.028847	0	0
aminomuconate-semialdehyde dehydrogenase	AM6SAD	0.024801	0.028847	0	0
2-aminomuconate reductase	AMCOXO	0.024801	0.028847	0	0
formate dehydrogenase	FDH	0.027221	0.031267	0.001646	0.001646
N-Formyl-L-kynurenine amidohydrolase	FKYNH	0.024801	0.028847	0	0
3-Hydroxy-L-kynurenine hydrolase	HKYNH	0.024801	0.028847	0	0
kynurenine 3-monooxygenase	KYN3OX	0.024801	0.028847	0	0
picolinic acid decarboxylase	PCLAD	0.024801	0.028847	0	0
L-Tryptophan:oxygen 2,3-oxidoreductase (decyclizing)	TRPO2	0.024801	0.028847	0	0
L-tryptophan transport in via sodium symport	TRPt4	0.026587	0.030633	0.001214	0.001214
argininosuccinate lyase	ARGSL	1.74E-14	1.398211	-1.5E-15	0.74598
L-glutamine transport via electroneutral transporter	GLNtm	0	1.280819	-5.6E-16	0.72901
3-Methyl-2-oxopentanoate mitochondrial transport via proton symport	3MOPt2im	0	-4.6E-15	0.00422	0.004585
acetyl-CoA C-acetyltransferase, mitochondrial	ACACT10m	0	-4.6E-15	0.00422	0.004585
acyl-CoA dehydrogenase (2-methylbutanoyl-CoA), mitochondrial	ACOAD10m	0	-4.6E-15	0.00422	0.004585
2-Methylprop-2-enoyl-CoA (2-Methylbut-2-enoyl-CoA), mitochondrial	ECOAH9m	0	-4.6E-15	0.00422	0.004585
3-hydroxyacyl-CoA dehydrogenase (2-Methylacetoacetyl-CoA), mitochondrial	HACD9m	0	-4.6E-15	0.00422	0.004585
L-isoleucine transport in via sodium symport	ILEt4	0.014332	0.014332	0.013967	0.014332
isoleucine transaminase	ILETA	0	-4.6E-15	0.00422	0.004585
2-oxoisovalerate dehydrogenase (acylating; 3-methyl-2-oxopentanoate), mitochondrial	OIVD3m	3.47E-18	-4.6E-15	0.00422	0.004585
Propionyl-CoA carboxylase, mitochondrial	PPCOACm	0	-4.6E-15	0.00422	0.004585
L-Isoleucine exchange	EX_ile_L(e)	-0.01433	-0.01433	-0.01433	-0.01397
methylmalonyl-CoA epimerase/racemase	MMEEm	4.57E-15	-5.6E-17	-0.00458	-0.00422
Reversible reaction					
Only in the positive direction (forward)					
Only in the negative direction (backward)					
Rigid Reaction (Flux is fixed, does not vary)					

Table 7.3. Details of the exome variants used as constraints.

NSP unique genes mutations (Homozygous) correlated to the model reactions based on GPR											
<i>In silico</i> model details				Genes with alterations (Homozygous)		Genes with alterations (Heterozygous)		Unique genes (Homozygous)		Unique Mutations in common genes (Homozygous)	
Gene	Rxn ID	RxnName	Rxn Subsystem	U87MG	NSP	U87MG	NSP	U87MG	NSP	U87MG	NSP
CYC1	CYOR_u10m	CYOR u10m	Oxidative Phosphorylation	N	Y	Y	Y	N	Y	N	N
CYC1	CYOOm2	CYOOm2	Oxidative phosphorylation	N	Y	Y	Y	N	Y	N	N
ME1	ME2	malic enzyme (NADP)	Pyruvate Metabolism	N	Y	N	N	N	Y	N	N
NSDHL	C3STDH1Pr	C-3 sterol dehydrogenase (4-methylzymosterol)	Cholesterol Metabolism	N	Y	N	N	N	Y	N	N
NSDHL	C4STMO2Pr	C-4 methyl sterol oxidase	Cholesterol Metabolism	N	Y	N	N	N	Y	N	N
SLC38A4	PHEt4	L-phenylalanine transport in via sodium symport	Transport, Extracellular	N	Y	Y	Y	N	Y	N	N
SLC38A4	SERt4	L-serine via sodium symport	Transport, Extracellular	N	Y	Y	Y	N	Y	N	N
SLC38A4	GLYt4	glycine transport via sodium symport	Transport, Extracellular	N	Y	Y	Y	N	Y	N	N
SLC38A4	GLNt4	L-glutamine reversible transport via sodium symport	Transport, Extracellular	N	Y	Y	Y	N	Y	N	N
SLC38A4	LEUt4	L-leucine transport in via sodium symport	Transport, Extracellular	N	Y	Y	Y	N	Y	N	N
SLC38A4	PROt4	Na+/Proline-L symporter	Transport, Extracellular	N	Y	Y	Y	N	Y	N	N
SLC38A4	ASNt4	L-asparagine transport in via sodium symport	Transport, Extracellular	N	Y	Y	Y	N	Y	N	N

U87MG unique genes mutations (Homozygous) correlated to the model reactions based on GPR											
<i>In silico</i> model details				Genes with alterations (Homozygous)		Genes with alterations (Heterozygous)		Unique genes (Homozygous)		Unique Mutations in common genes (Homozygous)	
Gene	Rxn ID	RxnName	Rxn Subsystem	U87MG	NSP	U87MG	NSP	U87MG	NSP	U87MG	NSP
AMT	GCCam	glycine-cleavage complex (lipoylprotein), mitochondrial	Glycine, Serine, and Threonine Metabolism	Y	N	N	N	Y	N	N	N
AMT	GCCbim	glycine-cleavage complex (lipoylprotein) irreversible, mitochondrial	Glycine, Serine, and Threonine Metabolism	Y	N	N	N	Y	N	N	N
AMT	GCCcm	glycine-cleavage complex (lipoylprotein), mitochondrial	Glycine, Serine, and Threonine Metabolism	Y	N	N	N	Y	N	N	N

Reaction (Rxn) IDs, Reaction (Rxn) names and subsystems are used as such from the model. Gene-protein relationship from the model is used to connect the genes to the reaction in the network. Exome variants from the Chapter 4 have been listed that are unique for each cell type. Y = Yes - Variants identified using Exome sequencing; N = No – No variants identified using Exome sequencing.

Flux variability analysis was performed on the constraints based representation of *in silico* U87MG and NSP using COBRA (Constraints based reconstruction and analysis) toolbox in MATLAB platform. This analysis identifies the minimum and maximum ranges of flux in each reaction in the network (Table 7.2 and Figure 7.7 B) and also identifies reactions that can hold unique flux. Differential flux distribution profiles for U87MG and NSP in reactions related to the valine, leucine, and isoleucine subsystem (Figure 7.7 B) was delineated. Also, flux distribution was varied in the urea cycle.

Especially, the ornithine carbamoyl transferase reaction changes from irreversible to reversible in case of U87MG. This major change was validated from the Exome data wherein the ODC gene has a unique deletion profile in U87MG (**Chapter 4**). This FVA analysis predicts the genotypic variations from the phenotypic constraints provided in the model. Further, homozygous non-synonymous variants from Exome data have been used as constraints (Table 7.3), for the reactions involving genes with mutations, to make the model more cell-specific. This was performed to validate the genotype to phenotype relationship that can be predicted from the constraints based models. The complete details of the model and constraints are provided in Appendix B.

7.6. Discussion

The findings and inferences from this thesis identified the potential rewired central metabolism (Figure 7.8) and its contributors from signaling network that can form the potential survival strategy/adaptability mechanism of resistant cells using data-driven approaches and predictive modeling. The major metabolic reprogramming (highlighted in Figure 7.8) can be based on the glutaminolysis that takes place from glutamine and its contribution to ornithine via carbamoyl phosphate (Figure 7.3). Hence, the proposed rewired metabolism is highly due to the preferential utilization of glutamine (Chapter 2) and as reported in our analysis (Immanuel et al. 2018). This is also regulated by the potential contributions from genotypic changes in the signal and regulatory networks that includes mTOR, PTEN and other DNA methylating genes (highlighted in red boxes in Figure 7.8).

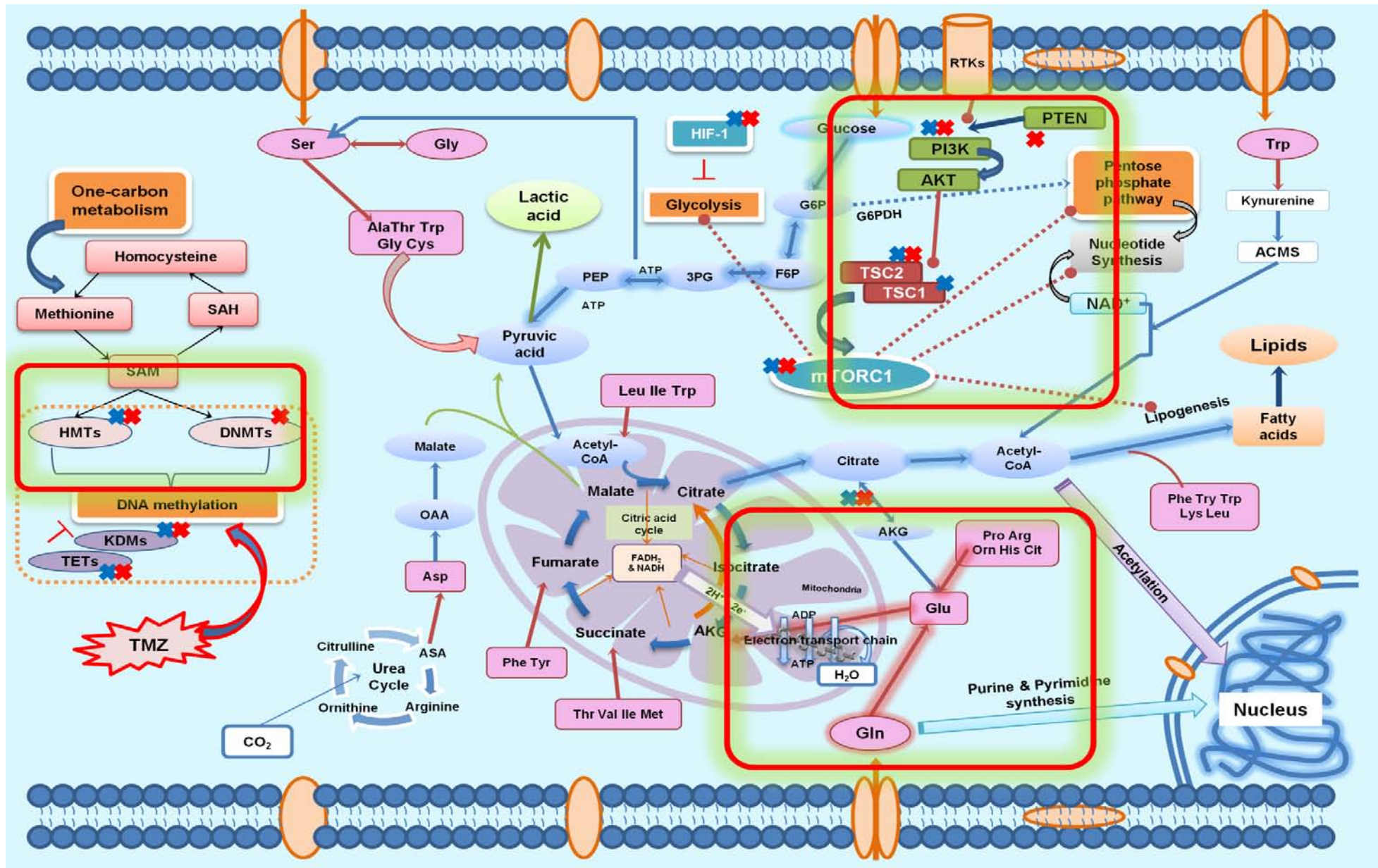


Figure 7.8: Metabolic reprogramming depicted based on the inferences from all the datasets in this thesis.

7.7. Conclusions

High throughput data acquisition is revolutionizing research in almost all fields including cancer. The amount of data acquired in research is tremendously increasing. Hence it is very important to skill the level of expertise in handling big data sets, especially when working with human inferences. Though the data acquisition process by itself needs highly developed platforms, one of the crucial steps in any analysis is how to drive knowledge and inferences from the acquired data. **Systems biology** is one such platform where it offers many advantages in handling high throughput datasets of any data types. Herein, **integrative systems approaches** have been deployed to connect all the experimental data derived in this thesis from **Chapter 2 to 6**, starting from growth kinetics, differential dose response, metabolite profiling, exome sequencing to phenotypic characterization. Systems biology approaches **in this chapter** included pathway analysis using Pathway StudioTM, metabolite quantification profiles and mathematical models to analyze the flux distributions in each reaction in the network using constraints based models. All these “**state of the art**” approaches led to the identification and characterization of temozolomide resistant Neurospheres from U87MG, Glioblastoma cell line. This study also delineated the metabolic reprogramming in these resistant cells that could potentially contribute to the survival strategies of these resistant cells as differential glutamine preferences, changes in the exome variants in master controller genes and DNA repair genes. Such analyses broaden the scope of this thesis to a **scalable pipeline** that can be applied to other cancer types and can be translated to clinical findings, thus **bridging the gap** between data acquisition and deriving inferences. Such findings would also definitely ramify novel insights to the problem of drug resistance highlighting that it is just not the drug efflux or the drug inefficiency, but also the capability of the cell to adapt and resist such environments that makes the condition more complex to combat cancer resistance. Thus methods for data integration are critical to unify inferences that can drive hypothesis generation and discovery.

Chapter 8

Conclusions and Future scope

"Scientists often have a naïve faith that if only they could discover enough facts about a problem, these facts would somehow arrange themselves in a compelling and true solution".

-Theodosius Dobzhansky

"History repeats, but science reverberates."

- Siddhartha Mukherjee, The Emperor of All Maladies

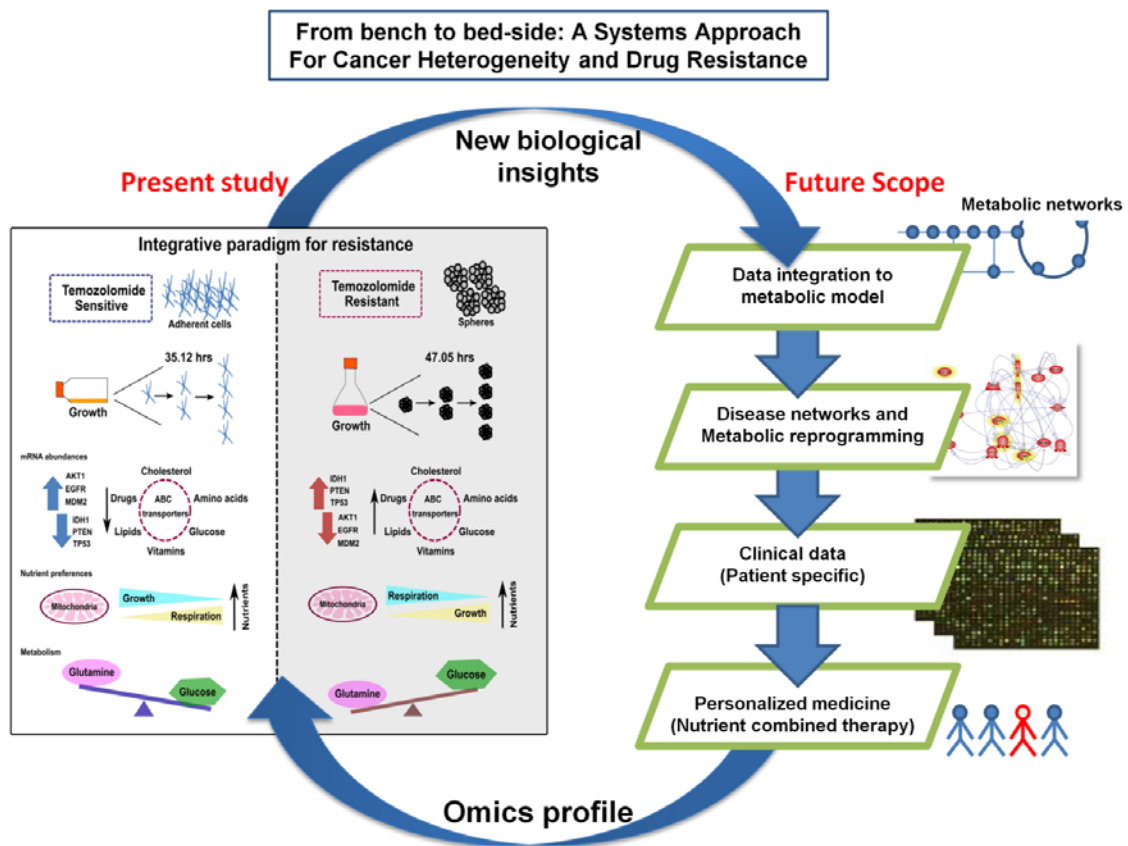


Figure 8.1: Integrative paradigm developed for cancer drug resistance from this study and its future scope on translational research.

The fundamental question in biology is to understand what defines the cells, the individuals and the populations as different from one another. The answer is that these are shaped by the genotype-phenotype relationship. The work described in this dissertation is a “systems biology approach” to delineate the molecular basis of differences between drug resistant and susceptible cells of glioblastoma.

My doctoral research presents not only the elucidation of differential components of molecular hierarchies in glioblastoma cells that are susceptible and resistant to the chemotherapeutic drug TMZ but also an integrated analysis to unravel some of the mechanistic aspects of drug resistance. In this context, this thesis begins with the discovery and isolation of morphologically different cells in a glioblastoma cell line that were separated and banked for further characterization. The genotype (exome) was delineated and the unique variations in each cell type identified. Transcript levels were ascertained for selected CAN genes and ABC transporters generally implicated in resistance in cancer. Metabolism orchestrates cell function/growth and hence the intracellular metabolite level was dynamically fingerprinted. The contributing micro-environments were also quantitated in an attempt to understand the choices the cell makes to remain proliferative in the presence of a drug. Since biological systems are complex and their function is more than the sum of their parts, all the data was integrated to analyze the emergent properties resultant from the interaction. Reprogrammed metabolism as a consequence of varied genotypes was identified and the connections to the methylating action of the drug temozolomide were elucidated.

Thus, in this thesis, I have advanced the current understanding of temozolomide resistance in a model glioblastoma cell line by developing an integrated paradigm that addresses many levels of molecular hierarchy in the cell. To our knowledge, this high-throughput poly-OMIC data integration has never before been performed to describe glioblastoma heterogeneity and to address the role of reprogrammed metabolism in TMZ resistance.

8.1. Recapitulation

A broad recap of some of the main concepts described and realized in this thesis is discussed here.

- Temozolomide (TMZ) resistant Neurospheroids (NSP) were identified in the U87MG human glioblastoma cell line.
- NSP shows varied dose-response, 40% higher IC₅₀ and 30% lower growth rate.

- Altered Glucose and Glutamine uptake in U87MG and NSP shaped metabolic dynamics; Glutamine is preferentially utilized by NSP.
- Differential mRNA levels of CAN genes & ABC transporters drive respiration and growth.
- Differential expression of ABC transporters not only affects the drug uptake but also potentially contributes to varied substrate uptake and reprogrammed metabolism.
- 44 genes with metabolic ontology are mutated in NSP alone, while 15 are mutated in U87MG.
- Many signaling, regulatory genes that control metabolism are mutated including mTORC1, PTEN, and cMyc.
- Metabolism is programmed in the presence of temozolomide by oncogenic and micro-environmental signals.
- AKG/Succinate ratios determine the methylating level of temozolomide.
- Ornithine, pyrimidine metabolism, and urea cycle play a role in the survival of NSP even in the presence of the drug.
- Rotenone and berberine, complex I inhibitors can inhibit the growth of NSP.
- Constraints-based metabolic modeling using a core model of human metabolism predicted varied flux wiring patterns, pathway utilization, and NAD recycling.
- Integrative paradigm identifies potential metabolic drivers for TMZ resistance.

8.2. Unknown frontiers of chemotherapeutic resistance

Some of the more global questions that are addressed in the thesis and yet need the final validations and answers are

- 1) How do metabolic reprogramming and epigenetic alterations shape the cancer cell response to drugs?
- 2) How do genetic variations and gene expression impact reprogrammed metabolism and resistance to alkylating drugs?
- 3) Can one identify adjuvants in metabolism to supplement chemotherapy and tailor micro-environments for personalized medicine?

The answers to these questions inadvertently lie in our ability to make measurements at the molecular level for heterogeneous cells in individuals, integrated models for further understanding and translation into the diagnosis for tailoring microenvironments. The

precision of tailoring specific microenvironments near the tumor cells would predominantly dictate the future of personalized medicine and individualized therapy in cancer.

8.3. Future scope and directions

The future scope of this study lies in its extension or translation to clinical samples from patients. The pipeline developed to study drug resistance in cancer is completely scalable to clinical data from patients thus can potentially transform research from bench to bedside (Figure 8.1). Moreover, intra-tumor heterogeneity is a complex problem that needs to be addressed through continuous monitoring and changing treatment strategies. The use of data-driven models and constraints based models hold the potential to design targeted and specific therapy for the patients either with primary tumors or relapse.

8.4. Single cell analysis

Rapid and inexpensive single-cell sequencing is driving new visualizations of cancer instability and evolution. Thus single cell analysis is critical in understanding intra-tumor heterogeneity. The study of clonal evolution can allow the tape of each cancer cell's life to be deciphered, revealing the temporal order of genomic events and shedding light on constraints and contingencies to cancer evolutionary trajectories. All the methods explored in this thesis can be extended to single cell analysis and the heterogeneity of drug response be understood. Some of the advances in single cell analysis are seen in the **preliminary data gathered at Manchester Institute of Biotechnology, UK** using sphere fluidics.

The droplets were generated using a droplet formation technique (Figure 8.2) and validated using fluorescence imaging (Figure 8.3).

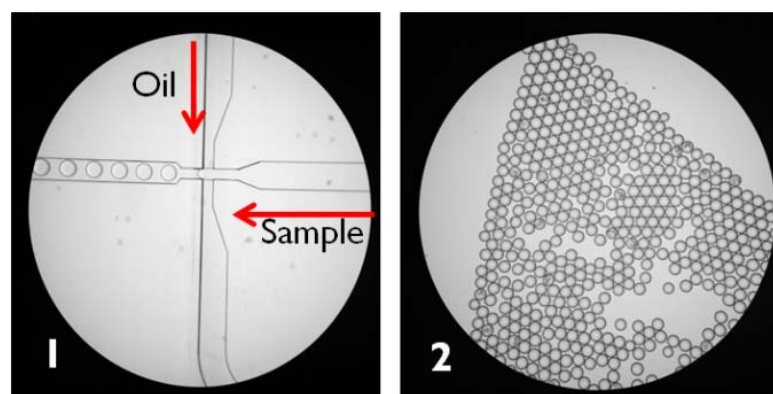


Figure 8.2: Encapsulation of samples with cells inside droplets. 1) Droplet creation-images were taken under a microscope. 2) Droplets are of ~300 picoM.

U87MG cells stained with Hoechst 33342 dye were encapsulated in oil by optimizing the flow rate that defines the size of the droplet that is formed. These droplets thus formed can be separated to get single cell encapsulation to further grow in the defined conditions.

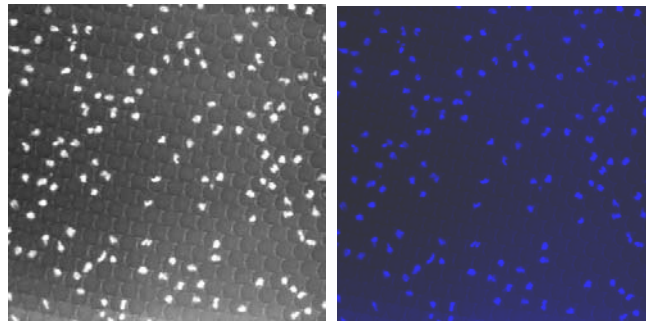


Figure 8.3: Fluorescence microscope image of droplets created for U87MG cells stained with Hoechst 33342 dye. 1) Bright field image of the droplets 2) Blue fluorescence image.

The stability of the droplets to undergo qPCR assays has been tested by incubating the droplets placed on a slide to test their stability at different temperatures varying from 20°C to 70°C (Figure 8.4).

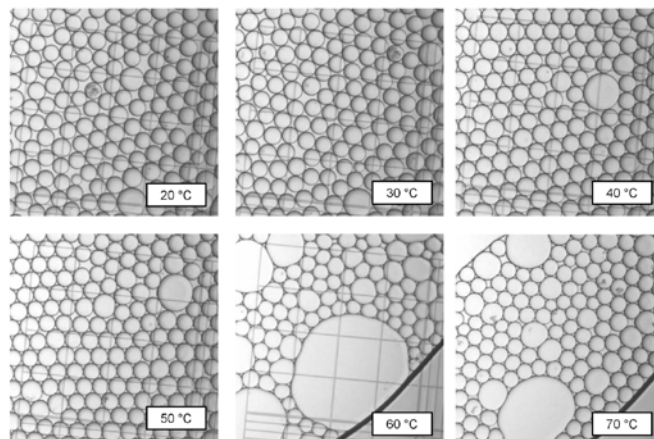


Figure 8.4: Stability of droplets under varied temperature conditions. Droplets were heated at different temperatures and then the image is captured under a microscope. The irregularity in the shape of the droplets is shown at different temperatures.

This thesis forms the base and the proliferation of such isolated single cells would give way for multiple measurements including gene expression and metabolite profiles that can drive precision medicine and thus holds promising future ramifications.

“No research is ever quite complete. It is the glory of a good bit of work that it opens the way for something still better, and this repeatedly leads to its own eclipse”

- Mervin Gordon

Appendices

Appendix A: (All the supplementary data generated in this doctoral research have been listed in the form of tables and figures).

U87MG cell line has recently in 2016 undergone some controversies in its characteristics due to the continuous passaging at ATCC according to the study mentioned in the Nature journal (Allen et al. 2016). This states that some batches of this cell line dispatched from ATCC lost its originality. In our study, I have performed the cell line authentication to check the authenticity of the U87MG cell line used for this complete doctoral research. This identified that this cell line **matched 100% with the ATCC STR profiles** as given in the Table A1.

Table A1: Cell line authentication results for U87MG.

U87MG cell line authentication (STR Profiling)													
% Match >= 80%	Sample Count	Match	Atcc No.	Name	D5S 818	D13 S317	D7S82 0	D16 S539	vW A	TH0 1	AM EL	TPO X	CSF IPO
100	15	15	HTB-14	U-87 MG	11,12	8,11	8,9	12	15,17	9.3	X,Y	8	10,11
81.82	11	9	HTB-183	NCI-H661	11	11	8,10	12	17	8	X,Y	8	10
83.33	12	10	CRL-5842	NCI-H774	11	8	9,11	12	15,17	6,9,3	X	8	10
80	15	12	SC-RS01314-MCB	Asuragen RU03	11,12	8,11	9,12	12	14,17	8	X,Y	8	10,11

Table A2: Growth rates in the presence and absence of temozolomide.

Gompertz growth parameters	Nmax (cell numbers)		μMax (hr ⁻¹)		R squared	
	NSP	U87MG	NSP	U87MG	NSP	U87MG
No Drug	1.304*10 ⁶	1.383*10 ⁶	0.01473	0.02316	0.9733	0.9690
10μM TMZ	1.009*10 ⁶	7.327*10 ⁵	0.01102	0.02534	0.9421	0.9816
100μM TMZ	1.301*10 ⁶	1.283*10 ⁶	0.03898	-0.009934	0.6795	0.9193
700μM TMZ	1.739*10 ⁶	1.927*10 ⁶	-0.006475	-0.03191	0.9449	0.9932

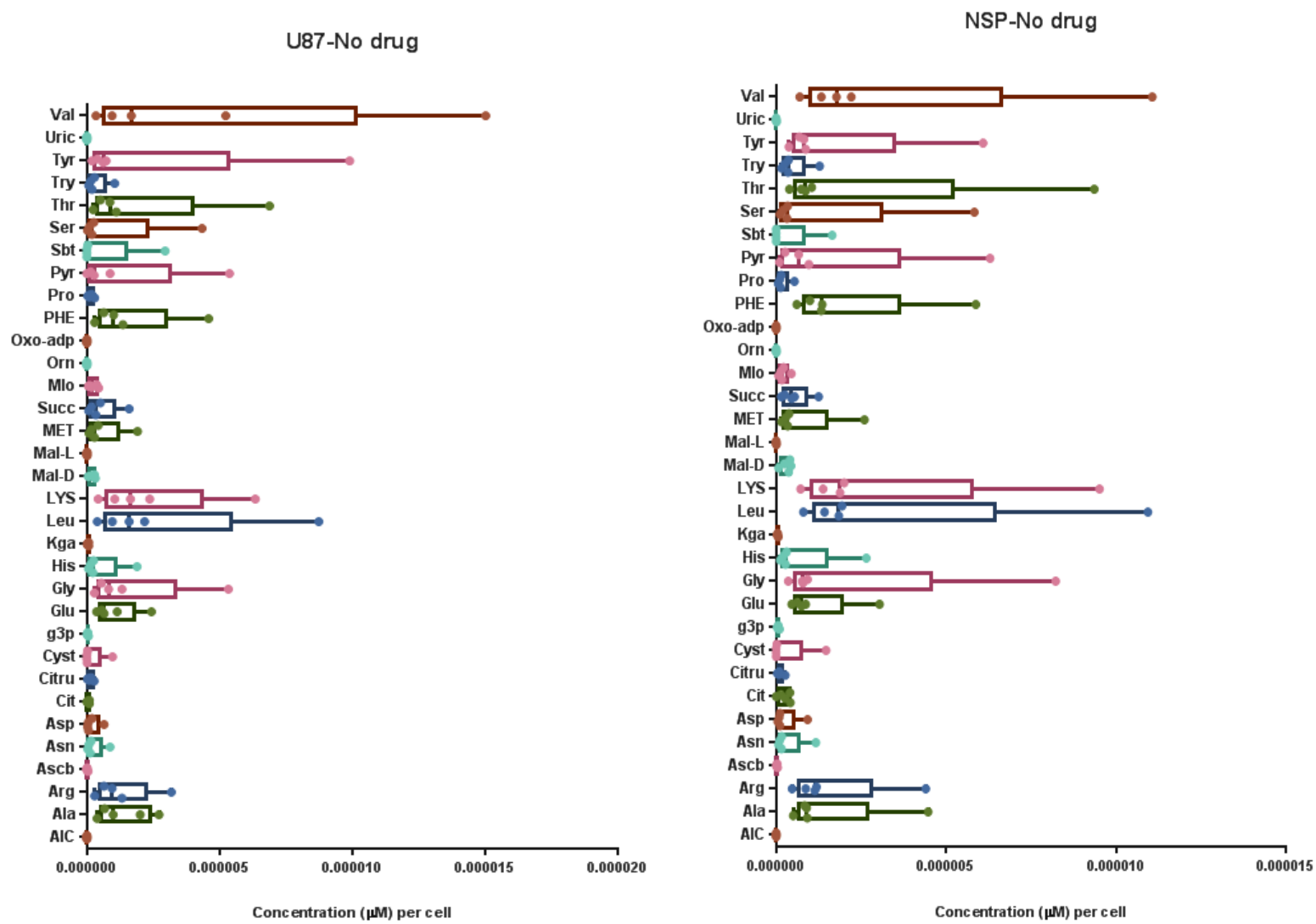


Figure A1: Intracellular profiles of U87MG and NSP in no drug experiment.

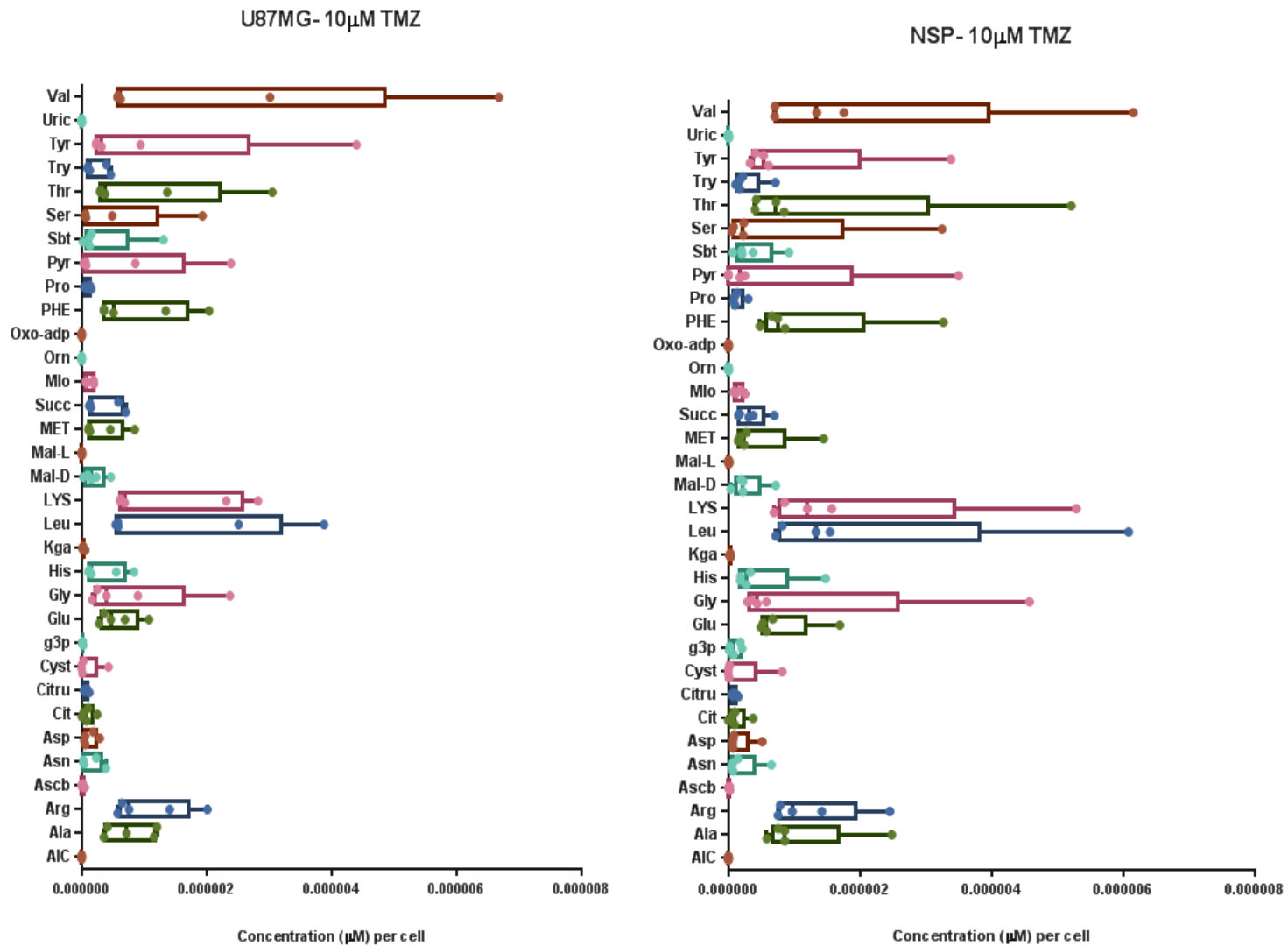


Figure A2: Intracellular profiles of U87MG and NSP in the presence of 10 μM TMZ.

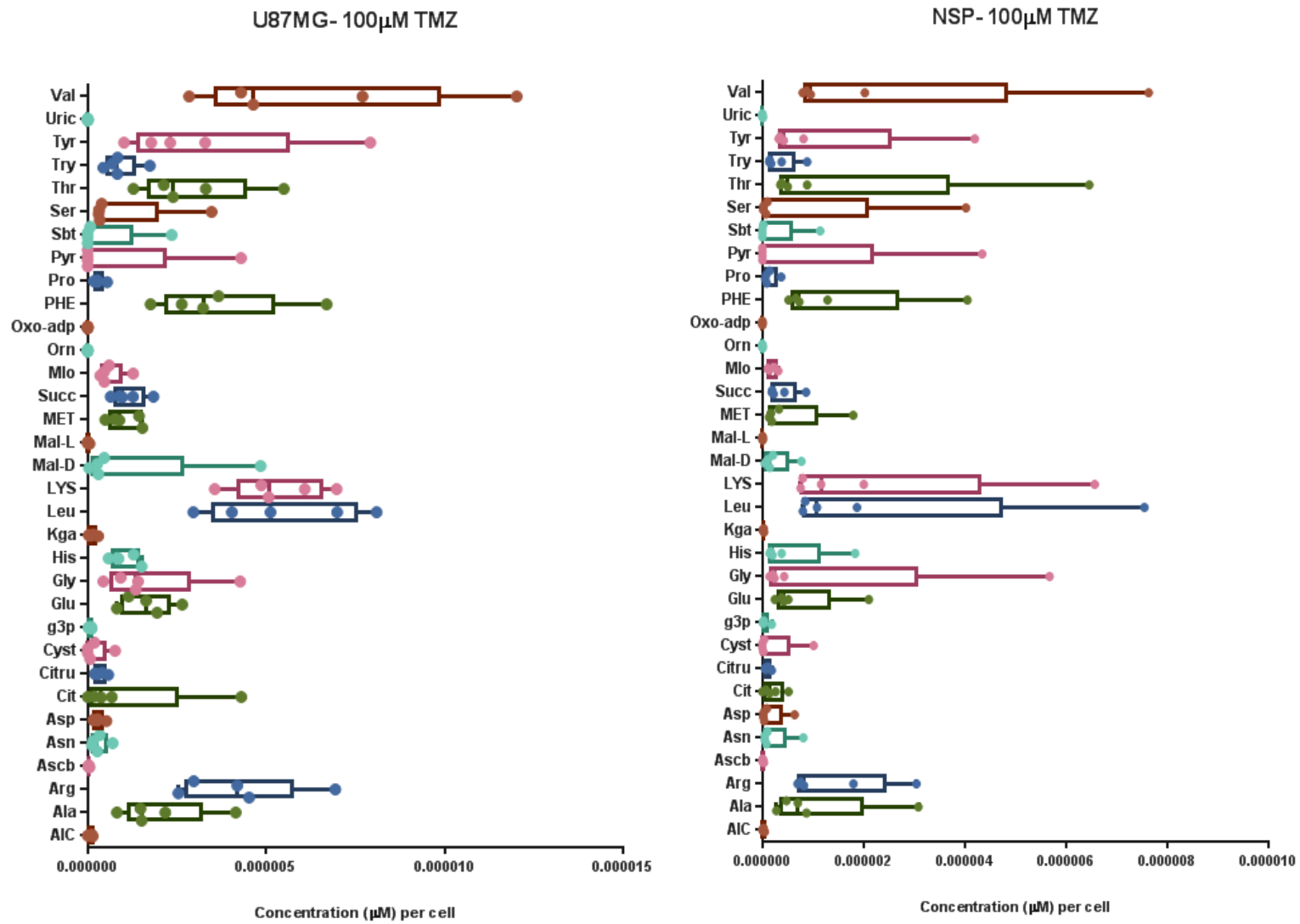


Figure A3: Intracellular profiles of U87MG and NSP in the presence of 100 μM TMZ.

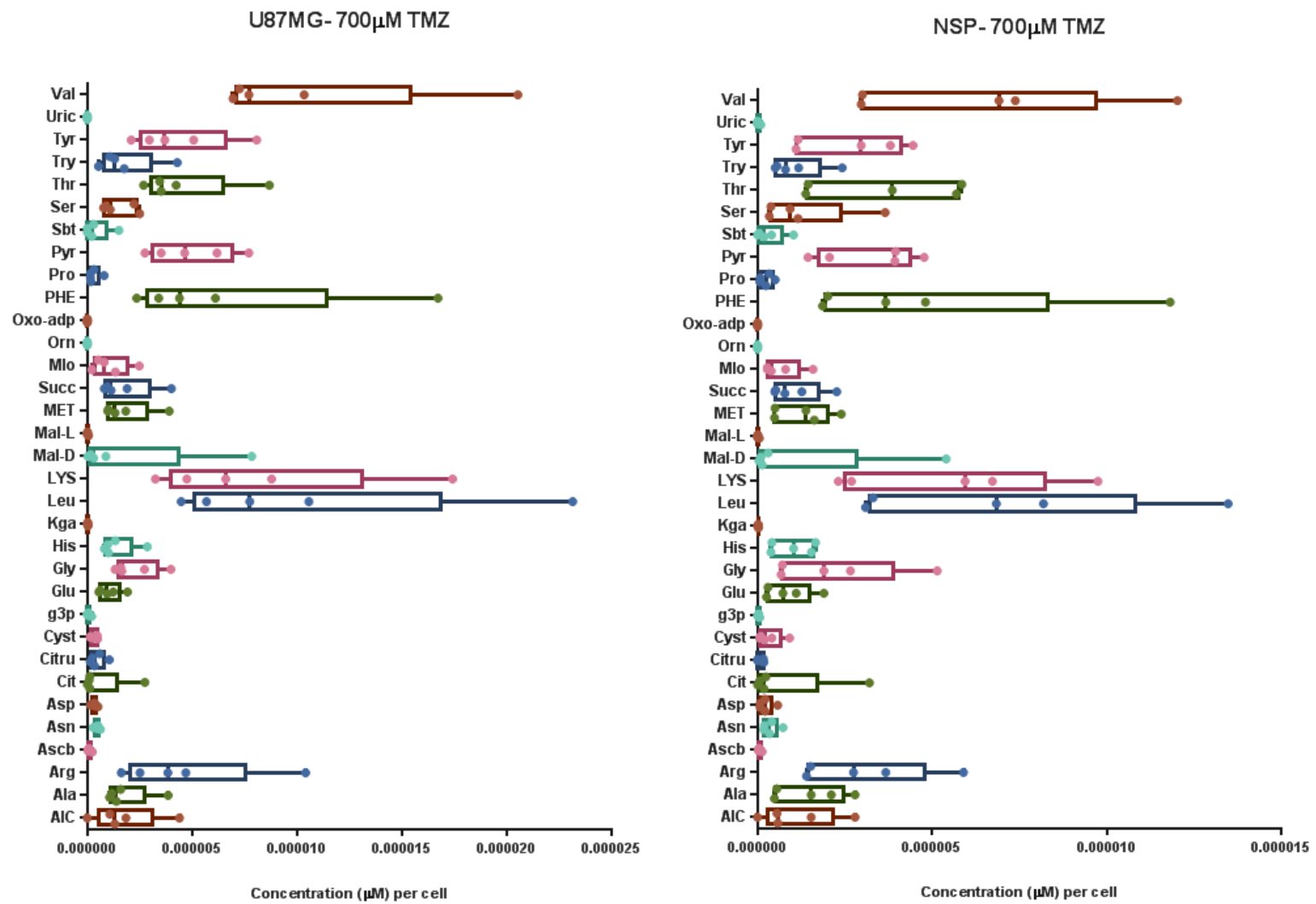


Figure A4: Intracellular profiles of U87MG and NSP in the presence of 700 μM TMZ.

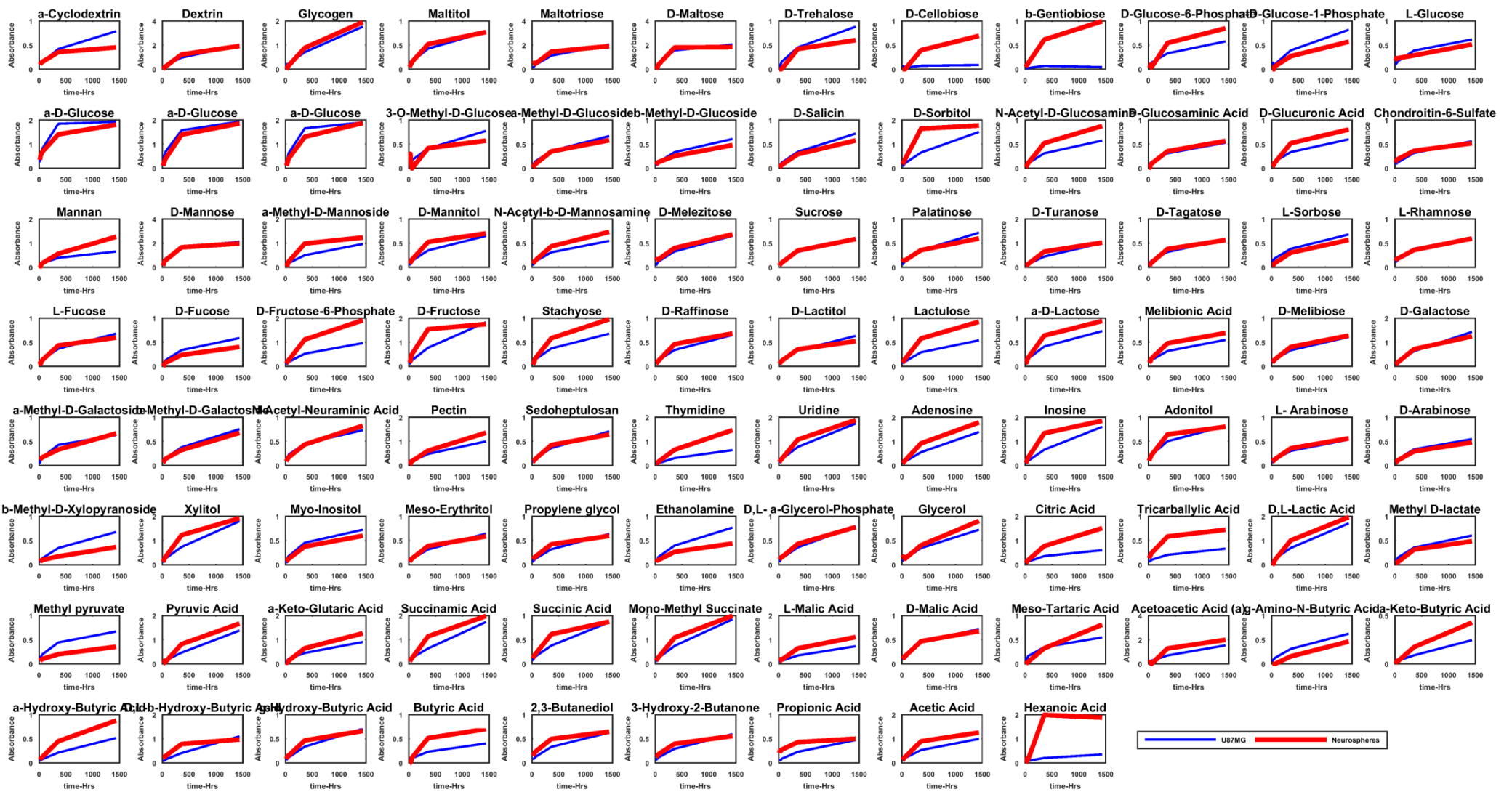


Figure A5: Growth profiles from PMM-1 plate

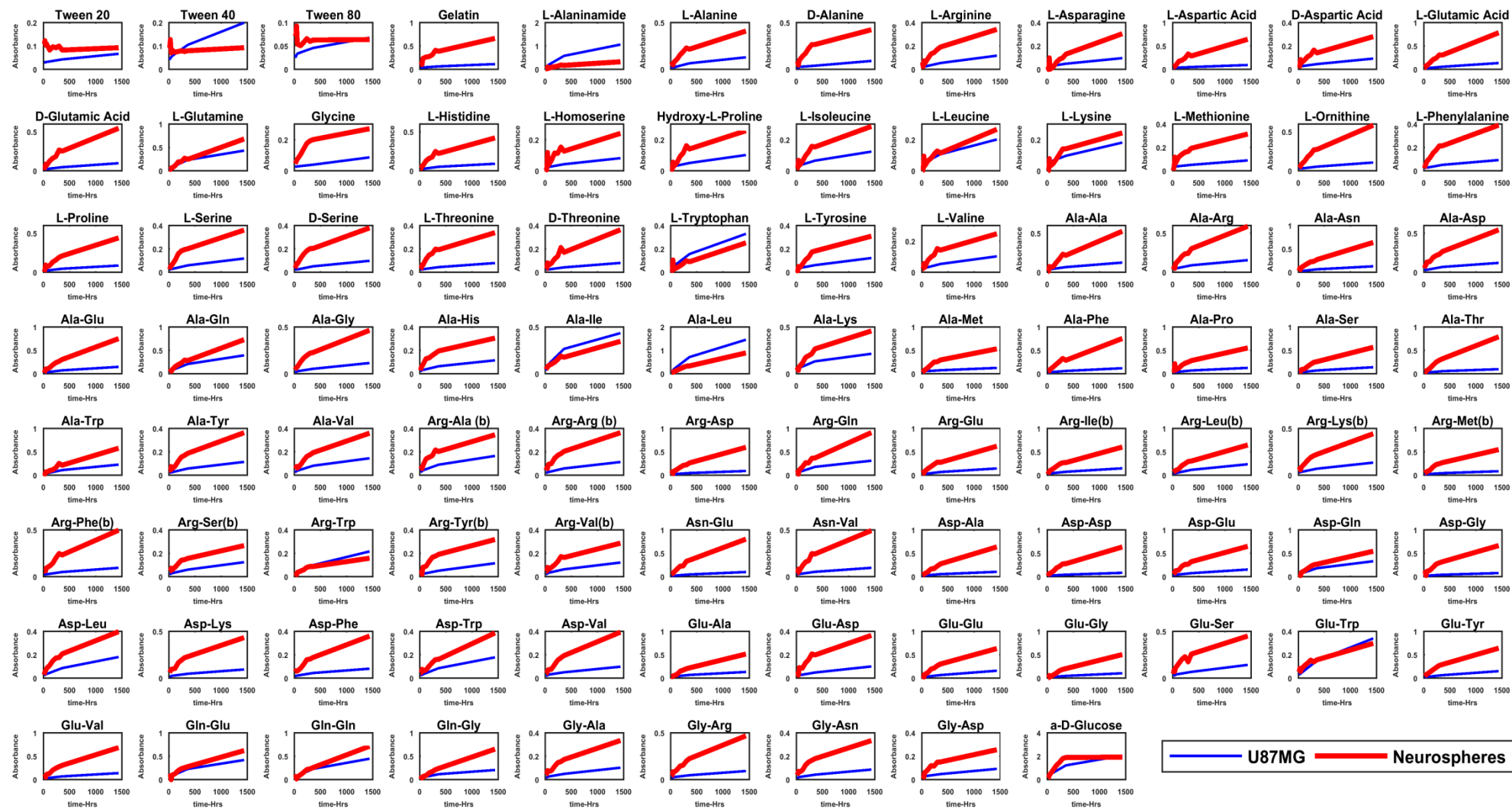


Figure A6: Growth profiles from PMM-2 plate

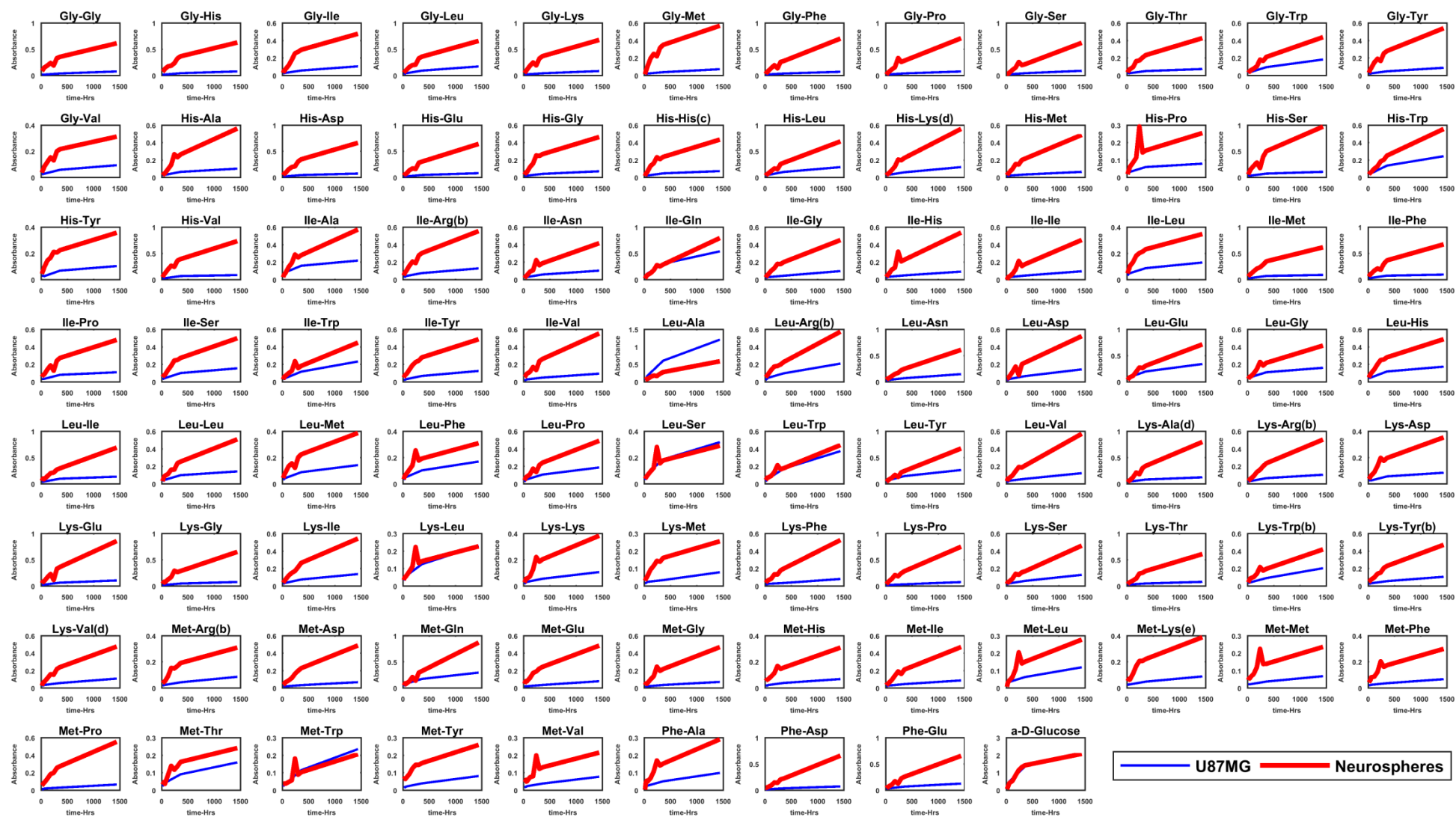


Figure A7: Growth profiles from PMM-3 plate

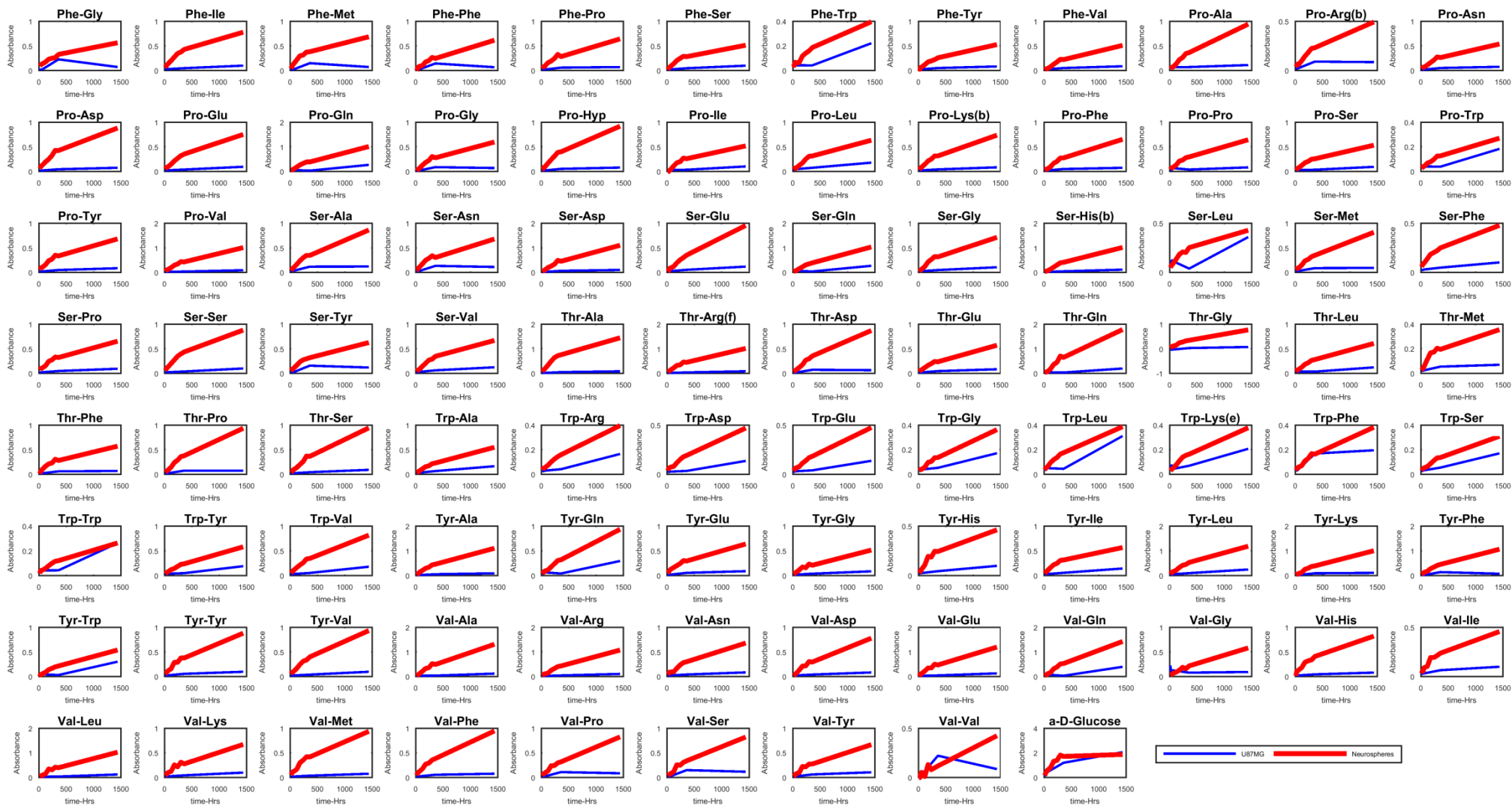


Figure A8: Growth profiles from PMM-4 plate

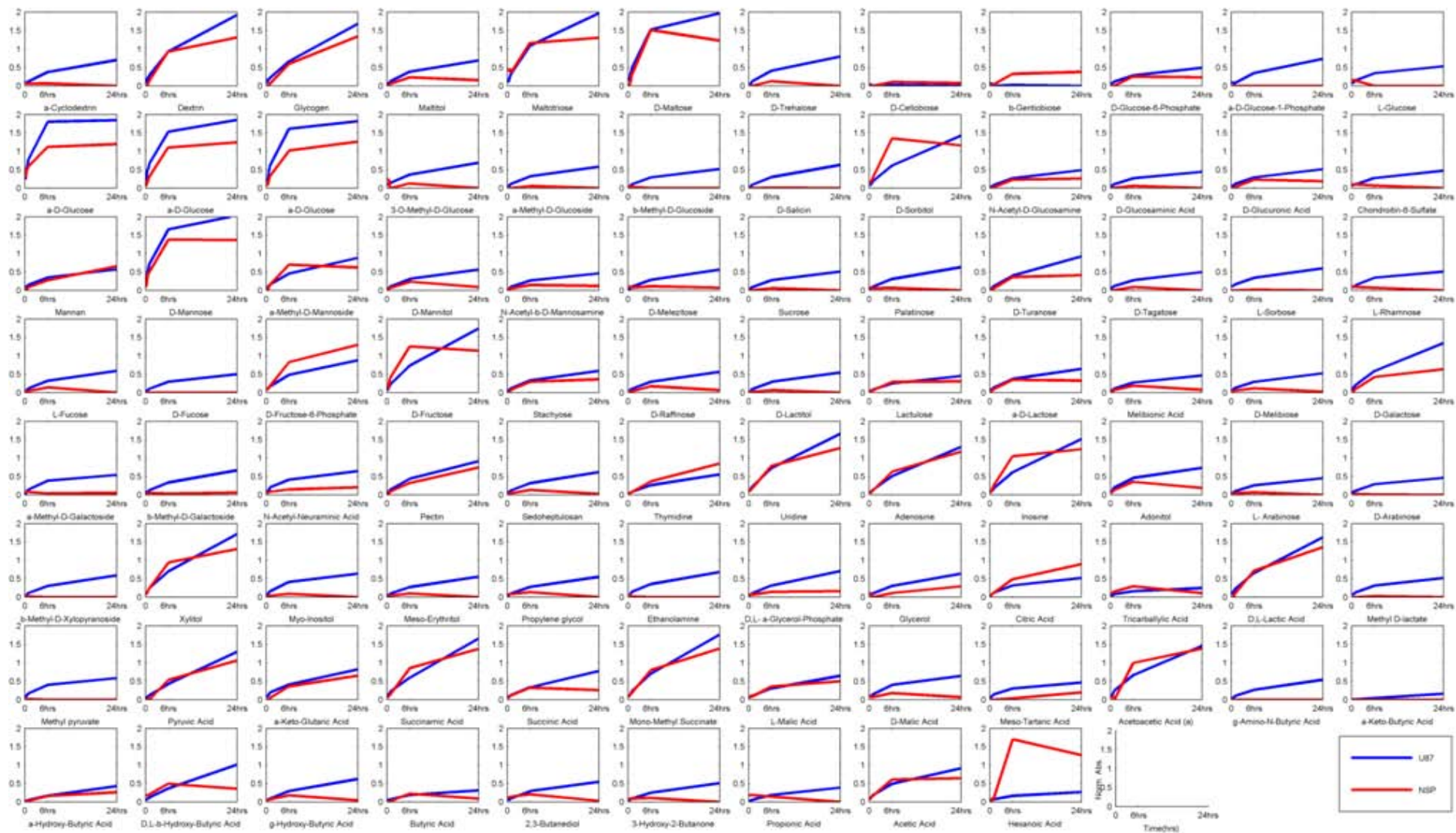


Figure A9: Respiration profiles from PMM-1 plate

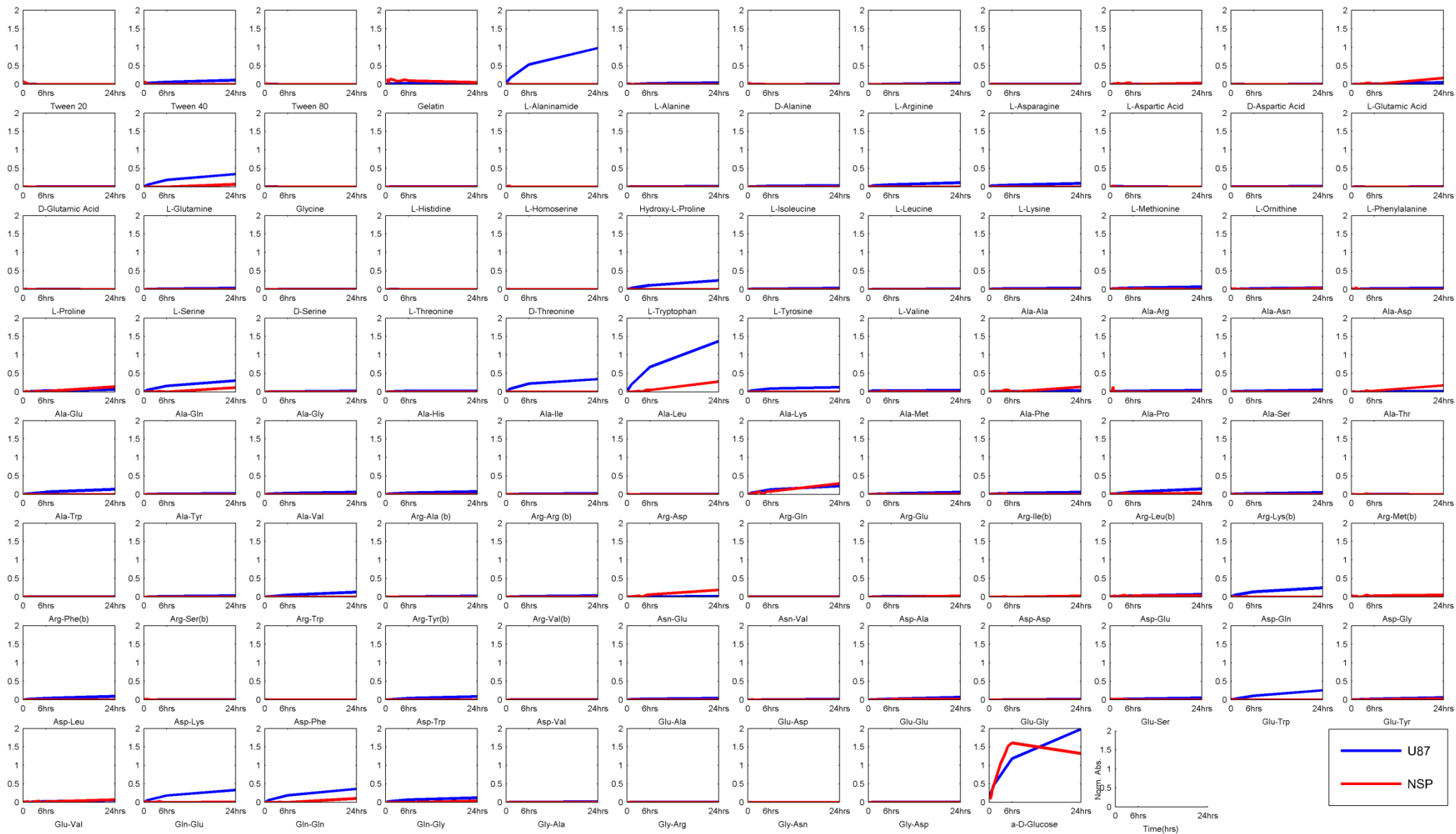


Figure A10: Respiration profiles from PMM-2 plate

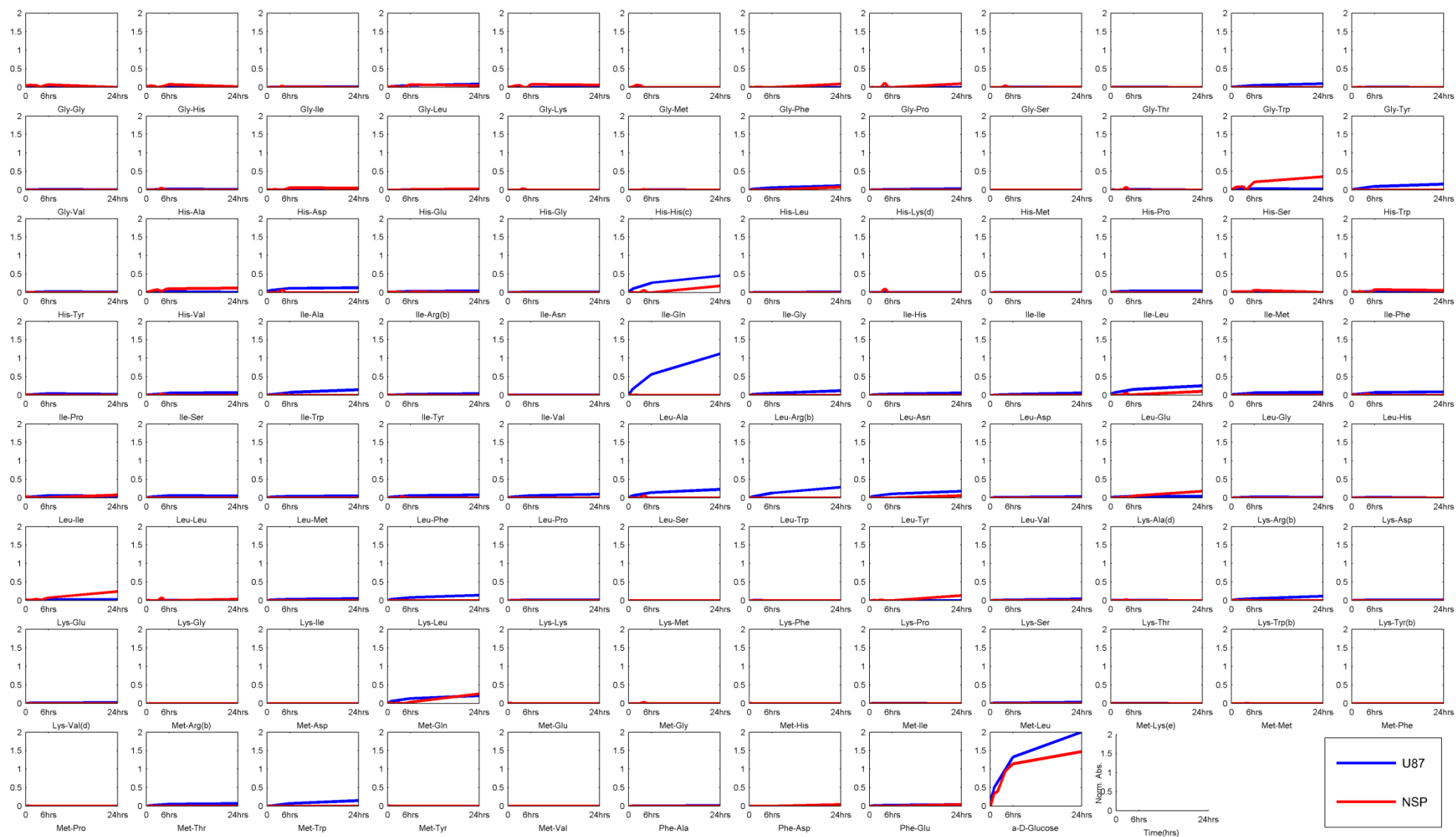


Figure A11: Respiration profiles from PMM-3 plate

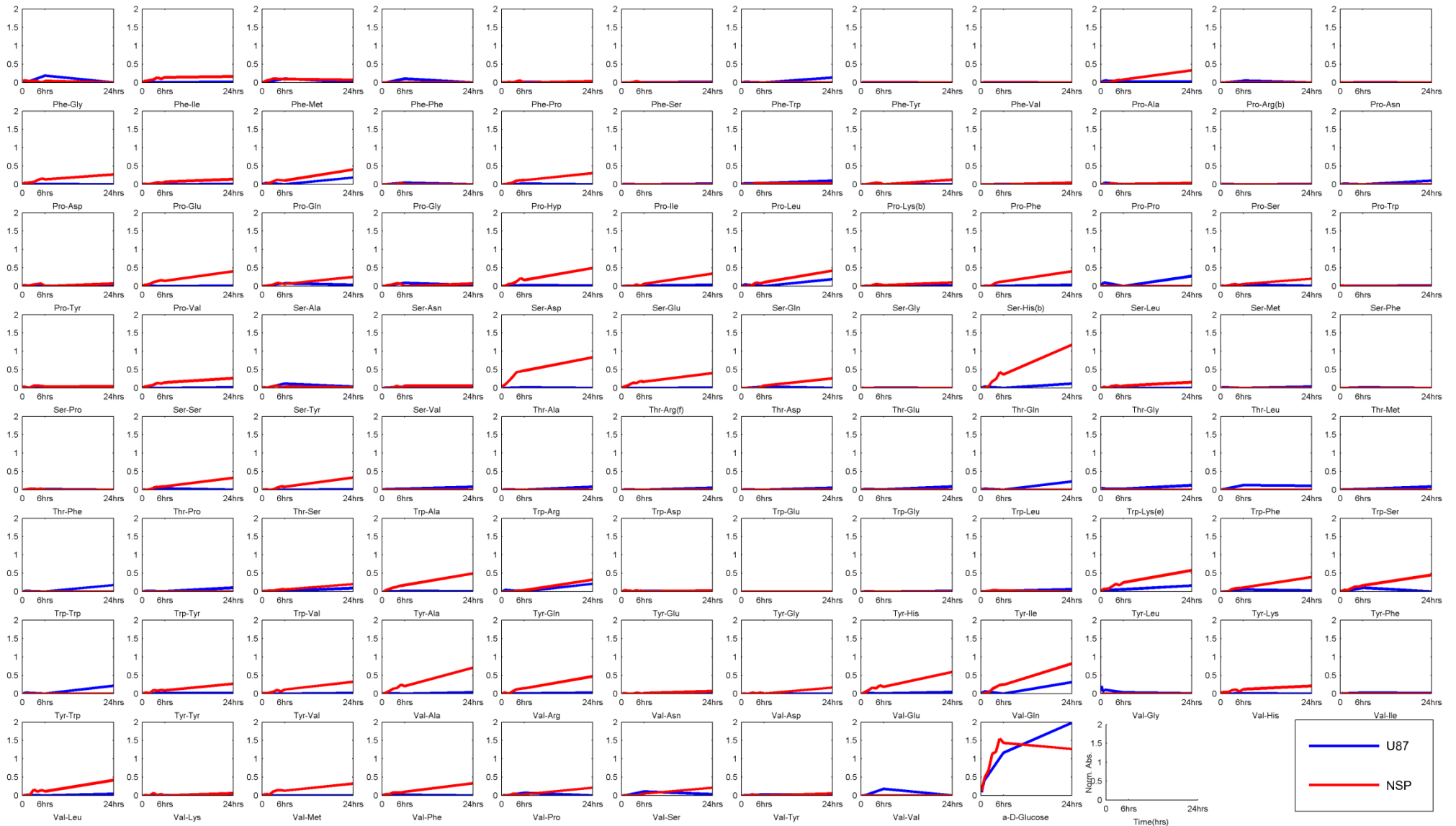


Figure A12: Respiration profiles from PMM-4 plate

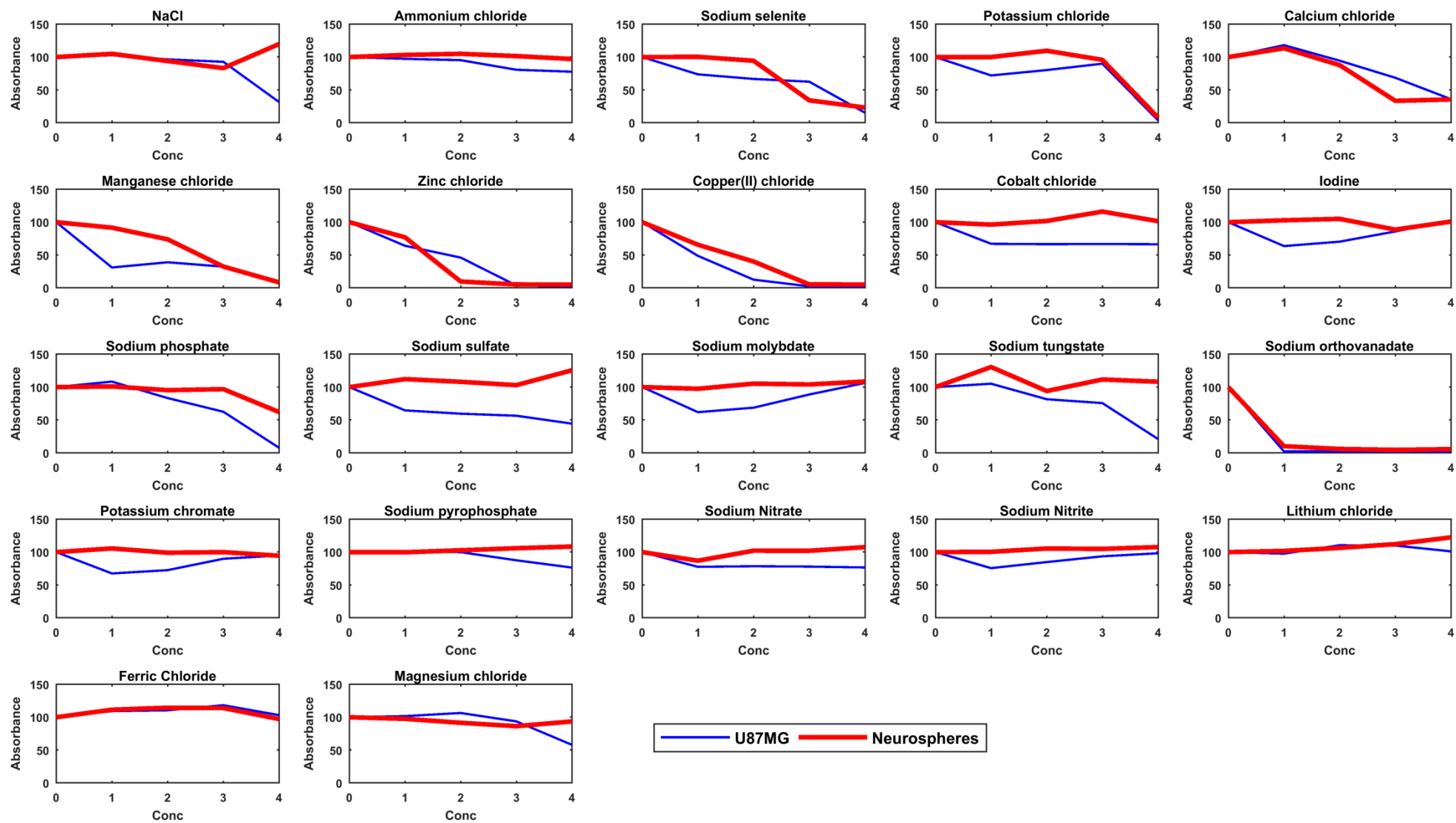


Figure A13: Growth profiles from PMM-5 plate

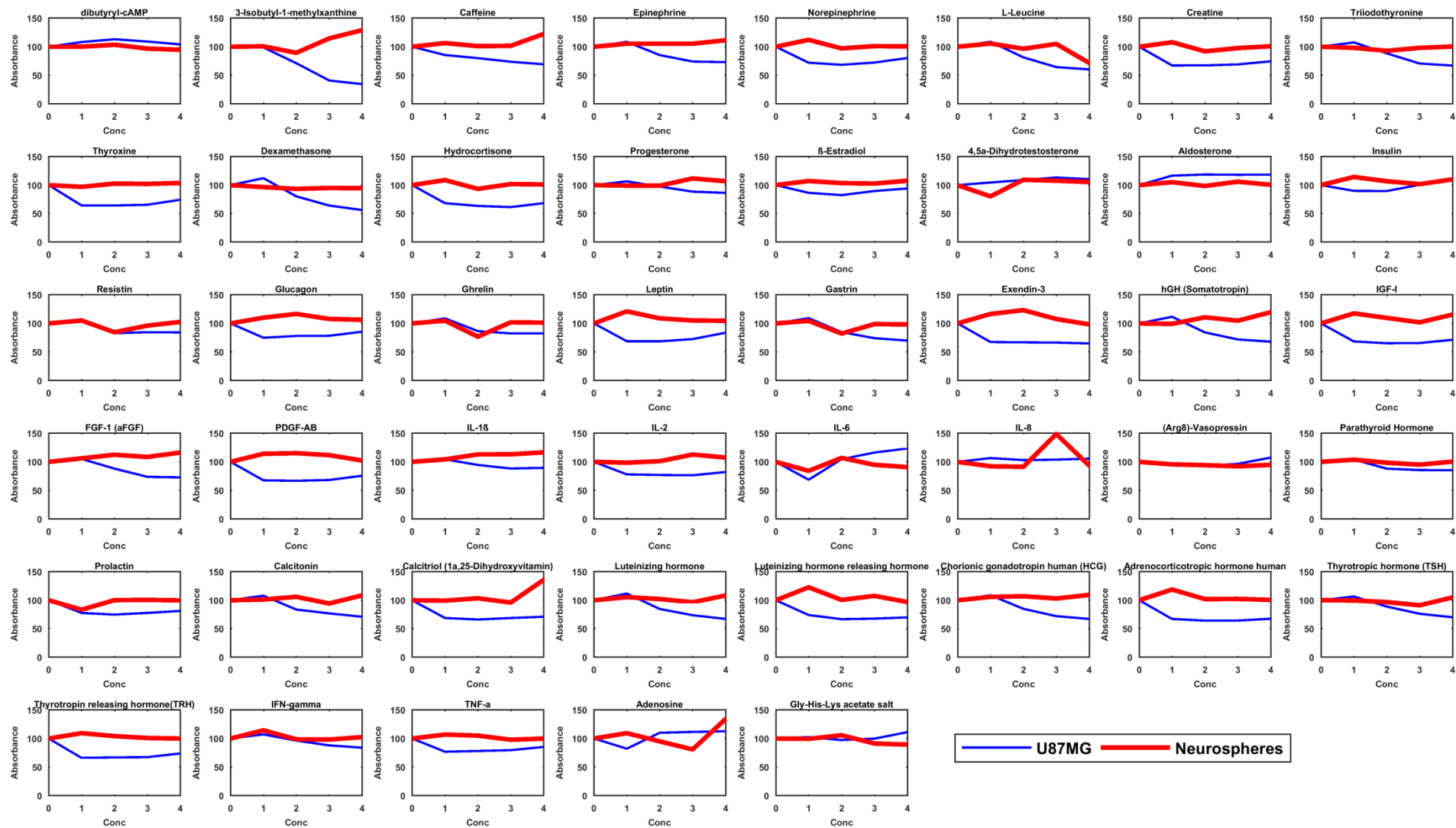


Figure A14: Growth profiles from PMM-6 to 8 plate

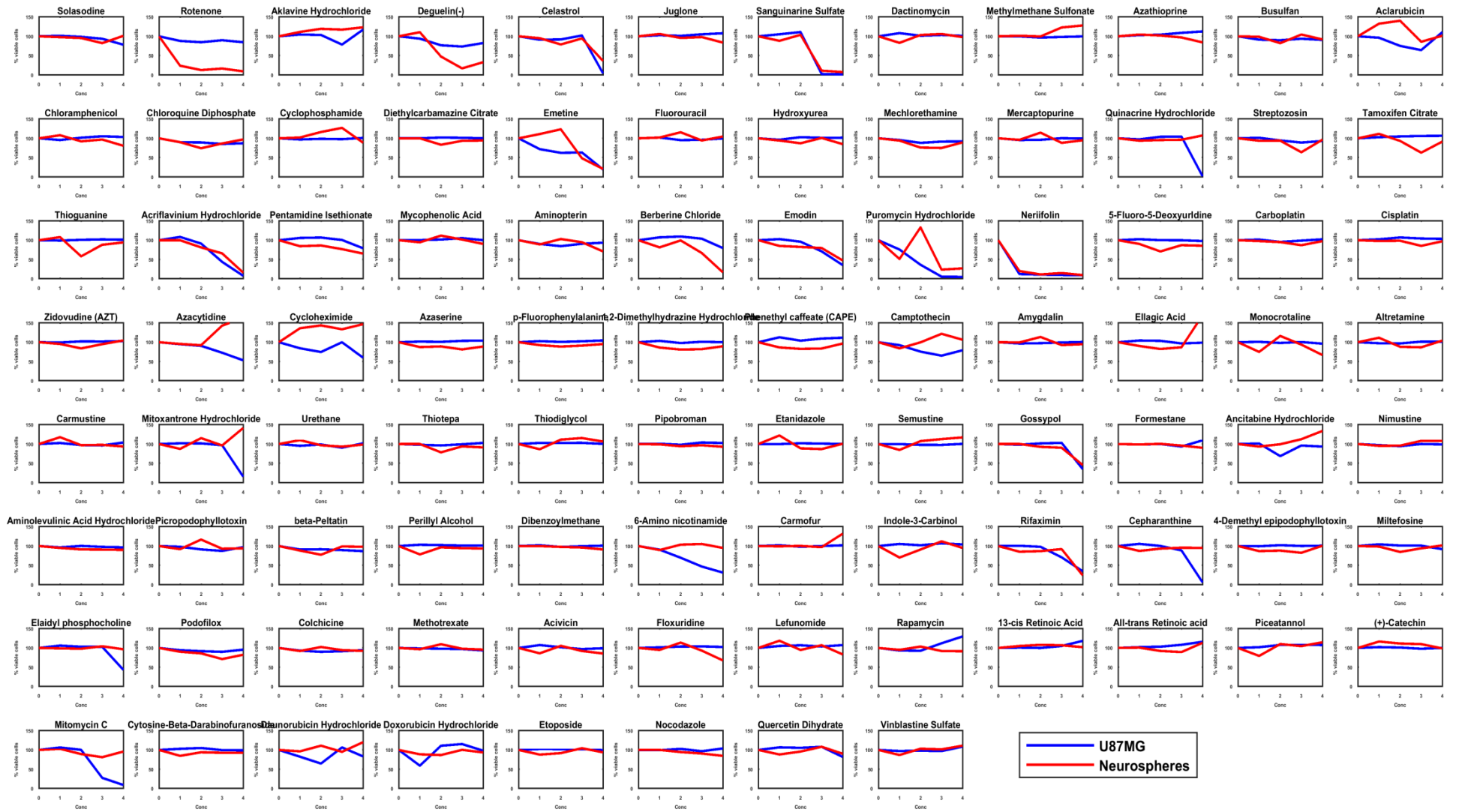


Figure A15: Growth profiles from PMM-11 to 14 plate

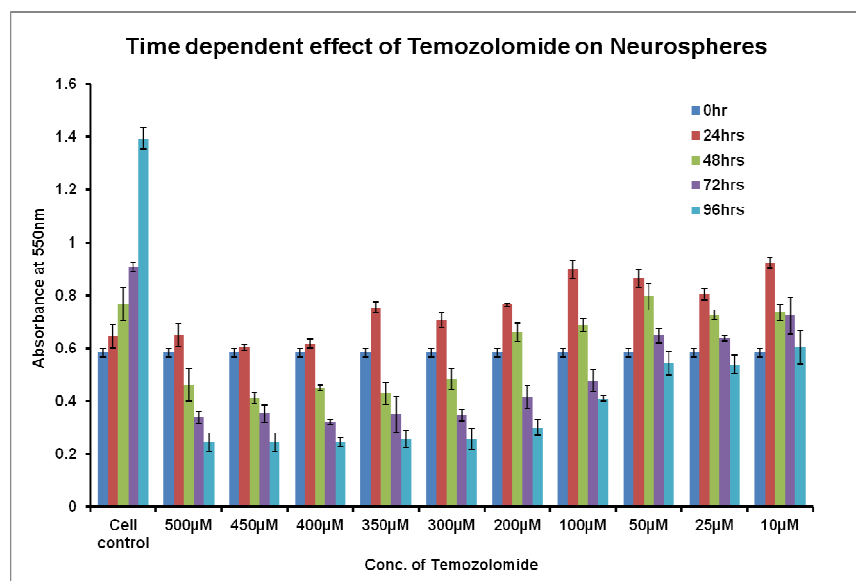


Figure A16: Time dependent effect of Temozolomide on Neurospheres

Appendix B: (Additional soft data)

- Some of the high-throughput supplementary data generated in this doctoral research have been listed in the form of **excel sheets** and **provided in the CD** attached at the end of the hard copy of this thesis and also with the soft copy of the thesis.
 - 1) **Data integration 1:** mRNA abundances of ABC transporters were linked to the drugs and their U87MG and NSP profiles from BIOLOG panels.
 - 2) **Data integration 2:** All the reactions from *in silico* model have been linked to the genes and their exome variants with functional annotations.
 - 3) **Exome characterization:** The functional annotation of all the variants identified using exome sequencing in this study.
 - 4) **LC-MS/MS data:** All the metabolic profiles from this study are provided.
 - 5) **PathwayStudio analysis:** Output datasheet with number of references associated with each relation in the network.
 - 6) Comparison of Exome data (this study) with patient data from literature.
- Complete data obtained via exome sequencing in this doctoral research has been submitted in the open source database from NCBI, Sequence Read Archive (SRA) and can be found at <https://www.ncbi.nlm.nih.gov/sra>. The details are available with the author and can be shared on request for reference.

Appendix C: (Contributions to other projects)

Generation of tryptophan over producing knockout strains of

Escherichia coli

C.1. Background of the study

Moving across cell hierarchies from genes to rewiring metabolic networks to host-cells expressing desired phenotypes can be investigated using metabolic engineering and genome editing. Such approach promises the development of strains that can be stable compared to the plasmid transformants. Tryptophan, one of the aromatic amino acids, is being attempted to be manufactured from bacterial strains in industry (Ikeda 2006; Zhao et al. 2011; Burgard et al. 2003). The synthesis of aromatic amino acids is challenging owing to the poor efficiency of strains. L- Tryptophan, in particular, is one of the difficult attempts by industrial processes because of its high production costs (Ikeda 2006; Qiang et al. 2012).

Here-in, tryptophan pathway has been genome engineered in *E. coli* K12 host to improve the yields of tryptophan. Three genes were selected – *pgi*, *pheA* and *trpR* that are crucial and affect the levels of tryptophan through precursor accumulation, reduction in flux through phenylalanine synthesis and feedback inhibition (Figure 1) respectively (Patnaik & Liao 1994; Chhvez et al. 2005; Ahn et al. 2011; Zhao et al. 2011; Bongaerts et al. 2001) were selected. These genes were deleted (knockout) in the base strain using homologous recombination strategies. The deletion strains of *E. coli* K12 (Δpgi , $\Delta pheA$ and $\Delta trpR$) thus generated in this study increased the precursor tryptophan levels two-fold.

This study is further followed up for the biosynthesis violacein, an industrially important compound with antioxidant activities with great potential as a drug exhibiting antibacterial, antitumoral, antiviral, trypanocidal and antiprotozoan properties (Füller et al. 2016; Durán et al. 2016; Choi et al. 2015; Queiroz et al. 2012). The knockout strains increased the levels of tryptophan as estimated in MALDI-MS/MS analysis. Since tryptophan is the precursor for violacein (Sánchez et al. 2006; Fang et al. 2015), the use of these knockout strains increased the violacein biosynthesis by applying synthetic and systems biology approaches in addition to the genome editing.

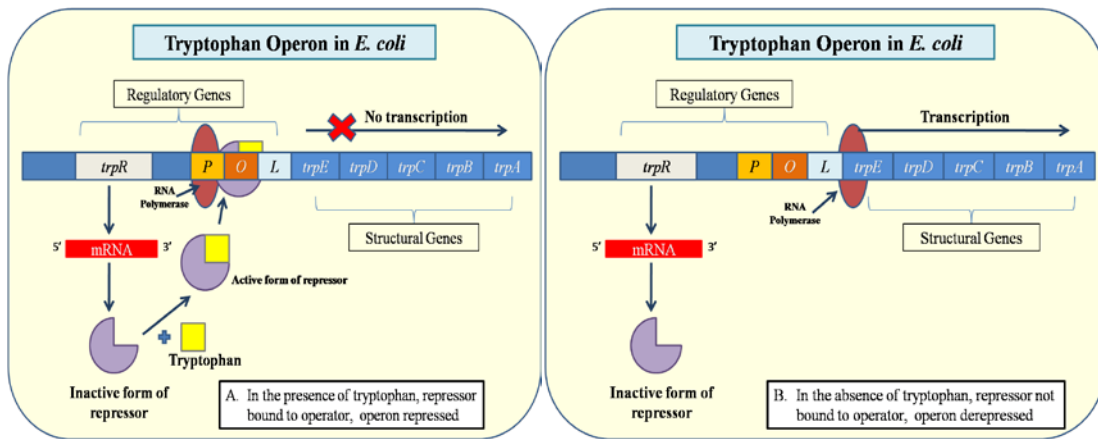


Figure C1: Tryptophan operon regulation in *E. coli*. A) Feedback inhibition B) No inhibition

C.2. Methods

C.2.1. *E. coli* strains and culture conditions

Escherichia coli K12 (*E. coli* K12) strain was used in this study for generation of knockout strains and *E. coli* DH10 β as control for growth experiments. Luria-Bertani (LB) medium (HiMedia Laboratories) was used for all growth and transformation experiments. Luria–Bertani agar (LBA) was used for colony purification. Kanamycin at a final concentration of 15 μ g/ml was used for the selection of transformants in the knockout protocol. All experiments were performed in triplicates unless mentioned otherwise.

C.2.2. Construction of *E. coli* knockout strains

The knockout strains were created using the standard method of homologous recombination with the λ Red recombinase system (Datsenko & Wanner 2000). The Quick and Easy *E. coli* Gene Deletion Kit (Gene Bridges) was used for the construction of knockout strains (Δ *pgi*, Δ *trpR* and Δ *pheA* strains) as per manufacturer's protocol. Briefly, FRT-flanked resistance cassette was used for the disruption or replacement of the targeted gene that allowed the subsequent removal of the selection marker by an FLP-recombinase step. The initial step of gene deletion started with the generation of a PCR product with FRT cassette containing the flanking sequence from the gene of interest (*pgi*, *pheA* and *trpR*) using primers listed in Table C1. Transformation of pRED-ET plasmid into *E. coli* host was performed using electroporation. After the induction of pRED-ET protein synthesis, the transformation of PCR product containing FRT cassette was done using electroporation. Homologous recombination was performed at 30°C

incubation. An increase of the temperature to 37°C resulted in a loss of the expression plasmid after recombination. pFLP706 was used for removal of the antibiotic resistance marker from the *E. coli* genome. Selection of successful transformants was done using the culture conditions similar to that described earlier.

C.3. Results

C.3.1. Confirmation using gel electrophoresis

Generation of knockout strains was based on the homologous recombination that flips the targeted sequence with the known non-coding FRT sequence. The PCR product thus amplified by using the primers (Table C1), were analyzed (Figure C2) before and after deletion to check the removal of gene sequence from the specific location in the genome of *E. coli*.

Table C1: Primers used for the generation of knockout strains

Gene Name	Primer	Primer Sequence
Δpgi	Primer 1	ACTAAAACCATCACATTTTTCTGTG
	Primer 4	ACAGACAAGGGGATTTATCTGATAAAA
$\Delta pheA$	Primer 1	AGAATGCGAAGACGAACAAT
	Primer 4	ATTGAGTTGCTGGAGCAGG
$\Delta trpR$	Primer 1	ATATGCTATCGTACTCTTTAGCG
	Primer 4	TGGCGCTGAGTCCGTTTCATAAT

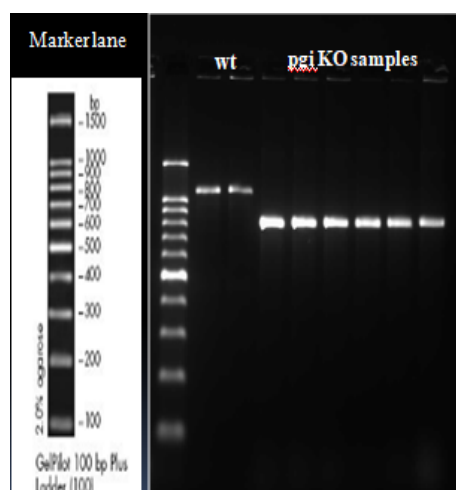


Figure C2: PCR profiles of *pgi* KOs.

C.3.2. Growth of wild-type *E. coli* K12 and knockout strains

Metabolic pathway engineering of *E. coli* K12 through gene deletions identified genes, *pgi* and *pheA* that potentially increase tryptophan levels. The *pgi* gene diverts flux through the pentose phosphate shunt, increasing precursor for aromatic amino acid (AA) synthesis and cofactor NADPH levels; and *pheA* gene diverts flux from the other competing aromatic AA phenylalanine and tyrosine

into tryptophan synthesis. Additionally, *trpR* gene was knocked out to de-regulate feedback inhibition of tryptophan synthesis. Growth rates (Table C2) and biomass yields of the deletion strains Δpgi , $\Delta trpR$ and $\Delta pheA$ (Figure C3) in *E. coli* on Luria-Bertani (LB) media were similar to the wild-type strain *E. coli* K12 and the control DH10 β .

Table C2: Growth rates of knockout strains in LB media.

<i>E. coli</i> Strain	Growth rate in LB (hr^{-1})
<i>DH10B</i>	0.5412
<i>K12</i>	0.5251
<i>K12 :ΔtrpR</i>	0.4725
<i>K12 :Δpgi</i>	0.4987
<i>K12 :ΔpheA</i>	0.4858

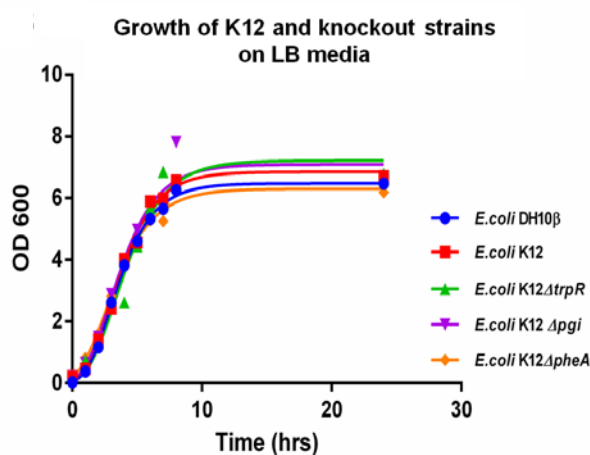


Figure C3: Growth profiles of *E. coli* K12 and deletion strains on LB media.

C.3.3. Tryptophan levels in knockout strains

The level of intracellular tryptophan has been estimated using relative quantification in MALDI-MS/MS analysis. All knockout strains showed a two-fold increase in tryptophan (Figure C4).

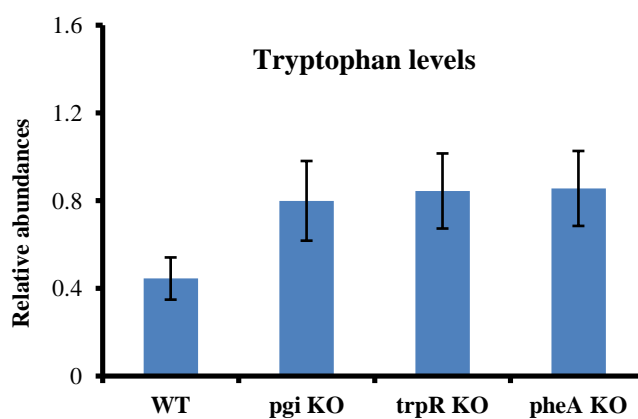


Figure C4: Tryptophan levels from MALDI-Analysis

C.3.4. Applications of generated knockout strains

The three knockout strains Δpgi , $\Delta trpR$ and $\Delta pheA$ are being used in our lab as base strains in the design for violacein producing strains. This is possible by metabolic engineering them further with synthetic biology to add violacein pathway that has five consecutive genes, *vioABCDE* coded by *vio* operon.

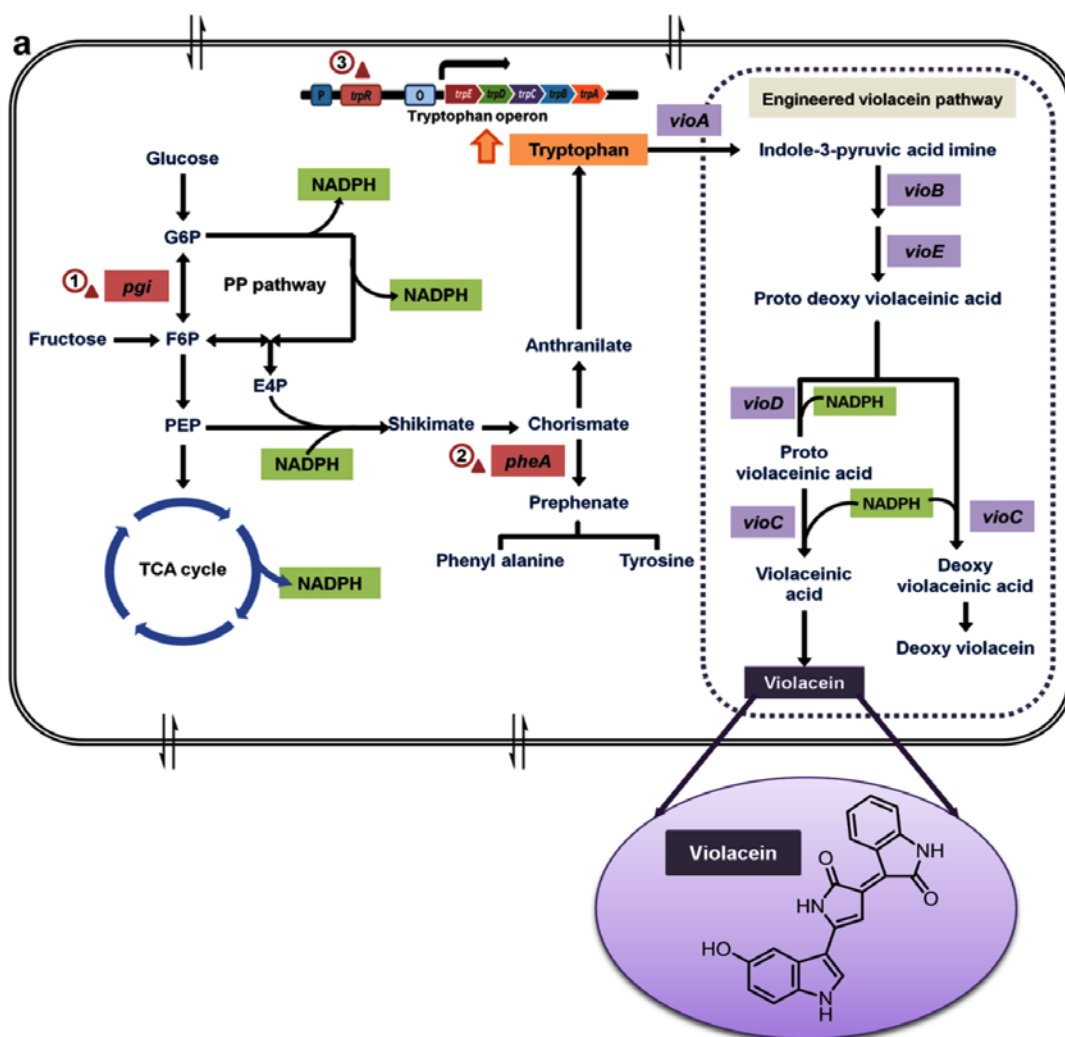


Figure C5: Pathway engineering for increasing tryptophan yields and adding violacein operon by synthetic biology, will give increased violacein yields as a product.

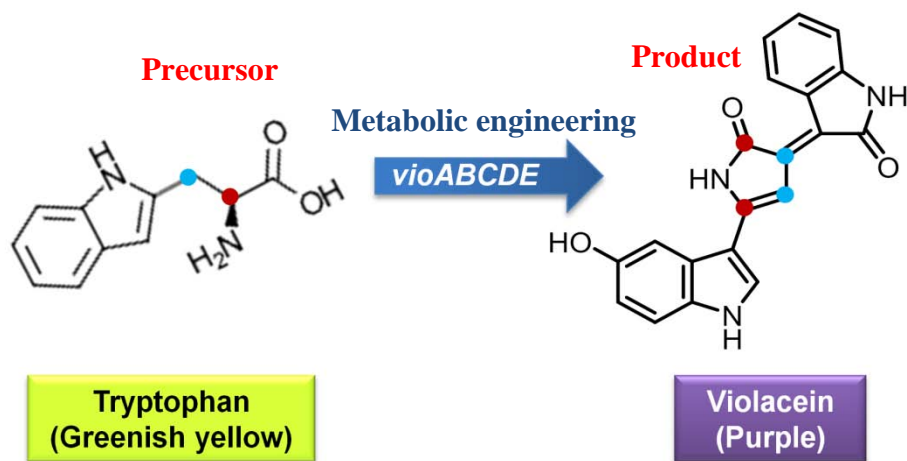


Figure C6: Two molecules of tryptophan (greenish yellow) combine to form violacein (Purple).

The genome engineered strains of *E. coli* thus has many applications and can be used as a host strain for different value-added products that involves tryptophan as a precursor or intermediate. In other applications, Δpgi strain has also been used as a base strains for value-added products like poly-lactic acid (bioplastics) where the carbon source is tailored for increasing the yields.

Bibliography

- Abaan, Ogan D, Eric C Polley, Sean R Davis, Yuelin J Zhu, Sven Bilke, Robert L Walker, Marbin Pineda, et al. 2013. “The Exomes of the NCI-60 Panel: A Genomic Resource for Cancer Biology and Systems Pharmacology.” *Cancer Research* 73 (14). NIH Public Access: 4372–82. doi:10.1158/0008-5472.CAN-12-3342.
- Ahn, Jungoh, Bevan K S Chung, Dong Yup Lee, Myongsoo Park, Iftexhar A. Karimi, Joon Ki Jung, and Hongweon Lee. 2011. “NADPH-Dependent Pgi-Gene Knockout Escherichia Coli Metabolism Producing Shikimate on Different Carbon Sources.” *FEMS Microbiology Letters* 324 (1): 10–16. doi:10.1111/j.1574-6968.2011.02378.x.
- Allen, M., M. Bjerke, H. Edlund, S. Nelander, and B. Westermarck. 2016. “Origin of the U87MG Glioma Cell Line: Good News and Bad News.” *Science Translational Medicine* 8 (354): 354re3-354re3. doi:10.1126/scitranslmed.aaf6853.
- Almeida Sassi, Felipe De, Algimir Lunardi Brunetto, Gilberto Schwartzmann, Rafael Roesler, and Ana Lucia Abujamra. 2012. “Glioma Revisited: From Neurogenesis and Cancer Stem Cells to the Epigenetic Regulation of the Niche.” *Journal of Oncology* 2012. doi:10.1155/2012/537861.
- Altman, Brian J., Zachary E. Stine, and Chi V. Dang. 2016. “From Krebs to Clinic: Glutamine Metabolism to Cancer Therapy.” *Nature Reviews Cancer* 16 (10): 619–34. doi:10.1038/nrc.2016.71.
- Altschuler, Steven J., and Lani F. Wu. 2010. “Cellular Heterogeneity: Do Differences Make a Difference?” *Cell* 141 (4): 559–63. doi:10.1016/j.cell.2010.04.033.
- Auger, Nathalie, Krystell Wanherdrick, Ahmed Idbah, Marie-emmanuelle Legrier, Bernard Dutrillaux, Marc Sanson, and Marie-france Poupon. 2006. “Genetic Alterations Associated with Acquired Temozolomide Resistance in SNB-19 , a Human Glioma Cell Line.” *Molecular Cancer Therapeutics* 9 (5): 2182–93. doi:10.1158/1535-7163.MCT-05-0428.
- Banelli, Barbara, Elisa Carra, Federica Barbieri, Roberto Würth, Federica Parodi, Alessandra Pattarozzi, Roberta Carosio, et al. 2015. “The Histone Demethylase KDM5A Is a Key Factor for the Resistance to Temozolomide in Glioblastoma.”

- Cell Cycle* 14 (21): 3418–29. doi:10.1080/15384101.2015.1090063.
- Bar, Eli E. 2011. “Glioblastoma, Cancer Stem Cells and Hypoxia.” *Brain Pathology* 21: 119–29. doi:10.1111/j.1750-3639.2010.00460.x.
- Berardinis, Ralph J. De, and Navdeep S. Chandel. 2016. “Fundamentals of Cancer Metabolism.” *Science Advances*. American Association for the Advancement of Science. doi:10.1126/sciadv.1600200.
- Bernhart, Eva, Sabine Damm, Andrea Wintersperger, Trevor DeVaney, Andreas Zimmer, Tony Raynham, Christopher Ireson, and Wolfgang Sattler. 2013. “Protein Kinase D2 Regulates Migration and Invasion of U87MG Glioblastoma Cells in Vitro.” *Experimental Cell Research* 319 (13). Elsevier: 2037–48. doi:10.1016/j.yexcr.2013.03.029.
- Bhattacharya, Sumitra, John D Jackson, Ani V Das, Wallace B Thoreson, Charles Kuszynski, Jackson James, Shantaram Joshi, and Iqbal Ahmad. 2003. “Direct Identification and Enrichment of Retinal Stem Cells / Progenitors by Hoechst Dye Efflux Assay.” *Investigative Ophthalmology and Visual Science* 44 (6): 2764–73. doi:10.1167/iovs.02-0899.
- Bleau, Anne Marie, Dolores Hambarzumyan, Tatsuya Ozawa, Elena I. Fomchenko, Jason T. Huse, Cameron W. Brennan, and Eric C. Holland. 2009. “PTEN/PI3K/Akt Pathway Regulates the Side Population Phenotype and ABCG2 Activity in Glioma Tumor Stem-like Cells.” *Cell Stem Cell* 4 (3). Elsevier Ltd: 226–35. doi:10.1016/j.stem.2009.01.007.
- Bongaerts, J, M Krämer, U Müller, L Raeven, and M Wubbolts. 2001. “Metabolic Engineering for Microbial Production of Aromatic Amino Acids and Derived Compounds.” *Metabolic Engineering* 3 (4): 289–300. doi:10.1006/mben.2001.0196.
- Brandes, Alba A, Alicia Tosoni, Enrico Franceschi, Michele Reni, Gemma Gatta, and Charles Vecht. 2008. “Glioblastoma in Adults.” *Critical Reviews in Oncology/Hematology* 67: 139–52. doi:10.1016/j.critrevonc.2008.02.005.
- Broadley, Kate W R, Martin K. Hunn, Kathryn J. Farrand, Kylie M. Price, Carole Grasso, Rose J. Miller, Ian F. Hermans, and Melanie J. McConnell. 2011. “Side Population Is Not Necessary or Sufficient for a Cancer Stem Cell Phenotype in Glioblastoma Multiforme.” *Stem Cells* 29 (3): 452–61. doi:10.1002/stem.582.

- Burgard, Anthony P., Priti Pharkya, and Costas D. Maranas. 2003. "Optknock: A Bilevel Programming Framework for Identifying Gene Knockout Strategies for Microbial Strain Optimization." *Biotechnology and Bioengineering* 84 (6): 647–57. doi:10.1002/bit.10803.
- Burrell, Rebecca a, Nicholas McGranahan, Jiri Bartek, and Charles Swanton. 2013. "The Causes and Consequences of Genetic Heterogeneity in Cancer Evolution." *Nature* 501 (7467): 338–45. doi:10.1038/nature12625.
- Bustin, Stephen a, Vladimir Benes, Jeremy Garson, Jan Hellemans, Jim Huggett, Mikael Kubista, Reinhold Mueller, et al. 2009. "The MIQE Guidelines: Minimum Information for Publication of Quantitative Real-Time PCR Experiments." *Clinical Chemistry* 55 (4): 000-012. doi:10.1373/clinchem.2008.112797.
- Calibasi Kocal, Gizem, Sinan Güven, Kira Foygel, Aaron Goldman, Pu Chen, Shiladitya Sengupta, Ramasamy Paulmurugan, Yasemin Baskin, and Utkan Demirci. 2016. "Dynamic Microenvironment Induces Phenotypic Plasticity of Esophageal Cancer Cells Under Flow." *Scientific Reports* 6 (1). Nature Publishing Group: 38221. doi:10.1038/srep38221.
- Cantor, Jason R., and David M. Sabatini. 2012. "Cancer Cell Metabolism: One Hallmark, Many Faces." *Cancer Discovery* 2: 881–98. doi:10.1158/2159-8290.CD-12-0345.
- Carey, Bryce W., Lydia W S Finley, Justin R. Cross, C. David Allis, and Craig B. Thompson. 2014. "Intracellular α -Ketoglutarate Maintains the Pluripotency of Embryonic Stem Cells." *Nature* 518 (7539): 413–16. doi:10.1038/nature13981.
- Chang, Geoffrey. 2003. "Multidrug Resistance ABC Transporters." *FEBS Letters* 555 (1): 102–5. doi:10.1016/S0014-5793(03)01085-8.
- Chang, Han, Donald G. Jackson, Paul S. Kayne, Petra B. Ross-Macdonald, Rolf Peter Ryseck, and Nathan O. Siemers. 2011. "Exome Sequencing Reveals Comprehensive Genomic Alterations across Eight Cancer Cell Lines." *PLoS ONE* 6 (6). doi:10.1371/journal.pone.0021097.
- Cheng, Wei-chung, I-fang Chung, Chen-yang Chen, Hsing-jen Sun, Jun-jeng Fen, Wei-chun Tang, Ting-yu Chang, Tai-tong Wong, and Hsei-Wei Wang. 2014. "DriverDB: An Exome Sequencing Database for Cancer Driver Gene Identification." *Nucleic Acids Research* 42 (D1): D1048–54. doi:10.1093/nar/gkt1025.

- Cheung, B. W Y, Linda L. Cartier, Henry Q. Russlie, and Ronald J. Sawchuk. 2005. "The Application of Sample Pooling Methods for Determining AUC, AUMC and Mean Residence Times in Pharmacokinetic Studies." *Fundamental and Clinical Pharmacology* 19: 347–54. doi:10.1111/j.1472-8206.2005.00329.x.
- Chhvez, Maria Incs, Alfredo Martinez, Francisco Bolivar, and Guillermo Gosset. 2005. "Metabolic Pathway Engineering for Microbial Production of Aromatic Amino Acids," 2005.
- Choi, Seong Yeol, Kyoung-hye Yoon, Jin Il Lee, and Robert J. Mitchell. 2015. "Violacein: Properties and Production of a Versatile Bacterial Pigment." *BioMed Research International* 2015: 1–8. doi:10.1155/2015/465056.
- Chong, Jasmine, Othman Soufan, Carin Li, Iurie Caraus, Shuzhao Li, Guillaume Bourque, David S Wishart, and Jianguo Xia. 2018. "MetaboAnalyst 4.0: Towards More Transparent and Integrative Metabolomics Analysis." *Nucleic Acids Research*, May. doi:10.1093/nar/gky310.
- Clark, Michael James, Nils Homer, Brian D. O'Connor, Zugen Chen, Ascia Eskin, Hane Lee, Barry Merriman, and Stanley F. Nelson. 2010a. "U87MG Decoded: The Genomic Sequence of a Cytogenetically Aberrant Human Cancer Cell Line." Edited by Marshall S. Horwitz. *PLoS Genetics* 6 (1): e1000832. doi:10.1371/journal.pgen.1000832.
- Clark, Michael James, Nils Homer, Brian D. O'Connor, Zugen Chen, Ascia Eskin, Hane Lee, Barry Merriman, and Stanley F Nelson. 2010b. "U87MG Decoded: The Genomic Sequence of a Cytogenetically Aberrant Human Cancer Cell Line." Edited by Marshall S. Horwitz. *PLoS Genetics* 6 (1): e1000832. doi:10.1371/journal.pgen.1000832.
- Cruz, M. H., Å. Sidén, G. M. Calaf, Z. M. Delwar, and J. S. Yakisich. 2012. "The Stemness Phenotype Model." *ISRN Oncology* 2012: 1–10. doi:10.5402/2012/392647.
- Dang, Chi V. 2012a. "Links between Metabolism and Cancer." *Genes and Development* 26: 877–90. doi:10.1101/gad.189365.112.
- Datsenko, K A, and B L Wanner. 2000. "One-Step Inactivation of Chromosomal Genes in Escherichia Coli K-12 Using PCR Products." *Proceedings of the National*

Academy of Sciences 97 (12): 6640–45. doi:10.1073/pnas.120163297.

- Daye, Dania, and Kathryn E. Wellen. 2012. “Metabolic Reprogramming in Cancer: Unraveling the Role of Glutamine in Tumorigenesis.” *Seminars in Cell and Developmental Biology* 23 (4). Elsevier Ltd: 362–69. doi:10.1016/j.semcdb.2012.02.002.
- DeBerardinis, R. J., and N. S. Chandel. 2016. “Fundamentals of Cancer Metabolism.” *Science Advances* 2 (5). American Association for the Advancement of Science: e1600200–e1600200. doi:10.1126/sciadv.1600200.
- Drummond, R J, and A T Phillips. 1977. “Intracellular Amino Acid Content of Neuronal, Glial, and Non-Neural Cell Cultures: The Relationship to Glutamic Acid Compartmentation.” *Journal of Neurochemistry* 29: 101–8.
- Duckwall, Casey Scott, Taylor Athanasaw Murphy, and Jamey Dale Young. 2013. “Mapping Cancer Cell Metabolism with(13)C Flux Analysis: Recent Progress and Future Challenges.” *Journal of Carcinogenesis* 12: 13. doi:10.4103/1477-3163.115422.
- Durán, Nelson, Giselle Z. Justo, Marcela Durán, Marcelo Brocchi, Livia Cordi, Ljubica Tasic, Guillermo R. Castro, and Gerson Nakazato. 2016. “Advances in Chromobacterium Violaceum and Properties of Violacein-Its Main Secondary Metabolite: A Review.” *Biotechnology Advances* 34 (5). Elsevier Inc.: 1030–45. doi:10.1016/j.biotechadv.2016.06.003.
- Etchegaray, Jean-Pierre, and Raul Mostoslavsky. 2016. “Interplay between Metabolism and Epigenetics: A Nuclear Adaptation to Environmental Changes.” *Molecular Cell* 62 (5). Elsevier Inc.: 695–711. doi:10.1016/j.molcel.2016.05.029.
- Fang, Ming-Yue, Chong Zhang, Song Yang, Jin-Yu Cui, Pei-Xia Jiang, Kai Lou, Masaaki Wachi, and Xin-Hui Xing. 2015. “High Crude Violacein Production from Glucose by Escherichia Coli Engineered with Interactive Control of Tryptophan Pathway and Violacein Biosynthetic Pathway.” *Microbial Cell Factories* 14 (1): 1–13. doi:10.1186/s12934-015-0192-x.
- Farrés, Mireia, Stefan Platikanov, Stefan Tsakovski, and Romà Tauler. 2015. “Comparison of the Variable Importance in Projection (VIP) and of the Selectivity Ratio (SR) Methods for Variable Selection and Interpretation.” *Journal of*

- Chemometrics* 29 (10). Wiley-Blackwell: 528–36. doi:10.1002/cem.2736.
- Feron, Olivier. 2009. “Pyruvate into Lactate and Back: From the Warburg Effect to Symbiotic Energy Fuel Exchange in Cancer Cells.” *Radiotherapy and Oncology* 92 (3). Elsevier Ireland Ltd: 329–33. doi:10.1016/j.radonc.2009.06.025.
- Frattoni, Veronique, Vladimir Trifonov, Joseph Minhow Chan, Angelica Castano, Marie Lia, Francesco Abate, Stephen T Keir, et al. 2013. “The Integrated Landscape of Driver Genomic Alterations in Glioblastoma.” *Nature Genetics* 45 (10). Nature Publishing Group: 1141–49. doi:10.1038/ng.2734.
- Friedman, Hs, T Kerby, and H Calvert. 2000. “Temozolomide and Treatment of Malignant Glioma.” *Clinical and Translational Medicine* 6 (July): 2585–97.
- Füller, Janis J., René Röpke, Joern Krausze, Kim E. Rennhack, Nils P. Daniel, Wulf Blankenfeldt, Stefan Schulz, Dieter Jahn, and Jürgen Moser. 2016. “Biosynthesis of Violacein, Structure and Function of l-Tryptophan Oxidase VioA from *Chromobacterium Violaceum*.” *The Journal of Biological Chemistry* 291 (38): 20068–84. doi:10.1074/jbc.M116.741561.
- Furnari, Frank B, Timothy F Cloughesy, Webster K Cavenee, and Paul S Mischel. 2015. “Heterogeneity of Epidermal Growth Factor Receptor Signalling Networks in Glioblastoma.” *Nature Reviews Cancer* 15 (5). Nature Publishing Group: 302–10. doi:10.1038/nrc3918.
- Gaspar, Nathalie, Lynley Marshall, Lara Perryman, Dorine a. Bax, Suzanne E. Little, Marta Viana-Pereira, Swee Y. Sharp, et al. 2010. “MGMT-Independent Temozolomide Resistance in Pediatric Glioblastoma Cells Associated with a PI3-Kinase-Mediated HOX/Stem Cell Gene Signature.” *Cancer Research* 70 (22): 9243–52. doi:10.1158/0008-5472.CAN-10-1250.
- Gaude, Edoardo, and Christian Frezza. 2014. “Defects in Mitochondrial Metabolism and Cancer.” *Cancer & Metabolism* 2 (1): 10. doi:10.1186/2049-3002-2-10.
- Geck, Renee C., and Alex Toker. 2016. “Nonessential Amino Acid Metabolism in Breast Cancer.” *Advances in Biological Regulation*. Pergamon. doi:10.1016/j.jbior.2016.01.001.
- Gerner, Eugene W., and Frank L. Meyskens. 2004. “Polyamines and Cancer: Old Molecules, New Understanding.” *Nature Reviews Cancer*. Nature Publishing

Group. doi:10.1038/nrc1454.

Glavinas, Hristos, Peter Krajcsi, Judit Cserepes, and Balazs Sarkadi. 2008. “The Role of ABC Transporters in Drug Absorption, Distribution, Metabolism, Excretion and Toxicity (ADME-Tox).” *Drug Discovery Today* 13 (9–10): 379–93. doi:10.1016/j.drudis.2007.12.010.

Golebiewska, Anna, Sébastien Bougnaud, Daniel Stieber, Nicolaas H C Brons, Laurent Vallar, Frank Hertel, Barbara Klink, Evelin Schröck, Rolf Bjerkvig, and Simone P. Niclou. 2013. “Side Population in Human Glioblastoma Is Non-Tumorigenic and Characterizes Brain Endothelial Cells.” *Brain* 136: 1462–75. doi:10.1093/brain/awt025.

Golebiewska, Anna, Nicolaas H C Brons, Rolf Bjerkvig, and Simone P. Niclou. 2011. “Critical Appraisal of the Side Population Assay in Stem Cell and Cancer Stem Cell Research.” *Cell Stem Cell* 8 (2): 136–47. doi:10.1016/j.stem.2011.01.007.

Goodell, Margaret A. 2005. “Stem Cell Identification and Sorting Using the Hoechst 33342 Side Population (SP).” *Current Protocols in Cytometry*, 1–11.

Grasbon-Frodl, Eva M., Friedrich Wilhelm Kreth, Michael Rüter, Oliver Schnell, Karl Bise, Jörg Felsberg, Guido Reifenberger, Jörg Christian Tonn, and Hans A. Kretschmar. 2007. “Intratumoral Homogeneity of MGMT Promoter Hypermethylation as Demonstrated in Serial Stereotactic Specimens from Anaplastic Astrocytomas and Glioblastomas.” *International Journal of Cancer* 121 (11): 2458–64. doi:10.1002/ijc.23020.

Günther, W, E Pawlak, R Damasceno, H Arnold, and a J Terzis. 2003. “Temozolomide Induces Apoptosis and Senescence in Glioma Cells Cultured as Multicellular Spheroids.” *British Journal of Cancer* 88: 463–69. doi:10.1038/sj.bjc.6600711.

Haga, S, E Hinoshita, K Ikezaki, M Fukui, G L Scheffer, T Uchiumi, and M Kuwano. 2001. “Involvement of the Multidrug Resistance Protein 3 in Drug Sensitivity and Its Expression in Human Glioma.” *Japanese Journal of Cancer Research: Gann* 92 (2): 211–19.

Hainaut, Pierre, and Amelie Plymoth. 2012. “Cancer as a Metabolic Disease.” *Current Opinion in Oncology* 24 (1): 56–57. doi:10.1097/CCO.0b013e32834e388a.

Hanahan, D, and R A Weinberg. 2000. “The Hallmarks of Cancer.” *Cell* 100 (1): 57–70.

doi:10.1007/s00262-010-0968-0.

- Hanahan, Douglas, and Robert A. Weinberg. 2011. “Hallmarks of Cancer: The next Generation.” *Cell*.
- Hardie, D. Grahame. 2013. “The LKB1-AMPK Pathway-Friend or Foe in Cancer?” *Cancer Cell* 23 (2). Elsevier: 131–32. doi:10.1016/j.ccr.2013.01.009.
- Heiden, Matthew G Vander, Lewis C Cantley, and Craig B Thompson. 2009. “Understanding the Warburg Effect: The Metabolic Requirements of Cell Proliferation.” *Science (New York, N.Y.)* 324 (2009): 1029–33. doi:10.1126/science.1160809.
- Higgins, Christopher F. 2001. “ABC Transporters: Physiology, Structure and Mechanism – an Overview.” *Res. Microbiol* 152: 205–10. doi:10.1016/S0923-2508(01)01193-7.
- Hirschmann-Jax, C, a E Foster, G G Wulf, J G Nuchtern, T W Jax, U Gobel, M a Goodell, and M K Brenner. 2004. “A Distinct ‘Side Population’ of Cells with High Drug Efflux Capacity in Human Tumor Cells.” *Proceedings of the National Academy of Sciences of the United States of America* 101 (39): 14228–33. doi:10.1073/pnas.0400067101.
- Hoelzinger, Dominique B, Luigi Mariani, Joachim Weis, Tanja Woyke, Theresa J Berens, Wendy S McDonough, Andrew Sloan, Stephen W Coons, and Michael E Berens. 2005. “Gene Expression Profile of Glioblastoma Multiforme Invasive Phenotype Points to New Therapeutic Targets.” *Neoplasia (New York, N.Y.)* 7 (1): 7–16. doi:10.1593/neo.04535.
- Hoey, Timothy. 2010. “Drug Resistance, Epigenetics, and Tumor Cell Heterogeneity.” *Science Translational Medicine* 2 (28): 28ps19. doi:10.1126/scitranslmed.3001056.
- Holohan, Caitriona, Sandra Van Schaeybroeck, Daniel B Longley, and Patrick G Johnston. 2013. “Cancer Drug Resistance: An Evolving Paradigm.” *Nature Reviews. Cancer* 13 (10). Nature Publishing Group: 714–26. doi:10.1038/nrc3599.
- Hsu, Peggy P., and David M. Sabatini. 2008. “Cancer Cell Metabolism: Warburg and Beyond.” *Cell* 134 (5): 703–7. doi:10.1016/j.cell.2008.08.021.
- Huang, Huiyong, Hong Lin, Xiang Zhang, and Juan Li. 2012. “Resveratrol Reverses Temozolomide Resistance by Downregulation of MGMT in T98G Glioblastoma Cells by the NF- κ B-Dependent Pathway.” *Oncology Reports* 27 (6): 2050–56.

doi:10.3892/or.2012.1715.

- Ikedo, Masato. 2006. "Towards Bacterial Strains Overproducing L-Tryptophan and Other Aromatics by Metabolic Engineering." *Applied Microbiology and Biotechnology* 69 (6): 615–26. doi:10.1007/s00253-005-0252-y.
- Immanuel, Selva Rupa C., Avinash D. Ghanate, Dharmeshkumar S. Parmar, Fiona Marriage, Venkateswarlu Panchagnula, Philip J. Day, and Anu Raghunathan. 2018. "Integrative Analysis of Rewired Central Metabolism in Temozolomide Resistant Cells." *Biochemical and Biophysical Research Communications* 495 (2): 2010–16. doi:10.1016/j.bbrc.2017.12.073.
- Inda, Maria-del-mar, Rudy Bonavia, and Joan Seoane. 2014. "Glioblastoma Multiforme: A Look Inside Its Heterogeneous Nature," 226–39. doi:10.3390/cancers6010226.
- Johannessen, Tor-Christian Aase, Lars Prestegarden, Amra Grudic, Monika E. Hegi, Berit Bølge Tysnes, and Rolf Bjerkvig. 2013. "The DNA Repair Protein ALKBH2 Mediates Temozolomide Resistance in Human Glioblastoma Cells." *Neuro-Oncology* 15 (3): 269–78. doi:10.1093/neuonc/nos301.
- Jones, Russell G., David R. Plas, Sara Kubek, Monica Buzzai, James Mu, Yang Xu, Morris J. Birnbaum, and Craig B. Thompson. 2005. "AMP-Activated Protein Kinase Induces a P53-Dependent Metabolic Checkpoint." *Molecular Cell* 18: 283–93. doi:10.1016/j.molcel.2005.03.027.
- Khan, Zarine, Amal Shervington, Chinmay Munje, and Leroy Shervington. 2013. "The Complexity of Identifying Cancer Stem Cell Biomarkers." *Cancer Investigation* 31 (October 2012): 404–11. doi:10.3109/07357907.2013.802800.
- Khodursky, a B, B J Peter, N R Cozzarelli, D Botstein, P O Brown, C Yanofsky, a B Khodursky, B J Peter, N R Cozzarelli, and C Yanofsky. 2000. "DNA Microarray Analysis of Gene Expression in Response to Physiological and Genetic Changes That Affect Tryptophan Metabolism in Escherichia Coli." *Proceedings of the National Academy of Sciences of the United States of America* 97 (22): 12170–75. doi:10.1073/pnas.220414297.
- Kim, Jungim, Jeongsu Han, Yunseon Jang, Soo Jeong Kim, Min Joung Lee, Min Jeong Ryu, Gi Ryang Kweon, and Jun Young Heo. 2015. "High-Capacity Glycolytic and Mitochondrial Oxidative Metabolisms Mediate the Growth Ability of

- Glioblastoma.” *International Journal of Oncology* 47 (3): 1009–16. doi:10.3892/ijo.2015.3101.
- King, C. Ryan, Paul J. Rathouz, and Dan L. Nicolae. 2011. “Computational and Statistical Approaches to Analyzing Variants Identified by Exome Sequencing.” Edited by Jonathan Marchini. *Genome Biology* 12 (9): 227. doi:10.1371/journal.pgen.1001202.
- Kline, Berry J, and Ph D Richmond. 1981. “Determination of Mean Valproic Acid Serum Level by Assay of a Single Pooled Sample.” *Clin. Pharmacol. Th* 29 (3): 408–13.
- Kohsaka, S., L. Wang, K. Yachi, R. Mahabir, T. Narita, T. Itoh, M. Tanino, T. Kimura, H. Nishihara, and S. Tanaka. 2012. “STAT3 Inhibition Overcomes Temozolomide Resistance in Glioblastoma by Downregulating MGMT Expression.” *Molecular Cancer Therapeutics* 11: 1289–99. doi:10.1158/1535-7163.MCT-11-0801.
- Kreeger, Pamela K., and Douglas a. Lauffenburger. 2009. “Cancer Systems Biology: A Network Modeling Perspective.” *Carcinogenesis* 31 (1): 2–8. doi:10.1093/carcin/bgp261.
- Kreth, Simone, Jens Heyn, Stefan Grau, Hans a. Kretzschmar, Rupert Egensperger, and Friedrich W. Kreth. 2010. “Identification of Valid Endogenous Control Genes for Determining Gene Expression in Human Glioma.” *Neuro-Oncology* 12 (6): 570–79. doi:10.1093/neuonc/nop072.
- Kucharzewska, Paulina, Helena C. Christianson, and Mattias Belting. 2015. “Global Profiling of Metabolic Adaptation to Hypoxic Stress in Human Glioblastoma Cells.” Edited by Nikos K Karamanos. *PLoS ONE* 10 (1): e0116740. doi:10.1371/journal.pone.0116740.
- Lee, Sang Y. 2016. “Temozolomide Resistance in Glioblastoma Multiforme.” *Genes & Diseases* 3 (3). Elsevier: 198–210. doi:10.1016/J.GENDIS.2016.04.007.
- Lewis, Nathan E., and Alyaa M. Abdel-Haleem. 2013. “The Evolution of Genome-Scale Models of Cancer Metabolism.” *Frontiers in Physiology* 4 (September). Frontiers: 237. doi:10.3389/fphys.2013.00237.
- Li, Sichen, Arthur P Chou, Weidong Chen, Ruihuan Chen, Yuzhong Deng, Heidi S Phillips, Julia Selfridge, et al. 2013. “Overexpression of Isocitrate Dehydrogenase

- Mutant Proteins Renders Glioma Cells More Sensitive to Radiation” 15 (1): 57–68.
- Little, Suzanne E, Sergey Popov, Alexa Jury, Dorine A Bax, Lawrence Doey, S. Al-Sarraj, Juliane M Jurgensmeier, and Chris Jones. 2012. “Receptor Tyrosine Kinase Genes Amplified in Glioblastoma Exhibit a Mutual Exclusivity in Variable Proportions Reflective of Individual Tumor Heterogeneity.” *Cancer Research* 72 (7): 1614–20. doi:10.1158/0008-5472.CAN-11-4069.
- Liu, Pengyuan, Carl Morrison, Liang Wang, Donghai Xiong, Peter Vedell, Peng Cui, Xing Hua, et al. 2012. “Identification of Somatic Mutations in Non-Small Cell Lung Carcinomas Using Whole-Exome Sequencing.” *Carcinogenesis* 33 (7): 1270–76. doi:10.1093/carcin/bgs148.
- Losman, Julie Aurore, and William G. Kaelin. 2013. “What a Difference a Hydroxyl Makes: Mutant IDH, (R)-2-Hydroxyglutarate, and Cancer.” *Genes and Development* 27 (8): 836–52. doi:10.1101/gad.217406.113.
- Maher, Elizabeth A. 2001. “Malignant Glioma: Genetics and Biology of a Grave Matter.” *Genes & Development* 15 (11): 1311–33. doi:10.1101/gad.891601.
- Mardis, Elaine R. 2008. “The Impact of Next-Generation Sequencing Technology on Genetics.” *Trends in Genetics* 24 (3): 133–41. doi:10.1016/j.tig.2007.12.007.
- Marjanovic, Nemanja D., Robert a. Weinberg, and Christine L. Chaffer. 2013. “Cell Plasticity and Heterogeneity in Cancer.” *Clinical Chemistry* 59 (1): 168–79. doi:10.1373/clinchem.2012.184655.
- Mathis, Robert Austin, Ethan S. Sokol, and Piyush B. Gupta. 2017a. “Cancer Cells Exhibit Clonal Diversity in Phenotypic Plasticity.” *Open Biology* 7 (2): 160283. doi:10.1098/rsob.160283.
- Mazurek, Sybille, C. Bruce Boschek, Ferdinand Hugo, and Erich Eigenbrodt. 2005. “Pyruvate Kinase Type M2 and Its Role in Tumor Growth and Spreading.” *Seminars in Cancer Biology* 15 (4): 300–308. doi:10.1016/j.semcancer.2005.04.009.
- Med, J Exp. 1996. “Hoechst 33342 HSC Staining and Stem Cell Purification Protocol.” *J Exp Med* 183: 1797–1806.
- Megova, Magdalena, Jiri Drabek, Vladimira Koudelakova, Radek Trojanec, Ondrej Kalita, and Marian Hajduch. 2014. “Isocitrate Dehydrogenase 1 and 2 Mutations in Gliomas.” *Journal of Neuroscience Research* 92 (12): 1611–20.

doi:10.1002/jnr.23456.

- Meldrum, Cliff, Maria A Doyle, and Richard W Tothill. 2011. "Next-Generation Sequencing for Cancer Diagnostics: A Practical Perspective." *The Clinical Biochemist. Reviews* 32 (4). The Australian Association of Clinical Biochemists: 177–95.
- Metzker, Michael L. 2010. "Sequencing Technologies - the next Generation." *Nature Reviews. Genetics* 11 (1): 31–46.
- Muñoz-Pinedo, C, N El Mjiyad, and J-E Ricci. 2012. "Cancer Metabolism: Current Perspectives and Future Directions." *Cell Death and Disease* 3: e248. doi:10.1038/cddis.2011.123.
- Ng, P C. 2008. "Genetic Variation in an Individual Human Exome." *PLoS Genet.* 4. Macmillan Publishers Limited. All rights reserved: e1000160.
- Ng, Sarah B, Kati J Buckingham, Choli Lee, Abigail W Bigham, Holly K Tabor, Karin M Dent, Chad D Huff, et al. 2010. "Exome Sequencing Identifies the Cause of a Mendelian Disorder." *Nature Genetics* 42 (1): 30–35. doi:10.1038/ng.499.
- Ng, Sarah B, Emily H Turner, Peggy D Robertson, Steven D Flygare, Abigail W Bigham, Choli Lee, Tristan Shaffer, et al. 2009. "Targeted Capture and Massively Parallel Sequencing of 12 Human Exomes." *Nature* 461 (7261). Macmillan Publishers Limited. All rights reserved: 272–76.
- Nieminen, Anni I, Vilja M Eskelinen, Heidi M Haikala, Topi a Tervonen, Yan Yan, Johanna I Partanen, and Juha Klefström. 2013. "Myc-Induced AMPK-Phospho P53 Pathway Activates Bak to Sensitize Mitochondrial Apoptosis." *Proceedings of the National Academy of Sciences of the United States of America* 110 (20): E1839-48. doi:10.1073/pnas.1208530110.
- Nikitin, Alexander, Sergei Egorov, Nikolai Daraselia, and I. Mazo. 2003. "Pathway Studio--the Analysis and Navigation of Molecular Networks." *Bioinformatics* 19 (16): 2155–57. doi:10.1093/bioinformatics/btg290.
- Noushmehr, Houtan, Daniel J. Weisenberger, Kristin Diefes, Heidi S. Phillips, Kanan Pujara, Benjamin P. Berman, Fei Pan, et al. 2010. "Identification of a CpG Island Methylator Phenotype That Defines a Distinct Subgroup of Glioma." *Cancer Cell* 17 (5): 510–22. doi:10.1016/j.ccr.2010.03.017.

- Ostrom, Quinn T, Luc Bauchet, Faith G Davis, Isabelle Deltour, James L Fisher, Chelsea Eastman Langer, Melike Pekmezci, et al. n.d. “The Epidemiology of Glioma in Adults: A ‘State of the Science’ Review.” doi:10.1093/neuonc/nou087.
- Parker, Nicole R., Amanda L. Hudson, Peter Khong, Jonathon F. Parkinson, Trisha Dwight, Rowan J. Ikin, Ying Zhu, et al. 2016. “Intratumoral Heterogeneity Identified at the Epigenetic, Genetic and Transcriptional Level in Glioblastoma.” *Scientific Reports* 6 (1). Nature Publishing Group: 22477. doi:10.1038/srep22477.
- Parker, Nicole Renee, Peter Khong, Jonathon Fergus Parkinson, Viive Maarika Howell, and Helen Ruth Wheeler. 2015. “Molecular Heterogeneity in Glioblastoma Potential Clinical Implications” 5 (March): 1–9. doi:10.3389/fonc.2015.00055.
- Parsons, D Williams, Siân Jones, Xiaosong Zhang, Jimmy Cheng-ho Lin, Rebecca J Leary, Philipp Angenendt, Parminder Mankoo, et al. 2010. “NIH Public Access” 321 (5897). doi:10.1126/science.1164382.An.
- Patel, Anoop P., Itay Tirosh, John J. Trombetta, Alex K. Shalek, Shawn M. Gillespie, Hiroaki Wakimoto, Daniel P. Cahill, Brian V. Nahed, William T. Curry, Robert L. Martuza, David N. Louis, Orit Rozenblatt-Rosen, et al. 2014. “Single-Cell RNA-Seq Highlights Intratumoral Heterogeneity in Primary Glioblastoma.” *Science* 344 (6190): 1396–1401. doi:10.1126/science.1254257.
- Patel, Anoop P, Itay Tirosh, John J Trombetta, Alex K Shalek, Shawn M Gillespie, Hiroaki Wakimoto, Daniel P Cahill, Brian V Nahed, William T Curry, Robert L Martuza, David N Louis, Orit Rozenblatt-rosen, et al. 2014. “Single-Cell RNA-Seq Highlights Intratumoral Heterogeneity in Primary Glioblastoma.” *Science* 344 (6190): 1396–1401.
- Patnaik, Ranjan, and James C Liao. 1994. “Engineering of Escherichia Coli Central Metabolism for Aromatic Metabolite Production with near Theoretical Yield . Engineering of Escherichia Coli Central Metabolism for Aromatic Metabolite Production with Near Theoretical Yield.” *Appl. Environmental Microbiol.* 60 (11): 3903–8.
- Pei, Jian, Kyung-sub Moon, Sango Pan, Kyung-hwa Lee, Hyang-hwa Ryu, Tae-young Jung, In-young Kim, Woo-yeol Jang, Chae-hun Jung, and Shin Jung. 2014. “Proteomic Analysis between U87MG and U343MG-A Cell Lines: Searching for Candidate Proteins for Glioma Invasion” 2 (1): 22–28.

- Persano, Luca, Elena Rampazzo, Giuseppe Basso, and Giampietro Viola. 2013. "Glioblastoma Cancer Stem Cells: Role of the Microenvironment and Therapeutic Targeting." *Biochemical Pharmacology* 85 (5). Elsevier Inc.: 612–22. doi:10.1016/j.bcp.2012.10.001.
- Persson, Anders I., and William a. Weiss. 2009. "The Side Story of Stem-like Glioma Cells." *Cell Stem Cell* 4 (3). Elsevier Inc.: 191–92. doi:10.1016/j.stem.2009.02.004.
- Portnow, Jana, Behnam Badie, Mike Chen, An Liu, Suzette Blanchard, and Timothy W. Synold. 2009. "The Neuropharmacokinetics of Temozolomide in Patients with Resectable Brain Tumors: Potential Implications for the Current Approach to Chemoradiation." *Clinical Cancer Research* 15 (22): 7092–98. doi:10.1158/1078-0432.CCR-09-1349.
- Qazi, M. A., P. Vora, C. Venugopal, S. S. Sidhu, J. Moffat, C. Swanton, and S. K. Singh. 2017. "Intratumoral Heterogeneity: Pathways to Treatment Resistance and Relapse in Human Glioblastoma." *Annals of Oncology*. doi:10.1093/annonc/mdx169.
- Qian, Xiao-Min, Zhen-Dong Shi, Yu Ren, Chao-Yong Liu, Ya-Ru Ji, Li-Xia Long, Peiyu Pu, Jing Sheng, Xu-Bo Yuan, and Chun-Sheng Kang. 2013. "Synergistic Inhibition of Human Glioma Cell Line by Temozolomide and PAMAM-Mediated MiR-21i." *Journal of Applied Polymer Science* 127: 570–76. doi:10.1002/app.37823.
- Qiang, L, T Wu, H-W Zhang, N Lu, R Hu, Y-J Wang, L Zhao, et al. 2012. "HIF-1 α Is Critical for Hypoxia-Mediated Maintenance of Glioblastoma Stem Cells by Activating Notch Signaling Pathway." *Cell Death and Differentiation* 19: 284–94. doi:10.1038/cdd.2011.95.
- Queiroz, Karla C S, Renato Milani, Roberta R. Ruela-de-Sousa, Gwenny M Fuhler, Giselle Z Justo, Willian F Zambuzzi, Nelson Duran, et al. 2012. "Violacein Induces Death of Resistant Leukaemia Cells via Kinome Reprogramming, Endoplasmic Reticulum Stress and Golgi Apparatus Collapse." Edited by Rafael Linden. *PLoS ONE* 7 (10): e45362. doi:10.1371/journal.pone.0045362.
- Ramão, Anelisa, Marcela Gimenez, Helen J Laure, Clarice Izumi, Rodrigo Cesar S Vida, Sueli Oba-Shinjo, Suelly Kn Marie, and Jose C Rosa. 2012. "Changes in the Expression of Proteins Associated with Aerobic Glycolysis and Cell Migration Are Involved in Tumorigenic Ability of Two Glioma Cell Lines." *Proteome Science* 10 (1): 53. doi:10.1186/1477-5956-10-53.

- Ramirez, Yulian P., Jessica L. Weatherbee, Richard T. Wheelhouse, and Alonzo H. Ross. 2013. "Glioblastoma Multiforme Therapy and Mechanisms of Resistance." *Pharmaceuticals* 6: 1475–1506. doi:10.3390/ph6121475.
- Ramirez, Yulian, Jessica Weatherbee, Richard Wheelhouse, and Alonzo Ross. 2013. "Glioblastoma Multiforme Therapy and Mechanisms of Resistance." *Pharmaceuticals* 6 (12): 1475–1506. doi:10.3390/ph6121475.
- Rees, Douglas C., Eric Johnson, and Oded Lewinson. 2009. "ABC Transporters: The Power to Change." *Nature Reviews Molecular Cell Biology* 10 (3): 218–27. doi:10.1038/nrm2646.
- Ríos, Marcos, Marc Foretz, Benoit Viollet, Angel Prieto, Maximo Fraga, Jose a. Costoya, and Rosa Senarís. 2013. "AMPK Activation by Oncogenesis Is Required to Maintain Cancer Cell Proliferation in Astrocytic Tumors." *Cancer Research* 73: 2628–38. doi:10.1158/0008-5472.CAN-12-0861.
- Rolfsson, Ottar, Bernhard Ø Palsson, and Ines Thiele. 2011. "The Human Metabolic Reconstruction Recon 1 Directs Hypotheses of Novel Human Metabolic Functions." *BMC Systems Biology* 5 (1): 155. doi:10.1186/1752-0509-5-155.
- Ros, S., C. R. Santos, S. Moco, F. Baenke, G. Kelly, M. Howell, N. Zamboni, and a. Schulze. 2012. "Functional Metabolic Screen Identifies 6-Phosphofructo-2-Kinase/Fructose-2,6-Biphosphatase 4 as an Important Regulator of Prostate Cancer Cell Survival." *Cancer Discovery* 2: 328–43. doi:10.1158/2159-8290.CD-11-0234.
- Safa, Ahmad R, Mohammad Reza Saadatzadeh, Aaron A. Cohen-Gadol, Karen E Pollok, and Khadijeh Bijangi-Vishehsaraei. 2015. "Glioblastoma Stem Cells (GSCs) Epigenetic Plasticity and Interconversion between Differentiated Non-GSCs and GSCs." *Genes & Diseases* 2 (2). Elsevier Taiwan LLC and the: 152–63. doi:10.1016/j.gendis.2015.02.001.
- Sahoo, Swagatika, Maiké K. Aurich, Jon J. Jonsson, and Ines Thiele. 2014. "Membrane Transporters in a Human Genome-Scale Metabolic Knowledgebase and Their Implications for Disease." *Frontiers in Physiology* 5 MAR (March): 1–24. doi:10.3389/fphys.2014.00091.
- Sánchez, César, Alfredo F. Braña, Carmen Méndez, and José a. Salas. 2006. "Reevaluation of the Violacein Biosynthetic Pathway and Its Relationship to

- Indolocarbazole Biosynthesis.” *ChemBioChem* 7 (8): 1231–40. doi:10.1002/cbic.200600029.
- Scourzic, Laurianne, Enguerran Mouly, and Olivier A. Bernard. 2015. “TET Proteins and the Control of Cytosine Demethylation in Cancer.” *Genome Medicine* 7 (1): 1–16. doi:10.1186/s13073-015-0134-6.
- Seznec, Janina, Simone Weit, and Ulrike Naumann. 2010. “Gene Expression Profile in a Glioma Cell Line Resistant to Cell Death Induced by a the Chimeric Tumor Suppressor-1 (CTS-1), a Dominant-Positive Variant of P53—the Role of NFκB.” *Carcinogenesis* 31 (3): 411–18. doi:10.1093/carcin/bgp319.
- Sharma, Vivek, Deobrat Dixit, Sadashib Ghosh, and Ellora Sen. 2011. “COX-2 Regulates the Proliferation of Glioma Stem like Cells.” *Neurochemistry International* 59 (5). Elsevier B.V.: 567–71. doi:10.1016/j.neuint.2011.06.018.
- Snuderl, Matija, Ladan Fazlollahi, Long P. Le, Mai Nitta, Boryana H. Zhelyazkova, Christian J. Davidson, Sara Akhavanfard, et al. 2011. “Mosaic Amplification of Multiple Receptor Tyrosine Kinase Genes in Glioblastoma.” *Cancer Cell* 20 (6). Elsevier Inc.: 810–17. doi:10.1016/j.ccr.2011.11.005.
- Sottoriva, Andrea, Inmaculada Spiteri, Sara G M Piccirillo, Anestis Touloumis, V Peter Collins, John C Marioni, Christina Curtis, Colin Watts, and Simon Tavaré. 2013. “Intratumor Heterogeneity in Human Glioblastoma Reflects Cancer Evolutionary Dynamics.” *Proceedings of the National Academy of Sciences of the United States of America* 110 (10): 4009–14. doi:10.1073/pnas.1219747110.
- Štefková, Jana, R. Poledne, and J. A. Hubáček. 2004. “ATP-Binding Cassette (ABC) Transporters in Human Metabolism and Diseases.” *Physiological Research* 53 (3): 235–43.
- Szakács, Gergely, András Váradi, Csilla Ozvegy-Laczka, and Balázs Sarkadi. 2008. “The Role of ABC Transporters in Drug Absorption, Distribution, Metabolism, Excretion and Toxicity (ADME-Tox).” *Drug Discovery Today* 13 (9–10): 379–93. doi:10.1016/j.drudis.2007.12.010.
- Szerlip, Nicholas J, Alicia Pedraza, Debyani Chakravarty, Mohammad Azim, J. McGuire, Yuqiang Fang, T. Ozawa, et al. 2012. “Intratumor Heterogeneity of Receptor Tyrosine Kinases EGFR and PDGFRA Amplification in Glioblastoma

- Defines Subpopulations with Distinct Growth Factor Response.” *Proceedings of the National Academy of Sciences* 109 (8): 3041–46. doi:10.1073/pnas.1114033109.
- Titov, D. V., V. Cracan, R. P. Goodman, J. Peng, Z. Grabarek, and V. K. Mootha. 2016. “Complementation of Mitochondrial Electron Transport Chain by Manipulation of the NAD⁺/NADH Ratio.” *Science* 352 (6282): 231–35. doi:10.1126/science.aad4017.
- Turner, Nicholas C., and Jorge S. Reis-Filho. 2012. “Genetic Heterogeneity and Cancer Drug Resistance.” *The Lancet Oncology* 13 (4). Elsevier Ltd: e178–85. doi:10.1016/S1470-2045(11)70335-7.
- Ulrey, Clayton L., Liang Liu, Lucy G. Andrews, and Trygve O. Tollefsbol. 2005. “The Impact of Metabolism on DNA Methylation.” *Human Molecular Genetics* 14 (1): 139–47. doi:10.1093/hmg/ddi100.
- Vacas-Oleas, Andrés. 2013. “In Vitro Tumorigenicity and Stemness Characterization of the U87MG Glioblastoma Cell Line Based on the CD133 Cancer Stem Cell Marker.” *Journal of Bacteriology & Parasitology* S1 (1): 1–7. doi:10.4172/scientificreports.609.
- Vandesompele, Jo, Katleen De Preter, Filip Pattyn, Bruce Poppe, Nadine Van Roy, Anne De Paepe, and Frank Speleman. 2002. “Accurate Normalization of Real-Time Quantitative RT-PCR Data by Geometric Averaging of Multiple Internal Control Genes.” *Genome Biology* 3 (7): RESEARCH0034. doi:10.1186/gb-2002-3-7-research0034.
- Vasiliou, Vasilis, Konstandinos Vasiliou, and Daniel W Nebert. 2009. “Human ATP-Binding Cassette (ABC) Transporter Family.” *Human Genomics* 3 (3): 281–90. doi:10.1186/1479-7364-3-3-281.
- Verhaak, Roel G.W., Katherine A Hoadley, Elizabeth Purdom, Victoria Wang, Yuan Qi, Matthew D Wilkerson, C Ryan Miller, et al. 2010. “Integrated Genomic Analysis Identifies Clinically Relevant Subtypes of Glioblastoma Characterized by Abnormalities in PDGFRA, IDH1, EGFR, and NF1.” *Cancer Cell* 17 (1). Elsevier: 98–110. doi:10.1016/j.ccr.2009.12.020.
- Vlashi, E., C. Lagadec, L. Vergnes, T. Matsutani, K. Masui, M. Poulou, R. Popescu, et al. 2011. “Metabolic State of Glioma Stem Cells and Nontumorigenic Cells.”

- Proceedings of the National Academy of Sciences* 108: 16062–67. doi:10.1073/pnas.1106704108.
- Wang, Z, B Wang, Y Shi, C Xu, H L Xiao, L N Ma, S L Xu, et al. 2014. “Oncogenic MiR-20a and MiR-106a Enhance the Invasiveness of Human Glioma Stem Cells by Directly Targeting TIMP-2.” *Oncogene*, no. February 2013: 1–13. doi:10.1038/onc.2014.75.
- Warburg, Otto. 1956. “On the Origin of Cancer Cells.” *Science* 123 (3191): 309–14.
- Warburg, Otto, Franz Wind, and N Negelein. 1923. “The Metabolism of Tumors in the Body.” *Biochem. Z. Biochem. Z. Biochem. Z. Biol. Chem* 309 (2): 397–519.
- Ward, Patrick S., and Craig B. Thompson. 2012. “Metabolic Reprogramming: A Cancer Hallmark Even Warburg Did Not Anticipate.” *Cancer Cell* 21 (3). Elsevier Inc.: 297–308. doi:10.1016/j.ccr.2012.02.014.
- Wei, Xiaomu, Vijay Walia, Jimmy C Lin, Jamie K Teer, Todd D Prickett, Jared Gartner, Sean Davis, et al. 2011. “Exome Sequencing Identifies GRIN2A as Frequently Mutated in Melanoma.” *Nature Genetics* 43 (5): 442–46. doi:10.1038/ng.810.
- Weisenberger, Daniel J. 2014. “Characterizing DNA Methylation Alterations from The Cancer Genome Atlas.” *Journal of Clinical Investigation* 124 (1): 17–23. doi:10.1172/JCI69740.
- Wesolowski, J R, P Rajdev, and S K Mukherji. 2010. “Temozolomide (Temodar).” *American Journal of Neuroradiology* 31 (8): 1383–84. doi:10.3174/ajnr.A2170.
- Wise, D. R., P. S. Ward, J. E. S. Shay, J. R. Cross, J. J. Gruber, U. M. Sachdeva, J. M. Platt, R. G. DeMatteo, M. C. Simon, and C. B. Thompson. 2011. “Hypoxia Promotes Isocitrate Dehydrogenase-Dependent Carboxylation of α -Ketoglutarate to Citrate to Support Cell Growth and Viability.” *Proceedings of the National Academy of Sciences* 108 (49): 19611–16. doi:10.1073/pnas.1117773108.
- Wrensch, Margaret, Yuriko Minn, Terri Chew, Melissa Bondy, and Mitchel S Berger. 2002. “Epidemiology of Primary Brain Tumors Literature 1.” *Neuro-Oncology*, 278–99.
- Xia, J., R. Mandal, I. V. Sinelnikov, D. Broadhurst, and D. S. Wishart. 2012. “MetaboAnalyst 2.0--a Comprehensive Server for Metabolomic Data Analysis.” *Nucleic Acids Research* 40 (W1): W127–33. doi:10.1093/nar/gks374.

- Xia, J., N. Psychogios, N. Young, and D. S. Wishart. 2009. "MetaboAnalyst: A Web Server for Metabolomic Data Analysis and Interpretation." *Nucleic Acids Research* 37 (Web Server): W652–60. doi:10.1093/nar/gkp356.
- Xia, Jianguo, Igor V. Sinelnikov, Beomsoo Han, and David S. Wishart. 2015. "MetaboAnalyst 3.0—making Metabolomics More Meaningful." *Nucleic Acids Research* 43 (W1): W251–57. doi:10.1093/nar/gkv380.
- Xia, Jianguo, and David S. Wishart. 2011a. "Metabolomic Data Processing, Analysis, and Interpretation Using MetaboAnalyst." *Current Protocols in Bioinformatics* 34 (1): 14.10.1-14.10.48. doi:10.1002/0471250953.bi1410s34.
- Xia, Jianguo, and David S Wishart. 2011b. "Web-Based Inference of Biological Patterns, Functions and Pathways from Metabolomic Data Using MetaboAnalyst." *Nature Protocols* 6 (6): 743–60. doi:10.1038/nprot.2011.319.
- Xue Xue, Xing-Jie Liang. 2012. "Overcoming Drug Efflux-Bsed Multidrug Resistance in Cancer with Nanotechnology." *Chinese Anti Cancer Association*, 100–109. doi:10.5732/cjc.011.10326.
- Yecies, Jessica L, and Brendan D Manning. 2011. "Transcriptional Control of Cellular Metabolism by MTOR Signaling." *Cancer Research* 71 (8). American Association for Cancer Research: 2815–20. doi:10.1158/0008-5472.CAN-10-4158.
- Yeung, Y. T., K. L. McDonald, T. Grewal, and L. Munoz. 2013. "Interleukins in Glioblastoma Pathophysiology: Implications for Therapy." *British Journal of Pharmacology* 168 (3): 591–606. doi:10.1111/bph.12008.
- Yuan, Shuqiang, Yunxin Lu, Jing Yang, Gang Chen, Sangbae Kim, Li Feng, Marcia Ogasawara, et al. 2015. "Metabolic Activation of Mitochondria in Glioma Stem Cells Promotes Cancer Development through a Reactive Oxygen Species-Mediated Mechanism." *Stem Cell Research & Therapy* 6 (1). BioMed Central: 198. doi:10.1186/s13287-015-0174-2.
- Zhang, Jihong, Malcolm F.G. Stevens, and Tracey D. Bradshaw. 2011. "Temozolomide: Mechanisms of Action, Repair and Resistance." *Current Molecular Pharmacology* 5: 102–14. doi:10.2174/1874467211205010102.
- Zhao, Y, E B Butler, and M Tan. 2013. "Targeting Cellular Metabolism to Improve Cancer Therapeutics." *Cell Death & Disease* 4 (3). Nature Publishing Group: e532.

doi:10.1038/cddis.2013.60.

Zhao, Yue, Li Fu, Rong Li, Li-Na Wang, Yan Yang, Na-Na Liu, Chun-Mei Zhang, et al. 2012. “Metabolic Profiles Characterizing Different Phenotypes of Polycystic Ovary Syndrome: Plasma Metabolomics Analysis.” *BMC Medicine* 10 (1). BioMed Central: 153. doi:10.1186/1741-7015-10-153.

Zhao, Zhi Jun, Chun Zou, Yi Xing Zhu, Jun Dai, Sheng Chen, Dan Wu, Jing Wu, and Jian Chen. 2011. “Development of L-Tryptophan Production Strains by Defined Genetic Modification in Escherichia Coli.” *Journal of Industrial Microbiology and Biotechnology* 38 (12): 1921–29. doi:10.1007/s10295-011-0978-8.

Zielinski, Daniel C, Neema Jamshidi, Austin J Corbett, Aarash Bordbar, Alex Thomas, and Bernhard O Palsson. 2017. “Systems Biology Analysis of Drivers Underlying Hallmarks of Cancer Cell Metabolism.” *Scientific Reports* 7 (January). Nature Publishing Group: 41241. doi:10.1038/srep41241.

Zou, Yongxiang, Guanzhong Qiu, Lei Jiang, Zheng Cai, Wei Sun, Hongkang Hu, Chengyin Lu, Weilin Jin, and Guohan Hu. 2017. “Overexpression of Ubiquitin Specific Proteases 44 Promotes the Malignancy of Glioma by Stabilizing Tumor-Promoter Securin” 8 (35): 58231–46. doi:10.18632/oncotarget.16447.

List of Publications

1. **S.R.C. Immanuel**, A.D. Ghanate, D.S. Parmar, F. Marriage, V. Panchagnula, P.J. Day, A. Raghunathan, Integrative analysis of rewired central metabolism in temozolomide resistant cells, *Biochem. Biophys. Res. Commun.* 495 (2018) 2010–2016. **doi:10.1016/j.bbrc.2017.12.073**.
2. **S.R.C. Immanuel**, D. Banerjee, M.P. Rajankar, A. Raghunathan, Integrated constraints based analysis of an engineered violacein pathway in *Escherichia coli*, *BioSystems*. 171 (2018). **doi:10.1016/j.biosystems.2018.06.002**.
3. **S.R.C. Immanuel**, A. Raghunathan, Metabolic perturbations in temozolomide resistant cells deduced by core metabolic model. *In preparation*.
4. **S.R.C. Immanuel**, A. D. Ghanate, D. S. Parmar, M. Mohole, A. Raghunathan, Bridging the gap: Role of scalable metabolic models in connecting metabolism to personalized medicine. *In preparation*.
5. Dharmesh S. Parmar, Avinash Ghanate, **S.R.C. Immanuel**, Anu Raghunathan, Venkateswarlu Panchagnula. Mass spectrometry analysis method for quantification of amino acids and other metabolites in cell culture samples. *Submitted*.



Integrative analysis of rewired central metabolism in temozolomide resistant cells

Selva Rupa C. Immanuel^{a, b, c}, Avinash D. Ghanate^{b, c}, Dharmeshkumar S. Parmar^{b, c}, Fiona Marriage^a, Venkateswarlu Panchagnula^{b, c}, Philip J. Day^a, Anu Raghunathan^{b, c, *}

^a Division of Evolution and Genomic Sciences, The Manchester Institute of Biotechnology, University of Manchester, United Kingdom

^b Chemical Engineering Division, CSIR-National Chemical Laboratory, Pune, India

^c Academy of Scientific & Innovative Research (AcSIR), CSIR-National Chemical Laboratory, Pune, India

ARTICLE INFO

Article history:

Received 4 December 2017

Accepted 14 December 2017

Available online 14 December 2017

Keywords:

Temozolomide resistance

Metabolic rewiring

Glutamine

Metabolite profiling

mRNA abundances

U87MG

ABSTRACT

An authenticated U87MG clonal glioblastoma cell line was investigated to identify a sub-population of neurospheroidal (NSP) cells within the main epithelial population (U87MG). The NSP cells sorted using Fluorescence Assisted Cell Sorting (FACS) showed varied morphology, 30% lower growth rates, 40% higher IC₅₀ values for temozolomide drug and could differentiate into the glial cell type (NDx). Metabolite profiling using HR-LCMS identified glucose, glutamine and serine in both populations and tryptophan only in U87MG as growth limiting substrates. Glycine, alanine, glutamate and proline were secreted by U87MG, however proline and glycine were re-utilized in NSP. Exo-metabolite profiling and phenotypic microarrays identified differential metabolism of primary carbon sources glucose and derived pyruvate for U87MG; glutamine and derived glutamate metabolism in NSP. Differential mRNA abundance of AKT1, PTEN, PIK3CA controlling metabolism, drug efflux, nutrient transport and epigenetic control MDM2 are potentially critical in shaping DNA methylation effects of temozolomide. Our study provides a new insight into the combined effect of these factors leading to temozolomide resistance in NSP.

© 2017 Elsevier Inc. All rights reserved.

1. Introduction

Temozolomide (TMZ), anti-cancer prodrug of Temodar, is an imidazotetrazine that has increased the prognosis of highly aggressive Glioblastoma Multiforme (GBM) [1]. The therapeutic index is dependent on molecular markers like O⁶-methylguanine methyltransferase (MGMT) and/or lack of DNA repair in GBM [2]. Other contributors include isocitrate dehydrogenase type 1 and type 2 (IDH1/2) mutations that metabolically reprogram the cell to form neo-metabolite 2-hydroxyglutarate [3] and the epigenetic status controlling cytosine-phosphate-guanine (CpG) island methylator phenotype (G-CIMP) [4]. U87MG, a completely sequenced [5] and commonly studied grade IV glioma cell line [6] is wildtype for IDH1/IDH2 is sensitive to temozolomide [1]. Cell line model systems, indispensable tools in providing preclinical biological insight, are known to harbor minority populations of

putative stem-like cells, molecularly defined by dye extrusion phenotypes that may cause resistance to chemotherapy [7,8]. With increased discovery of gene and protein expression signatures [4] and detailed molecular characterization to characterize the drug sensitivity, rigorous phenotyping of these sub-populations, in addition to morphology and drug efflux is critical to understand resistance.

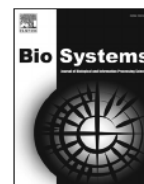
In this study, a sub-population of neurospheroidal cells (NSP) morphologically distinct from epithelial cells were identified in U87MG (Grade-IV GBM cell line) and sorted using Fluorescence Assisted Cell Sorting (FACS). To our knowledge, this is the first study addressing the functional characterization in terms of integrating knowledge related to drug efflux, growth/proliferation, nutrient preferences and metabolite profiling to drug dose response establishing an integrated resistance paradigm.

2. Materials and methods

Cell culture: An authenticated U87MG cell line (HTB-14; Human Glioblastoma Multiforme from ATCC; Supplementary File 2,3)

* Corresponding author. Biochemical Engineering unit, Chemical Engineering division, CSIR, National Chemical Laboratory (CSIR-NCL), Pune, India.

E-mail address: anu.raghunathan@ncl.res.in (A. Raghunathan).



Integrated constraints based analysis of an engineered violacein pathway in *Escherichia coli*

Selva Rupa Christinal Immanuel¹, Deepanwita Banerjee¹, Mayoreshwar P. Rajankar¹, Anu Raghunathan*

Chemical Engineering Division, CSIR-National Chemical Laboratory, Dr. Homi Bhabha Road, Pune, 411008, India

ARTICLE INFO

Keywords:

Violacein
Escherichia coli
Synthetic biology
Metabolism
Flux balance analysis

ABSTRACT

Strategies towards optimal violacein biosynthesis, a potential drug molecule, need systems level coordination of enzymatic activities of individual genes in a multigene operon *vioABCDE*. Constraints-based flux balance analysis of an extended *iAF1260* model (*iAF1260vio*) with a reconstructed violacein module predicted growth and violacein yields in *Escherichia coli* accurately. Shadow price (SP) analysis identified tryptophan metabolism and NADPH as limiting. Increased tryptophan levels in Δ *pgi* & Δ *pheA* were validated using *in silico* gene deletion analysis. Phenotypic phase plane (PhPP) analysis highlighted sensitivity between tryptophan and NADPH for violacein synthesis at molar growth yields. A synthetic *VioABCDE* operon (SYNO) sequence was designed to maximize Codon Adaptive Index (CAI: 0.9) and tune translation initiation rates (TIR: 2–50 fold higher) in *E. coli*. All pSYN *E. coli* transformants produced higher violacein, with a maximum six-fold increase in yields. The rational design *E. coli* Δ *pheA* SYN: gave the highest violacein titers (33.8 mg/l). Such integrated approaches targeting multiple molecular hierarchies in the cell can be extended further to increase violacein yields.

1. Introduction

The grand challenge of metabolic engineering lies in the complexity and redundancy of cellular pathways and the evolutionary drive to maximize growth/fitness rather than a forced bioengineering objective. Constraints based flux balance analysis (FBA) of metabolic models has been used to design strains *in silico* that simultaneously maximize fitness and the desired product (Burgard et al., 2003; Rupp et al., 2010; Varma and Palsson, 1993). These models predict intracellular reaction fluxes and identify strategies for substrate uptake, energy and cofactor balance. Although, these models can drive rational strain design, the predictions of such evolutionary optimality models are more in tune with adapted strains (Ibarra et al., 2002). Metabolic engineering of value added products through synthetic biology strategies to fast forward the adaptive evolution process are becoming more rampant.

When complex pathways are introduced inside the cell, limitations including intermediate toxicity, low enzyme activity, metabolic burden (cofactor imbalance etc.) need to be overcome for high performance. Such bottlenecks can be addressed using pathway engineering that exploits the synergies of synthetic biology, metabolic engineering and systems biology (Nielsen and Keasling, 2011, 2016; Stephanopoulos, 2012; Wu et al., 2016; Yadav et al., 2012). Successful metabolic

engineering for platform cell factories to produce a wide range of fuels and chemicals necessitates identifying the sensitivity of product/process to nutrient precursors and cofactors *a priori*. Such complementation supports coupling of cellular objectives of growth and energy to desired bioengineering objectives. Comprehensive computational strain designs for stoichiometric growth-coupling of desired products of central metabolism have been identified through pathway analysis (Klamt and Mahadevan, 2015; Von Kamp and Klamt, 2017).

Violacein is a bacterial bis-indole pigment of commercial interest having antibacterial, antitumoral, antiviral, trypanocidal and anti-protozoan properties (Durán and Menck, 2001; Durán et al., 2007; Ferreira et al., 2004; Queiroz et al., 2012). It is formed by the condensation of two L-tryptophan molecules controlled by the enzymes of a complex biosynthetic pathway (Fig. 1). The impact of the double bonds, conjugation and hydroxyl groups potentially attribute chromophoric properties (Fig. 1B) to final violet colored product violacein of the pathway (Hoshino, 2011). Violacein has been tested to show anti-bacterial (gram positive), antineoplastic and antifungal properties (Durán et al., 2016). Other tryptophan based small molecule therapeutics like rebeccamycin and staurosporine have been reported as important anti-tumor molecules (Howard-Jones and Walsh, 2006).

The violacein biosynthetic pathway is complex due to a coordinated

* Corresponding author.

E-mail address: anu.raghunathan@ncl.res.in (A. Raghunathan).

¹ Equal contributing author.

SELVA RUPA CHRISTINAL IMMANUEL

C/O. Dr. Anu Raghunathan,
Chemical Engineering and Process Development Division (CEPD),
CSIR-National Chemical Laboratory (CSIR-NCL),
Dr Homibhabha Road, Pashan,
Pune- 411008. Maharashtra. India.



PROWESS

- **Animal cell culture:** Basic maintenance of cancer cell lines & primary astrocytes. Use of key techniques including FACS, MTT assay, SRB assay, BIOLOG phenotypic microarray, Fluorescence Imaging of cells, qPCR, Extraction of metabolites for quantitation using high resolution LC-MS/MS and MALDI MS/MS analysis.
- **Molecular biology:** Gene Knockout using homologous recombination in bacteria, Molecular cloning, construction of recombinant DNA and its transformation using electroporation, Genomic and Proteomic techniques (PCR, Agarose GE, 2D PAGE, Isoelectric focusing, Western blotting, DNA and Protein Purification).
- **High-throughput Data Analysis:** Exome Sequencing data analysis using Oncotator web tool, Comparison with Human genome build hg19, Identification of SNPs and INDELS, and Plotting using MATLAB.
- **MATLAB:** Computational simulations including robustness analysis, flux variability analysis etc., using COBRA toolbox and Flux balance analysis (FBA) using tomlab and glpk solver.

PROFESSIONAL EXPERIENCE

- * **INSPIRE Fellow (SRF-P), July 2011 to present**, PhD Student at CSIR-National Chemical Laboratory, Pune. India.
Thesis Advisor: Dr. Anu Raghunathan, Chemical Engineering Division.
Thesis Focus: Metabolic Reprogramming Of The Cell - Understanding the Systemic Signatures And Growth In Cancer
- * **Newton Bhabha Research Fellow, June 2015 to December 2015.** British council - DST India PhD placement under Newton Bhabha scheme. Worked in Manchester Institute of Biotechnology (MIB), University of Manchester, **United Kingdom.**
Research Collaborator: Dr. Philip J. Day and Prof. Douglas Kell (MIB,UK).
Research Focus: Glioblastoma heterogeneity: Quantitative real time PCR analysis to address temozolomide resistance.
- * **Assistant Professor, July 2010 to June 2011.** P.G. Department of Molecular Biology, Bishop Heber College, Trichy, India.

AWARDS AND MERITS

- * **Newton Bhabha PhD placement 2015-2016** Fully funded fellowship from British council and DST-India for 6 months to visit UK and do a part of my PhD research in MIB, UK.
- * **Best Poster in Chemical Engineering** Award for presenting my research work on National Science Day 2014, at CSIR- National Chemical Laboratory, Pune, India.

SELVA RUPA CHRISTINAL IMMANUEL

- * **Prof. A. Narayasamy Endowment Gold Medal** in recognition of outstanding performance in M.Tech degree examination held by University of Madras, Chennai, India.
- * **Best Outgoing Student Award** during the period of 2004-2007 by Bharath College of Science and Management, Thanjavur, India.
- * Ullas Trust **Young Achiever's Scholarship** for the year 2003-2004 by Ullas trust, Chennai, India.
- * Awarded the Merit Certificate in recognition of the high position secured in the list of meritorious candidates qualifying for the awards in tenth public examination held in 2002 by the **Tamilnadu Education Department**, under **National Scholarship Scheme**.

RESEARCH EXPERIENCE

- * **Newton Bhabha Research Fellow, June 2015 to December 2015.** British council - DST India PhD placement under Newton Bhabha scheme. Worked in Manchester Institute of Biotechnology (MIB), University of Manchester, **United Kingdom**.
Research Collaborator: Dr. Philip J. Day and Prof. Douglas Kell (MIB, UK).
Research Focus: Glioblastoma heterogeneity: Quantitative real time PCR analysis to address temozolomide resistance.
- * **M. Tech. Thesis:** *In situ* biofunctionalization of gold nanoparticles with antibiotics for increased activity against microbes and bacterial cell imaging using AFM.
Supervisor: Dr. Pankaj Poddar, CSIR-National Chemical Laboratory (NCL), Pune, India.
- * **M. Sc., Project:** Molecular Cloning of Urease Gene from *Arabidopsis thaliana* and an attempt to increase its expression using f-CNT.
Supervisor: Dr. P. Karthe, Center of advanced study in crystallography and biophysics, University of Madras, Chennai, India.

EDUCATIONAL QUALIFICATION

Qualification	Institution/University	Year of passing	Percentage	Class	Rank Obtained
M. Tech., (Nanoscience & Nanotechnology)	Centre for Nanosciences and Nanotechnology, University of Madras , Chennai. Tamil Nadu.	2010	81.36% CGPA: 5.53/6 Grade: O	First class Outstanding	1st Rank (University Level)
B. Sc., (Bio-technology)	Bharath College of Science & Management, Thanjavur. Tamil Nadu. (Bharathidasan University)	2007	80.45%	First class with distinction	8th Rank (University Level)
HSC	Bentick Higher Secondary School, Choolai, Chennai. Tamil Nadu.	2004	75.5%	First class	Not applicable
SSLC	S.H.N. Ethel Harvey GHSS, Sattur. Tamil Nadu.	2002	95%	First class with distinction	Not applicable

SELVA RUPA CHRISTINAL IMMANUEL

CO-CURRICULAR ACTIVITIES

Poster presentation

1. Poster title: Capturing metabolic reprogramming using mass spectrometry – CORE analysis towards understanding tumor heterogeneity and cancer drug resistance
Conference: *The Gaskell Birthday Symposium – A Celebration of Mass Spectrometry (2015)*, University of Manchester, United Kingdom.
2. Poster title: Deciphering Cancer Exome At A Systems-Level
Conference: *C-DAC Bioinformatics symposium*, CDAC, Pune, India.
3. Poster title: *Drug Resistant Population In Human Glioblastoma Multiforme Cells: Identification And Phenotypic Characterization. ***Best Poster Award**
Conference: *National Science Day (2014)*, CSIR-National Chemical Laboratory, Pune. India.
4. Poster title: Drug Resistant Population In Human Glioblastoma Multiforme Cells: Identification And Phenotypic Characterization Using Hoechst 33342 Staining.
Conference: *International Conference on Biotechnology and Bioinformatics (ICBB-2014)*, Pune, India.
5. Poster title: A Systems Approach for Metabolic Engineering of Tryptophan in *Escherichia coli*
Conference: *AiCHE-2013*, Hilton San Francisco Union Square, San Francisco.

Conference attended

1. *The Gaskell Birthday Symposium – A Celebration of Mass Spectrometry (2015)*, University of Manchester, United Kingdom.
2. *C-DAC Bioinformatics symposium (2015)*, CDAC, Pune, India.
3. *International Conference on Biotechnology and Bioinformatics (ICBB-2014)*, Pune, India.

Workshop attended

1. *MetaMod 2016 - Workshop on ScrumPy and Systems biology*, NCL-IISER, Pune, India.